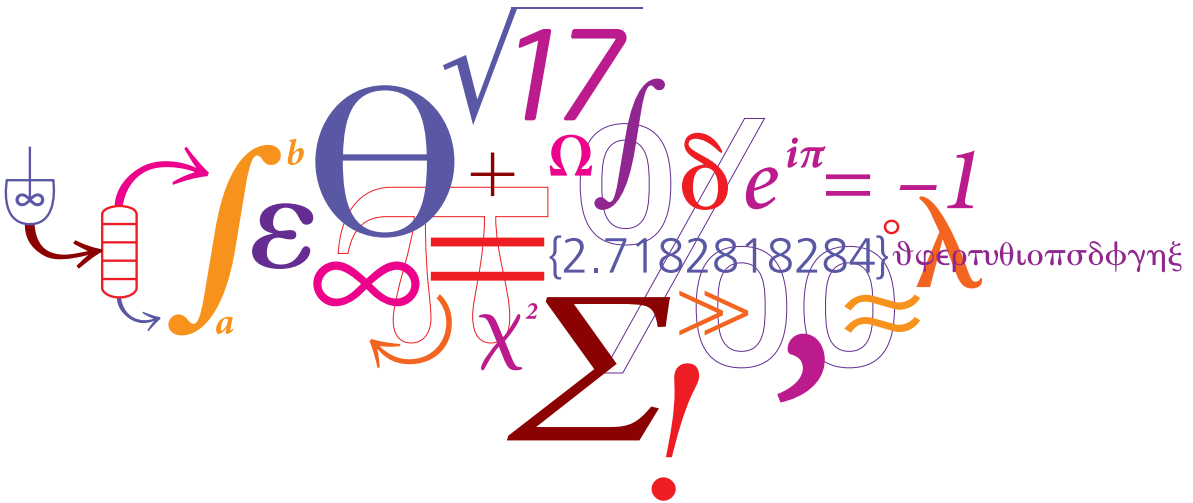


# CO<sub>2</sub> capture using aqueous ammonia



**Victor Darde**  
 Ph.D. Thesis  
 August 2011

# CO<sub>2</sub> capture using aqueous ammonia

**Victor Darde**  
Ph.D. Thesis  
August 2011

Copyright©: **Victor Darde**

August 2011

Address: Center for Energy Resources Engineering

**Department of Chemical and**

**Biochemical Engineering**

**Technical University of Denmark**

Søltofts Plads, Building 229

DK-2800 Kgs. Lyngby

Denmark

Phone: +45 4525 2800

Fax: +45 4525 4588

Web: [www.cere.dtu.dk](http://www.cere.dtu.dk)

Print: **J&R Frydenberg A/S**

København

December 2011

ISBN: 978-87-92481-56-6

## Preface

The thesis is submitted in partial fulfillment of the requirements for the Ph.D. degree at the Technical University of Denmark (DTU). This work has been done at the Department of Chemical and Biochemical Engineering of DTU and at the department of Chemical Engineering of DONG Energy Power as an industrial PhD project. It has been supervised by Associate Professor Kaj Thomsen from DTU and Willy van Well from DONG Energy Power. It has been financed by DONG Energy Power and by the Danish ministry of science, technology and innovation. It has started February 1<sup>st</sup> 2008 and ended August 31<sup>st</sup> 2011.

I would like to express my gratitude to Kaj Thomsen for his exceptional supervision during this project. Thank you for constant support and your valuable help during this thesis. I have benefited immensely from the programs, software, models and data base that you have developed over the years and that you have allowed me to use. I have learned a lot from you and have appreciated each of our many discussions and debates. Thank you for also for your patience during these years. It has been inspiring working with you.

Thanks to Willy van Well for his remarkable guidance during this thesis. Your knowledge regarding the world of CO<sub>2</sub> capture has been rousing. Thank you for your support and your help on the many times where it was needed. I am very grateful for the huge enthusiasm you have shown for every aspects of this work, from the very beginning to the very end. I have appreciated a lot the trust that I have put in me and the many advices, suggestions and technical recommendations that you have given me and that have improved a lot the quality of this work. It has been very fruitful and fulfilling years thanks to you.

At the Technical University of Denmark, there are several people that have contributed to this work.

I express my gratitude to Erling Stenby for giving me the possibility to work in such an enriching environment, for believing in the project and for showing such interest for it.

Thank you very much to Philip Loldrup Fosbøl for your immense help during this work and for the countless technical discussions that we have had. Your knowledge, skills and patience have been key assets for the completion of this work. Thank you also for translating the abstract in Danish.

I express my admiration and gratefulness to Bjørn Maribo-Mogensen for the work he has done developing the Extended UNIQUAC user model. It has been inspiring working with you.

Thank you to Leila Faramarzi for the many fruitful discussions and for the many advices that you have given me regarding this work.

Thank you to Povl Valdemar Andersen and Zacarias Teclé for their help regarding the experimental work. A warm thank to Henning Vitus Koldbech for his enthusiasm regarding the manufacturing of the

experimental apparatus. Thank you Anne Louise Biede and Patricia Wagner for solving any problem I could experience in no time. Thanks also to Lars Jensen.

Many people from DONG Energy Power have contributed to the completion of this work. I have especially benefited a lot from the help of Jacob Knudsen. Thank you also to Flemming Kanstrup, Jørgen Nørklit Jensen and Thomas Pedersen for their advices and suggestions. Thank you to Alice Jochumsen for her patience and kindness during these years. Thank you to Ole Hede Larsen, Folmer Fogh and especially Rudolph Blum for showing such enthusiasm and interest for this project.

Several external people have also directly contributed to this project.

Thank you to Ross Dugas from the University of Texas for his recommendations regarding the experimental apparatus.

A warm thank to Sebastian Linnenberg from the Hamburg Technical University for his patience and for his brilliant contribution to the integration study. Thanks also to Jochen Oexmann that has given valuable suggestions regarding the simulation of the process and the integration study.

I am thankful to Davide Bonalumi from the University of Milano for his suggestions regarding the process simulation study.

On a more personal basis, I would like to thank warmly my family for their support during these years and for allowing me to reach that point despite some difficult times.

Thank you to my friends that have made my life so enjoyable. Specially, thanks to Julie, Jose, Silvio, Ana, Matthieu, Wenjing and the Jam.

Finally, special thanks to Inês for her constant support during the good and the less good times. Muito obrigado por tudo linda.

Victor Darde

## Abstract

The subject of this thesis is the study of the post combustion carbon dioxide capture process using aqueous solutions of ammonia. Amine solutions have been commonly used for the commercial production of CO<sub>2</sub> and have been tested for CO<sub>2</sub> capture on pilot scale. The main disadvantages related to the use of amine solutions are the high heat consumption (3500-4000 kJ/kg CO<sub>2</sub>) and the high degradation rate of the amines.

The capture process using aqueous ammonia exists in two variants. The first variant absorbs the CO<sub>2</sub> at low temperature (2-10°C). It is being developed by Alstom and is called Chilled Ammonia Process (CAP). The second process absorbs CO<sub>2</sub> at ambient temperature (25-40 °C). According to the CAP patent, the heat requirement for CO<sub>2</sub> desorption is significantly lower than for conventional amine processes. In addition, by using ammonia, degradation problems can be avoided and a high carbon dioxide capacity can be achieved. Hence, this process shows good perspectives. However, a scientific understanding of the processes is required. In this work, the performance of the CO<sub>2</sub> capture process using aqueous ammonia has been analyzed.

In order to describe the CO<sub>2</sub>-NH<sub>3</sub>-H<sub>2</sub>O system, an advanced thermodynamic model is required. The Extended UNIQUAC model for the CO<sub>2</sub>-NH<sub>3</sub>-H<sub>2</sub>O system proposed by Thomsen and Rasmussen (1999) was upgraded in order to enlarge its valid temperature range to 0-150 °C. Additional types of experimental data have been used during the parameter fitting in order to increase the accuracy of the model. A thermodynamic study of the process based on the information from the patent has been performed. The heat requirement in the desorber was found to be 1850 kJ/kg CO<sub>2</sub> captured for a chosen non-optimized configuration. This is significantly lower than the heat required for the monoethanolamine (MEA) based process. However, our study showed also a high vapor pressure of ammonia in the absorber and thereby the need for extensive washing sections.

The rate of absorption of carbon dioxide by the solvent is a key parameter regarding the sizing of the absorber column. The study of the rate of absorption of carbon dioxide by ammonia solvent has been conducted by using a wetted wall column. The absorption rate was measured from 6 to 31 °C for aqueous ammonia between 1 and 10 wt% NH<sub>3</sub> with a loading varying from 0 to 0.8 mol CO<sub>2</sub>/molNH<sub>3</sub>. It was compared to the rate of absorption using 30 wt% MEA at 40°C as reference. The study has shown that MEA at 40 °C absorbs carbon dioxide significantly faster than ammonia at low temperature. Hence, a larger contact area between the gas and the liquid would be necessary in the absorber in the context of the CAP. In addition, the rate of absorption has been modeled. The model could successfully predict the experimental measurements of the absorption rate of CO<sub>2</sub> in loaded ammonia solutions.

In order to make a process optimization study, flow sheet calculations are required. Therefore the Extended UNIQUAC thermodynamic model has been implemented in the commercial simulator

ASPEN Plus by applying a user model (Maribo-Mogensen *et al.*, 2009). This allows for using the functionalities of ASPEN Plus coupled with the calculation abilities from the thermodynamic model. This tool has been applied to compare the performance of the e-NRTL model implemented in Aspen with the Extended UNIQUAC model. The calculation of the latter has been shown to be significantly more accurate than the corresponding calculations with the e-NRTL model for the temperature and ammonia concentration range used in the capture process. This study has been made in collaboration with university of Milano.

By applying the Extended UNIQUAC user model, both variants of the process have been simulated in ASPEN Plus by performing equilibrium calculations. The simulation takes into account the chilling of the solvent and flue gas, the ammonia removal from the flue gas and the recovery of the washed ammonia. In order to account for the low rate of absorption and the deviation from equilibrium, a low Murphree efficiency has been applied in the absorber. Two process configurations have been analyzed and a sensitivity analysis over the main process parameters has been studied. The lowest total heat requirement for the desorber and NH<sub>3</sub>-stripper of 2700 kJ/kg CO<sub>2</sub> captured could be observed for low absorption temperature implying precipitation. However, the process absorbing carbon dioxide at low temperature without solid formation was also found to be promising.

In order to estimate the effect of the capture on a coal-fired power plant, an integration study has been performed in collaboration with Hamubrg University of Technology. In order to take into account the location of the plant, two cooling water temperatures have been considered. A study allowing for minimizing the net efficiency penalty from the capture has been conducted and compared with the MEA-based process. For both configurations, the net efficiency penalty observed was significantly lower than the one observed with MEA when low temperature cooling water is available. A net efficiency penalty of 9.5 %pts. was calculated for one of the configurations, against 10.9 %pts. for the MEA-based process. When cooling water is available at 20 °C, the process was not competitive with the MEA-based one. Using the modeling of the rate of absorption of carbon dioxide by aqueous ammonia and the simulation results, the dimensions of the absorber columns has been estimated. An absorber about twice as high as the one used for the MEA-based process was found to be required to reach 90% capture rate.

## Resumé på dansk

Denne PhD afhandling omhandler kuldioxidopsamling fra kulfyrede kraftværker ved brug af vandige opløsninger af ammoniak. Aminopløsninger har almindeligvis været brugt til kommerciel produktion af CO<sub>2</sub> og er blevet testet i pilotskala til CO<sub>2</sub>-opsamling fra kraftværker. De største ulemper ved anvendelse af aminopløsninger er et højt varmekonsum (3500-4000 kJ/kg CO<sub>2</sub>) og en stor amidnedbrydning.

Opsamlingsprocessen med vandig ammoniak findes i to varianter: I den første proces absorberes CO<sub>2</sub> ved lav temperatur (2-10 °C). Denne variant udvikles i virksomheden Alstom og kaldes "Chilled Ammoniak Processen" (CAP) (Gal, 2006). I den anden proces absorberes CO<sub>2</sub> i stedet ved stuetemperatur (25-40 °C). Ifølge patentet for CAP burde varmekonsumet være væsentlig lavere i ammoniak processen sammenlignet med amin processen. Derudover har ammoniak ingen nedbrydningsproblemer og kan optage mere kuldioxid. Derfor er ammoniak processen lovende. Det er dog nødvendigt at skabe en videnskabelig forståelse af processen og derfor analyseres ammoniak CO<sub>2</sub>-opsamlingsprocessen i dette studie.

For at beskrive systemet, behøves der er en avanceret termodynamisk model. I dette studie blev den udvidede UNIQUAC model af Thomsen og Rasmussen (1999) opgraderet for systemet CO<sub>2</sub>-NH<sub>3</sub>-H<sub>2</sub>O med henblik på at udvide temperaturgyldighedsområdet til 0-150 °C. Under arbejdet med parameterestimeringen er der brugt flere eksperimentelle data end oprindeligt for at øge nøjagtigheden af modellen. Der er udført et termodynamisk studie af processen ved brug af oplysninger fra CAP patentet. Varmeforbruget blev fundet til at være 1850 kJ/kg CO<sub>2</sub> opsamlet for en given ikke-optimeret konfiguration. Dette er væsentlig lavere sammenlignet med den konventionelle monoethanolamin (MEA) proces. Studiet viste til gengæld også et højt ammoniak damptryk i absorbereren og dermed et behov for fordynende vaskesektioner.

Hastigheden hvormed kuldioxid absorberes i opsamlingsvæsken er en vigtig parameter i forbindelse med dimensionering af absorberkolonnen. I dette studie er CO<sub>2</sub> opsamlingshastigheden blevet undersøgt eksperimentelt ved hjælp af en befugtetvægskolonne (wetted wall column). Absorptionshastigheden blev målt mellem 6 og 31 °C i vandige ammoniak med 1 til 10 vægtprocent NH<sub>3</sub> og med et CO<sub>2</sub> indhold på 0 til 0,8 mol CO<sub>2</sub>/mol NH<sub>3</sub>. Resultaterne blev sammenlignet med absorptionshastigheden i 30 vægtprocent MEA. Undersøgelsen viste, at den typiske proces af MEA ved 40 °C absorberer kuldioxid betydeligt hurtigere end lav temperatur CAP ammoniak. Derfor er det nødvendigt at skabe et større kontaktareal imellem røggassen og opsamlingsvæsken for at opnå den samme oprensning. Derudover er absorptionshastigheden blevet modelleret. Modellen kan anvendes til at forudsige CO<sub>2</sub> absorptionshastigheden i CO<sub>2</sub>-holdige ammoniakopløsninger.

Den udvidede termodynamiske UNIQUAC model blev implementeret i den kommercielle proces simulator ASPEN Plus under anvendelse af en bruger model (Maribo-Mogensen et al., 2009) til at



kunne udføre procesoptimeringsstudier. Dette giver mulighed for at kombinere Aspen Plus og specialiserede termodynamiske beregninger. Værktøjet er blevet anvendt til sammenligning af resultaterne fra e-NRTL i Aspen Plus med resultater fra den udvidede UNIQUAC model. Beregningerne har vist sig at være betydeligt mere præcise end de tilsvarende beregninger med e-NRTL modellen for relevante temperaturer og ammoniakkoncentrationer.

Ligevægtssimuleringer, ved brug af den udvidede UNIQUAC brugermodel i Aspen Plus for ammoniak CO<sub>2</sub>-opsamling, er blevet foretaget. Der er taget hensyn til nedkøling af opløsningsmidlet og røggassen, samt fjernelse af ammoniak fra den rensede røggas og regenerering af vaskevandet. For at tage højde for den lave absorptionshastighed og afvigelsen fra ligevægt, er der anvendt en lav Murphrees-effektivitet i absorbersimuleringerne. To proceskonfigurationer er blevet analyseret og der er foretaget variationsanalyse over de vigtigste procesvariable. Det mindste varmebehov blev observeret ved lav absorptionstemperatur med udfældning af faste stoffer. Processer uden faststofdannelse anses dog også for at være lovende.

For at bestemme den mere overordnede effekt af CO<sub>2</sub> opsamling på kulfyrede kraftværker, er der blevet foretaget en procesintegrationsundersøgelse. For at tage hensyn til den geografiske placeringen af anlægget, er der t blevet anvendt to forskellige kølevandstemperaturer. Begge proces konfigurationer er blevet analyseret. Der er gennemført et studie med henblik på at minimere det totale effektivitetstab ved elektricitetsproduktion under udnyttelse af CO<sub>2</sub>-opsamling. Der er foretaget en sammenligning med resultaterne for den konventionelle MEA proces. Begge ammoniak konfigurationer gav et betydeligt mindre effektivitetstab end ved MEA brug. Ved hjælp af modellering af kuldioxidabsorptionshastigheden i vandige ammoniakopløsninger og simuleringresultaterne, har det været muligt at dimensionere absorberkolonnerne. Sammenlignet med MEA processen kræves en større absorber for at opnå 90 procent opsamling.

# Table of Content

Preface .....	I
Abstract.....	III
Resumé på dansk .....	V
Table of Content.....	VII
1 General introduction.....	1
1.1 Global warming and climate change: causes and consequences .....	1
1.2 Climate change mitigation.....	3
1.3 Carbon dioxide capture and storage.....	5
1.3.1 Carbon dioxide capture techniques.....	5
1.3.2 Options regarding the carbon dioxide transport and disposal .....	10
1.3.3 Considerations regarding the cost of the process.....	12
1.4 Post-combustion capture by chemical absorption.....	12
1.4.1 Description of the flow sheet.....	12
1.4.2 Considerations regarding the solvent .....	14
1.4.3 Current development of chemical solvents and perspectives .....	15
1.5 Carbon dioxide capture using aqueous ammonia .....	17
1.5.1 Description of the process.....	17
1.5.2 Literature review.....	19
1.5.3 Thesis motivation and outline .....	21
1.6 References .....	22
2 Thermodynamic modeling of mixtures of carbon dioxide, ammonia and water .....	29
2.1 Introduction .....	29
2.2 Phase equilibria.....	30
2.2.1 Chemistry .....	30

2.2.2	Standard state chemical potential, enthalpy of formation, heat capacity .....	33
2.3	Description of the thermodynamic model .....	35
2.3.1	Local composition models .....	35
2.3.2	Extended UNIQUAC model.....	35
2.4	Evaluation of the parameters .....	38
2.4.1	Parameter fitting procedure .....	38
2.4.2	Parameters fitted.....	41
2.5	Experimental data used for the estimation of the parameters and results.....	44
2.5.1	Binary NH <sub>3</sub> -H <sub>2</sub> O data.....	44
2.5.2	Binary CO <sub>2</sub> -H <sub>2</sub> O data.....	49
2.5.3	Ternary data.....	53
2.6	Conclusion.....	65
2.7	References .....	66
3	Thermodynamic analysis of CO <sub>2</sub> capture process using aqueous ammonia.....	75
3.1	Introduction .....	75
3.2	Equilibrium composition of the process stream.....	75
3.2.1	Absorption.....	75
3.2.2	Desorption .....	81
3.2.3	Comparison with the calculations using the old set of Extended UNIQUAC parameters .....	83
3.3	Heat requirement in the desorber .....	83
3.4	Conclusion.....	88
3.5	References .....	89
4	Experimental measurement and modeling of the rate of absorption of carbon dioxide by aqueous ammonia	91
4.1	Introduction .....	91
4.2	Measurement of carbon dioxide absorption rate by aqueous ammonia .....	91

4.2.1	Review of the experimental apparatus .....	91
4.2.2	Description of the wetted wall column apparatus.....	99
4.2.3	Definition and measurement of the overall mass transfer coefficient.....	102
4.2.4	Experimental procedure .....	106
4.3	Rate of absorption and expression of the overall kinetic constant.....	108
4.3.1	Overall kinetic constant using aqueous ammonia solutions.....	108
4.3.2	Overall kinetic constant using MEA solutions .....	111
4.4	Characterization of the wetted wall column.....	112
4.4.1	Determination of the gas side mass transfer coefficient, $k_G$ .....	112
4.4.2	Determination of the physical liquid mass transfer coefficient $k_L^0$ .....	116
4.5	Liquid side mass transfer coefficient .....	117
4.5.1	Considerations regarding the accuracy of the measurements.....	118
4.5.2	Liquid side mass transfer coefficient with aqueous MEA.....	120
4.5.3	Liquid side mass transfer coefficient with aqueous ammonia.....	121
4.6	Overall chemical rate of absorption of CO <sub>2</sub> by aqueous ammonia .....	126
4.6.1	Modeling.....	126
4.6.2	Comparison of the models.....	129
4.7	Conclusion.....	133
4.8	Nomenclature.....	133
4.9	References .....	135
5	Validation of the Aspen User model and comparison with the e-NRTL model.....	139
5.1	Introduction .....	139
5.2	Description of the Aspen user model .....	139
5.2.1	Introduction to the implementation of Extended UNIQUAC on Aspen Plus.....	139
5.2.2	Main challenges related to the development of the user model.....	140

5.2.3	Applicability and limitation of the user model .....	141
5.3	Validation of the interface .....	142
5.4	Comparison with the e-NRTL model.....	146
5.4.1	Introduction .....	146
5.4.2	Evaluation of the thermodynamic models with experimental data.....	146
5.4.3	Simulation of the CO <sub>2</sub> capture process using aqueous ammonia with e-NRTL and xUM .....	161
5.5	Conclusion.....	168
5.6	References .....	169
6	Simulation of CO <sub>2</sub> capture using aqueous ammonia using the Extended UNIQUAC model .....	171
6.1	Introduction .....	171
6.2	Simulation of the CO <sub>2</sub> capture process using aqueous ammonia.....	171
6.2.1	Description of the process configurations .....	171
6.2.2	Description of the flow sheet and design specifications .....	173
6.2.3	Boundary conditions for the base case scenario .....	176
6.3	Results and discussion.....	178
6.3.1	Base case scenario .....	178
6.3.2	Results sensitivity analysis Configuration A.....	180
6.3.3	Results sensitivity analysis Configuration B.....	188
6.3.4	Discussion regarding the simulation.....	194
6.3.5	Analysis of the simulation results .....	194
6.4	Conclusion.....	196
6.5	References .....	197
7	Integration study of the CO <sub>2</sub> capture process using aqueous ammonia.....	199
7.1	Introduction .....	199
7.2	Modeling methodology .....	199

7.2.1	Power plant.....	199
7.2.2	CO <sub>2</sub> capture process.....	201
7.2.3	Mechanical chiller system.....	205
7.2.4	Compressors.....	206
7.2.5	Integration with CO <sub>2</sub> capture unit.....	207
7.3	Results.....	209
7.3.1	Reference process with MEA.....	209
7.3.2	Results configuration A.....	211
7.3.3	Results Configuration B.....	224
7.4	Conclusion.....	228
7.5	References.....	229
8	Conclusions and recommendations.....	231
8.1	Conclusive remarks.....	231
8.2	Challenges and recommendations.....	233
9	Appendix.....	235
9.1	Appendix A.....	235
9.1.1	Additional information regarding the Wetted Wall column apparatus.....	235
9.1.2	References.....	237
9.2	Appendix B.....	237
9.3	Appendix C.....	239
9.3.1	List of publications.....	239
9.3.2	List of presentations at international conferences.....	239



# 1 General introduction

## 1.1 Global warming and climate change: causes and consequences

The global warming phenomenon relates to the fast increase of the average air and ocean temperature since the second half of the twentieth century. Figure 1-1 shows the global temperature anomaly from 1850 to 2005 considering the 1961-1990 baseline.

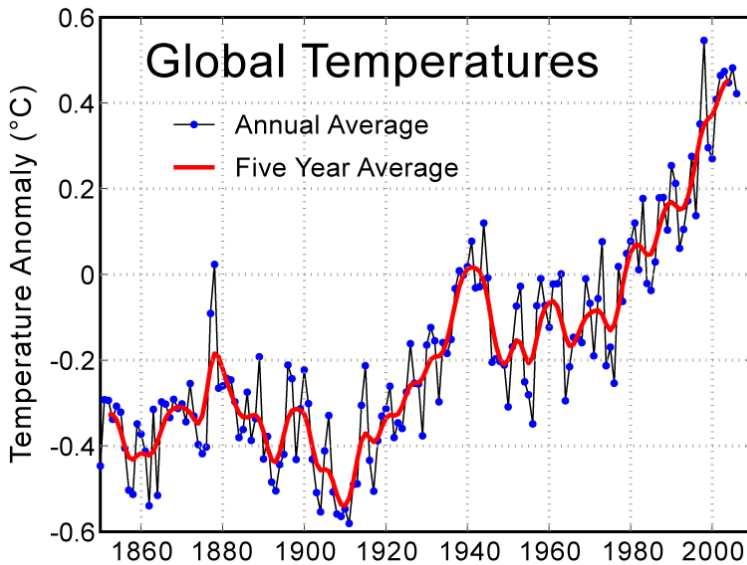


Figure 1-1: Global temperature anomaly for the past 150 years from the 1961-1990 baseline (Brohan *et al.*, 2006)

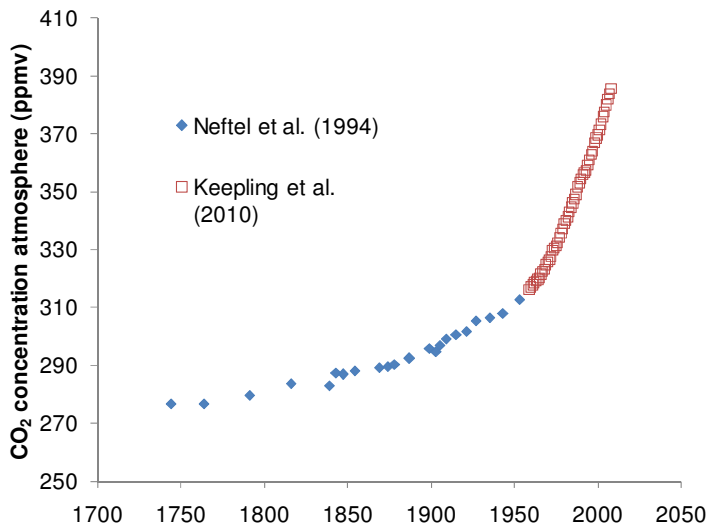
The concern about the rising of temperature encouraged the creation of the International Panel on Climate Change (IPCC) in 1988. The main task of the IPCC is to review the information related to global warming and to propose synthesis and recommendations based on the scientific analysis of this information. According to the IPCC, the average temperature has increased by approximately 0.74 °C from 1906 to 2005, and the increase of the temperature was twice as fast during the second half of that period (IPCC, 2007a).

The greenhouse effect is a natural phenomenon that consists of absorbing the Earth's surface thermal radiation by atmospheric greenhouse gases and re-emitting it in all directions. The main gases that contribute to this effect are: water (H<sub>2</sub>O), carbon dioxide (CO<sub>2</sub>) and methane (CH<sub>4</sub>). Ozone (O<sub>3</sub>), nitrous oxide (N<sub>2</sub>O) and some fluorinated gases are some of the other gases that contribute to this effect. This phenomenon is necessary to regulate the Earth's surface temperature and has always



occurred. Without this effect, the temperature of the Earth would be 20 to 30 °C lower (The Royal Society, 2005).

Greenhouse gases (GHG) are naturally present in the atmosphere. Keeling *et al.* (2010) have measured the evolution of the concentration of carbon dioxide from 1958 to 2010. Before that period, the concentration of carbon dioxide in the atmosphere has been estimated by analyzing the composition of ice cores (Neftel *et al.* 1994). The results from these measurements are shown in Figure 1-2. A similar trend can be observed for methane or nitrous oxide (IPCC, 2007a).



**Figure 1-2 Concentration of carbon dioxide in the atmosphere from 1700 to 2008 (Neftel *et al.*, 1994 and Keeling *et al.*, 2010)**

The analysis of ice cores shows that over the past 40,000 years the concentration of carbon dioxide has been below 300 ppm. This shows that it is very likely that it is the increase of anthropogenic production of GHG that has caused a fast increase of the concentration of the GHG in the atmosphere in the last two centuries. This increase is especially significant for the past 60 years. The same conclusion is valid for methane or nitrous oxides.

The IPCC (2007b) concluded that “most of the observed increase in globally averaged temperatures since the mid-20th century is very likely due to the observed increase in anthropogenic greenhouse gas concentrations”.

The potential consequences of global warming have been analyzed by constructing and analyzing scenarios based on different level of GHG emissions. If no measure is taken, the global temperature increase could reach more than 5 °C by 2100. The consequences of climate change could therefore be

very big and global. It has been studied that this phenomenon would likely favor the increase of the frequency of extreme weather events, deeply change precipitation patterns and cause sea level rise among other dramatic consequences. It is also asserted that the changes caused by global warming will increase rapidly if the rise of the GHG concentration in the atmosphere continues. Hence, the IPCC indicates that measures have to be taken in order to reduce the anthropogenic emissions of greenhouse gases in order to limit the effect of climate change (IPCC, 2007b).

The IPCC has recommended to maintain the temperature increase below 2 °C by 2100 (IPCC, 2007b), which corresponds to an atmospheric concentration of carbon dioxide of about 450 ppm. This would imply a significant decrease of the anthropogenic carbon dioxide emissions.

## ***1.2 Climate change mitigation***

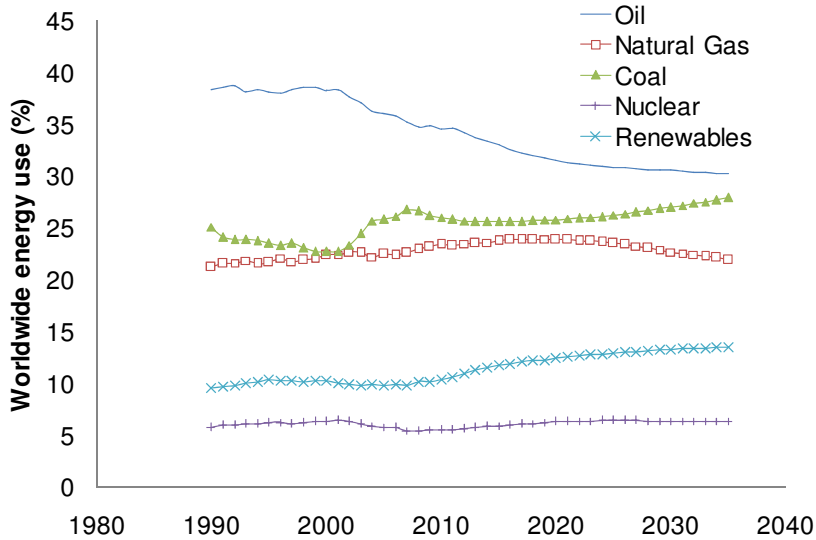
In order to know how to reduce greenhouse gas emissions, it is first necessary to analyze the distribution of the emissions by sector. The IPCC has defined seven main sectors that contribute the most to global emissions: energy supply, transport, building, industry, agriculture, forestry and waste management (IPCC, 2007c). For each of these sectors, key mitigation technologies have been identified.

Globally, the sector that causes the most carbon dioxide emissions is the energy sector. In Europe, in 2007, it represented 38% of the total carbon dioxide emissions (European commission, 2007). It has been asserted by the International Energy Agency (IEA) in 2007 that the global energy demand will increase by more than 60% from 1990 to 2035. The emissions of GHG from the energy sector typically come from large sources. There is therefore a high potential for reduction of carbon dioxide emissions from this sector by implementing relevant technologies.

Several options are investigated for mitigating the carbon dioxide emission from the energy sector:

- Use of renewable energies
- Use of nuclear energy
- Use of low carbon content fuel
- Increase the efficiency of the fuel conversion
- Carbon dioxide capture and storage

Figure 1-3 shows the past and projected use of energy distributed by source from 1990 to 2035 for the reference case defined by IEA in 2007. These data include the transport sector.



**Figure 1-3 Past and projected distribution of the worldwide source of energy (including transportation) (IEA, 2007)**

As shown in Figure 1-3, the switch from fossil fuel to renewable energy has already been initiated. Hydroelectricity has been used for decades and continues growing. The use of biomass and wind energy is also growing. However, due to their high cost, most of the options for renewable energy are currently non competitive with fossil fuels in market conditions. Developments of alternative technologies, such as solar energy are necessary before a massive implementation in the energy market is possible (IPCC, 2007c).

Nuclear energy already accounts for 7% of the global energy in the world (IPCC, 2007c). However, it faces barriers such as the uncertainty regarding long term waste management, safety issues, political adversity as well as adverse public opinion. The recent nuclear accident in Japan in March 2011 might increase public opposition to this source of energy.

Hence, fossil fuels will likely remain the major energy resource for the next decades. According to projections from IEA, the use of coal will increase in the next decades. It is therefore necessary to find solutions that permit the decrease the carbon dioxide emissions from coal fired power plants. While increasing the efficiency of power plants is a way to reach this objective, it might be a costly solution because the increase of the efficiency and the potential regarding the retrofitting of power plants are limited. Hence, carbon capture and storage seems to be a very promising method to significantly cut down the emissions of carbon dioxide from the growing energy demand.

Figure 1.4 shows the potential for emissions reduction from different technologies for the IEA’s Energy Technology Perspective (ETP) 2008, Blue Map scenario. This scenario corresponds to a

reduction of 50% of the CO<sub>2</sub> emissions in 2050 relative to 2005 levels. This analysis forecasts that CCS will contribute to about 20% of the global emission reduction by 2050 in the most cost effective manner. Without CCS, the overall cost to achieve the 50% CO<sub>2</sub> emission reduction goal would increase by 70% (IEA, 2010). This shows that this technology will play a predominant role in the coming period.

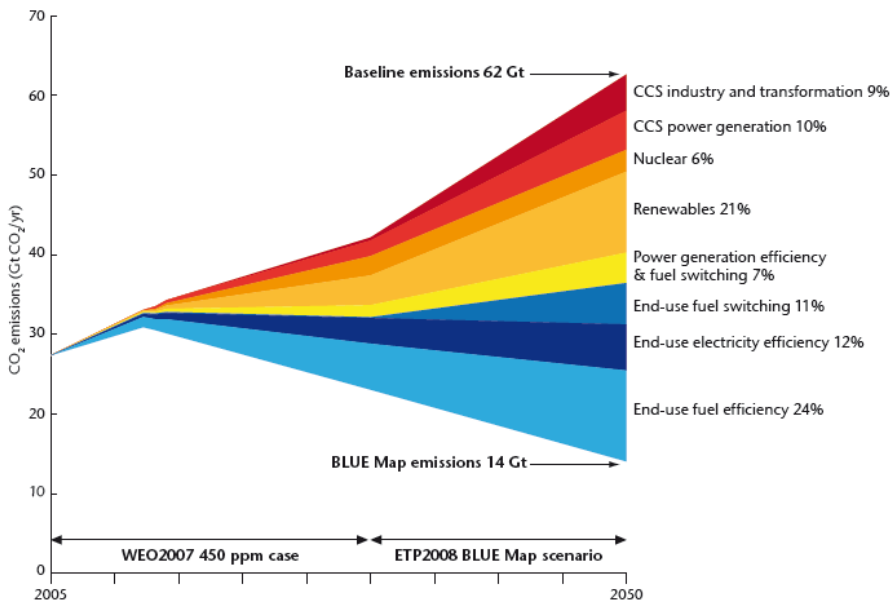


Figure 1-4 Assessment of the distribution of the contribution of the carbon dioxide emission reduction according to the ETP2008 Blue Map scenario (IEA, 2010)

### 1.3 Carbon dioxide capture and storage

The carbon dioxide and storage from fossil fuel power plants consists of separating the carbon dioxide from the rest of the flue gas. The purified carbon dioxide stream is then compressed and transported before it is injected in a geological formation in which long term storage can be assured.

#### 1.3.1 Carbon dioxide capture techniques

Carbon dioxide capture is a process that has been used since 1970, mainly to inject carbon dioxide in oil fields in order to enhance oil recovery (Dooley *et al.*, 2010). Different carbon dioxide capture techniques are currently investigated as shown in Figure 1-5. It should be noticed that this process is not reduced to the power generation and can also be applied to CO<sub>2</sub> emitting industries, such as cement production.

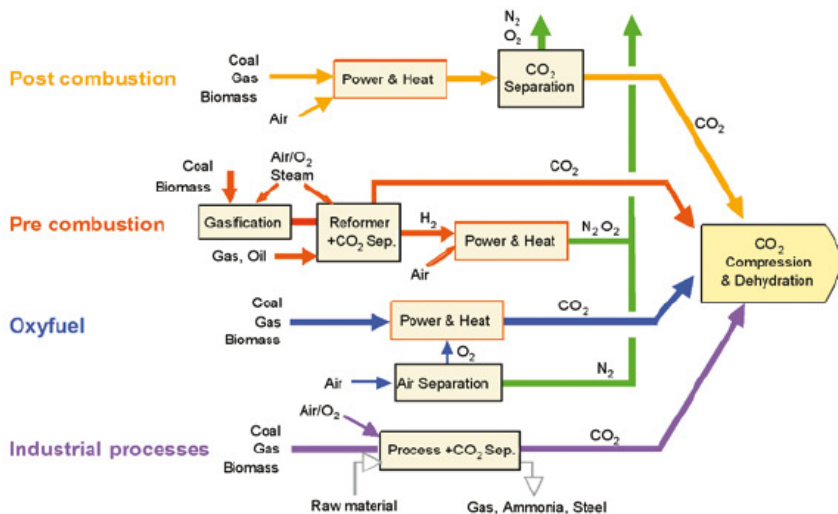


Figure 1-5 Schematic representation of the carbon dioxide capture techniques (IPCC, 2005)

### 1.3.1.1 Pre-combustion techniques

The pre combustion capture process, typically from an Integrated Gasification Combined Cycle (IGCC) plant requires two steps. First, the fuel, typically coal or biomass, is gasified in the presence of steam or oxygen/air, depending on the type of gasifier used. Under these conditions, a mixture of hydrogen and carbon monoxide (syngas) is produced. The second step consists of shifting the carbon monoxide to carbon dioxide in the presence of steam in a second reactor. This produces one mole of hydrogen and carbon dioxide per mole of carbon monoxide converted. The carbon dioxide is then separated from the hydrogen via physical (eg. Rectisol) or chemical absorption (SINTEF, 2009). The high concentration of carbon dioxide (16 to 60%) from the shift reactor and the elevated pressure is favorable to CO<sub>2</sub> separation (IPCC, 2005). The hydrogen stream produced can be used as a carbon free fuel to produce heat and electricity using a combination of gas and steam turbines.

IGCC is considered to be a technically feasible. In 2005, about 4 GW<sub>elec</sub> had been built (IPCC, 2005). Several new IGCC plants are to be commissioned before 2020 in the USA or in China. The main advantages seen in the IGCC plants with carbon dioxide capture are the low emissions of dust, nitrous and sulfur oxides. Such plants are usually cleaner than the conventional coal-fired power plants (Ratiffa-Brown *et al.*, 2002), and allow higher fuel flexibility than conventional power plants. However, the capital cost of such plant is significantly higher than a conventional power plant (Mondol *et al.*, 2009). Investigations regarding hydrogen-fired turbines are still required in order to increase the efficiency of the process, especially for large scale power plants. Furthermore, it is not possible to implement this type of capture process on existing conventional power plants. It should be noted that several variants of this technology are currently investigated.

### 1.3.1.2 Oxy-fuel techniques

The oxy-fuel techniques are being developed in two main variants: the oxy-fuel combustion process and the chemical looping combustion process.

A schematic view of the oxy fuel combustion process is shown in Figure 1-6. It consists of performing the combustion of the fuel (commonly coal) in a mixture of oxygen and carbon dioxide, a nitrogen-free atmosphere in order to produce steam that feeds a steam turbine. Oxygen is produced from air using an Air Separation Unit (ASU). The purity of the oxygen stream is typically superior to 95% (Buhre *et al.*, 2005). The flue gas is then cleaned from its solid matter and recycled with a chosen rate (typically 70-80%) to the boiler in order to control the temperature in the boiler. The concentration of carbon dioxide in the flue gas reaches 80% (IPCC, 2006). The flue gas is then cleaned from its sulfur content and condensed to remove the water. Further treatments might be needed in order to remove minor quantities of nitrogen and other compounds that can be contained in the flue gas before carbon dioxide is compressed and transported.

This technology shows good potential and allows for retrofitting to existing power plants. A 30 MW<sub>therm</sub> pilot plant has been operated from 2008 in Schwarze Pumpe by Vattenfall. The key point of the technology is the large and energy demanding ASU. In addition, more research regarding the combustion of the fuel in a mixture of carbon dioxide and oxygen is required.

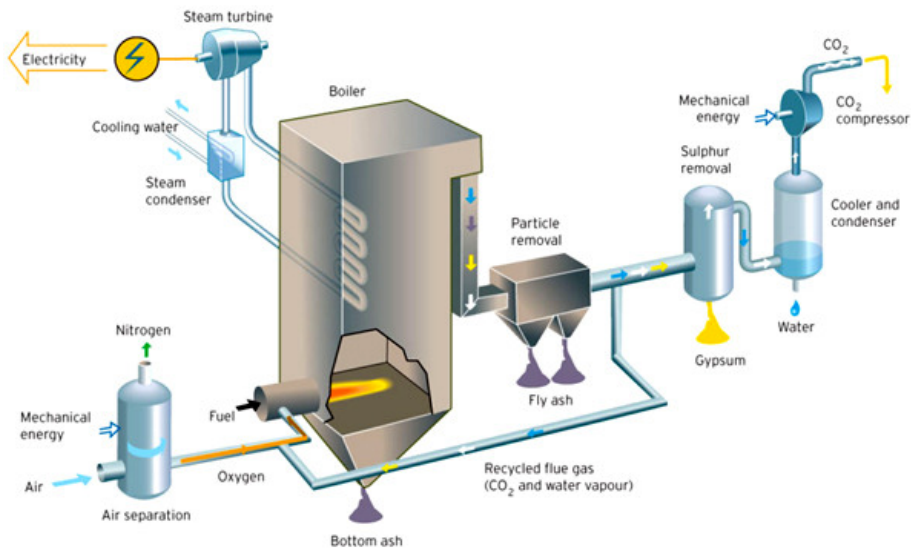


Figure 1-6 Schematic view of the oxyfuel combustion process (Vattenfall, 2010)

A schematic view of the chemical looping combustion process is shown in Figure 1-7. This technique consists of using a metal  $Me$  as an intermediate for providing the combustible with oxygen. Two reactors are necessary. In the first one, the metal is oxidized by oxygen, following the reaction:



The oxidized metal is transferred to the second reactor, and reacts with the fuel. In the case of methane, the reaction would be:



This reaction is highly exothermic and the energy can be used for power or heat production. Commonly used metals as oxygen carrier are nickel, copper, or iron oxides (IPCC, 2005).

Hence, this method permits  $CO_2$  separation without severe energy losses as there are two separated gas flows: one is composed mainly of  $N_2$  and  $O_2$ , with a very low content of  $CO_2$ . The other is mainly composed of  $CO_2$  and  $H_2O$ . Carbon dioxide can be easily recovered by cooling the exhaust gas and removing the condensed water (Ishida *et al.*, 2003). The technique is immature and requires years of development before it can be considered as an alternative on large scale emission sources.

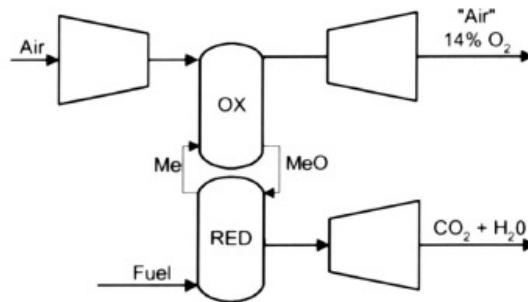


Figure 1-7 Schematic view of the chemical looping combustion process (Ishida *et al.*, 2003)

### 1.3.1.3 Post-combustion techniques

Post-combustion capture (PCC) processes consist of implementing a capture process without altering the combustion of the fuel. In most cases, PCC processes require the cleaning of the flue gas before the capture (removal of sulfur compounds and particulate matters) in order to avoid corrosion issues. Several techniques are investigated. This section provides a short description of some of the many techniques under development. These techniques are especially attractive as they permit the retrofitting of existing power plants.

The most prominent one is the chemical absorption by a liquid media. Commonly, the solvent used is amine based. It consists of the use of an absorber column where the flue gas and the solvent are contacted counter-currently and a desorber column where some heat is provided to release the gaseous carbon dioxide and regenerate the solvent. This technique will be studied in detail in the later sections of this study.

Membranes may be used to separate the carbon dioxide from the rest of the flue gas. Two main kinds of membrane techniques may be used. In the first case, membrane separation, carbon dioxide is separated by using the selective permeation of a nitrogen and carbon dioxide through the membrane. The gas flows thanks to the pressure difference between the sides of the membrane. Therefore this first variant is especially relevant for pressurized systems. Membrane technologies are in general more efficient when the compounds passing through the membrane are present in high concentration (IPCC, 2005). Hence, this technique represents a promising complement to pre-combustion techniques. Commercially available membranes are not able to deal with the high flow rates from power plants. In the second case, the membrane can also be used in an absorber as a porous media. The gas and the liquid solvent are separated flows, but the membrane permits the contact between the gas and the solvent and therefore the absorption of carbon dioxide by the solvent. Hence, the gas flows on the side of the membrane. This technique allows for a larger contact area compared to conventional columns.

An alternative technique relates to a rotating device that can be used in order to improve the contact between the gas and liquid phase by applying a centrifugal field. This field leads to the formation of droplets that increase the gas-liquid contact area. The principle of such process is similar to a classic absorption by amine solvents, but the absorber column is replaced by this device. For the moment, this technique is still experimental. The price and the maintenance are still prohibiting (Kelleher *et al.*, 1996).

Another option is to use compressors and coolers in order to solidify the carbon dioxide from the flue gas (anti-sublimation). The flue gas needs to be dehydrated before it is cooled down to avoid the formation of ice that would block its flow. For a concentration of carbon dioxide in the gas of 1%, the frosting temperature of carbon dioxide is about -120 °C (Clodic *et al.*, 2005). The carbon dioxide is then defrosted and sent to storage. The capture efficiency and the purity of the CO<sub>2</sub> stream can potentially be very high with this technique.

Adsorption techniques using activated carbon and other sorbents such as zeolites are currently under investigation. The desorption can be performed either by pressure or temperature swings. The pressure swing adsorption process requires a high concentration of carbon dioxide in the gas, which is not the case of the temperature swing adsorption. However, the later option requires long absorption-desorption cycles. These options are still under development, but the requirement for large equipments and a high efficiency penalty prevent them from being competitive. Hence, further developments are required. Decarbonisation technologies using calcium oxides as sorbent are also investigated. At high



temperature (above 600 °C), the sorption is fast. CO<sub>2</sub> from the hot flue gas reacts with CaO to produce CaCO<sub>3</sub>. The regeneration can be made at temperatures above 900 °C (IPCC, 2005). A fluidized bed technology is typically used for this technique.

### **1.3.2 Options regarding the carbon dioxide transport and disposal**

#### **1.3.2.1 Transport of carbon dioxide**

After its separation from the rest of the flue gas, the carbon dioxide is compressed to reach its supercritical conditions (above 73.4 bar and 31 °C). The transport from the emitting source to the storage is typically made by pipeline. In the United States, more than 2500 km of pipelines are used to transport carbon dioxide mainly to be used for enhanced oil recovery (IPCC, 2005). Another possibility is to use transport by truck for the case of low flow rate of flue gas. In the case of ocean storage, the transport of carbon dioxide by tankers is also investigated. The price of the storage heavily depends on the distance between the emitting and the storage sites.

It is important to ensure a relatively high purity of the CO<sub>2</sub> when it is transported and stored. No regulation is currently in place in Europe regarding the composition of the CO<sub>2</sub> stream to be transported. However, some recommendations have been formulated. The concentration of water should be limited to 500 ppm, meaning below the solubility of water in carbon dioxide in order to avoid corrosion issues. For health and safety considerations, the concentration of H<sub>2</sub>S and CO should be limited respectively to 200 and 2000 ppm. For the same reasons, the concentration of SO<sub>x</sub> and NO<sub>x</sub> should be limited to 100ppm (ENCAP project, 2010). The CACHET project has proposed to limit the concentration of all non-condensable gas to 3% in volume (Beavis *et al.*, 2008). In the case of storage in active oil fields (EOR), the concentration of oxygen should be limited to 1000 ppm and methane to 2% in volume.

#### **1.3.2.2 Storage options**

Different options are being investigated regarding the storage of CO<sub>2</sub>. One way resembles to the one that is used for the storage of natural gas. The pressurized CO<sub>2</sub> is injected in geological formations such as saline aquifers that allows for long term storage. Depleted gas reservoir options are also considered. The storage site must also be large enough so a large volume of CO<sub>2</sub> can be transported and stored from the pipeline. The storage must be monitored by using control wells to make sure there is no leakage and control the carbon dioxide plume underground. The worldwide storage capacity of these reservoirs is estimated to be in the range of 320 to 10<sup>4</sup> billion tones of CO<sub>2</sub> (Ormerod *et al.*, 1994). As a comparison, global emissions from coal firing in the world in 2010 are estimated at 2.3 billion tones (EIA, 2009). Inactive gas and oil reservoirs may represent a good solution as well. Abandoned reservoirs are estimated to be able to contain from 650 to 1800 billion tones of CO<sub>2</sub> in the world (Herzog *et al.*, 1997). It should be noted that the storage capacities are not evenly distributed around the globe. To illustrate this fact, the situation in Northern Europe can be put forward. Norway has a potential for a storage capacity over 84 billion tones CO<sub>2</sub>, typically in the same area as the oil and gas

fields in the North Sea (Boe *et al.*, 2002). A lot of interest is being shown in identifying and characterizing potential storage sites. On the other hand, Sweden shows a limited potential for CO<sub>2</sub> storage, as few geological formation can be suitable for this activity (VTT, 2010).

Few countries currently have the legislation in place regarding the underground storage of CO<sub>2</sub>. Regulations regarding the composition of the gas injected, the monitoring and the long term responsibility of the storage sites are required so that the implementation of this technology goes further. One of the largest scale projects for CO<sub>2</sub> storage has started in In Salah (Algeria). The project consists of re-injecting the carbon dioxide that is contained in the natural gas from the near gas field into a sandstone reservoir. The injection rate since 2004 is about 1.2 million tones per year (IPCC, 2005).

The storage in on-shore geological formations is one of the main options considered regarding carbon dioxide disposal. However, it should be noted that there is currently a strong public defiance regarding the process. The risks related to leakages and the lack of information about the process cause the public to be reluctant to the technology (IPCC, 2005). The storage of carbon dioxide captured from the oxy fuel pilot plant in Schwarze Pumpe had to be cancelled because of the opposition from local population. Public acceptance appears to be one of the big challenges to overcome.

The risks related to CO<sub>2</sub> storage are mainly linked to the leakage of CO<sub>2</sub>, either from the well or directly from a fracture in the rock. Carbon dioxide is not a poisonous gas. It is naturally present in the atmosphere. However, if its concentration in the air exceeds 7 to 10%, there is a risk of suffocation. This is why the choice of the storage site is critical in order to minimize these risks. It should also be noted that these types of hazards are handled effectively in the oil and gas industry.

The storage in deep ocean layer is also considered. CO<sub>2</sub> transported by pipeline or by ship is injected at a depth below 1000 meters in order to ensure its dissolution in sea water. The environmental consequences of such process are still investigated and not fully understood. The dissolution of a large quantity of carbon dioxide would lower the pH and might have deep impact on the marine environment. In addition, it is suspected that the dissolved carbon dioxide would eventually leave the ocean to reach equilibrium with the CO<sub>2</sub> concentration of the atmosphere. Mineralization is also considered as one of the storage options. Magnesium and calcium naturally react with carbon dioxide to form carbonates. These reactions are exothermic. In addition, there is a very large amount of magnesium available that could be used for this purpose. However, at ambient temperature and pressure, this reaction is very slow. Pretreatment of the minerals or temperature or pressure increase are investigated, but are currently too energy demanding to be competitive (IPCC, 2005).

### **1.3.2.3 Enhanced Oil Recovery (EOR)**

Carbon dioxide can be injected in oil fields to enhance oil recovery by increasing the oil mobility and reducing its viscosity. The carbon dioxide injection therefore improves the productivity of the reservoir

by facilitating the oil recovery. The Weyburn EOR project (Canada) injects 1.5 million tonnes CO<sub>2</sub> per year in the oil field to increase the productivity of the field. In 2008, the stored amount of CO<sub>2</sub> exceeded 12 million tonnes (Preston *et al.*, 2009). This option is attractive as the geology of the oil fields is well studied and because of the income from the recovered oil. However, oil fields have limited capacity (Gabrielsen, 2007). In addition, oil fields are commonly far away from the large CO<sub>2</sub> emitting sources. Hence, a pipeline network is required.

#### **1.3.2.4 Industrial use of CO<sub>2</sub>**

Additional industrial applications for carbon dioxide are currently being investigated. CO<sub>2</sub> can be used to enhance the recovery of methane while providing long term storage (Gale *et al.*, 2008). Carbon dioxide is also used for urea production and in the food industry, where the purity has to be very high. In the US in 2005, the total industrial use of carbon dioxide represents 1 to 2% of the CO<sub>2</sub> emissions from power generation (Jassim *et al.*, 2006).

### **1.3.3 Considerations regarding the cost of the process**

The cost of the process depends on many factors, the most prominent ones being the cost of electricity, the capture technique that is used and the type of source the carbon dioxide is emitted from. Two types of cost are generally reported: the cost per ton CO<sub>2</sub> captured and the cost per ton CO<sub>2</sub> avoided, the second one being systematically higher than the first. Alternatively the cost per kilowatt-hour produced may be used. It is generally estimated that the capture represents about 80% of the global cost while the rest is distributed between transport and storage (Rao *et al.*, 2002). The conventional capture process would increase fuel consumption of a coal fired power plant by 25% (IPCC, 2005). There is a wide range of cost that can be found for carbon capture and storage, depending on the technology used, the location of the capture and storage sites and the size of the carbon dioxide emitting source. Currently, the estimations of the cost of avoided CO<sub>2</sub> are significantly higher than the current price of a ton of carbon dioxide in the market. This shows that the price of CO<sub>2</sub> is currently too low to encourage the implementation of these technologies.

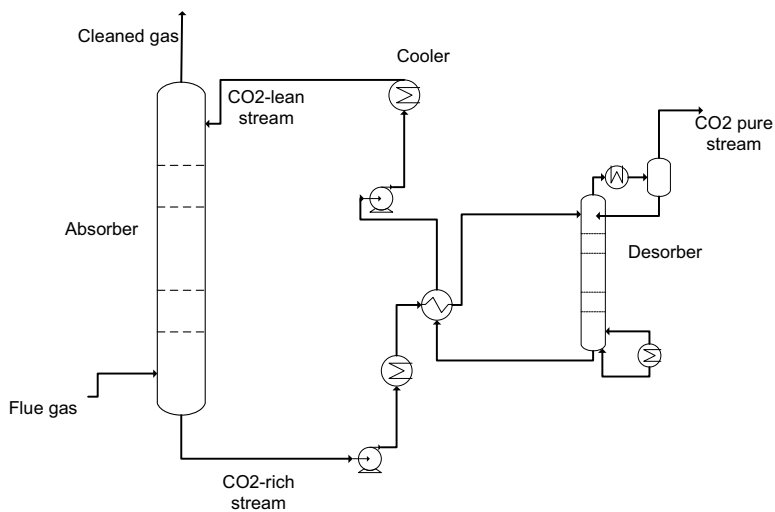
## ***1.4 Post-combustion capture by chemical absorption***

### **1.4.1 Description of the flow sheet**

Post-combustion CO<sub>2</sub> capture techniques by chemical absorption have been used for several decades in the industry. It consists of using a solvent that has the capacity to absorb acid gases such as carbon dioxide. The use of mono-ethanolamine (MEA) as a solvent for chemical absorption is a technique that has been tested on pilot plants and that is often used as a reference case for CO<sub>2</sub> capture from coal-fired power plants. MEA is a primary alkanolamine of the type  $R-NH_2$ , where  $R$  is an alkyl group, by opposition to secondary and tertiary alkanolamines, in the respective types  $R_1R_2NH$  and  $R_1R_2R_3N$  with  $R_i$  being alkyl groups. The CASTOR project in Esbjerg (Denmark) is one of the first post combustion capture pilot plants using chemical absorption. The first test campaign consisted of using MEA-based

solvents in order to prove the feasibility of the equipment before other solvents could be tested (Knudsen *et al.*, 2008).

A schematic flow sheet of a post combustion capture process by chemical absorption is shown in Figure 1-8. The flue gas typically produced by power generation and the amine-based solvent are contacted counter currently in a packed column commonly called absorber. The capture process is usually located after the flue gas cleaning systems, such as the particle removal and the flue gas desulfurization unit. The reaction of absorption is exothermic. The top of the column generally consists of a water wash that limits the emissions of amine in the atmosphere. The CO<sub>2</sub>-rich stream formed goes through a heat exchanger where its temperature rises and reaches a second column, the desorber that comprises a reboiler and a condenser. The heat provided permits the desorption of the carbon dioxide that leaves by the top of the column. It can then be dried and compressed before being transported. The regenerated solvent leaves by the bottom of the desorber as the CO<sub>2</sub>-lean stream, transfer the heat that it gained to the CO<sub>2</sub>-rich stream and flows back to the absorber after being cooled to the right temperature using an air or water cooler. A typical capture rate for such process is 90%.



**Figure 1-8 Schematic flow sheet of the carbon dioxide capture process using aqueous alkanolamine**

One of the main concerns related to the carbon capture process and its large scale implementation is the heat and electricity requirements of the process. The use of current post combustion capture process can reduce the efficiency of a coal-fired power plant by 10-13 %-pts. (Schach *et al.*, 2010). Studies regarding the optimization of the configuration of the process are being conducted. During the CESAR project, the configuration of the process used in the context of the CASTOR project was improved (use of absorption intercooler, redesign of the heat exchanger, use of vapor recompression...). It implied a significant decrease of the heat consumption with MEA. However, improvements of the configuration

of the process often imply additional investments. When dealing with the optimization of a capture process, a compromise between the capital and the operational costs must be found (Knudsen *et al.*, 2010).

A recent major concern is linked to the amine volatility. Despite the low volatility of the alkanolamine at absorber conditions and the use of washing section, alkanolamine emissions are observed. The concentration of the alkanolamine in the cleaned gas is very low, in the range of ppb, but the flow rate of flue gas from a large scale power plant is very big. Therefore the emissions become an issue. The alkanolamines released in the atmosphere are not stable and can degrade to form nitrosamines that are carcinogenic compounds (Knudsen *et al.*, 2009). The real degradation yield and the atmospheric chemistry of alkanolamines are still uncertain and research is being conducted to have a better understanding of the degradation phenomenon (Nielsen *et al.*, 2010). This volatility implies that an extensive washing of the gas is necessary on the top section of the absorber before it is released to the atmosphere.

#### **1.4.2 Considerations regarding the solvent**

One way to decrease the operational expenses of a post combustion process is to improve the performance of the solvent used. The process configuration that is used depends a lot on the solvent. Therefore the solvent used will also affect the capital expenses for the capture process. Different criteria have to be considered in the development of a new absorbent.

- The heat requirement for the regeneration is the most crucial criterion as it will strongly affect the operational cost. The heat requirement in the desorber is the sum of 3 contributions: the sensible heat to increase the temperature of the solvent to desorption conditions, the heat of evaporation to produce the steam in the reboiler and the heat required for the desorption of carbon dioxide (heat of absorption) (Freguia *et al.*, 2003). A lot of efforts are being made to develop solvents with a lower heat of absorption to reduce the heat requirement. Even though the heat of absorption is an important criterion, it has been shown that it is the overall heat requirement for the regeneration as well as the electricity requirements that have to be considered when a solvent is evaluated (Oexmann *et al.*, 2009). If a solvent, despite its high heat of absorption, allows for regeneration at high pressure, the amount of water that is vaporized is reduced and therefore the global heat requirement decreases as well. In addition, the electricity requirement for the compression of the carbon dioxide stream is lowered.
- The rate of reaction is strongly linked to the size of the absorber column. Hence, the capital cost for the capture process depends heavily on this factor. This rate varies significantly with the concentration, the temperature and the content of carbon dioxide in the solvent. Therefore the performance of the rate of reaction will be influenced by the process conditions.

- The cyclic capacity refers to the difference of the rich and the lean carbon dioxide loading. In this thesis, the carbon dioxide loading will systematically refer to the molar ratio between the carbon dioxide and the amine. The lean and rich loadings respectively refer to the loading in the CO<sub>2</sub>-lean and the CO<sub>2</sub>-rich streams. If the cyclic capacity is high, a lower flow rate of solvent can be circulated which implies a decrease of the heat requirement for the regeneration and of the electricity requirement for the pumping.
- The degradation rate of the solvent can imply strong constraints to its use. The thermal degradation properties of a solvent typically bring limitation to the pressure at which the desorber can be operated. Degradation with compounds present in the flue gas such as oxygen or sulfur compounds may also be observed. Degradation phenomena may lead to the formation of heat stable salt that can disturb the operation and cause the loss of active absorbent that needs to be replaced. In addition, degradation phenomenon may lead to the formation of volatile compounds and therefore entail emission issues.
- The vaporization of the solvent at absorber conditions has to be considered in order to assess the solvent loss during the capture. The extensive washing of the cleaned gas stream before it is released in the atmosphere is required.
- The toxicity and the environmental impacts of the solvent are important factors for healthy considerations.
- The corrosion of the solvent towards the equipment is a crucial parameter. The formation of heat stable salts is generally a factor that increases the corrosion properties of an amine solution (Roney *et al.*, 1997). Corrosion phenomenon damages the equipment used in the process and therefore causes additional maintenance costs and the use of costly materials.
- The cost of the solvent is also a parameter to consider.

As shown, these criteria are often linked and strongly influenced by the configuration of the process. Therefore, only a robust simulation of the process allows for assessing correctly the performance of an absorbent.

### **1.4.3 Current development of chemical solvents and perspectives**

A lot of interest is currently shown to develop absorbents with high performance towards CO<sub>2</sub> capture. Various types of molecules and salts are considered.

As mentioned above, MEA represents the reference solvent for post combustion carbon dioxide capture that has been used historically. This can be explained by the high reaction rate at absorber condition that allows for limiting the size of the absorber. In addition, the solvent is relatively cheap. However, as most primary and secondary amine, the heat of absorption of carbon dioxide by MEA solvent is high

(Carson *et al.*, 2000). In addition, MEA presents a high degradation rate at high temperature. Hence, the desorber cannot be operated at elevated pressure. Furthermore, the loading capacity and the cyclic capacity of the solvent are limited. At absorber conditions, the loading capacity of a primary or secondary amine is 0.5. This is due to the stability of the carbamate formed. The solvent is subject to degradation in presence of O<sub>2</sub> (Supap *et al.*, 2001) or SO<sub>x</sub> (Yeh *et al.* 1999). Generally, the concentration of MEA is limited to 30 wt% due to corrosion issues caused by degradation products. Inhibitors are currently developed in order to control the degradation so higher amine can be used (Delfort *et al.*, 2010). Because of these limitations, alternative absorbents are searched for.

Tertiary amines have also been considered, and especially N-methyldiethanolamine (MDEA). They are attractive thanks to their low heat of absorption of carbon dioxide that allows for a potentially lower heat requirement for the regeneration (Carson *et al.*, 2000) and their high loading capacity as they do not form carbamate (Mathonat, 1997). However, the rate of absorption of carbon dioxide by these amines is very low. Therefore they cannot be used for carbon dioxide capture from coal fired power plants where the partial pressure of carbon dioxide is too low. However, they are commonly used for removal of CO<sub>2</sub> and H<sub>2</sub>S from natural gas or to remove carbon dioxide from syngas (IPCC, 2005).

Sartori *et al.* (1987) have presented a group of primary and secondary amine characterized by the presence of a bulky group linked to the amino group. These sterically hindered amines do not form a stable carbamate. Therefore their loading capacities are higher than for common primary amines. 2-amino-2-methyl-1-propanol, or AMP, is a typical form of a sterically hindered primary amine that has been studied for carbon dioxide capture (Gabrielsen *et al.*, 2006). The properties of sterically hindered amines are generally closer to tertiary amine with respect to their low heat of absorption. Furthermore, the rate of reaction of carbon dioxide by AMP solutions was found to be significantly higher than the one found with MDEA (Gabrielsen *et al.*, 2007). Hence, sterically hindered amines could be a promising option for post-combustion carbon dioxide capture.

Numerous alkanolamine based solvents are currently being investigated. It is especially the vapor-liquid equilibrium data, heat of absorption data as well as measurement of rate of absorption that are of interest as they are often used for comparing amines with each other. Among others can be found Diethylnetriamine (DETA), Diglycolamine (DGA), Diethanolamine (DEA) or Ethylenediamine (EDA).

In order to combine the advantages from both classes of amines, blends of amines are currently investigated as a new generation solvent. The idea is to combine a fast reacting solvent with a solvent presenting a low heat of absorption. The blend of amine solvent presents a higher loading capacity than a primary amine and permits the reduction of the heat of absorption. The thermodynamic modelling of the blend of MEA and MDEA has been studied by Faramarzi *et al.* in 2009. Other types of blends than primary/tertiary amines are considered. Currently, studies using blends of MEA and piperazine are

being conducted and show the high potential of the solvent (Dang *et al.*, 2003). Potassium carbonate activated with Piperazine has also been studied (Cullinane *et al.*, 2003).

Several pilot plants have been recently operated by different private companies using blends of alkanolamines developed in-house. The compositions of these new generation solvents are not disclosed but the results presented are promising. Alstom (Vitse *et al.*, 2010), Hitachi (Yokohama *et al.*, 2010), KEPCO (Kim *et al.*, 2010), Mitsubishi (Tanaka *et al.*, 2009) and Toshiba (Ohashi *et al.*, 2010) have for example recently reported the use of new advanced solvents on pilot scale that showed high potential.

Recently, there is a growing interest on the use of amino-acid salt solutions to capture carbon dioxide. The main advantage of such molecules compared to conventional alkanolamines is that they are considered environmentally friendly. Aronu *et al.* (2010) have shown the potential for a low heat requirement for carbon dioxide capture using amino acid salt solutions.

Ionic liquids are also investigated for use as carbon dioxide absorbent. Their very low volatility is a significant advantage. Current studies show that the heat requirement obtained with some ionic liquids is competitive with the one obtained with MEA (Wappel *et al.*, 2010). Numerous studies are being conducted in order to develop ionic liquids with high performance towards CO<sub>2</sub> capture.

The use of aqueous ammonia as an absorbent for post combustion capture has been recently investigated. A growing interest has been shown for this solvent. Because of the volatility of ammonia and of the thermodynamic specificities of the CO<sub>2</sub>-NH<sub>3</sub>-H<sub>2</sub>O system, the complexity of the process increases. However, thanks to the potential for low heat requirement and the lack of degradation products, the capture process using aqueous ammonia is seen as a promising alternative for the capture of carbon dioxide from coal-fired power plant. This thesis focuses on the study of this technique.

## ***1.5 Carbon dioxide capture using aqueous ammonia***

### **1.5.1 Description of the process**

The ammonia process is found in two variants depending on the temperature of absorption. The first variant absorbs the CO<sub>2</sub> at low temperature (2-10 °C) and is therefore called chilled ammonia process (CAP). The low temperature process has the advantage of decreasing the ammonia slip in the absorber and decreasing the flue gas volume. This process allows precipitation of several ammonium carbonate compounds in the absorber. The second process absorbs CO<sub>2</sub> with aqueous ammonia solvent but avoids precipitation. It is mainly developed by Powerspan.

The CAP was patented in 2006 by Eli Gal. Figure 1-9 shows a simplified flow sheet of the capture process provided by Alstom (Kozak *et al.*, 2009). The process described in the patent requires several steps. First, the purpose of the process is to absorb the carbon dioxide at a low temperature. The patent indicates a temperature range from 0 to 20 °C, and preferably from 0 to 10 °C. Hence, it is first



necessary to cool down the flue gas that contains the CO<sub>2</sub>. This is done by using direct contact coolers at the entrance of the process. The temperature of the gas that leaves the cooling subsystem is comprised between 0 and 10 °C. This stream contains low moisture and almost no particulate matter, acidic or volatile species. Indeed, the low temperature decreases the vapor pressure of these compounds and causes their condensation into water.

Then, the flue gas enters the CO<sub>2</sub> capture and regeneration subsystem. This subsystem consists, like the capture processes using amines, of absorption and desorption columns. The exit stream from the absorber can be recycled to the absorber with a chosen recycling rate in order to increase the loading of the CO<sub>2</sub>-rich stream and to maintain a low temperature in the absorber. A hydro cyclone may be used in order to increase the solid content and the loading for the CO<sub>2</sub>-rich stream. The regeneration can be operated at elevated pressure. Despite the low temperature of absorption, the gas leaving the absorber has a high ammonia content. Hence, it is necessary to wash this gas. Similarly to the CO<sub>2</sub> absorption/desorption system, an absorber/stripper system is necessary to remove the gas from its ammonia content using a water wash stream. The ammonia must then be stripped in order to regenerate the washing stream. The ammonia removal is made at low temperature just like for the carbon dioxide. In Figure 1-9, the stripping of ammonia is made at elevated pressure, and the ammonia stream is sent to the carbon dioxide desorber. The gas exiting the water wash section is introduced to direct contact coolers used for the flue gas in order to further decrease its ammonia content before it is released.

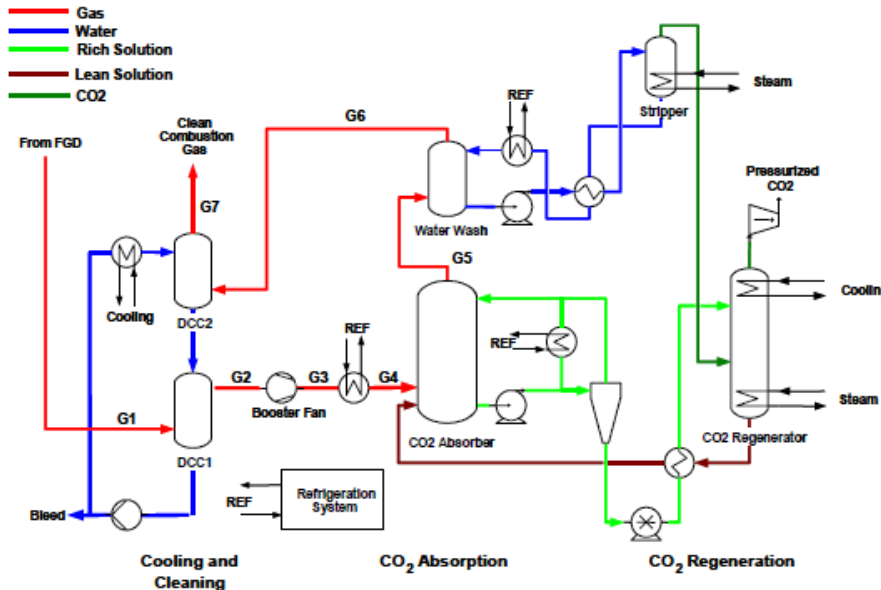


Figure 1-9 Flow sheet of the Chilled Ammonia Process (reproduced from Kozak *et al.*, 2009)

It is claimed in the patent that the CAP permits the reduction of the heat requirement in the desorber. Moreover, the desorption of carbon dioxide can be done at a temperature typically in the range 110-150 °C and at elevated pressure (10-50 bar) that implies some savings during the compression and limited vaporization of water. Overall, despite the chilling duty, the process is said to have a good potential. In addition, degradation issues observed with conventional processes using aqueous alkanolamines can be avoided and a high carbon dioxide capacity can be achieved. Furthermore, unlike the MEA-based process, ammonia is not degraded in the presence of sulfur compounds and SO<sub>x</sub> can potentially be removed from the flue gas during the carbon dioxide capture (Gal, 2006).

### 1.5.2 Literature review

Alstom has operated three demonstration projects. The We Energy Field pilot, inaugurated in 2008 in Wisconsin and the E-On Karlshamn (Sweden) commissioned in 2009 had a yearly capacity of 15,000 tones carbon dioxide. They have shown that a capture rate of 90% with high carbon dioxide purity for over 4500 hours was possible and were used as “a proof of concept”. The demonstration plant inaugurated with American Electric Power (AEP) in 2009 in Wisconsin has a capacity of 100,000 tones of carbon dioxide captured per year. The captured CO<sub>2</sub> is then stored in deep saline aquifers. However, until recently, very few results are communicated by Alstom in the open literature (Telikapalli *et al.*, 2010).

Powerspan has inaugurated a pilot facility with First Energy in Ohio in 2008. The pilot has a yearly capture capacity of 6,000 tones with a 90% capture rate. It allows for capturing carbon dioxide together with sulfur compounds in the flue gas (Mc Larnon *et al.*, 2009). However, again, very few concrete results from the pilot plant are available in the literature.

Few research studies on the process were available in the literature prior to the developments from Alstom. Yeh *et al.* (2005) have shown the high potential of aqueous ammonia as an absorbent. Their lab scale experiments showed the high cyclic capacity of the solvent and the low heat requirement compared to MEA-based process. The high loading capacity has been experimentally observed by Bai *et al.* (1997). Yeh *et al.* (1999) showed that under proper experimental conditions, the removal efficiency of aqueous ammonia solvent was superior to the one observed with MEA solvent. They conclude by stating that the heat requirement for the regeneration of the solvent is lower with ammonia than with MEA solvents.

Ciferno *et al.* (2005) have made a study on the use of aqueous ammonia to capture carbon dioxide from flue gas and compared it to MEA-based process. They emphasize the potential for low steam requirement, the higher loading capacity, the low cost of the chemical and the potential for production of ammonium sulfate  $(NH_4)_2SO_4$  as a by-product that could be valuable to the process. The study also points out the possibility for the process to capture NO<sub>x</sub> and SO<sub>x</sub> compounds together with the carbon dioxide. Hence, the process seems attractive compared to available technologies.

The results from the laboratory experiments made by Epri (Rhudy, 2006) are available. They show the high potential of the CAP compared to conventional amine based process. Especially, the heat requirement for the regeneration of the solvent is found to be significantly lower than the one found with MEA. According to these results, the net power output obtained for the CAP is higher than the one observed with MEA, but the net efficiency of a power plant with CO<sub>2</sub> capture with ammonia based solvents is found to be higher than the one using MEA based solvent.

Fosbøl *et al.* (2008) have evaluated the e-NRTL thermodynamic model for the CO<sub>2</sub>-NH<sub>3</sub>-H<sub>2</sub>O system implemented in Aspen Plus and have concluded that the version of the model tested is not accurate, pointing out issues regarding the solubility of ammonium bicarbonate.

Thanks to the intensive advertisement from Alstom, there has been a growing interest in the process in the scientific community. Several researchers have studied different aspects of the process.

Derks *et al.* (2009), Puxty *et al.* (2010) and Qin *et al.* (2010a) have measured and modeled the kinetic rate of absorption of carbon dioxide by aqueous ammonia and compared it with the one obtained with MEA at various concentrations and temperatures. The results from these studies are quite different from each other.

Qin *et al.* (2010b) have studied and modeled the heat of absorption of carbon dioxide by aqueous ammonia and suggested that their work should be used in the thermodynamic modeling of the CO<sub>2</sub>-NH<sub>3</sub>-H<sub>2</sub>O system.

Process evaluation studies based on thermodynamic modeling and process simulation from various researchers have been published. They are studied more in details in a later section of the thesis. Some of these studies are reported below.

Dave *et al.* (2009) have simulated the aqueous ammonia-based process with Aspen. They recommend to avoid precipitation of ammonium bicarbonate and to limit the ammonia slip during the absorption by using an ammonia concentration of 5 wt% and a temperature of absorption of 10 °C. They conclude that the performance of the process is equivalent to the MEA-based one.

Mathias *et al.* (2009) have simulated the CAP using the e-NRTL model available on Aspen to compare it with conventional amine process. Their conclusions are that CAP cannot compete with MEA-based process because of the high heat and electricity requirements.

Valenti *et al.* (2009) have made a study to evaluate the mass, energy and entropy flows in the CAP using a simple thermodynamic model. They include an estimation of the heat and power consumption as well as a cost for the capture. Their results show the very high potential of the process compared to the MEA-based processes. However, the study requires a more advanced thermodynamic model to improve its accuracy.

Continuing their work, Valenti *et al.* have published in 2011 an integration study of the process. Their work includes the simulation of the process in Aspen Plus. The specific heat duty and the efficiency penalty of the process are reported to be significantly lower than the ones observed with MEA. An estimation of the cost of the capture is also provided.

Versteeg *et al.* (2010) have studied the simulation of the process using Aspen Plus and have made a thorough analysis of the heat and electricity consumption of the different unit operations. In their paper they describe two cases using high and low ammonia concentrations in order to evaluate both variants of the process: with and without precipitation. They conclude that both variants of the process are less power demanding than the MEA-based case. A preliminary economical analysis is also included.

Jilvero *et al.* (2010) have published a preliminary study of the simulation of the CAP using a model developed by Kurz *et al.* (1995) to simulate the process and evaluate the heat and electricity requirements. They pointed out the importance of the temperature of the available cooling water. They have also made a preliminary integration study between the capture process and the power plant.

Most of the published studies show the high potential of the process. However, several points need to be studied in more details.

- The studies available show that the  $\text{CO}_2\text{-NH}_3\text{-H}_2\text{O}$  system is complex and that the thermodynamic models available in commercial simulators may not be accurate for the range of temperature and concentration used in the process.
- In addition, the recent results regarding the measurement of the kinetic rate of absorption of carbon dioxide by ammonia solvent are not in agreement. It is therefore difficult to draw any conclusion on this topic with the current level of information.
- Regarding the results from the process simulation studies, it is emphasized that the process of interest is more complex than conventional alkanolamine-based process. The chilling of the gas and solvents, the presence of solid compounds and the water wash / ammonia stripper system are some of the unit operations that have to be added to the simulation. This complexity implies that more options are to be considered regarding the optimization of the process and more parameters need to be studied.

### **1.5.3 Thesis motivation and outline**

The main objective of this thesis is to study the feasibility of  $\text{CO}_2$  capture from coal-fired power plant using aqueous ammonia and to increase the scientific level of information on this topic. This project is divided in seven main sections:

- First, the Extended UNIQUAC model developed by Thomsen and Rasmussen (1999) for the  $\text{CO}_2\text{-NH}_3\text{-H}_2\text{O}$  system is upgraded. In addition, the parameters of the model are refitted using

additional experimental data so that the valid temperature range is extended to 0-150 °C. The experimental data used in the fitting of the parameters include speciation and enthalpy measurements that improve the accuracy of the thermodynamic model.

- Based on the upgraded thermodynamic model and on the information from the patent, a thermodynamic analysis of the process is performed. It allows for roughly evaluating the performance of the process from a thermodynamic perspective. Conclusions regarding the configuration of the process can be drawn.
- The kinetic rate of absorption of carbon dioxide by ammonia solvent is studied by designing, building and using a new experimental apparatus. The rate of absorption is measured for a concentration of ammonia between 1 and 10 wt%, for a temperature between 6 and 31 °C and for a loading between 0 and 0.8. The results are compared to the one obtained with MEA solutions at 40 °C for a loading up to 0.4. The rate of absorption is successfully modeled.
- The thermodynamic model is implemented in the commercial simulator Aspen Plus through a user model developed within the department. The user model is tested and validated. The performance of the Extended UNIQUAC model is compared with the e-NRTL model available in Aspen.
- The Extended UNIQUAC thermodynamic model and the user model allows for performing flow sheet calculations and for simulating the process. A sensitivity analysis on various parameters is performed and two configurations of the process are tested. The results are compared with the MEA-based process.
- An integration study is conducted to evaluate the effect of the implementation of the process on a power plant. Both process configurations are considered. In order to account for the location of the plant, the study is made for two cooling water temperatures. Using the modeling of the rate of absorption, the size of the main unit operations is assessed. The performance of both variants of the process is evaluated and compared with the MEA-based process.
- Conclusions and recommendations are finally proposed and the main challenges regarding the continuation of this study are identified.

## 1.6 References

Aronu, U. E.; Svendsen, H. F.; Hoff, K. A. Investigation of amine amino acid salts for carbon dioxide absorption. *Int. J. Greenhouse Gas Control*, **2010**, *4*, 771.

Bai, H. L.; Yeh, A. C. Removal of CO<sub>2</sub> greenhouse gas by ammonia scrubbing. *Ind. Eng. Chem. Res.*, **1997**, *36*, 2490.

Bøe, R.; Magnus, C.; Osmundsen, P. T.; Rindstad, B. I. CO<sub>2</sub> point sources and subsurface storage capacities for CO<sub>2</sub> in aquifers in Norway. NGU Report, **2002**, 2002.010, 132 pp. [http://www.ngu.no/FileArchive/101/2002\\_010\\_skjerm.pdf](http://www.ngu.no/FileArchive/101/2002_010_skjerm.pdf), accessed November 2010.

Brohan, P.; Kennedy, J. J.; Harris, I. *et al.* Uncertainty estimates in regional and global observed temperature changes: A new data set from 1850. *J. Geoph. Res. Atm.*, **2006**, *111*, D12106.

Buhre, B. J. P.; Elliott, L. K.; Sheng C. D.; Gupta R. P. Wall, T. F. Oxy-fuel combustion technology for coal-fired power generation. *Progress in Energy and combustion science*, **2005**, *31*, 283.

Carson, J. K.; Marsh, K. N.; Mather, A. E. Enthalpy of solution of carbon dioxide in water with monoethanolamine, or diethanolamine, or N-methyldiethanolamine and water with monoethanolamine and N-methyldiethanolamine at 298.15K. *J. Chem Thermo.*, **2000**, *32*, 1285.

Ciferno J. P.; DiPietro, P.; Tarka, T. An Economic Scoping Study for CO<sub>2</sub> Capture Using Aqueous Ammonia. *National Energy Technology Laboratory*, **2005**.

Clodic, D; El Hitti, R.; Younes, M.; Bill, A.; Casier, F. CO<sub>2</sub> capture by anti-sublimation thermo-economic process evaluation. presented at the 4th Annual Conference on Carbon Capture & Sequestration, Alexandria (VA), USA, May **2005**.

Cullinane, J. T.; Rochelle, G. T. Carbon Dioxide Absorption with Aqueous Potassium Carbonate Promoted by Piperazine. *Greenhouse Gas Control Technology*, **2003**, *2*, 1603.

Dang, H.; Rochelle, G. T. CO<sub>2</sub> Absorption Rate and Solubility in Monoethanolamine / Piperazine / Water. *Separation Sci. & Tech.*, **2003**, *38*, 337.

Dave, N.; Do, T.; Puxty, G.; Rowland, R.; Feron, P. H. M.; Attala, M. I. CO<sub>2</sub> capture by aqueous amines and aqueous ammonia – A Comparison. *Greenhouse Gas Control Technologies 9, Energy procedia*, **2009**, *1*, 949.

Delfort, B.; Carette, P.; Bonnard, L. MEA 40% with Improved Oxidative Stability for CO<sub>2</sub> Capture in Post-Combustion. Presented at Greenhouse Gas Technology 10 (GHGT10), Amsterdam, **2010**.

Derks, P. W. J.; Versteeg, G. F. Kinetics of absorption of carbon dioxide in aqueous ammonia solutions. *Greenhouse Gas Control Technologies 9, Energy procedia*, **2009**, *1*, 1139.

Dooley, J. J.; Dahowski, R. T.; Davidson, C. L. CO<sub>2</sub>-driven enhanced oil recovery as a stepping stone to what? *US department of Energy*, **2010**. <http://web.mit.edu/mitei/docs/reports/eor-css/dooley.pdf>, accessed June 2011.

EIA. International Energy Outlook 2010. [http://www.eia.doe.gov/oiaf/ieo/graphic\\_data\\_highlights.html](http://www.eia.doe.gov/oiaf/ieo/graphic_data_highlights.html), accessed October 2010.

EIA. Carbon dioxide emission by sector. **2009**. [www.eia.doe.gov/oiaf/aeo/pdf/aeotab\\_18.pdf](http://www.eia.doe.gov/oiaf/aeo/pdf/aeotab_18.pdf). accessed October 2010.

ENCAP project, [www.encapco2.org](http://www.encapco2.org), accessed October 2010.

European commission (2007). CO2 emission by sector. [http://ec.europa.eu/energy/publications/doc/statistics/ext\\_co2\\_emissions\\_by\\_sector.pdf](http://ec.europa.eu/energy/publications/doc/statistics/ext_co2_emissions_by_sector.pdf), accessed October 2010.

Faramarzi, L.; Kontogeorgis, G. M.; Thomsen, K.; Stenby, E. H. Extended UNIQUAC model for thermodynamic modeling of CO<sub>2</sub> absorption in aqueous alkanolamine solutions. *Fluid Phase Equilib.*, **2009**, 282, 121.

Freguia, S.; Rochelle, G.T. Modeling of CO<sub>2</sub> capture by aqueous monoethanolamine. *AICHE J.* **2003**, 47, 1676.

Gabrielsen, J.; Michelsen, M. L.; Kontogeorgis, G. M.; Stenby, E. H. Modeling of CO<sub>2</sub> Absorber using an AMP Solution. *AICHE J.*, 2006, 52, 3443.

Gabrielsen, J.; Michelsen, M. L.; Kontogeorgis, G. M.; Stenby, E. H. Experimental validation of a rate-based model for CO<sub>2</sub> capture using an AMP Solution. *Chem. Eng. Sc.*, **2007**, 62, 2397.

Gabrielsen, J. CO<sub>2</sub> Capture from coal Fired Power Plants. Ph.D. Thesis, ISBN 978-87-91435-46-3 Technical University of Denmark, **2007**.

Gal, E. Ultra cleaning combustion gas including the removal of CO<sub>2</sub>. World Intellectual Property, **2006**, Patent WO 2006022885.

Gale, J.; Freund, P. Coal-Bed Methane Enhancement with CO<sub>2</sub> Sequestration Worldwide Potential. *Env. Gosc.* **2008**, 8, 210.

Herzog, H.; Drake, E. White Paper CO<sub>2</sub> Capture Reuse and Storage Technologies. *MIT* **1997**, DOE Order No. DE-AF22-96PC01257.

International Energy Agency. Energy Technology perspective. **2010**, IEA/OECD, Paris.

International Energy Agency. Technology Roadmap - Carbon Capture and Storage. **2010**, IEA/OECD, Paris.

IPCC Special Report on Carbon dioxide Capture and Storage. Intergovernmental Panel on Climate Change special report **2005**.

IPCC, Climate Change 2007: The Physical Science Basis. Fourth assessment report of the Intergovernmental Panel on Climate Change **2007a**.

IPCC, Climate Change 2007: Adaptation and vulnerability. Fourth assessment report of the Intergovernmental Panel on Climate Change **2007b**.

IPCC, Climate Change 2007: Mitigation of climate change. Fourth assessment report of the Intergovernmental Panel on Climate Change **2007c**.

Ishida, M.; Jin, H. A new advanced power-generation system using chemical-looping combustion. *Energy*, **2003**, 19, 415.

Jassim, M. S.; Rochelle, G. T. Innovative absorber/stripper configurations for CO<sub>2</sub> capture by aqueous monoethanolamine. *Ind. Eng. Chem. Res.*, **2006**, 45, 2465.

Jilvero, H.; Normann, F.; Anderson, K.; Johnsson, F. Thermal Integration and Modelling of the Chilled Ammonia Process. Presented at Greenhouse Gas Technology 10 (GHGT10), Amsterdam, **2010**.

Keeling, C. D.; and Whorf, T. P. 2010. Atmospheric CO<sub>2</sub> records from sites in the SIO air sampling network. In Trends: A Compendium of Data on Global Change. Carbon Dioxide Information Analysis Center, Oak Ridge National Laboratory, U.S. Department of Energy, Oak Ridge, Tenn., U.S.A. <http://cdiac.ornl.gov/ftp/trends/co2/maunaloa.co2>, accessed October 2010.

Kelleher, T.; Fair, J. R. Distillation Studies in High Gravity Contactor. *Ind. Eng. Chem. Res.*, **1996**, *35*, 4646.

Kim, J.; Lee, J.; Jang, K.; Shim, J. Performance evaluation of newly developed absorbents for CO<sub>2</sub> capture Presented at Greenhouse Gas Technology 10 (GHGT10), Amsterdam., **2010**.

Knudsen, J. N.; Jensen, J. N.; Biede, O.; 2008. Castor SP2: experiments on pilot plant. CASTOR-ENCAP-CACHET-DYNAMIS Common Technical Training Workshop, Lyon, **2008**.

Knudsen, J. N.; Andersen, J.; Jensen, J. N.; Biede, O. Evaluation of process upgrades and novel solvents for the post-combustion CO<sub>2</sub> capture process in pilot-scale. Presented at Greenhouse Gas Technology 10 (GHGT10), Amsterdam, **2010**.

Knudsen, S.; Karl, M.; Randall, S.; Summary Report: Amine Emissions to Air During Carbon Capture: Phase I: CO<sub>2</sub> and Amines Screening Study for Effects to the Environment. **2009**.

Kozak, F.; Petig, A.; Morris, E.; Rhudy, R.; Thimsen, D. Chilled Ammonia Process for CO<sub>2</sub> Capture. *Greenhouse Gas Control Technologies 9, Energy Procedia*, **2009**, *1*, 1419.

Kurz, F.; Rumpf, B.; Maurer, G. Vapor-liquid-solid equilibria in the system NH<sub>3</sub>-CO<sub>2</sub>-H<sub>2</sub>O from around 310 to 470 K: New experimental data and modeling. *Fluid Phase Equilibria*, **1995**, *104*, 261.

Mathias, P. M.; Reddy, S.; O'Connell, J. P. Quantitative Evaluation of the Aqueous-Ammonia Process for CO<sub>2</sub> capture fundamental Data and Thermodynamic Analysis. *Greenhouse Gas Control Technologies 9, Energy Procedia*, **2009**, *1*, 1227.

Mathonat, C.; Majer, V.; Mather, A. E.; Grolier, J. E. Enthalpies of absorption and solubility of CO<sub>2</sub> in aqueous solutions of methyldiethanolamine. *Fl. Ph. Eq.*, **1997**, *140*, 171.

McLarnon, C., R.; Duncan, J. L. Testing of ammonia based CO<sub>2</sub> capture with multi-pollutant control technology. *Energy Procedia*, **2009**, *1*, 1027–1034.

Mondol, J. D.; McIlveen-Wright, D.; Rezvani, S.; Huang, Y.; Hewitt, N. Techno-economic evaluation of advanced IGCC lignite coal fuelled power plants with CO<sub>2</sub> capture. *Fuel*, **2009**, *88*, 2495.

Neftel, A.; Friedli, H. *et al.* (1994). "Historical CO<sub>2</sub> record from the Siple Station ice core." In Trends: A Compendium of Data on Global Change. Carbon Dioxide Information Analysis Center, Oak Ridge National Laboratory, U.S. Department of Energy, Oak Ridge, Tenn., U.S.A. <http://cdiac.ornl.gov/ftp/trends/co2/siple2.013>, accessed October 2010.

Nielsen, C. J.; D'Anna, B.; Dye, C.; Grauss, M. *et al.* Atmospheric Chemistry of 2-aminoethanol (MEA). Presented at Greenhouse Gas Technology 10 (GHGT10), Amsterdam, **2010**.



- Oashi, Y.; Ogawa, T.; Egami, N. Development of Carbon Dioxide Removal System from the Flue Gas of Coal Fired Power Plant. Presented at Greenhouse Gas Technology 10 (GHGT10), Amsterdam, **2010**.
- Oexmann, J.; Kather, A. Minimising the regeneration heat duty of post-combustion CO<sub>2</sub> capture by wet chemical absorption: The misguided focus on low heat of absorption solvents. *Int. J. Greenhouse Gas Control* **2010**, *4*, 36.
- Ormerod W, The Disposal of Carbon Dioxide from Fossil Fuel Fired Power Stations, IEAGHG/SR3, IEA Greenhouse Gas R&D Programme, Cheltenham, UK **1994**.
- Prestona, C.; Whittakera, S.; Rostronb, B.; Chalaturnyk, R.; Whitec, D.; Hawkesd, C.; Johnsonc, C. W.; Wilkinsona, A.; Sacutaa, N. IEA GHG Weyburn-Midale CO<sub>2</sub> monitoring and storage project – moving forward with the Final Phase. *Greenhouse Gas Control Technologies 9, Energy procedia*, **2009**, *1*, 1703.
- Puxty, G.; Rowland. R; Attala, M. Comparison of the Rate of CO<sub>2</sub> Absorption into Aqueous Ammonia and Monoethanolamine. *Chem. Eng. Sc.*, **2010**, *65*, 915.
- Qin, F.; Wang, S.; Hartono, A.; Svendsen, H.F. Kinetics of CO<sub>2</sub> absorption in aqueous ammonia solution. *Int. J. Greenhouse Gas Control*, **2010a**, *4*, 729.
- Qin, F.; Wang, S.; Kim, I.; Svendsen, H.F.; Chen, C. Study of the Heat of Absorption of CO<sub>2</sub> in Aqueous Ammonia: Comparison between Experimental Data and Model Predictions. *Int. J. Greenhouse Gas Control*, **2010b**, *49*, 3776.
- Rao, A. B.; Rubin, E.S. A technical, economic, and environmental assessment of amine-based CO<sub>2</sub> capture technology for power plant greenhouse gas control. *Env. Sc. Technology*, **2002**, *20*, 4467.
- Ratiffa-Brown, J. A.; Manfreda, L. M.; Hoffmann, J. W.; Ramezan, M.; Stiegel, J. An Environmental Assessment of IGCC power systems. Presented at the Nineteenth Annual Pittsburgh Coal Conference, Pittsburgh, **2002**.
- Rooney, P. C.; Bacon, T. R.; DuPart, M. S. Effect of heat stable salts on MDEA solution corrosivity. *Hydrocarbon Processing*, **1997**.
- Sartori, G.; Savage, D. W. Sterically Hindered Amines for CO<sub>2</sub> Removal from Gases. *Ind. Eng. Chem. Fundamental*, **1983**, *22*, 239.
- Schach, M.; Schneider, R.; Schramm, H.; Repke, J. Techno-Economic Analysis of Postcombustion Processes for the Capture of Carbon Dioxide from Power Plant Flue Gas. *Ind. Eng. Chem. Res.*, **2010**, *49*, 2363.
- Supap, T.; Idem, R.; Veawab, A.; Aroonwilas, A.; Tontiwachwuthikul, P.; Chakma, A; Kybett, B. D. Kinetics of the Oxydative Degradation of Aqueous Monoethanolamine in a Flue Gas Trating Unit. *Ind. Eng. Chem. Res.* **2001**, *40*, 3445.
- Tanaka, H.; Iijima, M.; Mitchell, R. MHI's recent Post Combustion Co<sub>2</sub> Capture Achievments and Developments. Presented at the 12<sup>th</sup> meeting of the combustion capture network, Regina, **2009**.

Telikapelli, V.; Kozak, F.; Leandri, J.F.; Sherrick, B.; Black, J.; Muraskin, D.; Cage, M.; Hammond, M.; Spitznogle, G. CCS with the Alstom Chilled Ammonia Process Development Program – Field Pilot Results. Presented at Greenhouse Gas Technology 10 (GHGT10), Amsterdam, **2010**.

The Royal Society. A guide to facts and fictions about climate change.

[http://royalsociety.org/uploadedFiles/Royal\\_Society\\_Content/News\\_and\\_Issues/Science\\_Issues/Climate\\_change/climate\\_facts\\_and\\_fictions.pdf](http://royalsociety.org/uploadedFiles/Royal_Society_Content/News_and_Issues/Science_Issues/Climate_change/climate_facts_and_fictions.pdf), **2006**, accessed June 2011.

Thomsen, K.; Rasmussen, P. Modeling of vapor-liquid-solid equilibrium in gas-aqueous electrolyte systems. *Chemical Engineering Science*, **1999**, *54*, 1787.

Valenti, G.; Bonalumi, D.; Macchi, E. Energy and exergy analyses for the carbon capture with the chilled ammonia Process. *Greenhouse Gas Control Technologies 9, Energy procedia*, **2009**, *1*, 1059.

Valenti, G.; Bonalumi, D.; Macchi, E. A parametric investigation of the Chilled Ammonia Process from energy and economic perspectives. *Fuel*, **2011**, doi:10.1016/j.fuel.2011.06.035.

Vattefall,

[http://www.captureready.com/userfiles/image/Carbon%20Capture/Oxyfuel%20Combustion%20Capture%20Process\\_Vattenfall.jpg](http://www.captureready.com/userfiles/image/Carbon%20Capture/Oxyfuel%20Combustion%20Capture%20Process_Vattenfall.jpg) , Accessed October 2010.

VTT. Potential for carbon capture and storage (CCS) in the Nordic region. VTT research notes 2556, **2010**.

Versteeg, P.; Rubin, E. S. Technical and Economic Assessment of Ammonia-Based Post-Combustion CO<sub>2</sub> Capture. Presented at Greenhouse Gas Technology 10 (GHGT10), Amsterdam, **2010**.

Vitse, F.; Czarnecki, L.; Schimdt, D.; Schubert, C. Pilot Plant Assessments of UCARSOL FGC 3000 Performance on Advanced Flow Schemes for CO<sub>2</sub> capture from Flue Gas. Presented at Greenhouse Gas Technology 10 (GHGT10), Amsterdam, **2010**.

Yeh, A. C.; Bai, H. L. Comparison of ammonia and monoethanolamine solvents to reduce CO<sub>2</sub> greenhouse gas emissions. *Sc. Total Environment* **1999**, *228*, 121.

Yeh, J. T.; Resnik, K. P.; Rygle, K. Semi-batch absorption and regeneration studies for CO<sub>2</sub> capture by aqueous ammonia. *Fuel Processing Technology*, **2005**, *86*, 1533.

Yokoyama, K.; Takamoto, S.; Kikkawa, H.; Katsube, T. *et al.* Hitachi's Carbon Dioxide Scrubbing Technology with New Absorbent for Coal Fired Power Plants. Presented at Greenhouse Gas Technology 10 (GHGT10), Amsterdam, **2010**.

Zachos, J.; Pagani, M.; Sloan, L.; Thomas, E.; Billups, K. Trends, Rhythms and Aberrations in Global Climate 65Ma to present. *Science*, **2001**, *5517*, 686.



## 2 Thermodynamic modeling of mixtures of carbon dioxide, ammonia and water

### 2.1 Introduction

In order to accurately evaluate the performance of the carbon dioxide capture process using aqueous ammonia, it is necessary to use an accurate thermodynamic model that allows for calculating the equilibrium and thermal properties of the system  $\text{CO}_2\text{-NH}_3\text{-H}_2\text{O}$ . As seen previously, the model must be able to describe accurately the vapor-liquid equilibrium (VLE), the speciation and the solid-liquid equilibrium (SLE) as well as the enthalpy change from a mixture of water, carbon dioxide and ammonia in order to be usable for the simulation of the process. Hence, the model has to be accurate from 0 to 150 °C, for a pressure up to 10 MPa (100 bar) and for a large range of ammonia and carbon dioxide concentration.

In the past, several researchers have proposed models that allow for calculating the solubility of  $\text{CO}_2$  in aqueous alkanolamine. Kent *et al.* (1976) have developed a correlation that allowed them for calculating the partial pressure of carbon dioxide in aqueous MEA and DEA solutions, assuming that the activity coefficients were equal to unity and by fitting equilibrium constants. Gabrielsen has developed a simple correlation to calculate solubility of carbon dioxide in aqueous amine solutions as well as the enthalpy of absorption. The model has been tested with MEA, DEA, MDEA and AMP (Gabrielsen *et al.*, 2005, Gabrielsen *et al.*, 2006). However, this model is only valid for a narrow range of temperature and loadings.

The solutions that are modeled are electrolyte solutions. The most common models that are used are therefore the activity coefficient electrolyte models. The e-NRTL model proposed by Chen *et al.* (1982) is perhaps the most commonly used activity coefficient based thermodynamic model for industrial purposes. It is available on the widely used commercial simulator Aspen. This model has been used for modeling of carbon dioxide water and alkanolamine systems. Austgen *et al.* (1989) have proposed a model based on e-NRTL to predict the solubility of  $\text{CO}_2$  in aqueous MEA and DEA solutions. Several other models have followed. Posey and Rochelle (1997) have focused on the use MDEA for capturing  $\text{CO}_2$  and  $\text{H}_2\text{S}$  using the same method. Cullinane and Rochelle (2005) have proposed the thermodynamic model of aqueous potassium carbonate, piperazine and carbon dioxide using e-NRTL. Recently, Hessen *et al.* (2010) have applied the refined e-NRTL model proposed by Bollas *et al.* (2008) to model the  $\text{CO}_2\text{-MEA-H}_2\text{O}$  and  $\text{MDEA-CO}_2\text{-H}_2\text{O}$  systems.

Regarding the modeling of the  $\text{CO}_2\text{-NH}_3\text{-H}_2\text{O}$  system, several models are currently developed and used. Kurz *et al.* (1995) have proposed a model for this system based on the Pitzer electrolyte activity coefficient model (Pitzer, 1973) coupled with the SRK equation of state to calculate the gas phase fugacities for the system. The model uses empirical parameters that were fitted to VLE and SLE data from the literature. The VLE data were taken from various publications, including experimental data

measured within the research group (Goppert and Maurer, 1988, Müller *et al.*, 1988 Kurz *et al.*, 1995). The SLE data were taken from Jänecke *et al.* (1929a). The only solid considered by the model is the ammonium bicarbonate. In principles, the model requires 72 binary and 120 ternary parameters to be fitted. In practice, some binary parameters were retrieved from previous publications and some of the interactions between species were neglected to reduce the number of fitted parameters to 14. The model has been used by Jilvero *et al.* (2010) to simulate the process using Aspen.

As stated in 1.5.2, the original version of the e-NRTL model available in Aspen Plus V7.1 is not able to accurately describe the solubility of ammonium bicarbonate as it has been shown by Fosbøl (2008). It is necessary to refit the parameters to the experimental data to obtain accurate results. More details regarding the performance of the e-NRTL model for the the CO<sub>2</sub>-NH<sub>3</sub>-H<sub>2</sub>O system can be found in Chapter 5. The e-NRTL model has been refined by Mathias *et al.* (2010). The parameters have been fitted to VLE data from Goppert and Maurer (1988) and Kurz *et al.* (1995). Calorimetric data from Rumpf *et al.* (1998) were also used together with speciation data from Wen and Brooker (1995) and SLE data from Jänecke (1929a, 1929b). The model only handles the formation of ammonium bicarbonate as a solid. Mathias *et al.* (2010) did not provide a detailed description of the modifications made to the version of the model available in Aspen Plus.

In this study we use the Extended Universal Quasi Chemical model (Extended UNIQUAC) developed by Thomsen *et al.* (1999). A similar work applied to the carbon dioxide-alkanolamine-water system was presented by Faramarzi *et al.* (2009). The model provides activity coefficients for the liquid phase using the Extended UNIQUAC model. Gas phase fugacities are calculated using the Soave-Redlich-Kwong (SRK) equation of state for the volatile compounds. The model has been applied on different electrolyte systems. The original version of the model has shown to be capable of describing accurately the vapor-liquid-solid equilibria and thermal properties for the CO<sub>2</sub>-NH<sub>3</sub>-H<sub>2</sub>O system for a wide range of concentrations (up to 80 molal NH<sub>3</sub>), for a temperature in the range of 0-110 °C and for a pressure up to 10 MPa. However, the model does not cover the whole temperature range necessary to thoroughly evaluate the process (0-150 °C). In this new version of the model, additional experimental data were used in order to extend the valid temperature range up to 150 °C over a wide concentration range and pressures up to 10 MPa. Furthermore, the model has been upgraded and additional types of experimental data have been used to refit the parameters in order to increase its accuracy. This work has been published in Industrial & Engineering Chemistry Research (Darde *et al.*, 2010).

## **2.2 Phase equilibria**

### **2.2.1 Chemistry**

#### **2.2.1.1 Speciation**

The analysis of the CO<sub>2</sub>-NH<sub>3</sub>-H<sub>2</sub>O system implies the study of several equilibrium processes. The following reactions are considered in this new version of the model:



For each equilibrium, the sum of the chemical potential of the reactants is equal to the sum of the chemical potential of the products. Some conventions must be chosen to express these chemical potentials. In this model, water is considered to be the only solvent in the system. The symmetrical convention is adopted for water and rational unsymmetrical is chosen for the remaining species. Hence, the chemical potential of water in the liquid phase can be expressed as:

$$\mu_{\text{H}_2\text{O}(\text{l})} = \mu_{\text{H}_2\text{O}(\text{l})}^0 + RT \ln a_{\text{H}_2\text{O}(\text{l})} = \mu_{\text{H}_2\text{O}(\text{l})}^0 + RT \ln (\gamma_{\text{H}_2\text{O}(\text{l})} x_{\text{H}_2\text{O}(\text{l})}) \quad (2.6)$$

$\mu_{\text{H}_2\text{O}(\text{l})}^0$  ( $J \cdot \text{mol}^{-1}$ ) is the standard state chemical potential of water at temperature  $T$  (K),  $R$  ( $J \cdot \text{mol}^{-1} \cdot K^{-1}$ ) is the gas constant and  $a_{\text{H}_2\text{O}(\text{l})}$ ,  $\gamma_{\text{H}_2\text{O}(\text{l})}$  and  $x_{\text{H}_2\text{O}(\text{l})}$  are respectively the activity, the activity coefficient and the mole fraction of water in the liquid phase.

For the remaining species in the liquid phase, the chemical potential can be expressed as:

$$\mu_{i(\text{aq})} = \mu_{i(\text{aq})}^* + RT \ln a_{i(\text{aq})}^* = \mu_{i(\text{aq})}^* + RT \ln \gamma_{i(\text{aq})}^* x_{i(\text{aq})} \quad (2.7)$$

$\mu_{i(\text{aq})}^*$  is the unsymmetrical standard state chemical potential for the compound  $i$  in the solution, and  $a_{i(\text{aq})}^*$ ,  $\mu_{i(\text{aq})}^*$  and  $x_{i(\text{aq})}$  are respectively the activity, the unsymmetrical, rational activity coefficient and the mole fraction of compound  $i$  in the solution.

$$\ln K_j = -\frac{\Delta G^0}{RT} = \sum_i \nu_{i,j} \ln a_{i(\text{aq})} = \sum_i \nu_{i,j} \ln \gamma_{i(\text{aq})} x_{i(\text{aq})} \quad (2.8)$$

$K_j$  is the equilibrium constant of reaction  $j$  at temperature  $T$ ,  $\Delta G^0$  ( $J \cdot \text{mol}^{-1}$ ) is the change of the standard state Gibbs energy of formation for reaction  $j$  at the temperature  $T$ , or the change in standard state chemical potential for reaction  $j$  at temperature  $T$ ,  $\nu_{i,j}$  is the stoichiometric coefficient of compound  $i$  in reaction  $j$  and  $a_i$  is the activity coefficient of compound  $i$ .

### 2.2.1.2 Vapor-liquid equilibria



The critical conditions for ammonia ( $T_c = 132.4 \text{ }^\circ\text{C}$ ,  $P_c = 11.28 \text{ MPa}$ ) and carbon dioxide ( $T_c = 31.1 \text{ }^\circ\text{C}$ ,  $P_c = 7.39 \text{ MPa}$ ) are within the pressure and temperature ranges covered by the model. It was found that the extrapolation of equilibrium constants into the supercritical range was improved by using correlations for Henry's law constants rather than using the Gibbs-Helmholtz equation like it was done in the original model. Therefore, Henry's law constant correlations as a function of the temperature were included both for ammonia and carbon dioxide. The correlation used for ammonia in water (equation (2.12)) was proposed by Rumpf and Maurer (1993) for the temperature range from 273.15 to 433.15 K. The Henry's law constant is expressed in *MPa* and the temperature in Kelvin.

$$\ln(H_{NH_3,w}^*(MPa) \cdot M_w) = 3.932 - \frac{1879.02K}{T} - \frac{355134.1K^2}{T^2} \quad (2.12)$$

$M_w$  is the molar mass of water in  $\text{kg}\cdot\text{mol}^{-1}$  used in order to convert from the molality scale to the mole fraction scale. The correlation used for the Henry's constant for carbon dioxide in water (equation (2.13)) was proposed by Rumpf and Maurer (1993) for the temperature range from 273.15 to 473.15 K. The same units are used in this expression.

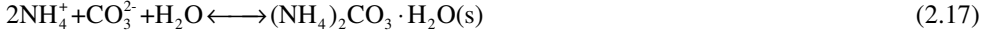
$$\ln(H_{CO_2,w}^*(MPa) \cdot M_w) = 192.876 - \frac{9624.4K}{T} + 1.441 \cdot 10^{-2} K^{-1} \cdot T - 28.749 \cdot \ln(T) \quad (2.13)$$

The pressure correction used for the Henry's law constant is a Poynting factor implemented as shown in equation (2.14).

$$P y_i \phi_i = H_{i,w}^*(T, P_w^s) \exp\left(\frac{v_{i,w}^\infty(T) \cdot (P - P_w^s)}{RT}\right) \gamma_i^* x_i \quad (2.14)$$

$H_{i,w}^*(T, P_w^s)$  is the Henry's constant of compound  $i$  in pure water on the mole fraction scale,  $v_i^\infty$  is the partial volume of compound  $i$  at infinite dilution. The partial volumes of ammonia and water were calculated by Rumpf and Maurer (1993) using the work from Brelvi and O'Connell (1972).

### 2.2.1.3 Solid-liquid equilibria



Hence, the model handles the formation of the same 5 different solids that are considered in the original version of the model:

- Ammonium bicarbonate:  $\text{NH}_4\text{HCO}_3$
- Ammonium carbonate:  $(\text{NH}_4)_2\text{CO}_3 \cdot \text{H}_2\text{O}$
- Ammonium carbamate:  $\text{NH}_2\text{COONH}_4$
- Ammonium sesqui-carbonate:  $(\text{NH}_4)_2\text{CO}_3 \cdot 2\text{NH}_4\text{HCO}_3$
- Ice:  $\text{H}_2\text{O}$

The solid-liquid equilibria can be expressed in a similar way as the speciation equilibrium. The activity of the solid compound in its phase is considered to be one. The chemical potential of the solid compound is therefore equal to its standard state chemical potential. Hence:

$$\ln K_j = -\frac{\Delta G^0}{RT} = \sum_i \nu_{i,j} \ln a_{i(aq)} \quad (2.20)$$

$K_j$  is the equilibrium constant of the reaction  $j$  at temperature  $T$ ,  $\Delta G^0$  ( $J \cdot \text{mol}^{-1}$ ) is the change of Gibbs energy of formation for reaction  $j$  at the temperature  $T$ .

The degree of saturation of a solution can be calculated with the saturation index (SI), defined by the ratio of the activity coefficients of the product of the reaction of dissolution of the solid over the equilibrium constant of the reaction of dissolution. If the solubility index is equal to unity, the solution is saturated. If it is superior, the solution is super saturated. If it is lower than one, the solution is not saturated. Hence, this index allows for determining if one or several salts are supersaturated in a solution.

## 2.2.2 Standard state chemical potential, enthalpy of formation, heat capacity

As in the original version of the model (Thomsen *et al.*, 1999), the standard state properties of most of the species considered by the model were taken from NIST tables. This includes the Gibbs energy and enthalpy of formation and the heat capacities. The standard state chemical potentials from NIST tables



are reported for 25 °C. At temperatures other than 25 °C, they are calculated using the Gibbs-Helmholtz equation (Thomsen *et al.*, 1996).

$$\frac{d \frac{\mu_i^*}{RT}}{dT} = -\frac{\Delta_f H_i^0}{RT^2} \quad (2.21)$$

$\Delta_f H_i^0$  is the enthalpy of formation at standard state of compound *i*.

The heat capacities are temperature dependant. The temperature dependence for the heat capacity is the same as the one used in the original version of the model (Thomsen *et al.*, 1999). It has been proposed by Helgeson *et al.* (1986).

$$C_{p,i}^* = a_i + b_i T + \frac{c_i}{T - 200K} \quad (2.22)$$

This temperature dependence allows for determining the temperature dependence of the standard-state enthalpy of formation:

$$\frac{d\Delta_f H_i^0}{dT} = C_{p,i}^* \quad (2.23)$$

Hence,

$$\Delta_f H_{i,T}^0 = \Delta_f H_{i,T_0}^0 + a_i (T - T_0) + 0.5b_i (T^2 - T_0^2) + c_i \ln \frac{T - 200K}{T_0 - 200K} \quad (2.24)$$

The temperature dependence of the chemical potential can be retrieved by using equations (2.21) and (2.24).

In the original version of the model, the heat capacities of the solids were considered as parameters to be fitted. In this new version, they have been calculated using Kopp's rule (Hurst *et al.*, 1992). The heat capacities of these solids were considered to be independent of temperature in the temperature range considered. The values of heat capacities can be found in Table 2-1. The Gibbs energy and the enthalpy of formation of these salts were fitted to experimental data.

**Table 2-1: Heat capacity of the solid compounds**

	$\text{NH}_4\text{HCO}_3$	$(\text{NH}_4)_2\text{CO}_3 \cdot \text{H}_2\text{O}$	$\text{NH}_2\text{COONH}_4$	$(\text{NH}_4)_2\text{CO}_3 \cdot 2\text{NH}_4\text{HCO}_3$
<b>Cp (J mol<sup>-1</sup> K<sup>-1</sup>)</b>	108	178	121	364

Furthermore, the Gibbs energy and enthalpy of formation as well as the heat capacity of the ammonium carbamate ion ( $\text{NH}_2\text{COO}^-$ ) were fitted to experimental data. In the original version of the model, these values were determined from the equilibrium constants measured by Faurholt *et al.* (1921).

## **2.3 Description of the thermodynamic model**

### **2.3.1 Local composition models**

The Extended UNIQUAC model is a local composition model that is based on the assumptions that the molecular composition is different from the bulk composition (Thomsen, 2006). This concept has been introduced by Wilson in 1964. Instead of considering an average composition, the local composition models take into account short-range intermolecular interactions. The most widely known local composition models are the NRTL (Renon and Prausnitz, 1968) and the UNIQUAC (Abrams and Prausnitz, 1975) models. They are specifically used to model electrolyte solutions.

Both the Extended UNIQUAC and the e-NRTL model couple a local composition model with an electrostatic term derived from the Debye-Hückel theory. The e-NRTL model uses the Pitzer Debye-Hückel term, while the Extended UNIQUAC uses the extended Debye-Hückel term that is simpler than the first one. However, according to Thomsen (2006), this does not make much difference in the results. In addition, the activity coefficient expressions used in the e-NRTL model are much more complicated than for UNIQUAC and imply a longer time for programming. The parameters used in e-NRTL are salt specific while the one used in Extended UNIQUAC are ion specific. The e-NRTL model therefore requires the use of a proper mixing rule to describe properly the properties of a salt solution.

The Extended UNIQUAC model has been successfully used for the  $\text{CO}_2\text{-NH}_3\text{-H}_2\text{O}$  system as the original version of the model used in this study (Thomsen *et al.*, 1999). Parameters for various ions are available (Thomsen, 1997). In addition, it has also been successfully developed for alkanolamine, carbon dioxide and water system (Faramarzi *et al.*, 2009).

### **2.3.2 Extended UNIQUAC model**

The model that is used in this study is the extended UNIQUAC model, proposed by Sander *et al.* (1986) and modified by Thomsen (1997). It is based on the UNIQUAC model added to a Debye-Hückel term in order to account for the electrostatic terms. The Debye-Hückel theory describes the interaction between ions in a solution. The interaction between the ions and the solvent, in our case water, are not taken into account. Hence the model can successfully model the long range interactions but miss a term that include short and intermediate range term interactions (Thomsen, 2006). The UNIQUAC model allows for calculating these interactions. In this model, similarly to the original version of the model, water is considered as being the only solvent, the rest of the species being solutes. This is a way to simplify the expression of the excess Gibbs energy that is not dependant on the solvent composition and to reduce the number of adjustable parameters.

The purpose of such models is to take into account the non-ideality of the solutions, and therefore to perform a calculation of the activity coefficient of the difference species. Hence, the study of the excess Gibbs energy is necessary, as the activity coefficients are derived from this energy.

The extended UNIQUAC model consists of three terms to calculate the excess Gibbs Energy of a solution: a combinatorial (entropic) term, a residual (enthalpic) term and an electrostatic term.

$$G^{ex} = G_{\text{Combinatorial}}^{ex} + G_{\text{Residual}}^{ex} + G_{\text{Extended Debye Hückel}}^{ex} \quad (2.25)$$

The combinatorial term is independent of the temperature. It only depends on the relative sizes of the species:

$$\frac{G_{\text{Combinatorial}}^{ex}}{RT} = \sum_i x_i \ln \frac{\phi_i}{x_i} + \frac{z}{2} \sum_i q_i x_i \ln \frac{\theta_i}{\phi_i} \quad (2.26)$$

$z$  is the coordination number of the lattice set to 10,  $x_i$  is the mole fraction of compound  $i$ ,  $\phi_i$  is the volume fraction and  $\theta_i$  is the surface area fraction. They are defined by equations (2.27) and (2.28).

$$\phi_i \equiv \frac{r_i x_i}{\sum_j r_j x_j} \quad (2.27)$$

$$\theta_i = \frac{q_i x_i}{\sum_j q_j x_j} \quad (2.28)$$

The parameters  $r_i$  and  $q_i$  are respectively the volume and the surface area parameters for the component  $i$ . Unlike in the UNIQUAC model, the Extended UNIQUAC model considers these parameters as adjustable ones that need to be fitted to experimental data to be determined.

The residual enthalpic term is dependent on the temperature.

$$\frac{G_{\text{Residual}}^{ex}}{RT} = - \sum_i q_i x_i \ln \left( \sum_j \theta_j \tau_{ji} \right) \quad (2.29)$$

With  $\tau_{ji}$  following equation (2.30)

$$\tau_{ji} = \exp\left(\frac{u_{ii} - u_{ji}}{T}\right) \quad (2.30)$$

$u_{ii}$  and  $u_{ji}$  are the interaction energy parameters. They are temperature dependant:

$$u_{ji} = u_{ji}^0 + u_{ji}^T (T - 298.15) \quad (2.31)$$

Hence, the enthalpic term comprises two adjustable parameters per pair of species considered.

The electrostatic term that is used is derived from the extended Debye-Hückel law (Guggenheim, 1949). It allows for accounting for the interactions between ions in a simpler way than the original Debye-Hückel law (Hückel *et al.*, 1925). The expression of the electrostatic term for the Gibbs energy as it is used in the model is:

$$G_{\text{Extended Debye Hückel}}^{\text{ex}} = -x_w M_w \frac{4A}{(Ba)^3} \left[ \ln(1 + BaI^{1/2}) - BaI^{1/2} + \frac{(Ba)^2 I}{2} \right] \quad (2.32)$$

$x_w$  and  $M_w$  ( $kg / mol$ ) are respectively the mole fraction and the molar mass of water. A typical value for  $Ba$  is  $1.5 (kg / mol)^{1/2}$ . This value has been used in the model.  $I$  is the ionic strength of the solution defined as:

$$I = \frac{1}{2} \sum_i m_i z_i^2 \quad (2.33)$$

Where  $m_i$  ( $mol / kgwater$ ) and  $z_i$  are respectively the molality and the charge number of ionic specie  $i$ .

$A$  is the Debye Hückel parameter defined as:

$$A = (2\pi N_A d_0)^{1/2} \left( \frac{e^2}{4\pi\epsilon_0\epsilon_r kT} \right)^{3/2} \quad (2.34)$$

Where  $N_A$  is the Avogadro number,  $d_0$  ( $kg / m^3$ ) is the density of water. In order to simplify the calculations, the mass and volumes of the ions are neglected.  $e$  (C) is the electronic charge,  $\epsilon_0$  and  $\epsilon_r$  ( $C^2 J^{-1} m^{-1}$ ) are respectively the permittivity in vacuum and the relative permittivity of pure water. The effect of ionic species on the dielectric constant is neglected.

There is no adjustable parameter related to the electrostatic term as the Debye Hückel parameter is only function of the density and relative permittivity of pure water. According to Thomsen (2006), the use of this simplified term accounting for the electrostatic interactions does not affect significantly the performance of the model.

The symmetrical activity coefficient  $\gamma_i$  of a specie  $i$  can be obtained by partial differentiation of the molar excess Gibbs energy with respect to the mole of the specie  $i$ .

$$\ln \gamma_i = \left[ \frac{\partial \left( \frac{nG^{\text{ex}}}{RT} \right)}{\partial n_i} \right]_{P,T,n_{j \neq i}} \quad (2.35)$$

The rational unsymmetrical activity coefficient of the species can be obtained by:

$$\gamma_i^* = \frac{\gamma_i}{\gamma_i^\infty} \quad (2.36)$$

Where  $\gamma_i^\infty$  is the activity coefficient at infinite dilution of specie  $i$ .

Hence, the logarithm of the symmetrical activity coefficient of a specie  $i$  is the sum of the three differentiations of the three term of the excess molar Gibbs energy. Therefore, the two following equations can be written:

$$\ln \gamma_w = \ln \gamma_w^{\text{Combinatorial}} + \ln \gamma_w^{\text{Residual}} + \ln \gamma_w^{\text{Extended Debye-Hückel}} \quad (2.37)$$

$$\ln \gamma_i^* = \ln \frac{\gamma_i^{\text{Combinatorial}}}{\gamma_i^{\text{Combinatorial}, \infty}} + \ln \frac{\gamma_i^{\text{Residual}}}{\gamma_i^{\text{Residual}, \infty}} + \ln \frac{\gamma_i^{\text{Extended Debye-Hückel}}}{\gamma_i^{\text{Extended Debye-Hückel}, \infty}} \quad (2.38)$$

The vapor-phase fugacities are calculated with the Soave-Redlich-Kwong (SRK) equation of state. The use of the SRK does not entail additional adjustable parameters as the classical mixing rules are used.

## 2.4 Evaluation of the parameters

### 2.4.1 Parameter fitting procedure

As seen before, the thermodynamic model has to describe accurately the vapor-liquid-solid equilibria as well as the speciation and the thermal properties. Experimental data from various experiments were

used during the fitting. The optimization procedure first required to define a function accounting for the deviation between the model and the experimental data for all types of experimental data.

The evaluation of model parameters was performed by minimizing the weighted sum of squared residuals. This sum is calculated using the function  $S$  :

$$\begin{aligned}
 S = & \sum_{\text{VLE data}} \left[ \frac{P_{\text{calc}} - P_{\text{exp}}}{0.04(P_{\text{exp}} + 0.05\text{Bar})} \right]^2 + \sum_{\text{H}^{\text{E}} \text{ data}} \left[ \frac{H_{\text{calc}}^{\text{E}} - H_{\text{exp}}^{\text{E}}}{120R_x} \right]^2 + \sum_{\text{H}^{\text{dil}} \text{ data}} \left[ \frac{H_{\text{calc}}^{\text{dil}} - H_{\text{exp}}^{\text{dil}}}{20R_x} \right]^2 + \\
 & \sum_{\text{H}^{\text{App mol}} \text{ data}} \left[ \frac{H_{\text{calc}}^{\text{dil}} - H_{\text{exp}}^{\text{dil}}}{20R_x} \right]^2 + \sum_{\text{H}^{\text{sol}} \text{ data}} \left[ \frac{H_{\text{calc}}^{\text{sol}} - H_{\text{exp}}^{\text{sol}}}{60R_x} \right]^2 + \sum_{\text{SLE data}} \left[ \frac{\Delta G^0 + RT \sum_i \nu_i \ln a_i}{0.04RT} \right]^2 + \\
 & \sum_{\text{Part Evap Data}} \left[ \frac{H_{\text{calc}} - H_{\text{exp}}}{0.02H_{\text{exp}}} \right]^2 + \sum_{\text{Spec data}} \left[ \frac{\left( \frac{m(\text{NH}_2\text{COO}^-)}{m(\text{CO}_2)_{\text{tot}}} \right)_{\text{calc}} - \left( \frac{m(\text{NH}_2\text{COO}^-)}{m(\text{CO}_2)_{\text{tot}}} \right)_{\text{exp}}}{0.012 \left( \frac{m(\text{NH}_2\text{COO}^-)}{m(\text{CO}_2)_{\text{tot}}} \right)_{\text{exp}}} \right]^2 + \\
 & \sum_{\text{Cp data}} \left( \frac{C_{\text{p calc}} - C_{\text{p exp}}}{10J \cdot \text{mol}^{-1} \cdot K^{-1}} \right)^2 + \sum_{\text{App Cp data}} \left( \frac{C_{\text{p calc}} - C_{\text{p exp}}}{10J \cdot \text{mol}^{-1} \cdot K^{-1}} \right)^2 + A
 \end{aligned} \tag{2.39}$$

“Calc” and “Exp” respectively signify the values calculated with the model and experimental values. The factors 0.04, 120, 20, 20, 60, 0.04, 0.02, 0.012, 10 and 10 are the weighting factors that were used for the vapor liquid equilibrium, excess enthalpy, enthalpy of dilution, apparent molar enthalpy, enthalpy of solution, solid liquid equilibrium, enthalpy change from partial evaporation, speciation heat capacity and apparent heat capacity data. The weighting factors have been chosen based on experience with modeling the  $\text{CO}_2\text{-NH}_3\text{-H}_2\text{O}$  system. The choice for these factors is crucial to allow the model for representing all the properties of the thermodynamic system satisfyingly. It is therefore necessary to test different weightings and to perform the fitting of the parameters for each of them until a solution that respect all the criteria is obtained

The term  $A$  accounts for the deviation related to the gas hydrate formation data. This term has been proposed by Munck and Skjold-Jørgensen (1988).

$$A = \sum_{\text{Gas hyd data}} \frac{\Delta\mu_0}{RT_0} - \ln \left( \frac{f_w^\alpha}{f_w^0} \right) + \sum_i \nu_i \ln \left( 1 - \sum_K Y_{Ki} \right) \tag{2.40}$$

Where  $\Delta\mu_0$  represents the difference in the chemical potential of water in the empty hydrate lattice and in the liquid state at 273.15 K,  $f_w$  represents the fugacity of water,  $\nu_i$  is the number of cavity of type  $i$

and  $Y_{ki}$  accounts for the probability of a cavity of type  $i$  being occupied by a hydrate forming molecule of type  $K$ .

The weighting factor for VLE data was chosen so that a difference of pressure of 4% between the experimental and calculated values would lead to a residual of 1 for relatively high pressure data. The added term 0.05 in the denominator of the VLE term of equation (2.39) allows for limiting the influence of the low pressure data. The calculated pressures in equation (2.39) are the bubble point pressures. Similarly to the original version of the model, only the total pressure reported in the publications were used in the parameter estimation. The determination of parameters using total pressure was shown by Barker in 1953 to be comparable in accuracy with the one using partial pressure experimental data. Van Ness *et al.* (1978) confirmed that the methods using the gas phase mole fraction in addition to the total pressure measurements were not superior to the one introduced by Barker. Hence, it is consistent not to use partial pressure data on top of the total pressure ones when both are available.

The weighting of the excess enthalpy data was chosen so that an absolute difference of 1000 J between the calculated and experimental values would give a residual of 1. The factor  $x = 1K$  has been added in the expression of  $S$  in equation (2.39) in order to make the expression dimensionless.

For the SLE term, the residual is zero when the correct salt is predicted at equilibrium. The SLE data are weighted so that a solubility index of 1.11 and 0.90 give a squared residual of 1. The weight of the SLE term has been increased compared to the original version of the model. This can be justified by the fact that additional VLE and enthalpy data have been used in this new version of the model, whereas the same number of SLE data has been used.

For the speciation data, it was chosen to use the difference between the ratio of molalities of ammonium carbamate ion and total molality of carbon dioxide in the mixture calculated by the model and from the experimental data as shown in equation (2.39).

Two different routines have been used to determine the parameters: a modified version of the Marquardt routine (Fletcher *et al.*, 1971) and a modified version of the Nelder-Mead routine.

In this new version of the model, 30 UNIQUAC model parameters and 13 standard state properties from various species were fitted using experimental data. The use of SRK equation of state does not imply additional parameters to be fitted as no interaction parameters are used for the gas phase.

The volume and surface area ( $r$  and  $q$ ) UNIQUAC parameters that were modified compared to the original version of the model are the ones for  $\text{NH}_3$ ,  $\text{CO}_2$  and  $\text{NH}_2\text{COO}^-$ .

For  $\text{CO}_2$ , the values of UNIQUAC volume and surface area parameters of carbon dioxide and water as well as the interaction energy UNIQUAC parameters between aqueous carbon dioxide species and

water were previously determined by Garcia (2005), for a temperature up to (250 °C) and using the same Henry's law constant correlation. Therefore, these values were used in the present model.

The VLE NH<sub>3</sub>-H<sub>2</sub>O binary data were used alone to fit the NH<sub>3</sub>  $r$  and  $q$  parameters as well as the different binary ammonia-water interaction parameters.

The rest of the parameters were systematically fitted using all the data in order to obtain an accurate representation of all the considered properties. This includes interaction parameters for the aqueous ternary species as well as  $r$  and  $q$  volume and surface area parameters for NH<sub>2</sub>COO<sup>-</sup>. In addition, the Gibbs energy and the enthalpy of formation of the four ammonia salts were fitted to experimental data.

The remaining standard state properties and parameters from UNIQUAC are identical to the ones used in the original model.

The optimization of such a high number of parameters is not a trivial task. Some parameters have more influence than others on the performance of the model. The fitting requires several optimization steps. Usually, the parameters were fitted as groups of four. The optimization was started with the most influent parameters on the VLE and thermal calculations, such as the parameters related to the ammonium carbamate ion. It was then extended to the other parameters. To test the performance of a set of parameters, all the results were carefully analyzed in order to make sure that all the properties were accurately described. This step may be very time consuming, especially the test of the performance of the model towards SLE, as a phase diagram had to be manually calculated for each of the set of parameters tested. The optimization quality depends heavily on the starting guess of the different parameters, which is why it was also tested to manually change the starting guess in order to observe the change in the results after optimization. In overall, the fitting of parameters required a lot of trial and error tests before obtaining a satisfying result.

## 2.4.2 Parameters fitted

The  $r$  and  $q$  UNIQUAC parameters determined for the various species of this system are presented in Table 2-2. The  $a$  and  $b$  parameters for the heat capacity of NH<sub>2</sub>COO<sup>-</sup> are given in Table 2-3. The estimated thermodynamic properties of NH<sub>2</sub>COO<sup>-</sup> and of the solid compounds that were determined by fitting to the experimental data are given in Table 2-4. The binary interaction parameters for the different compounds of the CO<sub>2</sub>-NH<sub>3</sub>-H<sub>2</sub>O system are given in Table 2-5 and Table 2-6.



Table 2-2: UNIQUAC r and q parameters fitted to experimental data. The values of parameters in bold have been changed from the original version of the model.

Species	r	q
H <sub>2</sub> O	0.9200	1.4000
NH <sub>3</sub> (aq)	<b>1.6292</b>	<b>2.9852</b>
CO <sub>2</sub> (aq)	<b>0.7500</b>	<b>2.4500</b>
NH <sub>4</sub> <sup>+</sup>	4.8154	4.6028
H <sup>+</sup>	0.1378	0.1·10 <sup>-15</sup>
OH <sup>-</sup>	9.3973	8.8171
CO <sub>3</sub> <sup>2-</sup>	10.828	10.769
HCO <sub>3</sub> <sup>-</sup>	8.0756	8.6806
NH <sub>2</sub> COO <sup>-</sup>	<b>4.3022</b>	<b>4.1348</b>

Table 2-3: a and b parameters for  $C_p^0$  (J mol<sup>-1</sup> K<sup>-1</sup>) (see equation (2.22))

Species	a	b	c
NH <sub>2</sub> COO <sup>-</sup>	-203.9191	0.082259	0.55163

Table 2-4: Thermodynamic properties estimated from experimental data

Species	Standard Gibbs energy of formation (kJ mol <sup>-1</sup> )	Standard enthalpy of formation (kJ mol <sup>-1</sup> )
NH <sub>2</sub> COO <sup>-</sup>	-379.355	-502.863
NH <sub>4</sub> HCO <sub>3</sub>	-667.068	-860.928
(NH <sub>4</sub> ) <sub>2</sub> CO <sub>3</sub> ·H <sub>2</sub> O	-929.281	-1239.826
NH <sub>2</sub> COONH <sub>4</sub>	-451.153	-656.845
(NH <sub>4</sub> ) <sub>2</sub> CO <sub>3</sub> ·2NH <sub>4</sub> HCO <sub>3</sub>	-2027.327	-2675.323

Table 2-5:  $u_{ij}^0 = u_{ji}^0$  parameters for calculating UNIQUAC interaction energy parameters ( $u_{ij} = u_{ij}^0 + u_{ij}^T (T - 298.15)$ ).

The values of parameters in bold have been changed from the original version of the model

Species	H <sub>2</sub> O	NH <sub>3</sub>	CO <sub>2</sub> (aq)	NH <sub>4</sub> <sup>+</sup>	H <sup>+</sup>	OH <sup>-</sup>	CO <sub>3</sub> <sup>2-</sup>	HCO <sub>3</sub> <sup>-</sup>	NH <sub>2</sub> COO <sup>-</sup>
H <sub>2</sub> O	0								
NH <sub>3</sub>	<b>594.72</b>	<b>1090.8</b>							
CO <sub>2</sub> (aq)	<b>8.8383</b>	2500.0	<b>302.25</b>						
NH <sub>4</sub> <sup>+</sup>	<b>52.7305</b>	<b>785.98</b>	<b>-424.01</b>	0					
H <sup>+</sup>	10000	10 <sup>9</sup>	10 <sup>9</sup>	10 <sup>9</sup>	0				
OH <sup>-</sup>	600.50	<b>1733.9</b>	2500.0	1877.9	10 <sup>9</sup>	1562.9			
CO <sub>3</sub> <sup>2-</sup>	361.39	<b>524.13</b>	2500.0	226.60	10 <sup>9</sup>	1588.0	1458.3		
HCO <sub>3</sub> <sup>-</sup>	577.05	<b>534.01</b>	<b>526.305</b>	505.55	10 <sup>9</sup>	2500.0	800.01	771.04	
NH <sub>2</sub> COO <sup>-</sup>	<b>28.2779</b>	<b>498.15</b>	2500.0	<b>44.849</b>	10 <sup>9</sup>	2500.0	2500.0	<b>613.25</b>	<b>3343.1</b>

Table 2-6:  $u_{ij}^T = u_{ji}^T$  parameters for calculating UNIQUAC interaction energy parameters ( $u_{ij} = u_{ij}^0 + u_{ij}^T (T - 298.15)$ ).

The values of parameters in bold have been changed from the original version of the model

Species	H <sub>2</sub> O	NH <sub>3</sub>	CO <sub>2</sub> (aq)	NH <sub>4</sub> <sup>+</sup>	H <sup>+</sup>	OH <sup>-</sup>	CO <sub>3</sub> <sup>2-</sup>	HCO <sub>3</sub> <sup>-</sup>	NH <sub>2</sub> COO <sup>-</sup>
H <sub>2</sub> O	0								
NH <sub>3</sub>	<b>7.1827</b>	<b>7.0912</b>							
CO <sub>2</sub> (aq)	<b>0.86293</b>	0	<b>0.35870</b>						
NH <sub>4</sub> <sup>+</sup>	<b>0.50922</b>	<b>6.1271</b>	<b>8.6951</b>	0					
H <sup>+</sup>	0	0	0	0	0				
OH <sup>-</sup>	8.5455	<b>0.1364</b>	0	0.34921	0	5.6169			
CO <sub>3</sub> <sup>2-</sup>	3.3516	<b>4.9305</b>	0	4.0555	0	2.7496	-1.3448		
HCO <sub>3</sub> <sup>-</sup>	-0.38795	<b>5.3111</b>	<b>-3.7340</b>	-0.00795	0	0	1.7241	-0.01981	
NH <sub>2</sub> COO <sup>-</sup>	<b>8.0238</b>	<b>6.6532</b>	0	<b>12.047</b>	0	0	0	<b>3.0580</b>	<b>-15.920</b>

The parameters are valid for a temperature up to 150 °C and for a concentration range up to 100 molal ammonia. Data at higher temperature (up to 200 °C) and higher molality of ammonia have been used but their limited number does not allow for guarantying the model is reliable.

## 2.5 *Experimental data used for the estimation of the parameters and results*

Besides the weighting factors, the choice of the experimental data that are used for the fitting is the second crucial factor for a good fitting. It is important to analyze the data thoroughly and to discard the ones that are not accurate and would lead to wrong parameters. This can be done in several ways. A literature study often provides information about the quality of the data if they are not too recent to be analyzed. Another obvious way is too compare data from different publications at similar conditions. This is not often possible. The data can then be analyzed by themselves. The reported experimental uncertainty, the details regarding the experiments and the trend of the data with an experimental parameter are good criteria regarding the quality of the data. It is sometimes necessary to make choices, as two sets of data are contradictory and would disturb the optimization process. This was the case of the SLE data, as it has been explained by Thomsen and Rasmussen (1999).

As stated by Thomsen and Rasmussen (1999), the accuracy of vapor pressure measurements using modern equipment is up to  $\pm 5\%$  (Rumpf *et al.*, 1994). The typical uncertainty of partial pressure measurements is 5-10% and can be as high as 15% in some experimental conditions (Göppert *et al.*, 1988). Hence, it can not be expected that a model reproduces partial pressure data with a deviation lower than 10%.

More than 3700 experimental data on the carbon dioxide-ammonia-water system from various publications have been used in this work in order to fit the parameters. In order to extend the valid temperature range and to improve the accuracy of the model, additional VLE data as well as new types of experimental data have been used during the parameter estimation compared to the original version of the model. The following sections describe the experimental data that have been used and the deviation between the calculations from the model and the experimental measurements. If nothing else is stated, the deviation is calculated as the average relative deviation as shown in equation (2.41).

$$\text{Dev} = 100 \left( \frac{\sum_{i=1}^N \frac{|\text{Exp}_i - \text{Cal}_i|}{\text{Exp}_i}}{N} \right) \quad (2.41)$$

### 2.5.1 Binary NH<sub>3</sub>-H<sub>2</sub>O data

Experimental data for the binary NH<sub>3</sub>-H<sub>2</sub>O system are necessary to model the properties of ternary mixtures. Binary NH<sub>3</sub>-H<sub>2</sub>O VLE data come from various publications. The data used to estimate the parameters include some that were not used by Thomsen and Rasmussen in the original version of the

model. These data were included in order to enlarge the valid temperature range of the parameters beyond the 110 °C limit of the original model. In total, more than 750 VLE data points for this binary system were used for the parameter estimation.

Not all the data found were used for the parameter estimation. Some were discarded based on evaluation. As stated by Thomsen and Rasmussen (1999), some data from Rizvi *et al.* (1985) at low temperature and pressure are quite scattered. Therefore these data points were not used to estimate the parameters. In addition, two data points at high temperature and high molality of ammonia (over 200 mol kg<sup>-1</sup>) were also discarded. One data point from Gillespie *et al.* (1987) at high temperature (176 °C) and high molality of ammonia (207 mol kg<sup>-1</sup>) was discarded. A single data point from Sassen *et al.* (1990) at high temperature (181 °C) and high molality of ammonia (222 mol kg<sup>-1</sup>) was discarded. Two data points from Mallet *et al.* (1897) at low temperature (-20 °C) and high molality of ammonia were discarded. Ten data points from Postma *et al.* (1920) at low temperature (less than -20 °C) were also discarded.

The description of the vapor-liquid equilibrium data for the ammonia-water system and the results from the total pressure calculations are included in Table 2-7. The data cover a temperature range from -9 to 200 °C. They cover a large range for the concentration of ammonia. The mass fraction range that is especially relevant for the carbon dioxide capture process using aqueous ammonia (5-30 wt%) is well represented.

The overall deviation between the experimental and calculated pressure is within our estimate of the experimental uncertainty and is therefore satisfactory. The average deviation between the calculations from the original model with the experimental data used in the fitting of the original parameters is also included. The deviation with the new set of parameters is very close to the one obtained with the original model while the number of data points used for the estimation has been multiplied by a factor of four.

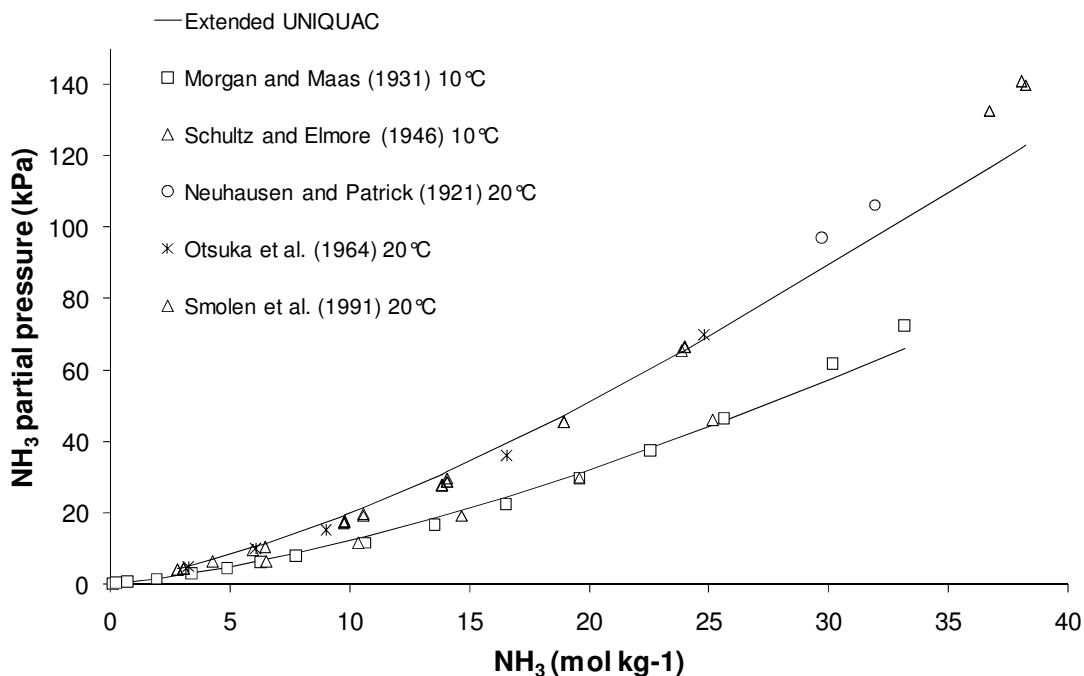
**Table 2-7: Results for the total vapor pressure of the binary water-ammonia system**

Wt% NH <sub>3</sub>	T, °C	P, MPa	Source	N	Deviation
0.34-35	0-25	0-0.1	Morgan and Maass (1931)	53	7.0 %
23-65	0-50	0.1-0.5	Neuhausen and Patrick (1921)	31	18.2%
0.51-26	60-147	0.05-1.6	Clifford and Hunter (1933)	46	4.0%
0.84-1.7	25	0-0.005	Abegg and Riesenfeld (1902)	2	0.49%
9.3-17	40-80	0.03-0.25	Kurz <i>et al.</i> (1995)	6	6.6%

20-30	0-60	0-0.3	Mittasch <i>et al.</i> (1926)	20	4.3%
9.2-30	10-35	0-0.1	Schultz and Elmore (1946)	10	8.0%
9.2-97	30-170	0.05-12.4	Rizvi (1985)	187	6.4%
1.3-99	40-176	0-11.1	Gillespie <i>et al.</i> (1987)	188	6.7%
3.3-31	100-200	0.18-3.1	Müller <i>et al.</i> (1988)	79	5.3%
2.2-33	100-150	0.4-2.4	Pawlikowski <i>et al.</i> (1982)	13	6.4%
3.0-30	20-100	0-0.3	Otsuka <i>et al.</i> (1960)	9	7.9%
3.1-23	40-70	0.1	Verbrugge (1979)	7	3.0%
12-51	0-120	0.12-0.93	Mollier (1908 and 1909)	34	9.1%
3.3-95	20-140	0-3.1	Smolen (1991)	188	6.9%
20-68	130-180	1.3-6.2	Guillevic <i>et al.</i> (1985)	13	7.2%
0-4.0	100-147	0.1-0.45	Polak and Lu (1975)	23	1.9%
18-79	18-194	1.2-13.5	Sassen <i>et al.</i> (1990)	50	4.4%
9.3-89	35-200	0.2-14.4	Harms-Watzenberg (1995)	35	6.2%
1.0	0-70	0.4-3.3	Cragoe <i>et al.</i> (1920)	15	10.7%
5.2-9.4	40-100	0.01-0.3	Rumpf <i>et al.</i> (1993b)	9	4.1%
1.2-17	40-120	0-0.55	Kurz (1994)	156	3.1%
48-88	112-200	0.7-14.5	Iseli (1985)	41	5.5%
4.9-9.3	40-120	0.02-0.45	Rumpf <i>et al.</i> (1999)	6	3.0%
18-82	60-100	0.16-2	Inomata <i>et al.</i> (1988)	8	7.5%
1.0-78	50-182	0-3.2	Jennings (1965)	68	5.7%
12-54	-9-53	0.05-0.1	Postma (1920)	14	14.5%

Total number of points and average deviation	1311	6.2%
Total number of points considered in the original model and average deviation with the original parameters	296	4.9%

Figure 2-1 plots the partial pressure of ammonia as a function of the molality of ammonia for ammonia-water mixtures at 10 and 20 °C, together with experimental data. A very good agreement can be seen until a high molality of ammonia. This shows that the model can accurately describe the volatility of ammonia for binary mixtures.



**Figure 2-1: Results for the partial pressure of ammonia as a function of the molality of ammonia for ammonia-water mixtures at 10 and 20 °C calculated with the model and experimental data**

Various kinds of enthalpy measurement data have also been used for the estimation of the parameters for the NH<sub>3</sub>-H<sub>2</sub>O binary system. Our analysis of the thermodynamic data revealed that some data points from these publications should be discarded from the data set used for the parameter estimation. Four data points from measurements of enthalpy of dilution from Berthelot *et al.* (1875) were discarded. In addition, one heat capacity data point from Wrewsky *et al.* (1924a) at 20 °C was discarded as they were

giving very high deviations with calculations from the model. The enthalpy of solution and excess enthalpy data from Mollier *et al.* (1908) and from Ramstetter *et al.* (1931) gave very high deviation with calculations from the model. The excess enthalpy measurements from Staudt (1984) were used in the parameter estimation but were given a low weight.

The details related to the heat capacity and the enthalpy of dilution data and the deviation between the experimental measurements and the model calculations are included in Table 2-8 and Table 2-9. The enthalpy of solution data from Wrewsky *et al.* (1924a) have been converted to enthalpy of dilution. The results obtained with the original parameters have also been included.

Figure 2-2 plots the experimental measurement of the enthalpy of dilution of aqueous ammonia solution from different publications at various temperatures and molalities of ammonia against the calculation from the Extended UNIQUAC model. The 10% deviation slopes have also been included. It shows that for most of the data, the deviation of model calculations from the experimental data is below 10% and is therefore satisfactory.

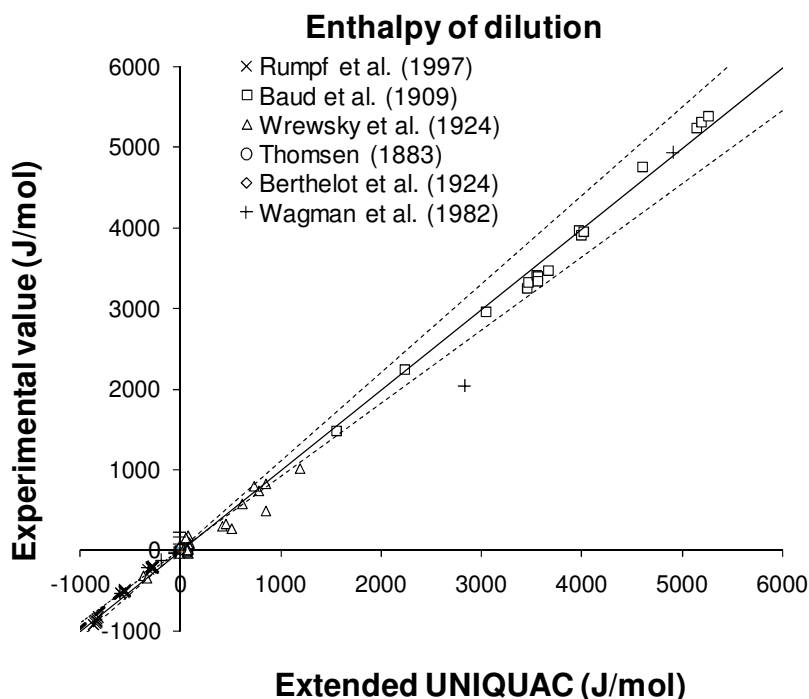


Figure 2-2: Results for the enthalpy of dilution data. The experimental results are plotted against the calculation from the model for the different sources

**Table 2-8: Results for the heat capacity of ammonia solutions**

Wt% NH <sub>3</sub>	T, °C	Source	N	Deviation
1.4-40	2-60	Wrewsky (1924b)	22	12.9%
0.88-4.0	18	Gawlick (1934)	8	10.8%
Total number of points and average deviation			30	10.9%

**Table 2-9: Results for the enthalpy of dilution of ammonia solutions**

Wt% NH <sub>3</sub>	T, °C	Source	N	Average absolute deviation (J mol <sup>-1</sup> )
23	18	Thomsen (1883)	3	185
14-49	14	Berthelot (1875)	6	225
1.7-24	287	Wrewsky (1924)	69	85.3
9.3-23	39-100	Rumpf (1997)	27	52.3
18-80	13	Baud (1909)	21	161
	25	Wagman <i>et al.</i> (1982)	13	169
Total number of points and average deviation			139	106
Total number of points considered in the original model and average deviation with the original parameters			97	111

## 2.5.2 Binary CO<sub>2</sub>-H<sub>2</sub>O data

The use of binary data for the CO<sub>2</sub>-H<sub>2</sub>O system was also necessary in this study. Even if the parameters used in the model were determined by Garcia *et al.*, it was important to test the performance of the model for this system for the different properties. Not all the data found in the published literature were used during the parameter estimation. Some of the experimental data were discarded after evaluation.



Diamond *et al.* (2003) reviewed the data from 25 experimental studies on solubility of CO<sub>2</sub> in water in the temperature range 0-25 °C and pressure up to 100 MPa. Garcia *et al* supplemented this review by including data at temperatures up to 250 °C. The choice of the binary CO<sub>2</sub>-H<sub>2</sub>O VLE data used for the parameter estimation was inspired by these studies.

As suggested by Diamond *et al.* (2003) and Garcia *et al.* (2006), the data from Wroblewski (1883), Sander (1912), Hähnel (1920), Kritschewsky *et al.* (1935), Vilcu and Gainar (1967), Stewart and Munjal (1970), Teng *et al.* (1997), and Servio and Englezos (2001) were discarded as they were considered to have a very low accuracy. The original data from Oleinik and Shagiakhmetov mentioned by Diamond were not found, and the data were therefore discarded as done by Garcia. The data from Kiepe *et al.* (2002) were not analyzed by Diamond *et al.* They were discarded in the work of Garcia *et al.* and in this work, as they seemed to be inaccurate. The data from Takenouchi and Kennedy (1965) were discarded as well as the experimental temperatures were beyond the model temperature range. The single data point from Hayduk (1971) was considered neither by Diamond *et al.* nor Garcia *et al.* This point was discarded from the data set used for the parameter estimation. In addition, as in the work of Garcia *et al.*, one data point at 146 °C from Cramer *et al.* (1982) was discarded due to doubts about its accuracy.

The list of experimental vapor-liquid equilibrium data that were used for parameter estimation and the deviation between the experimental and calculated total pressures can be found in Table 2-10. The list of experimental heat capacity data and the deviation from the model can be found in Table 2-11. The results obtained with the original parameters have also been included.

The description of the gas hydrate formation data that were used during the parameter estimation can be found in Table 2-12. The deviations were calculated using equation (2.41). Overall it can be stated that the model is able to describe accurately the properties of the binary carbon dioxide-water system.

**Table 2-10: Results for the total vapor pressure of the binary water-carbon dioxide system**

wt% CO <sub>2</sub>	T, °C	P, MPa	Source	N	Deviation
0.13-0.22	25	0.1	Geffcken (1904)	14	3.2%
0.87-3.8	100-120	2.3-11.1	Prutton and Savage (1945)	7	6.4%
2.2-5.0	0-5	0.8-2.1	Malegaonkar <i>et al.</i> (1997)	9	1.3%
0.04-0.35	0-45	0.1	Harned and Davis (1943)	18	1.3%
0-0.03	0-80	0-0.1	Dunsmore and Nancollas (1964)	63	0.5%
0-0.35	0-40	0.1	Markham and Kobe (1941)	4	1.4%

0.09-0.18	25-45	0.1	Yeh and Peterson (1964)	4	4.0%
0.02-0.2	0-25	0-0.18	Morgan and Maass (1931)	19	3.7%
0.44-3.4	30-60	0.9-4.0	Matous <i>et al.</i> (1969)	13	1.8%
0.04-0.22	13-76	0.1	Morrison and Billett (1952)	19	10.1%
0.09-0.31	0-35	0.1	Murray and Riley (1971)	8	2.8%
0.09-1.3	50-200	0.1-4.6	Zawisza and Malesinska (1981)	33	3.8%
0.44-3.8	80-200	2.3-10.2	Nighswander <i>et al.</i> 1989	33	5.4%
0.09-2.6	100-200	0.3-8.1	Müller <i>et al.</i> (1988)	48	1.9%
3.2	110-200	10	Takenouchi and Kennedy (1964)	3	2.9%
0.87-3.8	50	1-5.8	Rumpf B <i>et al.</i> (1994)	7	0.6%
0.44	170	2.5	Ellis and Golding (1963)	1	9.4%
0.04-0.22	15-55	0.1	Postigo <i>et al.</i> (1978)	5	7.1%
0.13-0.35	0-25	0.1	Kiss <i>et al.</i> (1937)	3	3.4%
0.87-5.0	50-100	2.5-12.7	Wiebe and Gaddy (1939)	13	4.4%
2.2-7.0	12-40	2.5-10.2	Wiebe and Gaddy (1940)	23	16.8%
0.22-2.2	10-30	0.1-2.03	Bartholomé and Hans (1956)	15	4.0%
0.09-2.6	0-50	0.1-0.9	Wasmund and Bultmann (1980a)	64	4.8%
0.09-2.6	0-50	0.1-0.9	Wasmund and Bultmann (1980b)	65	5.2%
0.18-3.8	0-15	0-2.2	Anderson (2002)	53	2.0%
3.0-5.4	25	2.2-5.3	Yang <i>et al.</i> (2000)	7	5.5%
0-0.18	10-40	0.01-0.1	Novak <i>et al.</i> (1961)	23	1.9%
0.13	20	0.1	Curry and Hazelton (1938)	4	5.7%
0.13	20-25	0.1	van Slyke (1939)	6	2.0%

1.3-5.0	20-50	5	Malinin and Kurovskaya (1975)	5	6.2%
2.2-5.0	20-65	5	Malinin and Savelyeva (1972)	14	5.4%
0.35-5.0	0-100	0.1-9.5	Zelvenskii (1937)	95	4.2%
2.6-5.0	50-80	4-13.1	Bamberger <i>et al.</i> (2000)	29	2.6%
0.13-0.44	20-45	0.1	Kunerth (1922)	8	2.2%
0-0.13	5-65	0.05-0.09	Zheng <i>et al.</i> (1997)	10	1.4%
0.44-1.3	30-200	0.8-4.1	Cramer (1982)	10	5.1%
0.04-0.22	115-200	0.5-1.8	Ellis (1959)	11	6.2%
0.22-6.2	15-95	0.7-10.1	Gillespie and Wilson (1981)	14	6.1%
Total number of points and average deviation				780	4.0%
Total number of points considered in the original model and average deviation with the original parameters				104	3.7%

**Table 2-11: Results for the apparent heat capacity data of the binary water-carbon dioxide system**

Wt% CO <sub>2</sub>	T, °C	Source	N	Deviation
0.05-0.43	25	Barbero (1983)	10	1.97%

**Table 2-12: Description of the gas hydrate formation data of the binary water-carbon dioxide system**

T, °C	Source	N
0-6	Dholabhai (1993)	4
0-10	Harvey (1987)	9
2-6	Dholabhai (1996)	2
0-9	Wendland (1999)	7
Total number of points and average deviation		22

### 2.5.3 Ternary data

Ternary data are of crucial importance to fit the parameters. In particular the parameters related to the ammonium carbamate ion were found to have a great influence on the equilibrium compositions. More than 1000 data points of VLE data were used over a wide range of temperatures, CO<sub>2</sub> loadings and molalities of ammonia and carbon dioxide. The list of experimental vapor-liquid equilibrium data that were used for parameter estimation and the deviation between the experimental and calculated vapor pressures can be found in Table 2-13. Only partial pressures of carbon dioxide and ammonia superior to 50 kPa and with a mole fraction in the gas phase higher than 0.08 were used in the calculation of the deviation. The reason is that according to Göppert and Maurer the reported partial pressures of ammonia are uncertain due to experimental difficulties at high temperature and high loading. The experimental uncertainties are caused both by the measurement of the partial pressure of ammonia, where the uncertainty is typically higher than 10%, and by the measurement of the molality of carbon dioxide in the solution that can lead to an additional deviation up to 5%. The results obtained with the original parameters have also been included. It can be seen that the results for the partial pressure of both carbon dioxide and ammonia are essentially equivalent for both versions. The original model covered most of the data point where the partial pressures were indicated and respected the criteria mentioned above. However, the deviation for the total pressure is slightly higher for the new version of the model than for the original version. This can be explained by the higher uncertainty of the experimental measurements at high temperature that are not considered in the original version of the model. As it can be seen in Table 2-13, data for temperatures up to 200 °C were included in the parameter estimation.

The data from Mezger *et al.* (1929) agree very poorly with comparable literature data. The four data points were therefore discarded. As reported by Thomsen and Rasmussen, the nine data points from Pawlikowski *et al.* (1982) deviate significantly from model calculations, both with respect to total and partial pressures. The total pressures given by Pawlikowski *et al.* are systematically higher than the calculated total pressures and the data are quite scattered compared to data from other publications. As stated by Thomsen and Rasmussen, some data points from Pexton (1938) and van Krevelen (1949) only reported one partial pressure and were discarded during the parameter estimation. When only the water pressure was missing, the water pressure was calculated as the saturated pressure of pure water and added to obtain a usable total pressure. According to Kurz *et al.* (1995), some of the pressures reported by Göppert and Maurer at 60 and 80 °C were measured while a solid phase was present in equilibrium. The same remark applies for 10 data points from Kurz *et al.* (1995). Hence, these data points were not used during the parameter estimation. Calculations with the Extended UNIQUAC model are in agreement with these observations. Some data from Verbrugge at 40 °C and low molality of ammonia and carbon dioxide only agree poorly with literature data. Hence, 21 data points were discarded. The experimental data points at higher temperature and molality of ammonia were used for the estimation of the parameters.

There is a large amount of ternary data experiments used for the fitting of the parameters. The typical concentration of ammonia used during the capture process (5-30 wt%) are well covered by the data. There is a significant amount of data at high temperature. It allows for being confident about the performance of the model at desorber conditions. However, no ternary data for temperature lower than 20 °C was used during the parameter estimation.

**Table 2-13: Results for the vapor pressures of the ternary carbon-dioxide-ammonia -water system**

Wt% NH <sub>3</sub>	Wt% CO <sub>2</sub>	T, K	P, MPa	Source	P	N	Deviation
0.83-3.41	0.43-5.7	20-60	0-0.075	Van Krevelen <i>et al.</i> (1949)	P (Total)	25	5.6%
					P(CO <sub>2</sub> )	1	20.2%
0.22-3.3	0.12-7.9	20-40	0-0.02	Pexton <i>et al.</i> (1938)	P (Total)	68	6.1%
					P(CO <sub>2</sub> )	1	0.14%
7.8-16	2.0-22	40-80	0.01-0.7	Kurz <i>et al.</i> (1995)	P (Total)	47	5.8%
					P(NH <sub>3</sub> )	13	2.8%
					P(CO <sub>2</sub> )	16	10.3%
0.80-21	0.74-29	60-120	0-7	Göppert and Maurer (1988)	P (Total)	530	6.6%
					P(NH <sub>3</sub> )	115	12.6%
					P(CO <sub>2</sub> )	462	9.5%
3.8-29	0.81-29	100-200	0.1-9.1	Müller (1988)	P (Total)	253	7.1%
					P(NH <sub>3</sub> )	201	15.3%
					P(CO <sub>2</sub> )	213	13.1%
1.5-20	1.3-17	20-100	0-0.26	Otsuka (1960)	P (Total)	60	11.8%
					P(NH <sub>3</sub> )	12	22.0%
					P(CO <sub>2</sub> )	5	40.3%

0.29-32	0.15-30	40-90	0.1	Verbrugge (1979)	P(Total)	71	6.1%
					P(NH <sub>3</sub> )	26	3.2%
					P(CO <sub>2</sub> )	1	0.59%
Total number of points and average deviation					P(Total)	1054	6.9%
					P(NH <sub>3</sub> )	367	13.8%
					P(CO <sub>2</sub> )	699	10.9%
Total number of points considered in the original model and average deviation with the original parameters					P(Total)	791	4.6%
					P(NH <sub>3</sub> )	367	12%
					P(CO <sub>2</sub> )	632	11%

Regarding the modeling of the CO<sub>2</sub> capture process, it is very important that the model describes accurately the partial pressure of ammonia and carbon dioxide in the absorber in order to assess correctly the amount of vaporized ammonia and the efficiency of the carbon dioxide absorption. Figure 2-3 and Figure 2-4, plot the calculated partial pressure of ammonia and carbon dioxide as a function of the molality of carbon dioxide at different molalities of ammonia at 20 °C together with experimental measurements. Figure 2-5 plots the calculated partial pressure of ammonia in ternary mixtures at 20 °C against the experimental data from Otsuka *et al.* (1960). The data are available at for a molality of ammonia up to 15 mol/kg water. The very good agreement between the calculation of the model and the experimental data show that the model is able to describe accurately the partial pressure of ammonia and carbon dioxide at low temperature and high concentration.

Figure 2-6 and Figure 2-7 plot the calculated partial pressures of ammonia and carbon dioxide as a function of the molality of carbon dioxide at different molalities of ammonia at 40 °C. It shows again a very good agreement between the model and the experiments and shows the ability for the model to describe accurately the partial pressures of ammonia and carbon dioxide during the absorption at that temperature. This is an important result, as this temperature could potentially be reached in some part of the absorber in the case of the carbon dioxide with aqueous ammonia without precipitation.

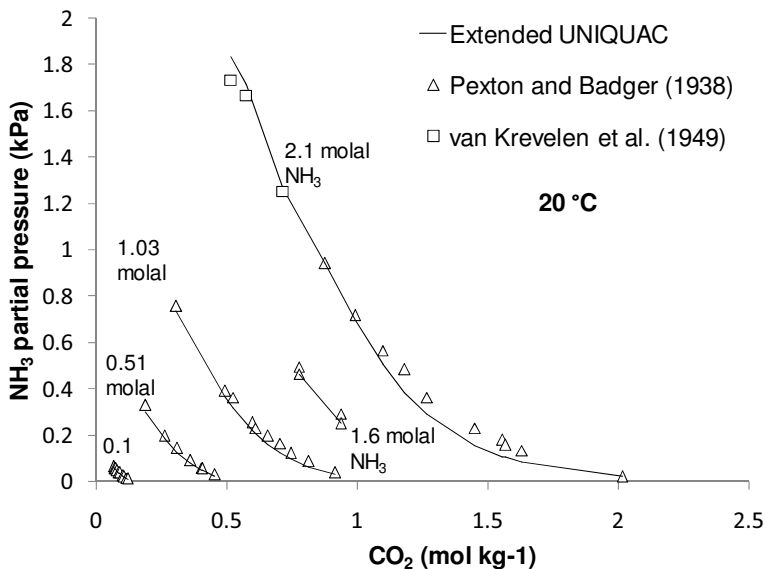


Figure 2-3: Partial pressure of ammonia for carbon dioxide-ammonia-water mixtures at 20 °C for different molalities of ammonia calculated with the model, and experimental data

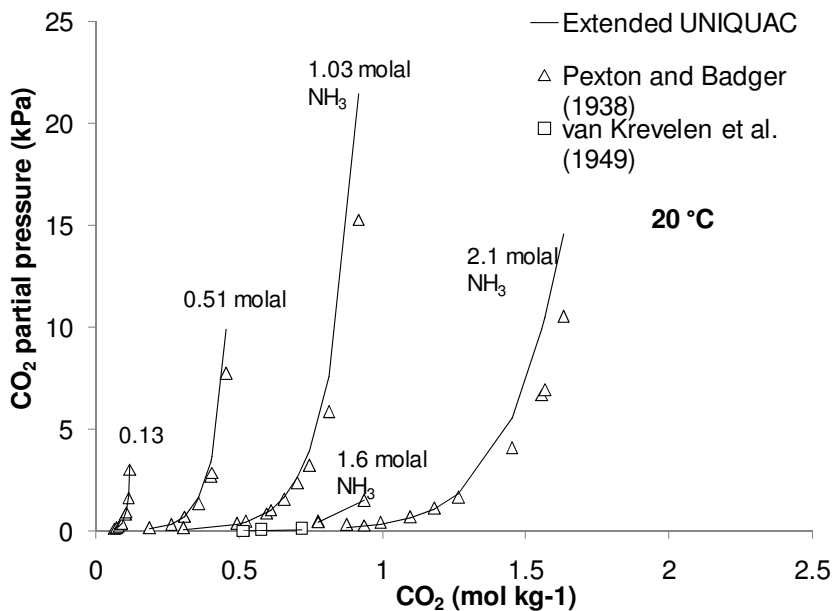


Figure 2-4: Partial pressure of carbon dioxide for carbon dioxide-ammonia-water mixtures at 20 °C for different molalities of ammonia calculated with the model, and experimental data

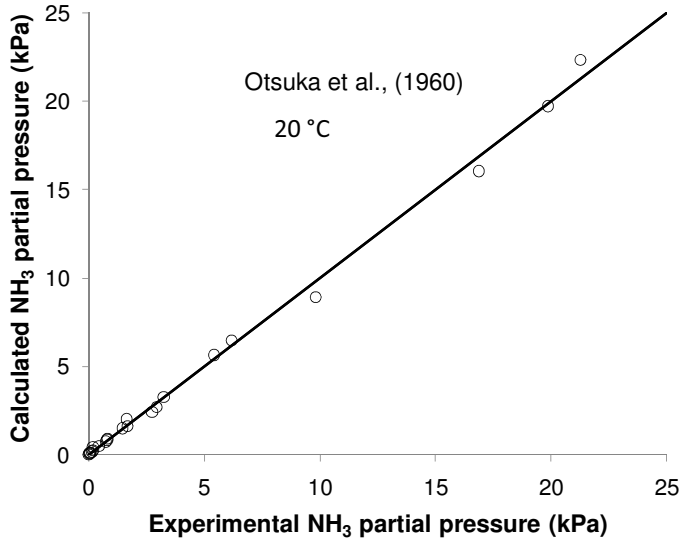


Figure 2-5: Partial pressure of ammonia for carbon dioxide-ammonia-water mixtures at 20 °C for different molalities of ammonia. Calculation with the model against experimental data from Otsuka *et al.* (1960)

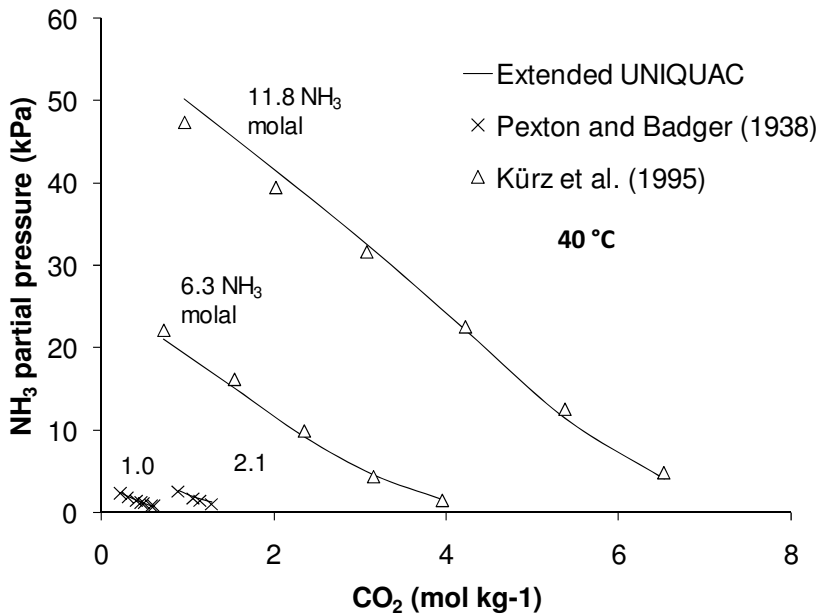
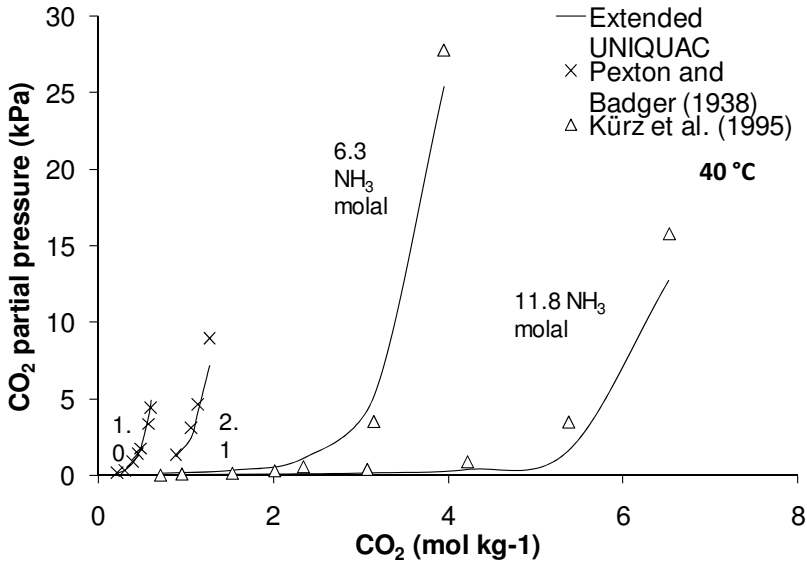


Figure 2-6: Partial pressure of ammonia for carbon dioxide-ammonia-water mixtures at 40 °C for different molalities of ammonia calculated with the model, and experimental data





**Figure 2-7: Partial pressure of carbon dioxide for carbon dioxide-ammonia-water mixtures at 40 °C for different molalities of ammonia calculated with the model, and experimental data**

A precise modeling of the pressures at high temperature is very important for the simulation of the desorber in the carbon dioxide capture process. Figure 2-8 and Figure 2-9 show respectively the partial pressure of carbon dioxide and ammonia for carbon dioxide-ammonia-water mixtures at 100 °C at various molalities of ammonia and carbon dioxide together with experimental data. It shows a good agreement between the model and the experimental data at that temperature.

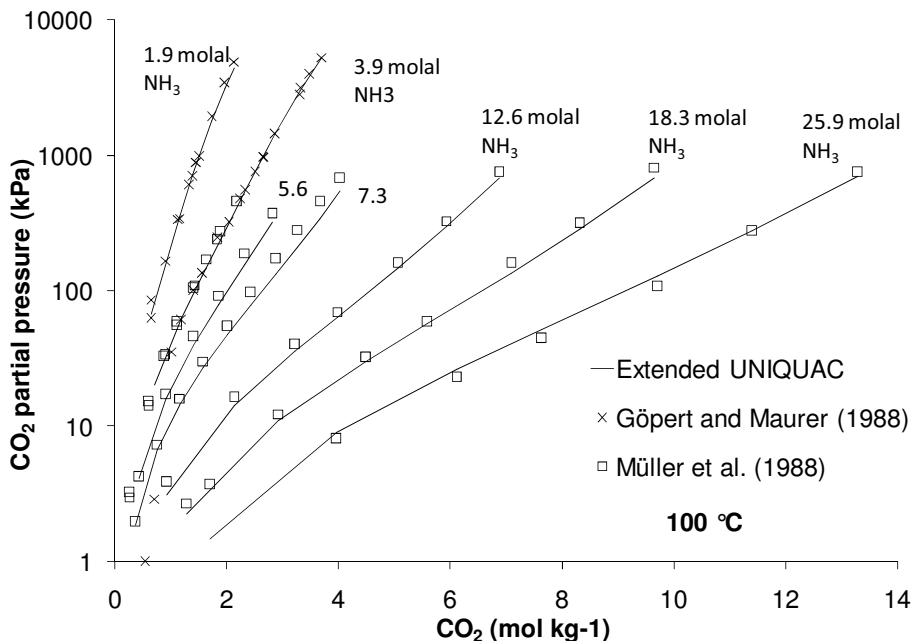


Figure 2-8: Partial pressure of carbon dioxide in carbon dioxide-ammonia-water mixtures at 100 °C for different molality of ammonia calculated with the model, and experimental data

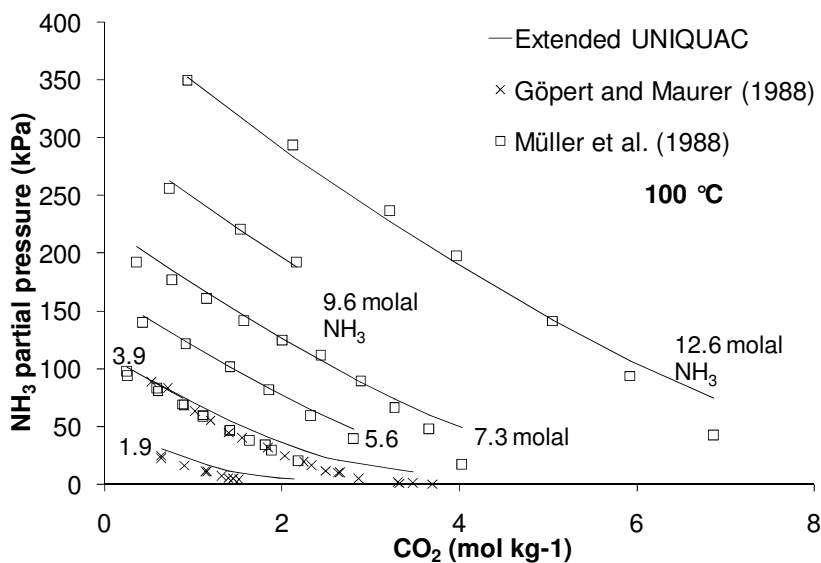
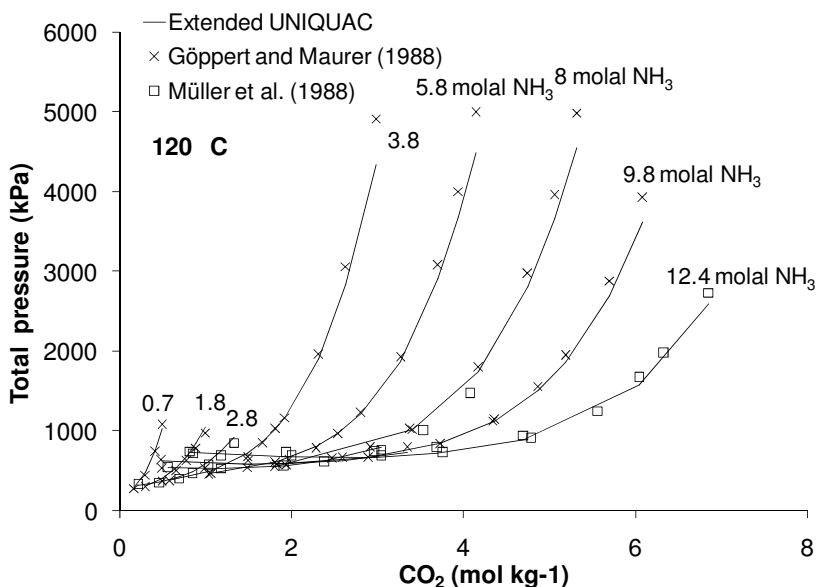
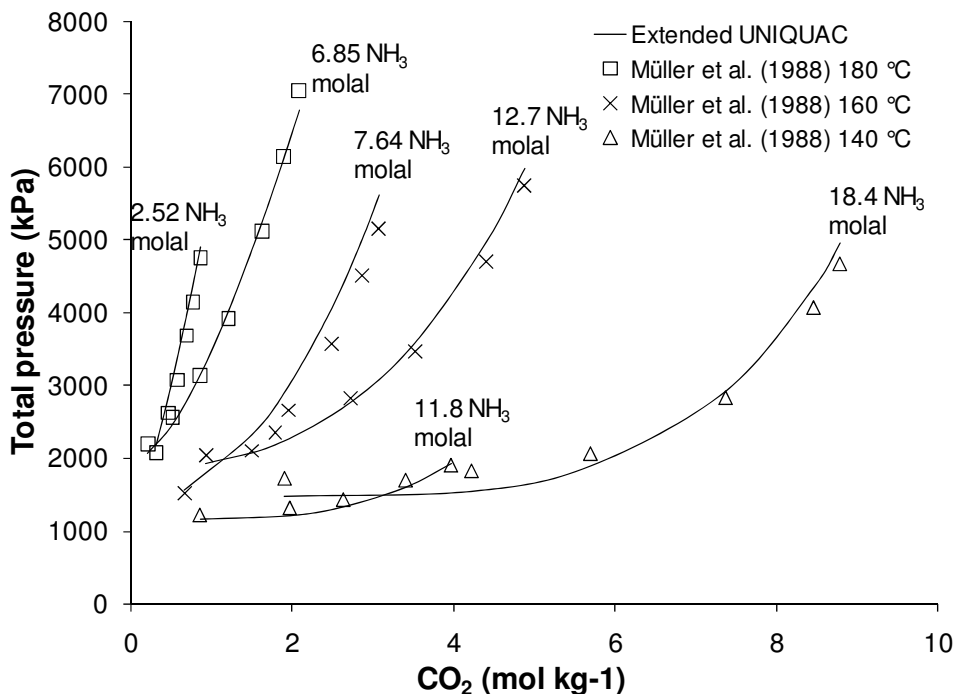


Figure 2-9: Partial pressure of ammonia in carbon dioxide-ammonia-water mixtures at 100 °C for different molality of ammonia calculated with the model, and experimental data

Some deviations can be observed for the partial pressure of ammonia at high molality of carbon dioxide and ammonia and high temperature (above 100 °C), where the partial pressure of ammonia is low while the total pressure reaches high level and increases rapidly. Similar deviations were reported by Göppert and Maurer (1988) when they modeled the experimental data measured by Kurz *et al.* (1995). As explained above, the uncertainty regarding the measurement of the partial pressure of ammonia at high temperature and high loading is uncertain. Figure 2-10 and Figure 2-11 show the total pressure of carbon dioxide-ammonia-water mixture at 120 °C, and at 140, 160 and 180 °C at different molalities of ammonia and carbon dioxide together with experimental data (Göppert and Maurer, 1988 and Müller *et al.*, 1988). It can be observed that the agreement between the model and the experimental measurements for the total pressure at temperatures up to 180 °C is satisfactory.



**Figure 2-10: Total pressure of carbon dioxide-ammonia-water mixtures at 120 °C for different molalities of ammonia calculated with the model, and experimental data (Müller *et al.*, 1988)**



**Figure 2-11: Total pressure of carbon dioxide-ammonia-water mixtures at 140, 160 and 180 °C for different molality of ammonia calculated with the model, and experimental data (Müller *et al.*, 1988)**

Solid-Liquid equilibrium data have also been used to fit the parameters. Similarly to the original version of the model, only the data from Jänecke *et al.* (1929a and 1929b) were used for the parameter estimation. The data from Guyer and Piechowicz, Terres and Behrens (1938), and Terres and Weiser (1921) are in disagreement with the nature of the salts formed.

Figure 2-12 plots the Extended UNIQUAC model calculations for the solubility isotherm for the carbon dioxide-ammonia-water system at 40 °C. Experimental data from Jänecke (1929a and 1929b) have been plotted as well. Figure 2-13 plots the phase diagram from 0 to 94 °C calculated with the Extended UNIQUAC model as well as the experimental data from various publications. The agreement with the data from Jänecke is satisfactory.

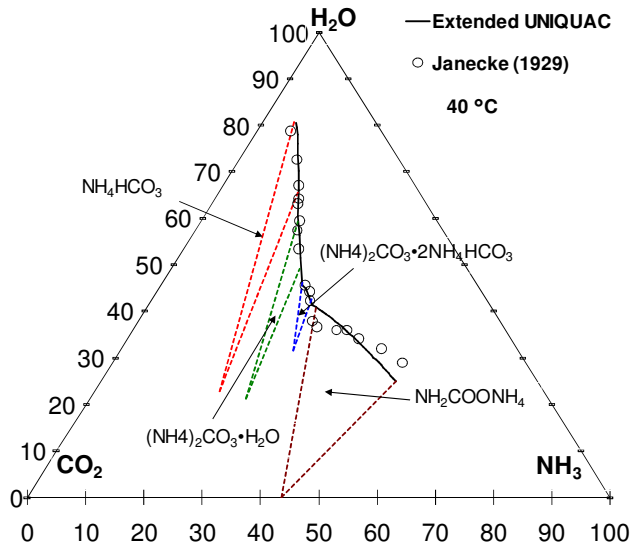


Figure 2-12: Solubility isotherm in the carbon dioxide-ammonia-water system at 40 °C. Tie lines connect each part of the isotherm to the points that correspond to the composition of the solid phase. The unit is mass %. Experimental data from Jänecke have been added.

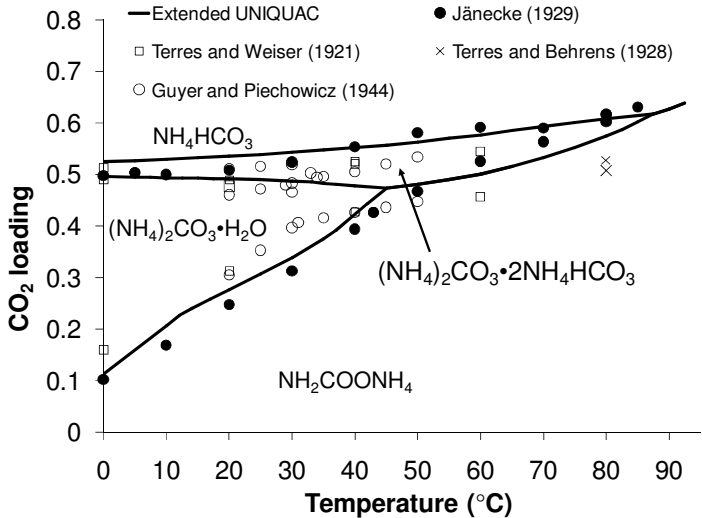


Figure 2-13: Phase diagram for the carbon dioxide-ammonia-water system from 0 to 94 °C. The ordinate is the CO<sub>2</sub> loading, defined as the molar ratio of carbon dioxide and ammonia. Experimental data have been added. It shows the calculated loadings and temperatures at which two or three solid phases are in equilibrium together with the corresponding experimental data.

Speciation data from Lichtfers (2000) were also used for parameter estimation. The data were measured at temperatures from 40 to 120 °C for mass fractions of ammonia up to 0.18. It is the molar ratio of ammonium carbamate ion and total ammonia species that has been used during the parameter estimation, as shown in equation (2.39). Some of the measurements at 40 °C seemed to be wrong. Similar sets of experiments have been done twice, giving different results. During the parameter estimation, among a total of 86 data points, eight data points at 40 and 60 °C were discarded, as the measurements were not in agreement with each other. Figure 2-14 and Figure 2-15 show the results from speciation calculated with the Extended UNIQUAC model plotted together with experimental measurement from Lichtfers at 60 °C for a molality of ammonia of 3.25 and at 120 °C for a molality of ammonia of 6.20. The agreement between the model calculations and the experimental measurements is satisfactory and shows that the model can accurately describe the speciation of carbon dioxide-ammonia-water mixtures in this temperature range.

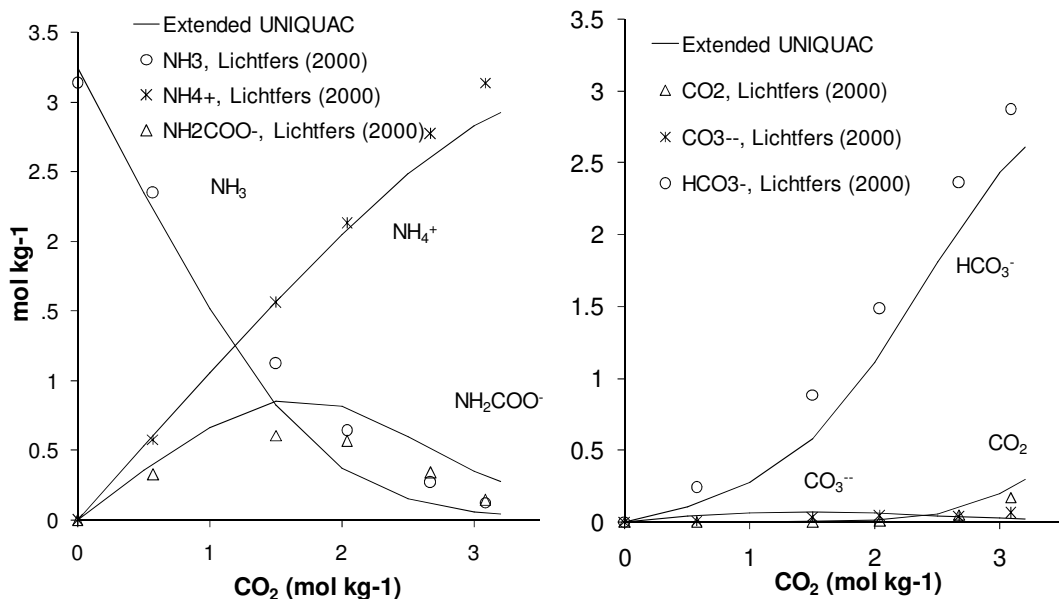
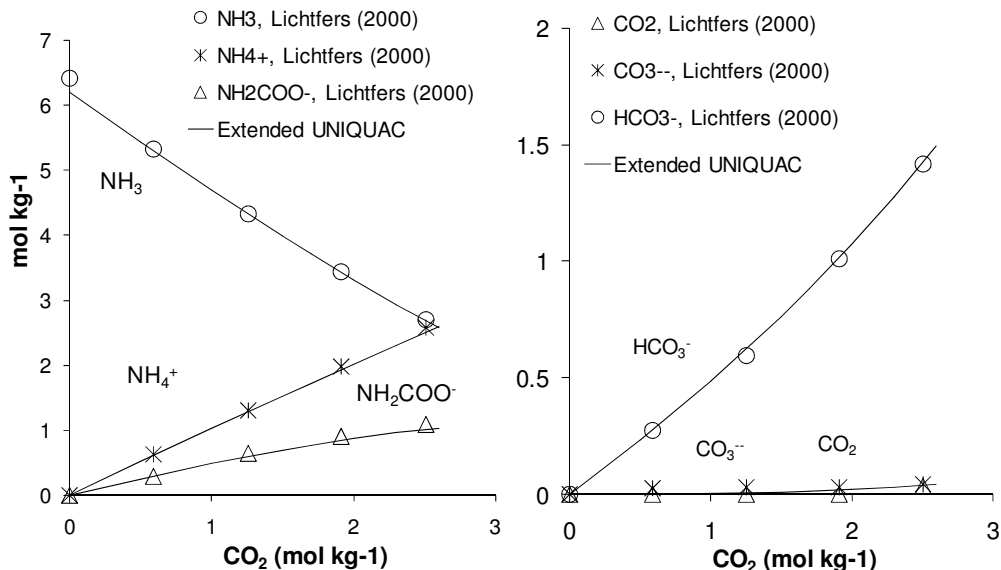


Figure 2-14: Speciation calculations expressed in molality, mol per kg water, for a mixture at T=60 °C and for m(NH<sub>3</sub>) = 3.25 mol/kg water. Experimental data from Lichtfers (2000) have been added.



**Figure 2-15: Speciation calculations expressed in mole for 1kg water for a mixture at T=120 °C and for m(NH<sub>3</sub>) = 6.20 mol/kg water. Experimental data from Lichtfers (2000) have been added**

In addition, the enthalpy measurement data from the partial evaporation of carbon dioxide ammonia and water mixtures from Rumpf *et al.* (1998) were used for the estimation of the parameters. These measurements consist of increasing the temperature of a mixture by a given figure, usually around 10 °C. The initial and final molalities of ammonia, the masses of liquid and gas leaving the calorimeter, the pressure and the enthalpy change in the calorimeter are reported. During the parameter estimation, it was chosen to use the value of the enthalpy change in the object function. The description of the experimental data and the deviation from model calculation can be found in Table 2-14. The relatively high deviation between the Extended UNIQUAC calculations and the experimental measurements may be explained by the lack of precision regarding the pressure measurement. For most of the data, the pressure measurement was given with an uncertainty higher than 1 kPa. For some of the data, the uncertainty is up to 10 kPa. The sensitivity of flash calculations to the pressure was tested by calculating the enthalpy change using the reported pressures plus 1 kPa. The enthalpy calculation increased by up to 9%. The flash calculation required for using this type of experimental data is therefore extremely sensitive to pressure. The data should have been measured with a much more accurate pressure sensor to be used for parameter estimation. Hence, it is not reasonable to expect a better agreement than 9% between the experimental results and the model calculations.

**Table 2-14: Results for the enthalpy change from the partial evaporation of carbon dioxide-ammonia-water mixtures**

Wt% NH <sub>3</sub>	T, °C	Source	N	Deviation
4-12	40-120	Rumpf (1998)	88	14.0%

The experimental measurements of the enthalpy of absorption of carbon dioxide by aqueous ammonia solutions from Qin *et al.* (2010) were not used for parameter estimation as the data were not available at that time. The data are for a mass fraction of ammonia of 2.5 wt%, at temperatures from 35 to 80 °C and for a loading from 0.05 to 1.1. The average deviation between the experimental data and the prediction from the model is 20.0%. It must be noted that two sets of experiments were reported for each of the temperatures considered and that the experimental results show large deviations between the two sets. As reported by Qin *et al.*, the repeatability of the experiments is uncertain due to the volatility of the solvent. Therefore, the uncertainty of the experiment with aqueous ammonia solutions was hard to assess, and the average deviation between the experiments and the model calculations is satisfactory. According to the results from the model, the temperature has only a low influence on the enthalpy of absorption that decreases from 85 and 65 kJ/mol CO<sub>2</sub> when the loading increases from 0 to 1 for 2.5 wt% aqueous ammonia solutions at 35 °C.

## 2.6 Conclusion

According to the results presented here, the agreement between the experimental data used for the fitting of the parameter and the calculation of the model is very satisfactory. However, to gain confidence regarding the accuracy of the model, some additional experimental data would be required. First, some VLE ternary data at low temperature would confirm that the model is capable of accurately calculate partial pressures of carbon dioxide and ammonia at absorber conditions in the context of the CAP. It should nevertheless be added that despite the lack of ternary data at low temperature, the very good fit for ternary data at 20 °C, for binary data at 10 °C and the satisfying results for the SLE at low temperature allows for believing that the model is accurate from 0 °C. Second, additional ternary enthalpy of absorption data would be a good test for the model. Furthermore, the comparison of the results of the model with new SLE data could be interesting. Finally, it would be interesting to compare the results of the model with additional speciation data.

Overall it can be stated that the upgraded version of the Extended UNIQUAC model has been shown to describe accurately the phase behavior and thermal properties for the complex system carbon dioxide-ammonia-water for a temperature range from 0 to 150 °C. This thermodynamic model therefore shows great potential regarding the modeling of the carbon dioxide capture process using aqueous ammonia. The model required fitting UNIQUAC volume and surface area parameters, binary interaction parameters as well as standard thermodynamic properties for the ammonium carbamate ion and the solids potentially formed. In total, 30 UNIQUAC parameters and 13 standard state properties were fitted to more than 3700 experimental data points from various types of experiments on this system.



## 2.7 References

- Abegg, R.; Riesenfeld, H. Über das Lösungsvermögen von Salzlösungen für Ammoniak nach Messungen seines Partialdrucks, *Zeit. für Physikalische Chemie*, **1902**, *40*, 84.
- Anderson G. K. Solubility of Carbon Dioxide in Water under Incipient Clathrate Formation Conditions. *J. Chem. Eng. Data*, **2002**, *47*, 219.
- Austgen, D. M.; Rochelle, G. T. ; Peng, X. *et al.* Model of Vapor Liquid equilibria for Aqueous Acid Gas Alkanolamine Systems using the Electrolyte NRTL Equation. *Ind. Eng. Chem. Res.*, **1989**, *28*, 1060.
- Bamberger, A.; Sieder, G.; Maurer, G. High-pressure (vapor plus liquid) equilibrium in binary mixtures of (carbon dioxide plus water or acetic acid) at temperatures from 313 to 353 K. *J. Supercrit. Fl.* **2000**, *17*, 97.
- Barbero, J. A.; Hepler, L. G.; McCurdy, K. G.; Tremaine, P. R. Thermodynamics of aqueous CO<sub>2</sub> and SO<sub>2</sub>. *Can. J. Chem.*, **1983**, *61*, 2509.
- Barker, J. A. Determination of activity coefficients from total pressure measurements. *Austral. J. Chem.* **1953**, *6*, 207.
- Bartholomé, E.; Friz, H. Löslichkeit von Kohlendioxyd in Wasser bei höheren Drucken. *Chemie Ingenieur Technik*, **1956**, *28*, 706.
- Baud, E.; Gayn L. The determination of hydrates, in solution, by thermic method application to the ammonia liquid system. *Ann.Chim.Phys.*, **1909**, *17*, 398.
- Berthelot, M. Dissolution des Acides et des Alcalis. *Ann. Chim. Phys.*, **1875**, *4*, 445.
- Brelvi, S.W.; O'Connell, J. P. Corresponding States Correlations for Liquid Compressibility and Partial Molar Volumes of Gases at Infinite Dilution in Liquids. *AICHE J.* **1972**, *218*, 1239.
- Bollas, G.; Chen, C.-C.; Barton, P. Refined electrolyte-NRTL model: activity coefficient expressions for application to multi-electrolyte systems. *AICHE. J.*, **2008**, *54*, 1608.
- Chen, C. C.; Britt, H. I.; Boston, J. F.; Evans, L. B. Local Composition Model for excess Gibbs Energy of Electrolyte Systems. 1. Single Solvent, Single Completely Dissociated Electrolyte Systems. *AICHE J.*, **1982**, *28*, 588.
- Clifford, I. L.; Hunter, E. The System Ammonia-Water at Temperatures up to 150 °C and at Pressures up to twenty atmospheres. *J. Phys. Chem*, **1933**, *37*, 101.
- Cragoe, C. S.; Meyers, C. H.; Taylor, C. S. The vapor pressure of ammonia. *J. Am. Chem. Soc.*, **1920**, *42*, 206.
- Cramer, S. D. The solubility of methane, carbon dioxide , and oxygen in brines from 0 ° to 300 °C. *US Bureau of Mines Report of Investigations*, **1982**, *1*, 8706.
- Cullinane, J. T.; Rochelle, G. T. ; Thermodynamics of aqueous potassium carbonate, piperazine, and carbon dioxide. *Fluid Phase Equilibria*, **2005**, *227*, 197.
- Curry, J.; Hazelton, C.L. The Solubility of Carbon Dioxide in Deuterium Oxide at 25oC. *J. Am. Chem. Soc.*, **1938**, *60*, 2771.

Darde, V., Thomsen, K., van Well, W.J.M. and Stenby, E.H.S. 2010b Modeling of carbon dioxide absorption by aqueous ammonia solutions using the Extended UNIQUAC model. *Ind. Eng. Chem. Res.*, **2010**, *49*, 12663.

Diamond, L. W.; Akinfiyev, N. N. Solubility of CO<sub>2</sub> in water from -1.5 to 100 °C and from 0.1 to 100 MPa: evaluation of literature data and thermodynamic modeling. *Fluid Phase Equilib.*, **2003**, *208*, 265.

Dholabhai, P. D.; Kalogerakis, N.; Bishnoi, P.R. Equilibrium Conditions for Carbon Dioxide Hydrate Formation in Aqueous Electrolyte Solutions. *J. Chem. Eng. Data*, **1993**, *38*, 650.

Dholabhai, P. D.; Parent, J. S.; Bishnoi, P. R. Carbon Dioxide Hydrate Equilibrium conditions in Aqueous Solutions Containing Electrolytes and Methanol Using a New Apparatus. *Ind. Eng. Chem. Res.* **1996**, *35*, 819.

Dunsmore, H. S.; Nancollas, G. H. Dissociation of the Bisulfate Ion. *J. Phy. Chem.*, **1964**, *68*, 1579.

Ellis, A.J. The solubility of carbon dioxide in water at high temperatures. *Am. J. Sc.*, **1959**, *257*, 217.

Ellis, A.J.; Golding R.M. The solubility of CO<sub>2</sub> above 100 °C in water and in NaCl solutions. *Am. J. Sc.*, **1963**, *261*, 47.

Faramarzi, L.; Kontogeorgis, G. M.; Thomsen, K.; Stenby, E. H. Extended UNIQUAC model for thermodynamic modeling of CO<sub>2</sub> absorption in aqueous alkanolamine solutions. *Fluid Phase Equilib.*, **2009**, *282*, 121.

Faramarzi, L. Post-Combustion Capture of CO<sub>2</sub> from Fossil Fueled Power Plants. Ph.D thesis, Technical University of Denmark, **2010**.

Faurholt, C. (1921). Über die Prozesse  $\text{NH}_2\text{COONH}_4 + \text{H}_2\text{O} \rightleftharpoons (\text{NH}_4)_2\text{CO}_3$  und  $\text{CO}_2 + \text{H}_2\text{O} \rightleftharpoons \text{H}_2\text{CO}_3$ . *Det Kgl. Danske Videnskabernes Selskab, Matematisk-fysiske Meddelelser III*, **1921**, *20*, 3.

Fletcher, R. A modified Marquardt subroutine for non-linear least squares, Harwell report (1971). <http://www.hsl.rl.ac.uk/> Accessed March 2010.

Fosbøl, P. L. The chilled ammonia process Evaluation of the energy requirements. Technical University of Denmark, internal report, **2008**.

Gabrielsen, J.; Michelsen, M. L.; Kontogeorgis, G. M; Stenby, E. H. A Model for Estimating CO<sub>2</sub> Solubility in Aqueous Alkanolamines. *Ind. Eng Chem. Res.*, **2005**, *44*, 3348.

Gabrielsen, J.; Michelsen, M. L.; Kontogeorgis, G. M; Stenby, E. H. Modeling of CO<sub>2</sub> Absorber using an AMP Solution. *AICHE J.*, **2006**, *52*, 3443.

Garcia, A. Measurement and Modeling of Scaling Minerals. Ph.D thesis, Technical University of Denmark, **2005**.

Garcia, A. V.; Thomsen, K.; Stenby, E. H. Prediction of mineral scale formation in geothermal and oilfield operations using the extended UNIQUAC model. *Geothermics* **2006**, *35*, 289.

Gawlick H. Messung von Verdampfungs-, Verdünnungs- und spezifischen Wärmen mit einem neuen Differentialcalorimeter Dissertation. *Braunschweig*, **1934**.

Geffcken, G. Beiträge zur kenntnis der löslichkeitsbeeinflussung. *Z. Physik. Chem.*, **1904**, *49*, 257.

Gillespie, P. C.; Wilson, G. M. Vapor-liquid and liquid-liquid equilibria: Water-Methan, Water-Carbon Dioxide, Water-Hydrogen Sulfide, Water-nPentane, Water-Methan-nPentane. *Gas Processor Association, Tulsa, Research Report*, **1982**, RR48.

Gillespie, P. C.; Wilding, V. W.; Wilson, G. M. Vapor-liquid equilibrium measurements on the ammonia-water system from 313 to 589 K. *AIChE J.* **1987**, *256*, 97.

Göppert, U.; Maurer, G. Vapor-liquid equilibria in aqueous solutions of Ammonia and Carbon Dioxide at Temperatures Between 333 and 393K. *Fluid Phase Equilibria*, **1988**, *41*, 153.

Guillevic, J-L. ; Richon, D. ; Renon, H. Vapor-Liquid Equilibrium Data for the Binary System Water-Ammonia at 403.1, 453.1, 503.1 K up to 7.0 MPa. *J. Chem. Eng. Data*, **1985**, *30*, 332.

Guyer, A.; Piechowicz, T. Lösungsgleichgewichte in wässrigen Systemen 4. *Hel. Chim. Act.*, **1944**, *27*, 858.

Hähnel, O. The strength of carbonic acid at higher pressures. *Centralblatt für Mineralogie, Geologie und Paläontologie*, **1920**, *25*, 25.

Harms-Watzenberg, F. Messung und Korrelation der thermodynamischen Eigenschaften von Wasser-Ammoniak-Gemischen. *Fortschrittberichte VDI*, **1995**, *3*, 380.

Harned, H.S.; Davis, R. The ionization constant of Carbonic Acid in water and the solubility of CO<sub>2</sub>. *J. Am. Chem. Soc.*, **1945**, *65*, 2030.

Harvey, A. H.; Prausnitz, J. M. Dielectric constants of fluid mixtures over a wide range of temperature and density. *J. Sol. Chem.*, **1987**, *16*, 857.

Hayduk, W.; Malik, V. K.; Density, Viscosity, and Carbon Dioxide solubility and diffusivity in aqueous ethylene glycol solutions. *J. Chem. Eng. Dat.*, **1971**, *16*, 143.

Helgeson, H. C.; Kirkham, D. H.; Flowers, G. C. Theoretical prediction of the thermodynamic behavior of aqueous electrolytes at high pressures and temperatures: IV. *Am. J. & i*, **1981**, *281*, 1249.

Hessen, E. T.; Haug-Warberg, T.; Svendsen, H. F. The refined e-NRTL model applied to CO<sub>2</sub>-H<sub>2</sub>O-alkanolamine systems. *Chem. Eng. Sc.*, **2010**, *65*, 3638.

Hurst, J. E.; Harrison, K. B. Estimation of Liquid and Solid heat capacities using a modified Kopp's rule. *Chem. Eng. Comm.* **1992**, *112*, 21.

Inomata, H. ; Ikawa, N., Arai, K. ; Saito, S. Vapor-Liquid Equilibria for the ammonia-methanol-water system. *J. Chem. Eng. Data*, **1988**, *33*, 26.

Iseli, M. Experimentelle und thermodynamische untersuchung des siedegleichgewichtes des systems NH<sub>3</sub>-H<sub>2</sub>O bei hohen drucken, *Dissertation, Eidgenössischen technischen hochschule*, **1985**, Zürich.

Jänecke, E. Über das System H<sub>2</sub>O, CO<sub>2</sub>, NH<sub>3</sub>. *Zeitschrift für Electrochemie*, **1929a**, *35*, 716.

Jänecke, E. Über die Löslichkeit von ammonbicarbonat in wasser bis zum schmelzpunkt. *Zeitschrift für Electrochemie*, **1929b**, *35*, 332.

Jennings, B. H. Ammonia-Water Properties. *Transactions of the American society of heating and refrigeration engineers*, **1965**, *71*, 21.

Jilvero, H.; Normann, F.; Anderson, K.; Johnsson, F. Thermal Integration and Modelling of the Chilled Ammonia Process. Presented at Greenhouse Gas Technology 10 (GHGT10), Amsterdam, **2010**.

Kent, R. L.; Eisenberg, B. Better data for amine treating. *Hydrocarbon Processing*, **1976**, *55*, 87.

Kiepe, J.; Horstmann; S. Fischer; K. Gmehling, J. Experimental Determination and Prediction of Gas Solubility Data for CO<sub>2</sub> + H<sub>2</sub>O Mixtures Containing NaCl or KCl. *Ind. Eng. Chem. Res.*, **2002**, *41*, 4393.

- Kiss, A. V.; Lajtai, I.; Thury, G. Über die Löslichkeit von Gasen in Wasser-Nichtelektrolytgemischen. *Z. anorg. allg. Chemie*, **1937**, 233, 346.
- van Krevelen, D. W.; Hofstijzer, P. J.; Huntjens, F. J. Composition and vapour pressures of aqueous solutions of ammonia, carbon dioxide and hydrogen sulphide. *Recueil des travaux chimiques des Pays-Bas*, **1949**, 68, 191.
- Kritschewsky, I. R.; Shaworonkoff, N. M.; Aepelbaum, V. A. (Cited by Diamond *et al.*) Gemeinsame Löslichkeit der Gase in Flüssigkeiten unter Druck. *Zeit. Phys. Chem. A*, **1935**, 175, 232.
- Kunerth, W. Solubility of CO<sub>2</sub> and N<sub>2</sub>O in certain solvents. *Phys. rev.*, **1922**, 2, 512.
- Kurz, F. Untersuchungen zur simultaneous Lösung von Ammoniak und Kohlendioxid in Wasser und salzhaltigen wässrigen Lösungen. *Dissertation, Universität Kaiserslautern*, **1994**.
- Kurz, F.; Rumpf, B.; Maurer, G. Vapor-liquid-solid equilibria in the system NH<sub>3</sub>-CO<sub>2</sub>-H<sub>2</sub>O from around 310 to 470 K: New experimental data and modeling. *Fluid Phase Equilibria*, **1995**, 104, 261.
- Lichtfers, U. Spektroskopische Untersuchungen zur Ermittlung von Speziesverteilungen im System Ammoniak-Kohlendioxid-Wasser. PhD dissertation, Kaiserslautern, Germany, **2000**.
- Malegaonkar, M. B.; Dholabhai, P. D.; Bishnoi, P. R. Kinetics of Carbon Dioxide and Methane Hydrate formation. *Can. J. Chem. Eng.*, **1997**, 75, 1090.
- Malinin, S. D.; Savelyeva, N. I. Experimental Investigation of CO<sub>2</sub> Solubility in NaCl and CaCl<sub>2</sub> Solutions at Temperatures of 25, 50, and 75° and elevated CO<sub>2</sub> pressures. *Geokhimiya*, **1972**, 6, 643.
- Malinin, S. D.; Kurovskaya, N. A. Carbon dioxide solubility in solutions of chlorides at elevated temperatures and carbon dioxide pressure. *Geokhimiya*, **1975**, 4, 547.
- Mallet, J. W. On the solubility of ammonia in water at temperatures below 0 °C. *Am. Chem. J.* **1897**, 19, 804.
- Markham, A. E.; Kobe, K. A. The solubility of Carbon dioxide and Nitrous oxide in aqueous Salt Solutions. *J. Am. Chem. Soc.*, **1941**, 63, 449.
- Markham, A. E.; Kobe, K. A. The solubility of Carbon dioxide in aqueous H<sub>2</sub>SO<sub>4</sub>, HClO<sub>4</sub>. *J. Am. Chem. Soc.*, **1941**, 63, 1165.
- Mathias, P. M.; Reddy, S.; O'Connell, J. P. Quantitative Evaluation of the Aqueous-Ammonia Process for CO<sub>2</sub> capture fundamental Data and Thermodynamic Analysis. *Int. J. Greenhouse Gas Control*, **2010**, 4, 174.
- Matous, J.; Sobr, J.; Novák, J.P.; Pick, J. Solubility of Carbon Dioxide in Water at Pressures up to 40 atm. *Collection Czechoslov. Chem. Commun.*, **1969**, 34, 3982.
- Mezger, R.; Payer, T. Kohlensäure Ammoniumverbindungen. *Das Gas- und Wasserfach*, **1925**, 68, 651.
- Mittasch, A.; Kuss, E.; Schlueter, H. Thicknesses and steam pressure of water ammoniac solutions and of fluid nitrogen tetraoxide for the temperature area 0 degrees to 60 degrees, *Zeitschrift für anorganische und allgemeine Chemie*, **1926**, 59, 1.
- Mollier, H. Dampfdruck von wässrigen Ammoniaklösungen. *Zeitschrift des Vereinigung deutsche Ingenieuren*, **1908**, 52, 1315.
- Mollier, H. Dampfdruck von wässrigen Ammoniaklösungen. *Forschungsarbeiten auf dem Gebiete des Ingenieurwesens*, **1909**, 63/64, 85.

- Morgan, O. M.; Maass, An investigation of the equilibria existing in gas-water systems forming electrolytes. *O. Can. j. Res.* **1931**, *5*, 162.
- Morrison, T. J.; Billett, F. The Salting-out of Non-electrolytes. Part I. The Effect of Ionic Size, Ionic Charge, and Temperature. *J. Chem. Soc.*, **1952**, *OCT.*, 3814.
- Müller, G.; Bender, E.; Maurer, G. Vapor-liquid-equilibrium in the ternary system ammonia-carbon dioxide-water at high water contents in the range 373K to 473K. *Ber. Bunsenges. Phys. Chem.* **1988**, *92*, 148.
- Munck, J.; Skjold-Jørgensen, S.; Rasmussen, P. Computations of the formation of gas hydrates. *Ch. Eng. Sc.*, **1988**, *43*, 2661.
- Murray, C. N.; Riley, J. P. The solubility of gases in distilled water and sea water - IV. Carbon dioxide. *Deep-Sea Research*, **1971**, *18*, 533.
- Nelder & Mead simplex algorithm c for function minimization. <http://lib.stat.cmu.edu/apstat/47>  
Accessed March 1<sup>st</sup> 2010.
- Novak, J.; Fried, V.; Pick, J. Löslichkeit des Kohlendiosyds in Wasser bei Verschiedenen Drücken und Temperaturen. *Collect. Czech. Chem. Commun.*, **1961**, *26*, 2266.
- van Ness, H. C.; Pedersen, F.; Rasmussen, P. Partial V. Data Reduction by Maximum Likelihood *AIChE J.*, **1978**, *24*, 1055.
- Neuhausen, B. S.; Patrick, W. A. A Study of the System Ammonia-Water as a Basis for a Theory of the Solution of Gases in Liquids. *J. Phys. chem.* **1921**, *25*, 693.
- Nighswander, J. A.; Kalogerakis, N.; Mehrota, A. K. Solubilities of carbon dioxide in water and 1 wt% NaCl. *J. Chem. Eng. Data*, **1989**, *34*, 355.
- NIST Chemical Thermodynamics Database Version 1.1, U.S. Department of Commerce, National Institute of Standards and Technology, Gaithersburg, MD 20899, **1990**.
- Otsuka, E.; Yoshimura, S.; Yakabe, M.; Inoue, S. Equilibrium of the NH<sub>3</sub>-CO<sub>2</sub>-H<sub>2</sub>O system. *Kogyo Kagaku Zasshi*, **1960**, *22*, 1914.
- Pawlikowski, E. M.; Newmann, J.; Prausnitz, J. M. Phase Equilibria for aqueous solutions of Ammonia and Carbon Dioxide. *Ind. Eng. Chem. Process. Des. Dev.* **1982**, *21*, 764.
- Pexton, S.; Badger, E. H. M. The Examination of Aqueous solutions containing only NH<sub>3</sub> and CO<sub>2</sub>. *J. Soc. Chem Ind.*, **1938**, *57*, 107.
- Pitzer, K. S. Thermodynamics of Electrolytes. I. Theoretical Basis and General Equations. *The Journal of Physical Chemistry*, **1973**, *77*, 268.
- Polak, J.; Lu, B. C-Y. Vapor-Liquid Equilibria in System Ammonia-Water at 14.69 and 65 psia. *J. Chem. Eng. Data*, **1975**, *20*, 182.
- Posey, M. L.; Rochelle, G. T. A thermodynamic model of methyldiethanolamine-CO<sub>2</sub>-H<sub>2</sub>S-water. *Ind. Eng. Chem. Res.*, **1997**, *36*, 3944.
- Postigo, M. A.; Pedrosa, G.; Katz, M. Nueva metodo experimental para la determinacion de solubilidad de gases en liquidos. *Anales Asoc. Quim. Argentina*, **1978**, *66*, 25.
- Postma, S. Le système ammoniacque – eau, *Recueils des travaux chimiques des Pays-Bas*, **1920**, *39*, 515.

- Prutton, C. F.; Savage, R. L. The solubility of Carbon Dioxide in Calcium Chloride-Water Solutions at 75, 100, 120 ° and high pressures. *J. Am. Chem. Soc.*, **1945**, *67*, 1550.
- Qin, F.; Wang, S.; Kim, I.; Svendsen, H. F.; Chen, C. Study of the Heat of Absorption of CO<sub>2</sub> in Aqueous Ammonia: Comparison between Experimental Data and Model Predictions. *Ind. Eng. Chem. Res.*, **2010**, *49*, 3776.
- Ramstetter, H.; Hantke, G. Eine neue Methode zur Messung von Wärmetönungen. *Z. phys. Chem.* **1931**, Bodenstein-Festband, 662.
- Renon, H.; Prausnitz, J. M. Local Compositions in Thermodynamic Excess Functions for Liquid Mixtures. *AIChE Journal*, **1968**, *14*, 135.
- Rizvi, S. S. H. Measurement and correlation of ammonia water equilibrium data, Dissertation, Department of Chemical and Petroleum Engineering, University of Calgary, Alberta, Canada, **1985**.
- Rumpf, B.; Maurer, G. Solubility of ammonia in aqueous solutions of sodium sulfate and ammonium sulfate at temperatures from 333.15K to 433.15K and pressure up to 3MPa. *Ind. Eng. Chem. Res.* **1993**, *32*, 1780.
- Rumpf, F.; Weyrich, F.; Nqurer, G. Simultaneous Solubility of NH<sub>3</sub> and SO<sub>2</sub> in H<sub>2</sub>O at temperatures from 313.15 to 373.15K and Pressures up to 2.2 MPa. *Fluid Phase Equilib.*, **1993**, *83*, 253.
- Rumpf, B.; Nicolaisen, H.; Öcal, C.; Maurer, G. Solubility of Carbon Dioxide in Aqueous Solutions of Sodium Chloride – Experimental results and correlation.. *J. Sol. Chem.*, **1994**, *23*, 431.
- Rumpf, B.; Weyrich, F.; Maurer, G. Enthalpy of dilution in aqueous systems of single solutes ammonia, sodium sulfate and ammonium sulfate: Experimental results and modeling. *Thermochemica Acta*, **1997**, *303*, 77.
- Rumpf, B.; Kamps, A. P. S.; Maurer, G. Simultaneous solubility of ammonia and hydrogen sulfide in water at temperatures from 313 K to 393 K. *Fluid Phase Equilib.*, **1999**, *158-160*, 923.
- Rumpf, B.; Weyrich, F.; Maurer G. Enthalpy changes upon Partial Evaporation of Aqueous Solutions containing Ammonia and Carbon Dioxide. *Ind. Eng. Chem. Res.*, **1998**, *37*, 2983.
- Sander, B.; Rasmussen, P. Fredenslund, Aa. Calculation of Solid-Liquid Equilibria in Aqueous Solutions of Nitrate Salts Using an Extended UNIQUAC Equation. *Chemical Engineering Science*, **1986**, *41*, 1197.
- Sander, W. Über die löslichkeit der kohlendäure in wasser und einigen andern lösungsmitteln unter höhern drucken. *Z. physik. Chem.*, **1912**, *78*, 513.
- Sassen, C. L.; van Kwartel, R. A. C.; van der Kool, H. J.; de Swan Arons, J. Vapor-Liquid Equilibria for the system Ammonia + Water up to the Critical Region. *J. Chem. Eng. Data*, **1990**, *35*, 140.
- Schultz, J. F.; Elmore, G. V. The System Ammonium Nitrate-Ammonia-Water, *Ind. Chem. Res.* **1948**, *38*, 296.
- Servio, P.; Englezos, P. Effect of temperature and pressure on the solubility of carbon dioxide in water in the presence of gas hydrate. *Fluid Phase Equilib.*, **2001**, *190*, 127.
- van Slyke, D. D. Determination of Solubilities of Gases in Liquids with Use of the Van Slyke-Neill Manometric Apparatus for both saturation and analysis. *J. Biol. Chem.*, **1939**, *130*, 545.
- Smolen, T. M.; Manley, D. B.; Poling, B. E. Vapor-Liquid Equilibrium data for the NH<sub>3</sub>-H<sub>2</sub>O System and Its Description with a modified cubic equation of state, *J. Chem. Eng. Data*, **1991**, *36*, 202.

Staudt, H. J. Experimentelle Bestimmung und Korrelation der excessenthalpie und des excessvolumens binärer wässriger amin – und Alkoholsysteme sowie des Systems Ammoniak-Wasser in Abhängigkeit von Druck, Temperatur und Zusammensetzung. *Dissertation, Universität Kaiserslautern*, **1984**.

Stewart, P. B.; Munjal, P. Solubility of carbon dioxide in pure water, synthetic sea water concentrates at 5 degrees to 2K degrees C and 10-atm to 45-atm pressure. *J. Chem. Eng. Dat.*, **1970**, *15*, 67.

Takenouchi, S.; Kennedy G. C. The binary system H<sub>2</sub>O-CO<sub>2</sub> at high temperatures and pressures. *Am. J. Sc.*, **1964**, *262*, 1055.

Takenouchi, S.; Kennedy, G. C. The Solubility of Carbon Dioxide in NaCl solutions at high temperatures and pressures. *American Journal of Science*, **1965**, *263*, 445.

Teng, H.; Yamasaki, M.; Chun, K.; Lee, H. Solubility of liquid CO<sub>2</sub> in water at 2 temperatures from 278K to 293K and pressures from 6.44 Pa to 29.49 MPa and densities of the corresponding aqueous solutions. *J.Chem.Thermodyn.*, **1997**, *29*, 1301.

Terres, E.; Weiser, H. Contribution to information on ammonia carbon acid compounds in the equation with their aqueous solutions. *Zeit. Elektrochemie Angewandte Physikalische Chem.*, **1921**, *27*, 177.

Terres, E.; Behrens, H. Information on the physical-chemical basis of the synthesis of urea from ammonia, carbonic acid and water. *Zeitschrift für physikalische Chemie*, **1938**, *139*, 695.

Thomsen, J. Wässrige lösung und hydratabildung. *Thermochemische Untersuchungen*, **1883**, *Band 3*, 34.

Thomsen, K.; Rasmussen, P.; Gani, R. Correlation and prediction of thermal properties and behaviour for a class of aqueous electrolyte systems. *Chem. Eng. Sc.*, **1996**, *51*, 3675.

Thomsen, K. Ph.D. Thesis, Department of Chemical Engineering, Technical University of Denmark, **1997**.

Thomsen, K.; Rasmussen, P. Modeling of vapor-liquid-solid equilibrium in gas-aqueous electrolyte systems. *Chemical Engineering Science*, **1999**, *54*, 1787.

Thomsen, K. Electrolyte Solutions: Thermodynamics, Crystallization, Separation method. Technical University of Denmark, **2006**.

Verbrugge, P. Vapour-Liquid Equilibria of the Ammonia-Carbon Dioxide-Water System, *Dissertation Delft University Press*, **1979**.

Vilcu, R.; Gainar, I. Löslichkeit der Gase unter Druck in Flüssigkeiten. I. Das System Kohlendioxid-Wasser. *Rev. Roum. Chim.*, **1967**, *12*, 181.

Wagman, D. D.; Evans, W. H.; Parker, V. B.; Schumm, R. H.; Halow, I.; Bailey, S. M. NIST Chemical Thermodynamics Database Version 1.1. *J. Phys. Chem. Ref. Data*, **1982**, *11*.

Wasmund, R.; Bultmann, H. Einfluss des Saccharosegehalts auf die CO<sub>2</sub>-Absorption wässriger Lösungen. *Zuckerind.*, **1980a**, *105*, 1085.

Wasmund, R.; Bultmann, H. Kohlendioxid-Absorption des reinen wassers in Abhängigkeit vom Druck und von der Temperatur. *Monatsschrift für Brauerei*, **1980b**, *16*, 857.

Wendland, M.; Hasse, H.; Maurer, G. Experimental pressure-temperature data on three- and four-phase equilibria of fluid, hydrate, and ice phases in the system carbon dioxide-water. *J. Chem. Eng. Data*, **1999**, *44*, 901.

Wiebe, R.; Gaddy, V. L. The solubility in water of carbon dioxide at 50, 75 and 100 °, at pressures to 700 Atmospheres. *J. Am. Chem. Soc.*, **1939**, *61*, 315.

- Wiebe, R.; Gaddy, V. L. The solubility of Carbon Dioxide in Water at Various Temperatures from 12 to 40 °C and at pressures to 500 atm. *J. Am. Chem. Soc.*, **1940**, *62*, 815.
- Wilson, G. M. Vapor-Liquid Equilibrium XI. A New Expression for the Excess Free Energy of Mixing. *J. Am. Chem. Soc.*, **1964**, *86*, 127.
- Wrewsky, M.; Sawaritzky, N. The formation enthalpy of watery solutions of HCl and NH<sub>3</sub> at different temperatures. *Zeitschrift Physikalische Chem. Stoch. Verwandtschaftslehre*, **1924a**, *112*, 90.
- Wrewsky, M.; Kaigorodoff, A. Heat capacity of watery solutions of hydrogen chloride and ammonium at different temperatures. *Zeitschrift Physikalische Chem. Stoch. Verwandtschaftslehre*, **1924b**, *112*, 83.
- Wroblewski, S.V. Cited by Diamond *et al.*, 2003) *Ann. Phys. Chem.*, **1883**, *18*, 290.
- Yang, S. O.; Yang, I. M.; Kim, Y. S.; Lee, C. S. Measurement and prediction of phase equilibria for water + CO<sub>2</sub> in hydrate forming conditions. *Fluid Phase Equilib.*, **2000**, *175*, 75.
- Yeh, S. Y.; Peterson, R. E. Solubility of Carbon Dioxide, Krypton, and Xenon in Aqueous Solutions. *J. Pharma. Sc.*, **1964**, *53*, 822.
- Zawisza, A.; Malesinska, B. Solubility of Carbon Dioxide in Liquid Water and of Water in Gaseous Carbon Dioxide in the range 0.2-5 MPa and at temperatures up to 473-K. *J. Chem. Eng. Data*, **1981**, *24*, 388.
- Zelvenskii, Y. D. The Solubility of Carbon Dioxide under Pressure. *Jour. Chem. Industry*, **1937**, *14*, 1250.
- Zheng, D-Q.; Tain-Min, G.; Knapp, H. Experimental and modeling studies on the solubility of CO<sub>2</sub>, CHClF<sub>2</sub>, CHF<sub>3</sub>, C<sub>2</sub>H<sub>2</sub>F<sub>4</sub> and C<sub>2</sub>H<sub>4</sub>F<sub>2</sub> in water and aqueous NaCl solutions under low pressures. *Fluid Phase Equilib.*, **1997**, *129*, 197.





## **3 Thermodynamic analysis of CO<sub>2</sub> capture process using aqueous ammonia**

### **3.1 Introduction**

The Extended UNIQUAC thermodynamic model allows for calculating the equilibrium liquid composition, the nature and amount of solid phases and the bubble point pressure of a given mixture of carbon dioxide water and ammonia.

Hence, thanks to the thermodynamic model available for the CO<sub>2</sub>-NH<sub>3</sub>-H<sub>2</sub>O system and based on the information from the patent of the CAP (Gal, 2006), it is possible to perform an analysis of the performance of the process based on thermodynamic calculations. The equilibrium composition of the process streams can be calculated and an assessment of the heat requirement can be made. This analysis allows for understanding the influence of some of the main parameters on the performance of the process. A similar thermodynamic analysis of the process using the Extended UNIQUAC model with the old set of parameters has been published (Darde *et al.*, 2010). In the present study, the upgraded Extended UNIQUAC model presented in Chapter 2 is used.

The concentration of ammonia to be used in the process is not mentioned in the patent. Some early presentations from Alstom mention a 28 wt% solution. In the present study, the analysis has been made for three different concentrations of ammonia. First, at 28 wt% (or 22.8 NH<sub>3</sub> molal), second at 10 wt% (6.5 NH<sub>3</sub> molal), which represents a molality close to the one observed for the reference solvent 30 wt% MEA (6.9 MEA molal), and finally at 5 wt% (3.1 NH<sub>3</sub> molal) in the context of a process without precipitation, such as the one developed by Powerspan (Mc Larnon *et al.*, 2009).

### **3.2 Equilibrium composition of the process stream**

#### **3.2.1 Absorption**

The CO<sub>2</sub> partial pressure of the flue gas of a coal-fired power plant is typically comprised between 0.10 and 0.15 bar. Hence, the equilibrium partial pressure of carbon dioxide of the CO<sub>2</sub>-rich stream must be lower than this value in order to maintain a driving force for the absorption.

According to the patent, in the case of the CAP, the absorption preferably occurs at a temperature between 0 and 10 °C. The lean loading is comprised between 0.25 and 0.67 and the rich loading between 0.5 and 1. Therefore, by maintaining a temperature of 10 °C, it is interesting to study the influence of the loading on the equilibrium composition of a mixture of water, carbon dioxide and ammonia. By using a temperature of 10 °C for the whole range of loadings, it is assumed that the temperature in the absorber is set constant despite the exothermic absorption.

### 3.2.1.1 28 wt% ammonia solutions

Figure 3-1, Figure 3-2 and Figure 3-3 respectively show the nature and amount of solid phases, the composition of the liquid phase and the bubble point pressures of 1 kg water equivalent 28 wt% ammonia solution as a function of the CO<sub>2</sub> loading at 10 °C. The results are based on the equilibrium composition calculated with the Extended UNIQUAC model. It should be noted that the loading that is used in the plot is the global loading of the mixture, including both the liquid and solid phases. When there is no solid phase, it is equal to the loading of the liquid phase. When solid compounds are present, the actual loading in the liquid phase is lower than the global one.

It can be observed that for a loading superior to 0.3, a solid phase of ammonium carbonate appears. When the loading increases another phase of sesqui-carbonate appears while the amount of ammonium carbonate decreases, followed by some ammonium bicarbonate. This shows that at these conditions, the CO<sub>2</sub>-lean stream entering the absorber presents a solid phase. It can be noticed that when two solid phases are present (for a loading from 0.48 to 0.65, and from 0.65 to 0.85), the composition of the liquid phase and the bubble point pressures are constant. This can be explained by the lack of degree of liberty that occurs when two solid phases are in equilibrium with the solution. The mass of solid increases continuously when the loading increases.

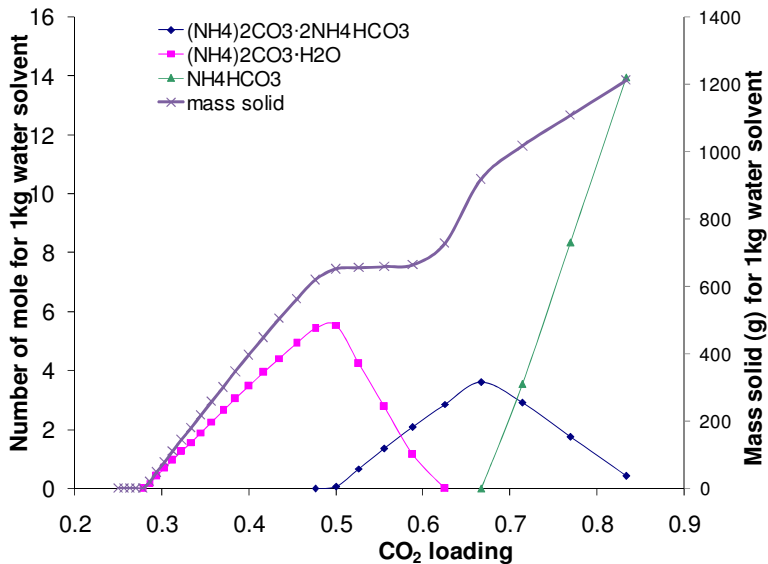


Figure 3-1: Nature and amount of solid phases of 28 wt% NH<sub>3</sub> with a temperature of 10 °C per kilogram water as a function of the CO<sub>2</sub> loading

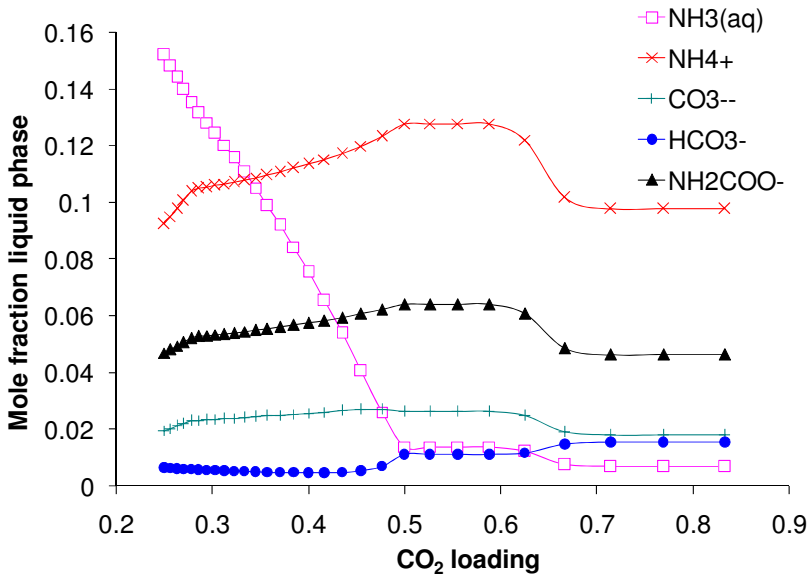


Figure 3-2: Equilibrium composition of the liquid phase of 28 wt% NH<sub>3</sub> for the main species at 10 °C as a function of the CO<sub>2</sub> loading. The water mole fraction is not represented.

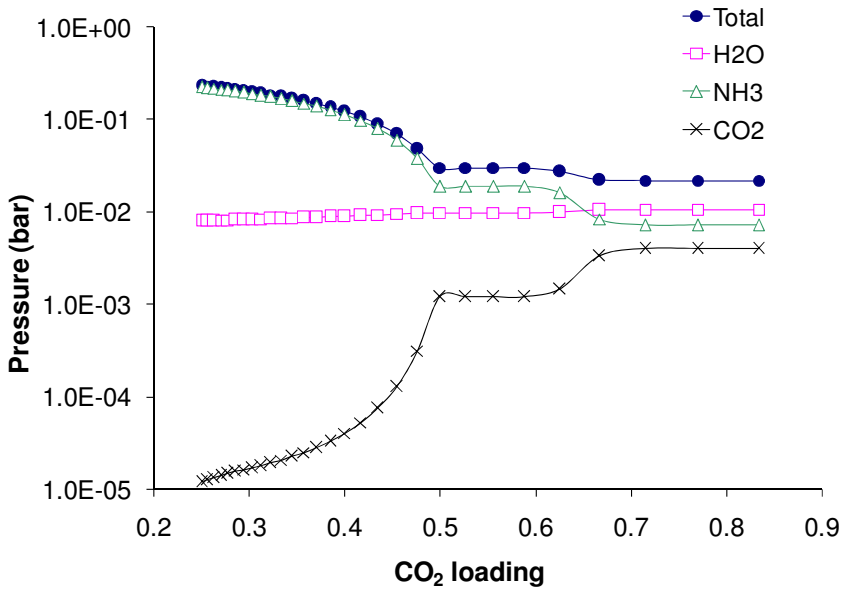


Figure 3-3: Bubble point pressures of 28 wt% NH<sub>3</sub> at 10 °C as a function of the CO<sub>2</sub> loading

The level of partial pressure of carbon dioxide shows that at low temperature and for the range of loadings considered, the solvent is suitable for absorption of carbon dioxide from coal-fired power plant.

The mole fraction of free ammonia dissolved in the liquid phase, and consequently the partial pressure of ammonia is significant for low loadings, which means that a large amount of ammonia is vaporized, even at this low temperature. The partial pressure of ammonia decreases rapidly with increasing loading, which shows that the vaporization of ammonia can be limited by applying a higher loading regime in the absorber. The high value for the partial pressure of ammonia at low temperature indicates that this high concentration of ammonia in the solvent is not recommended for the variant of the process absorbing carbon dioxide at higher temperature.

### **3.2.1.2 10 wt% ammonia solutions**

Figure 3-4 shows the bubble point pressures for a 10 wt% ammonia solution as a function of the loading at 10 °C. The composition of the liquid phase was found to be quite similar to the one presented for the 28 wt% NH<sub>3</sub> solvent. At 10 °C, for the range of loadings considered, only ammonium bicarbonate is formed for a loading higher than 0.55. Hence, according to the patent, when it flows to the absorber, the CO<sub>2</sub>-lean stream does not comprise any solid phase. The level of the carbon dioxide partial pressure shows the ability for the solvent to absorb carbon dioxide from coal-fired power plant at low temperature.

Compared to 28 wt% NH<sub>3</sub>, the same decrease of the partial pressure of ammonia with the loading can be observed. However, the pressure is much lower than the one observed with 28 wt% NH<sub>3</sub>, especially at low loading (see Figure 3-3). Hence, lowering the concentration of ammonia in the solvent permits the reduction of the ammonia slip from the absorber. It also allows for using a CO<sub>2</sub>-lean stream at a lower loading, and for performing the absorption at higher temperature.

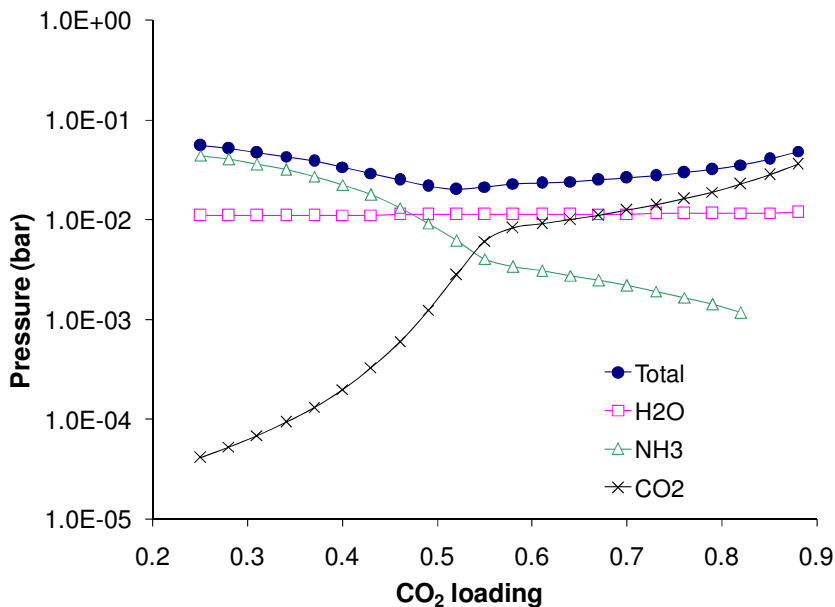


Figure 3-4: Bubble point pressures of 10 wt% NH<sub>3</sub> at 10 °C as a function of the CO<sub>2</sub> loading

### 3.2.1.3 5 wt% ammonia solutions

Figure 3-5 shows the bubble point pressure of a 5 wt% ammonia solvent as a function of the loading at 10 °C. Ammonium bicarbonate is formed for a loading above 0.67. According to the equilibrium partial pressure of carbon dioxide, for the loading range considered, the solvent is still suited for absorption of carbon dioxide from coal-fired power plant. The partial pressure of ammonia is significantly lower than for the previous ammonia concentrations studied.

The influence of the temperature on the partial pressure of carbon dioxide and ammonia is shown in Figure 3-6 and Figure 3-7. This study is relevant in the context of a process that does not use chilling water during the absorption. In addition, due to the exothermic reaction of absorption of CO<sub>2</sub>, the temperature in the absorber varies. Figure 3-6 shows that by increasing the temperature, the equilibrium partial pressure of carbon dioxide increases. Hence, an increase of the temperature at the bottom of the column for the low concentration of ammonia has a large effect on the maximum reachable rich loading, given the partial pressure of carbon dioxide in the flue gas. It should be noted that as a rate-based simulation would show, different parameters have an influence on the actual rich loading achieved during the absorption. As shown in Figure 3-7, increasing the temperature causes the rise of the ammonia partial pressure, and therefore the rise of the ammonia slip. Limiting the temperature at the top of the absorber is therefore an efficient way to reduce the vaporization of ammonia.

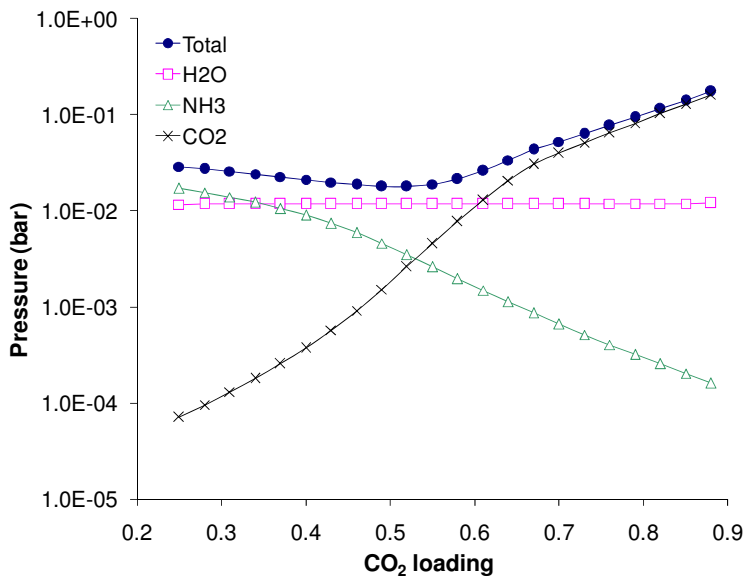


Figure 3-5: Bubble point pressures of 5 wt% NH<sub>3</sub> at 10 °C as a function of the CO<sub>2</sub> loading

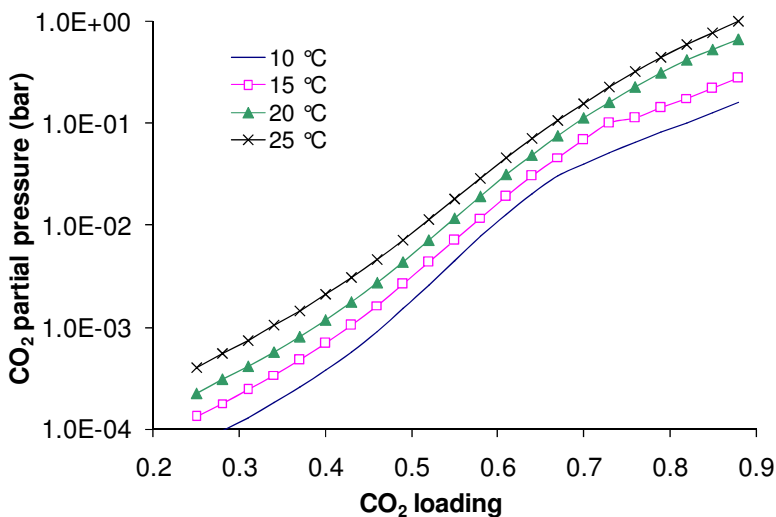


Figure 3-6: Bubble point carbon dioxide partial pressure of 5 wt% NH<sub>3</sub> as a function of the CO<sub>2</sub> loading and the temperature

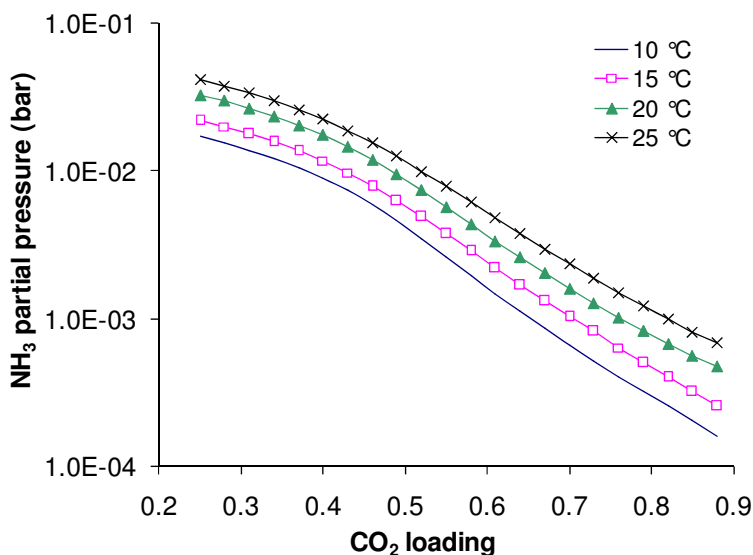


Figure 3-7: Bubble point ammonia partial pressure of 5 wt% NH<sub>3</sub> as a function of the CO<sub>2</sub> loading and the temperature

### 3.2.1.4 Conclusion

This study has shown that for the three concentrations studied, aqueous ammonia is able to capture carbon dioxide from coal-fired power plants at low temperature. The equilibrium calculations have confirmed the formation of solid compounds at low temperature for a sufficiently high concentration of ammonia. It was also shown that even at low temperature, the partial pressure of ammonia was significantly high, especially at low loading. This means that an extensive washing of the gas leaving the absorber is required. The temperature in the absorber is a very important parameter regarding the loading of the CO<sub>2</sub>-rich stream and the ammonia slip.

### 3.2.2 Desorption

Depending on the pressure at which the desorber is operated, the temperature in the reboiler may vary. The patent states a temperature in the range 100-150 °C. In this study, it was chosen to maintain the temperature at 120 °C. At this temperature and for the loading range considered, no solid phase can be found for the three concentrations studied.

Figure 3-8 and Figure 3-9 respectively show the composition of the bubble point gas phase and the bubble point pressures of a 28 wt% NH<sub>3</sub> solvent at 120 °C as a function of the loading.



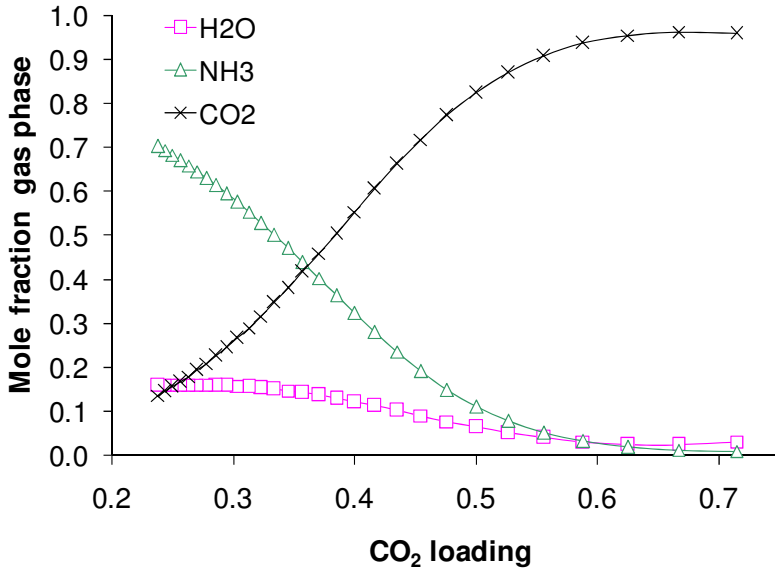


Figure 3-8: Composition of the bubble point gas phase of 28 wt% NH<sub>3</sub> at 120 °C as a function of the CO<sub>2</sub> loading

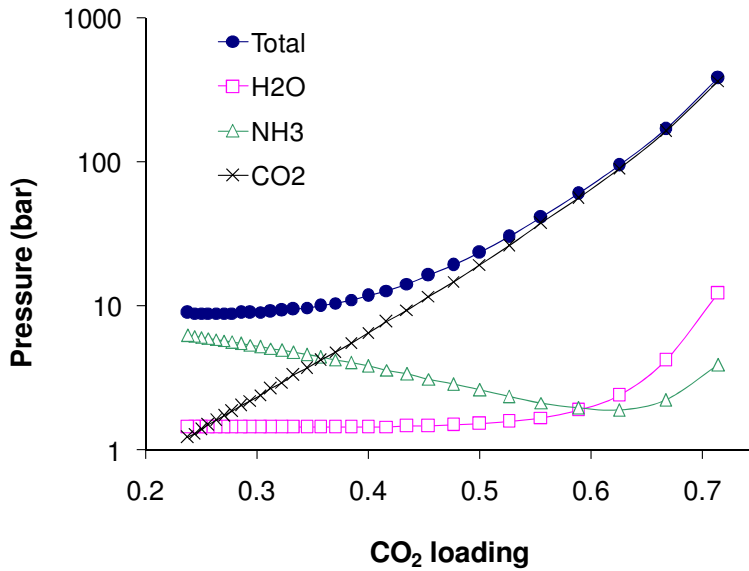


Figure 3-9: Bubble point pressures of 28 wt% NH<sub>3</sub> at 120 °C as a function of the CO<sub>2</sub> loading

The pressure calculated at high loading reaches very high values. This shows that the desorption can be made at elevated pressure. This is beneficial as some electricity savings can be made during the compression of carbon dioxide. In addition, as shown in Figure 3-8, the mole fraction of carbon dioxide at high loading is close to one. Providing that the CO<sub>2</sub>-rich stream that enters the desorber has a high CO<sub>2</sub> loading, this figure shows that at high temperature, it is possible to get a pressurized and nearly pure CO<sub>2</sub> stream. The use of a condenser and a washing section allow the cleaning of the CO<sub>2</sub> stream for water and ammonia.

The conclusions are similar with lower concentration of ammonia, the pressures reached under desorption are though more limited.

### **3.2.3 Comparison with the calculations using the old set of Extended UNIQUAC parameters**

The results obtained with the Extended UNIQUAC model from Thomsen and Rasmussen (1999) are quite similar. The same conclusions can be made and the levels of pressure at the temperatures considered in the study are in the same range for both versions of the model. Increasing the temperature in the desorber would however change significantly the calculation of the pressure. It can be noticed that for the 28 wt% NH<sub>3</sub> case at low temperature, no sesqui-carbonate is formed according to the calculations with the old parameters.

### **3.3 Heat requirement in the desorber**

The heat requirement in the desorber can be estimated by using the calculation of the enthalpy of the streams entering and leaving the column. Figure 3-10 shows a schematic flow sheet of the CO<sub>2</sub> desorber column. This study takes into account the amounts of water and ammonia that are swept along in the gas phase and eventually pumped to the desorber after the pure CO<sub>2</sub> stream passes through a condenser. The amount of water and ammonia vaporized is calculated using the bubble point pressure of the CO<sub>2</sub>-rich stream.

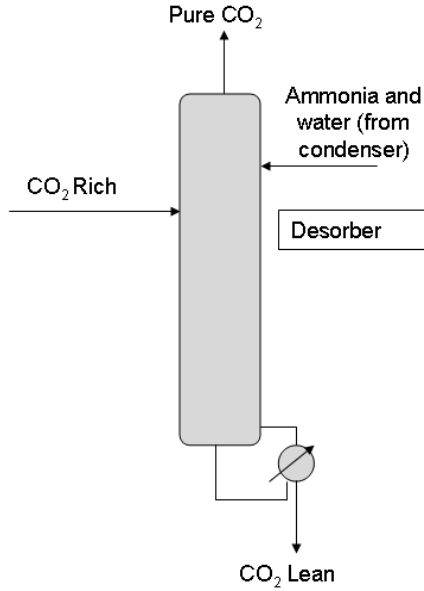


Figure 3-10: Flow sheet of the CO<sub>2</sub> desorber

A reference configuration has been set up according to the information from the patent (Gal, 2006). The main assumptions are summed up in Table 3-1. The temperatures of the stream entering and leaving the desorber have been specified based on experience from process simulation.

Table 3-1: Description of the stripper reference configuration

NH <sub>3</sub> wt%	T CO <sub>2</sub> -Lean	T CO <sub>2</sub> -Rich	T Pure CO <sub>2</sub>	Lean CO <sub>2</sub> loading	Rich CO <sub>2</sub> loading	T H <sub>2</sub> O + NH <sub>3</sub> from condenser
10	120 °C	110 °C	110 °C	0.33	0.67	25 °C

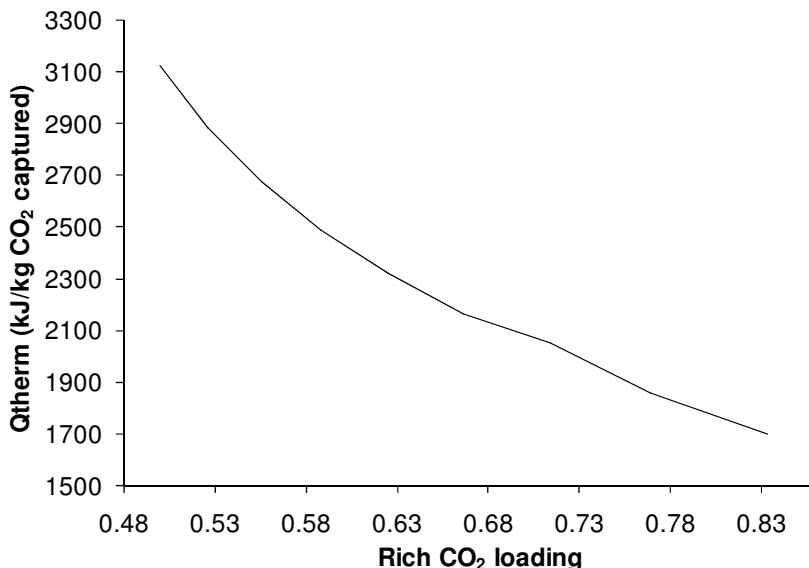
The heat requirement in the stripper is calculated according to equation (3.1). It is expressed in kJ/kg CO<sub>2</sub> captured. In these calculations, both the CO<sub>2</sub>-lean and CO<sub>2</sub>-rich streams consist of a 1 kg water solvent equivalent. The molality of ammonia is considered to be constant and calculated from the mass fraction of ammonia while the molality of carbon dioxide is calculated from the loadings.

$$ER_{des} = \frac{H_{CO_2Lean} + H_{Pure CO_2} - H_{CO_2Rich} - H_{NH_3/H_2O condenser}}{\text{Amount of CO}_2 \text{ in pure CO}_2\text{stream} * MW(CO_2)} \quad (3.1)$$

Different parameters were modified individually in order to assess their influence. The limit from this method is that these parameters are not independent from each other as a proper simulation of the

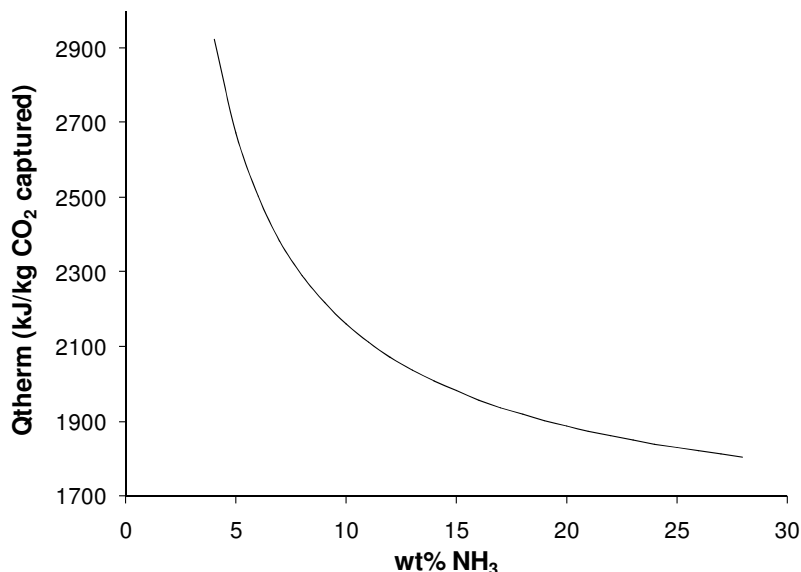
process would show. Hence, these calculations should not be seen as an accurate quantitative analysis of the heat requirement of the process. In addition, these calculations focus on the heat requirement in the CO<sub>2</sub> desorber and do not show the influence of the parameters on the chilling duty or the heat consumption in the ammonia stripper. Despite these limitations, the calculations can be used to study the general influence of various parameters and to draw general qualitative conclusions.

The influence of the rich loading on the heat requirement in the desorber can be seen in Figure 3-11. It shows a decrease of the heat requirement in the desorber when the rich loading increases at constant lean loading. This can be explained by the increase of the cyclic capacity that leads to the decrease of the sensible heat required to be added to the desorber for 1 kg water solvent. In addition, the heat of desorption of carbon dioxide from aqueous ammonia decreases when the loading increases. These equilibrium calculations show that the ability for aqueous ammonia solvent to reach high loading can be an asset to lower the heat consumption.



**Figure 3-11: Heat requirement as a function of the loading of the CO<sub>2</sub>-rich stream, at a constant mass fraction of 10 wt% ammonia**

Figure 3-12 shows the influence of the ammonia concentration in the solvent on the heat requirement in the desorber. The heat requirement decreases when the ammonia concentration increases, the decrease being faster between 5 and 10 wt% than between 10 and 28 wt%. This trend can be explained by the drop of the required sensible heat when the concentration of ammonia rises.



**Figure 3-12: Heat requirement as a function of the mass fraction of ammonia in the solvent**

The CASTOR project that consists of a pilot capture plant using aqueous MEA solution resulted in a heat consumption in the stripper of about 3700 kJ/kg CO<sub>2</sub> captured, with a capture efficiency of 90% (Knudsen *et al.*, 2008). Hence, based on the results from this study, the use of ammonia as a solvent is a promising way to achieve significant decrease in the heat consumption in the desorber. Moreover, as mentioned above, the equilibrium calculations show that it is possible to obtain a pressurized CO<sub>2</sub> stream, which would result in additional energy savings during the CO<sub>2</sub> compression.

The configuration considered here follows the recommendations from the patent. However, due to the presence of solid in the CO<sub>2</sub>-rich stream leaving the absorber, it is likely that the heat from the CO<sub>2</sub>-lean stream coming from the stripper is not sufficient to ensure the rise of temperature and the dissolution of solids and that some extra heat is required. Assuming that the temperature difference at the cold side of the heat exchanger is 5 °C, it is possible to evaluate the part of the heat that needs to be added. Based on the parameters from the reference configuration, assuming a mass fraction of ammonia in the solvent of 28 wt% and a temperature of the CO<sub>2</sub>-rich stream leaving the absorber of 15 °C, the heat required per kilogram water to rise the temperature of the CO<sub>2</sub>-rich stream up to 90 °C is 855 kJ. The enthalpy per kilogram of water that can potentially be transferred from the CO<sub>2</sub>-lean stream when its temperature decreases from 110 to 20 °C, is 587 kJ. Hence, only 69% of the rich stream can be heated by the exchange of heat. In that specific case, heating the 31% remaining represents an extra energy of 268 kJ for one kilogram water solvent, or 800 kJ/kg CO<sub>2</sub> captured. This extra heat could come from low quality heat available at the power plant or at the capture plant. Hence,

this heat could potentially be cheaper than the one used in the desorber. This high value for the required heat is mainly due to the high amount of solid at these conditions. The CO<sub>2</sub>-rich stream includes solid ammonium bicarbonate up to a temperature of 78 °C. When an initial mass fraction of ammonia of 10% is used in the solvent, by using the same temperatures and loadings for the streams entering and leaving the heat exchanger, enough heat can be recovered from the CO<sub>2</sub>-lean stream to heat up the CO<sub>2</sub>-rich stream. The difference with the 28 wt% NH<sub>3</sub> case is mainly due to the fact that the amount of solid formed with 10 wt% NH<sub>3</sub> is much lower. According to the equilibrium calculation, the ammonium bicarbonate solid phase disappears for a temperature higher than 33 °C.

Figure 3-13 plots the enthalpy necessary to heat the temperature of the CO<sub>2</sub>-rich stream up to 90 °C, and to ensure the dissolution of the solids, as a function of the temperature of the CO<sub>2</sub>-rich stream, from 15 to 90 °C. The figure also includes the enthalpy potentially transferred from the CO<sub>2</sub>-lean stream when its temperature decreases from 110 °C, as a function of the temperature of this stream. The loadings are the same as the ones described in the reference configuration. The calculations have been made for mass fractions of ammonia of 28 and 10%. The calculations take into account the enthalpy of both the solid and liquid phases and are based on one kilogram of water. It is assumed that the contents of water and ammonia are equal in both streams, as showed in Figure 3-10. Hence, the enthalpies of both streams are comparable. Figure 3-13 shows that considering the 28 wt% ammonia solvent, the enthalpy necessary to heat up the CO<sub>2</sub>-rich stream is larger than the enthalpy potentially transferred from the CO<sub>2</sub>-lean stream for a temperature lower than 68 °C. Hence, this shows that some extra energy is required to heat the CO<sub>2</sub>-rich stream due to the presence of solid in that stream up to a temperature of 73 °C. When 10 wt% NH<sub>3</sub> is considered, no additional heat is required.

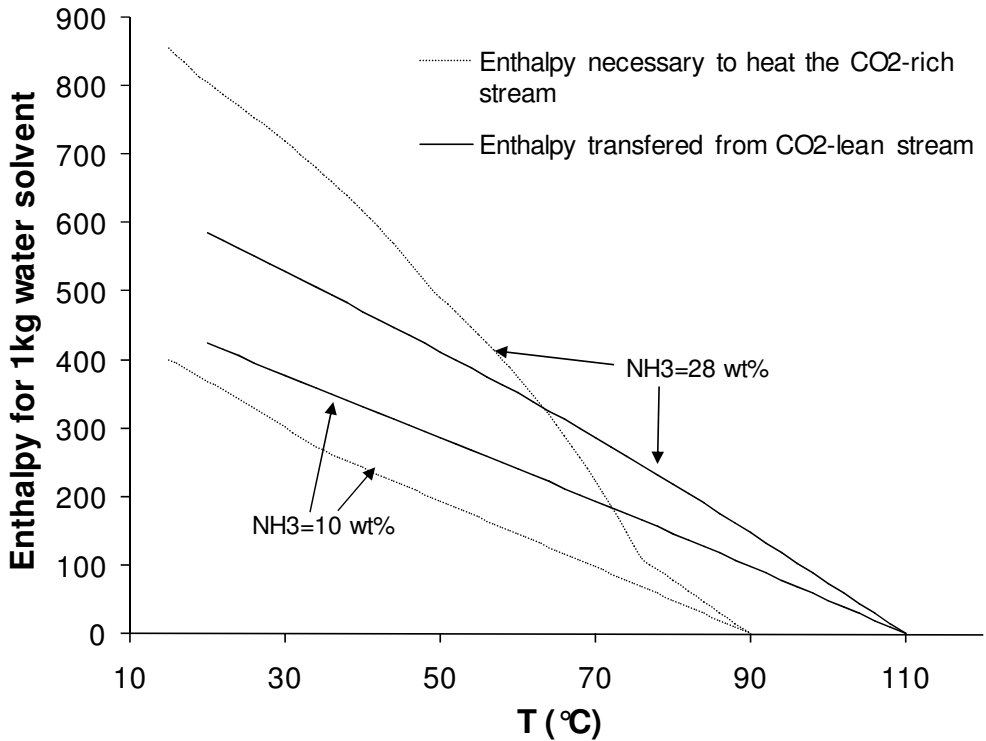


Figure 3-13: Enthalpy necessary to heat the CO<sub>2</sub>-rich stream as a function of the temperature of the CO<sub>2</sub>-rich stream for a CO<sub>2</sub> loading of 2/3, and enthalpy transferred from the CO<sub>2</sub>-lean stream as a function of the CO<sub>2</sub>-lean stream for a CO<sub>2</sub> loading of 1/3 with an initial mass fraction of ammonia of 10 and 28 wt%

### 3.4 Conclusion

The Extended UNIQUAC model was used to describe the equilibrium of the CO<sub>2</sub>-NH<sub>3</sub>-H<sub>2</sub>O system in order to perform a thermodynamic analysis of the CO<sub>2</sub> capture process using aqueous ammonia. Three concentrations of ammonia in the solvent were considered. Thanks to the indications from the patent and based on assumptions, it was possible to describe the composition of the main process streams. The equilibrium partial pressure of carbon dioxide showed the ability of the solvent for the three ammonia concentrations considered to capture carbon dioxide from coal-fired power plants at low temperature. This study showed that for the potential presence of precipitates in the absorber for high ammonia concentration in the solvent. The equilibrium calculation of the gas phase in the absorber showed a high mole fraction of ammonia. Hence, some cleaning subsystems at the top of the absorber should be considered in order to limit the emission of ammonia. The study has also shown the possibility to operate the desorber at high pressure.

From an enthalpy point of view, a reference configuration was used to assess the heat requirement in the desorber. Based on equilibrium calculations, this study showed that the use of aqueous ammonia as a solvent showed potential for a significant reduction of the heat consumption in the desorber compared to process using MEA. It also showed that when a high concentration of ammonia is used in the solvent, additional heat is required to heat the CO<sub>2</sub>-rich stream on top of the energy transferred from the CO<sub>2</sub>-lean stream in the heat exchanger.

This thermodynamic analysis allowed for making qualitative conclusions using equilibrium calculations. However, the evaluation of the process also requires the study of the kinetic rate of absorption of carbon dioxide by ammonia solvents. In addition, a process simulation study is necessary to evaluate thoroughly the performance of the technology. These studies are detailed in the following chapters.

### **3.5 References**

Darde, V.; Thomsen, K.; van Well W. J. M.; Stenby E. H. Chilled ammonia process for CO<sub>2</sub> capture, *Int. J. Greenhouse Gas Control*, **2010**, *4*, 131.

Gal, E. Ultra cleaning combustion gas including the removal of CO<sub>2</sub>. World Intellectual Property, **2006**, Patent WO 2006022885.

Knudsen, J. N.; Jensen, J. N.; Biede, O.; 2008. Castor SP2: experiments on pilot plant. CASTOR-ENCAP-CACHET-DYNAMIS Common Technical Training Workshop, Lyon, **2008**.

McLarnon, C., R.; Duncan, J. L. Testing of ammonia based CO<sub>2</sub> capture with multi-pollutant control technology. *Energy Procedia*, **2009**, *1*, 1027.





## **4 Experimental measurement and modeling of the rate of absorption of carbon dioxide by aqueous ammonia**

### ***4.1 Introduction***

The rate of absorption is a key parameter as it is a determining factor for the required contact area between the liquid and the gas. The rate of absorption is therefore strongly linked to the size of the absorber(s) and thereby to the capital expenditure for capturing carbon dioxide using ammonia. Hence, it is crucial to address this issue in order to evaluate processes based on ammonia, especially when a low absorption temperature is applied.

However, only few results are available on rate of absorption of carbon dioxide by ammonia solutions (Pinsent *et al.*, 1956, Derks *et al.*, 2009, Qin *et al.*, 2010 and Puxty *et al.*, 2010). Puxty *et al.* has developed a model to predict the rate of absorption in loaded aqueous ammonia solutions. The influence of temperature, ammonia concentration, and carbon dioxide loading on the kinetic rate of absorption were analyzed in this work. The rate of absorption of carbon dioxide in aqueous ammonia solvent was measured using a wetted wall column apparatus and compared to the rate measured for aqueous MEA solutions. The experiments cover the temperature range 6-31 °C, which is broader than the few other studies published on this topic. The ammonia concentration range used in the experiments of the present study is 1-10 wt% and the loading range is 0-0.8 mol carbon dioxide/mol ammonia. A 10 wt% ammonia solution corresponds approximately to 30 wt% MEA on an equi-molal basis.

In the following chapter, firstly, the experimental equipment designed and built in this study is described. Secondly the absorption mechanism and the expression of the kinetic rate of absorption are dealt with. Further, the wetted wall column is characterized with regard to the hydrodynamic conditions followed by the results of the liquid side mass transfer coefficient measurements. Finally the results from the modeling of the rate of absorption are given.

The results from this study have been published in International Journal for Greenhouse Gas Control (Darde *et al.*, 2011).

### ***4.2 Measurement of carbon dioxide absorption rate by aqueous ammonia***

#### **4.2.1 Review of the experimental apparatus**

As no experimental apparatus allowing for measuring the rate of absorption of carbon dioxide by liquid solvent was available at the Center for Energy Resources Engineering, it was necessary to choose, design and build an apparatus that could be used for this purpose. In the literature, different types of apparatus have been used to measure the absorption rate of carbon dioxide by a liquid solvent. This brief review describes the main types of apparatus.

### 4.2.1.1 Stirred cell reactor

The stirred cell reactor is a very common apparatus used to measure the absorption rates of a gas by a solvent. It has been especially used to measure the kinetics of absorption of carbon dioxide by alkanolamines. A scheme of the apparatus used by Vaidya and Mahajani (2005) is shown in Figure 4-1.

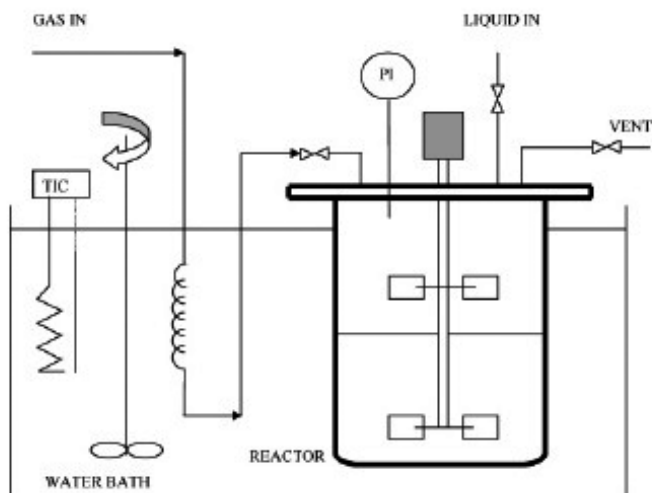


Figure 4-1: Schematic representation of a stirred cell reactor apparatus (Vaidya *et al.*, 2005)

The reactor is usually made of stainless steel. It is surrounded by a bath or a cylinder where water is circulated in order to maintain a constant temperature in the chamber. The reactor is filled with liquid and gas phases. The liquid and gas phases are commonly stirred separately with opposite directions and with adjustable speed. The speeds of the stirring appear to be a crucial parameter during the measurements.

At the beginning of an experiment, the liquid solvent, which is typically stored in a nitrogen atmosphere, is first injected in the cell. The thermodynamic equilibrium between the solvent and its vapour phase can be monitored by the pressure increase. After the equilibrium is achieved, the gas phase is injected inside the cell. The injection has to be rapid, as the absorption occurs very rapidly (Kucka L, 2003). The temperatures of the gas and liquid phase and the pressure in the cell are measured. The evolution of the pressure with time allows measuring the gas absorption rate. The apparatus allows adding inert gas to the absorbed gas in order to simulate the absorption of flue gas. An alternative to this apparatus is to maintain a constant pressure inside the cell by injecting an inert gas, typically nitrogen, at the same rate as the studied gas is absorbed. This apparatus has been used by Cadours in 2007 to measure the rate of absorption of carbon dioxide by DEA solutions. Derks et al

(2009) measured the rate of absorption of carbon dioxide by unloaded aqueous ammonia using this apparatus.

The main drawback of the use of this apparatus is the influence of the physical parameters such as the stirring speed or the depth of the stirrer in the liquid phase on the measurements. Hence, it is necessary to study the influence of the depth of the stirrer in the liquid phase, or of the stirring speed. It is therefore required to make sure that the stirring speed is constant during an experiment. In addition, the contact area between the liquid and the gas phases has to be well known despite the agitation. This is commonly done by adding baffles to the cell, as described by Lewis in 1954. A scheme of the cell used by Lewis is shown on Figure 4-2.

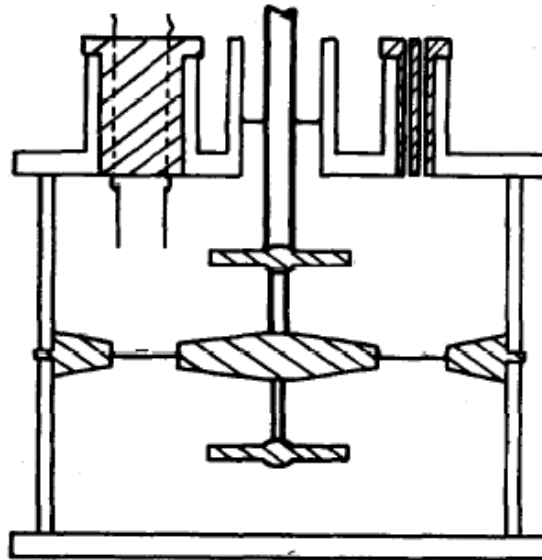


Figure 4-2: Schematic representation of a Lewis cell (Lewis, 1954)

A central baffle may prevent from the disturbance caused by the agitation. A circumferential wall baffle allows for limiting the irregular wall effects. The absorption therefore occurs in an annular gap between the two baffles thereby defining the contact area.

#### 4.2.1.2 Use of a Wetted-Wall Column

Several researchers have used wetted-wall-column apparatuses to study the absorption of gas by aqueous solutions. Among others, the study of the absorption of carbon dioxide by aqueous solutions

using a wetted-wall column has been performed by Cullinane and Rochelle in 2006, Pacheco in 1998 and Bishnoi *et al.* in 2000. Figure 4-3 shows a scheme of the wetted wall column used by Pacheco *et al.* (2000).

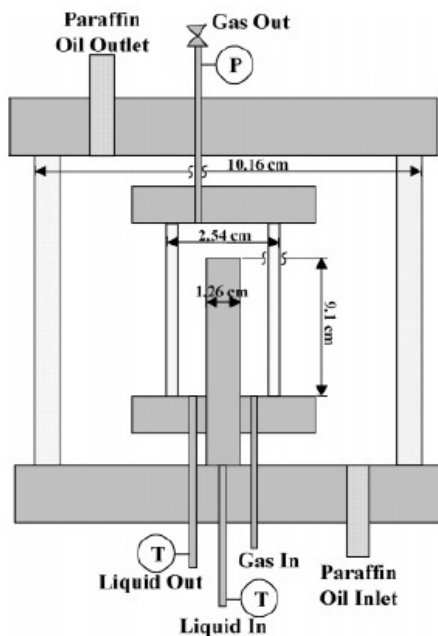


Figure 4-3: Schematic representation of a wetted wall column (Pacheco *et al.*, 2000)

The reaction chamber is commonly constructed from a stainless steel tube. The gas enters the base of the column and leaves the top of it. The liquid is pumped through the interior of a tube with a defined flow rate and is evenly distributed as a thin film along the outer surface of the tube. Therefore the total contact area between the liquid and the gas is defined by the diameter and the length of the tube. The gas and the liquid are contacted counter-currently. The chamber is surrounded by a glass cylinder. A second one encloses the chamber. Some paraffin oil or water is circulated in order to maintain a constant temperature in the reaction chamber. Therefore the temperature of absorption can be chosen. The temperatures of the gas and liquid are controlled before they reach the column. The absorption rate is measured by the difference between the inlet and outlet amount of carbon dioxide in the gas phase. The inlet and outlet concentration of gaseous carbon dioxide are measured using a CO<sub>2</sub> analyzer.

The main problems experienced when using this apparatus are the rippling of the surface of the liquid that entails uncertainties in the contact area. In addition, some researchers have reported the formation of an inactive film at the bottom of the column that leads to uncertainties about the actual height of the

film that should be used in the calculations, as reported by Yoon *et al.* in 2002. Hence, the effective height of the wetted surface has to be determined.

#### 4.2.1.3 Wetted-Sphere Absorber

Many researchers have used wetted-sphere absorber to study the reaction kinetics of the absorption of gas by a solvent. A scheme of the absorber used by Seo and Hong in 2000 is shown in Figure 4-4.

The reaction chamber consists of a glass tube. Inside the reaction chamber is placed the sphere assembly made of stainless steel. It consists of a tube with a sphere on top of it. The liquid is pumped inside the central tube and emerges at the top of the sphere. The liquid flows on the surface of the sphere as a thin and smooth film and then on the surface of the tube. The level of the liquid in the receiver is controlled by a liquid level controller. The flow of the liquid has to be optimized to get a stable film. The level of the tube has to be changed when the liquid flow rate is varied. The gas is first saturated with water and then enters the reaction chamber from its top and leaves from its top after having being absorbed by the liquid. The reaction chamber is surrounded by a wall glass cylinder where water is commonly circulated to maintain the temperature. The temperatures of the liquid and of the gas are controlled before they reach the reaction chamber.

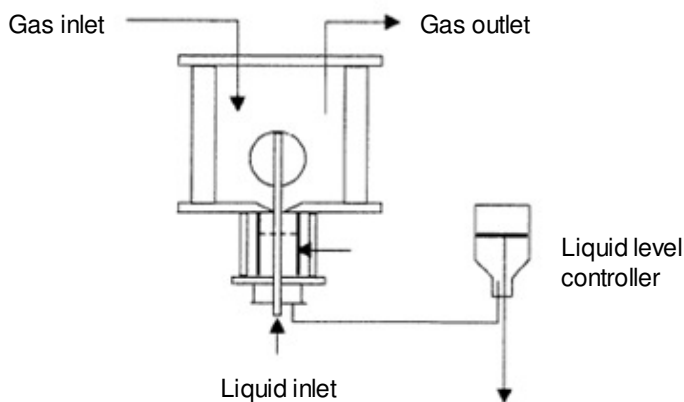


Figure 4-4: Schematic representation of a wetted-sphere absorber (Seo and Hong, 2000)

A hemispherical contactor has also been used by Jamal *et al.* in 2006 to measure the rate of absorption of carbon dioxide by AMP based solvents. The apparatus that was used is quite similar to the wetted-sphere absorber, but the full sphere is replaced by a hemisphere. Therefore, the rate of physical absorption and the contact time had to be determined by other formulas.

The main advantage of this apparatus compared to the wetted well absorber is that both the rippling and the stagnant layers effects that entailed inaccuracies are reduced.

#### 4.2.1.4 Laminar jet absorber

Laminar jet absorber apparatus have been used by several researchers to measure the absorption rate of carbon dioxide by different solvents. Figure 4-5 shows a scheme of the apparatus used by Aboudheir *et al.* in 2003 to study the kinetics of absorption of carbon dioxide by MEA solutions.

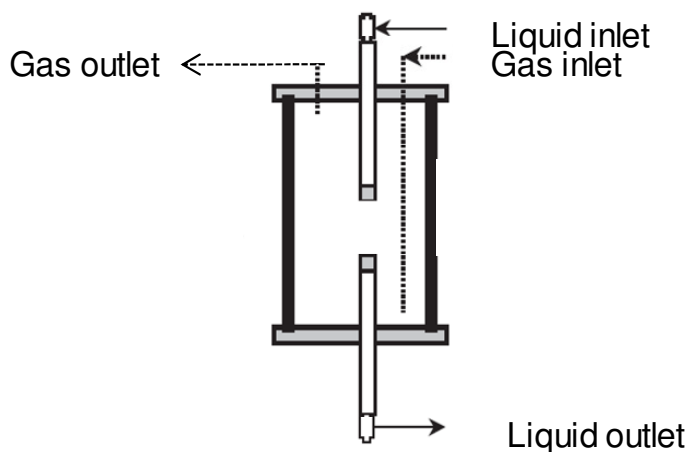


Figure 4-5: Schematic representation of a laminar jet reaction chamber (Aboudheir *et al.*, 2003)

The reaction chamber consists of a glass cylinder, enclosed in a jacket. The liquid is introduced in the reaction chamber by a tube made of steel. On bottom of this one is placed a circular nozzle in order to obtain a circular liquid jet of very small diameter. The liquid is collected in a receiver placed downwards and exits the reaction chamber. The gas is introduced in the reaction chamber and leaves it before it passes through a flow meter where its flow rate is measured. Both the diameter of the feeding tube and the distance between the bottom of the feeding tube and the top of the receiver have to be measured very accurately in order to get a precise contact time between the liquid and the gas. It is independent on the density or the viscosity of the liquid, according to Rinker *et al.* (2000).

According to Doraiswamy *et al.* in 1984, inert gas should not be introduced in the reaction chamber as its presence could change the mass transfer resistance from the gas-phase. The concentration of the absorbed gas can be varied by changing the total pressure in the apparatus.

The main disadvantage of this method is the limited distance between the feeding tube and the receiver. Therefore, the interfacial area and the contact time ranges are restricted.

#### 4.2.1.5 Disk Column

Disk column apparatus have also been used by researchers to study the kinetics of reaction of carbon dioxide with MDEA based solvent by Xu *et al.* in 1992. Figure 4-6 shows a scheme of the disk column that was used during these experiments. Hartono *et al.* (2009) and Qin *et al.* (2010) have recently used this apparatus to measure the rate of absorption of carbon dioxide by aqueous diethylenetriamine and aqueous ammonia.

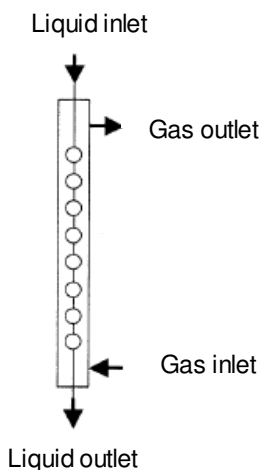


Figure 4-6: Schematic representation of a disk column (Xu *et al.*, 1992)

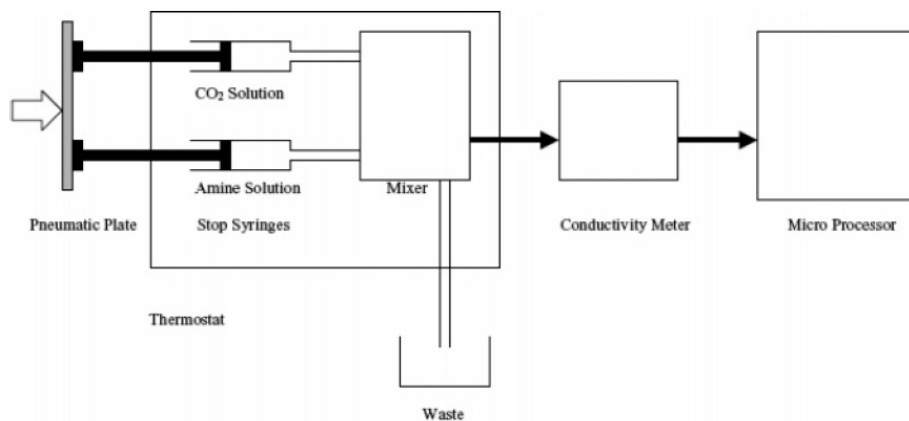
The gas enters the bottom of the column and flows upward, while the liquid is introduced from the top. Water is circulated in order to maintain a constant temperature. The outlet gas flow rate is measured by a flow meter to determine the absorption rate. The diameter, the thickness and the number of disks are key parameters that set the contact area. The main disadvantage of this method is that the compositions of both the gas and liquid phases may vary significantly in the column. Therefore, it is not possible to measure the specific absorption rate for a given composition (Vaidya *et al.*, 2007).

#### 4.2.1.6 Stopped Flow

The absorption rate of a gas by a solvent can also be performed using a stopped flow apparatus. This method excludes the influence of the mass transfer as it consists of bringing together two liquid phases. One is composed of the solvent solution, and the other of the gas dissolved in a liquid phase, typically water. Hence, it is purely the kinetics of the chemical reaction that is studied with this apparatus, as no gas phase is considered.

Figure 4-7 shows the apparatus used by Li *et al.* (2007) to measure the kinetics of reaction of carbon dioxide with different alkanolamines.





**Figure 4-7: Schematic representation of a stopped flow apparatus (Li *et al.*, 2007)**

In that study, the CO<sub>2</sub> solution was prepared by bubbling carbon dioxide in distilled water for a long time. The solutions are placed in two syringes. The pneumatic plates allows for injecting both solution in the mixer, and then to the conductivity meter cell where the ion formation can be studied as a function of time. This study allows determining the kinetics constant. Alternatively, a pH indicator has been used to perform this study. The absorption rate was determined using a color detector (Barth *et al.*, 1986).

The main disadvantage of this method is related to the limited concentration of carbon dioxide in the CO<sub>2</sub> solution. Hence, it is difficult to measure the kinetic rate for concentrated amine solutions (Vaidya *et al.*, 2007).

A similar method has been used by Pinsent *et al.* in 1956 to measure the rate of reaction between carbon dioxide and ammonia using carbon dioxide solutions. It is the evolution of the temperature that was measured in this study to determine the rate of reaction.

#### **4.2.1.7 Conclusion and choice of the apparatus**

The apparatus that was chosen to measure the kinetic rate of absorption of carbon dioxide by ammonia or alkanolamines is the wetted wall column (WWC). This choice is based on a literature study and on discussions with researchers. In order to justify this choice, the following sum-up describes the main features and drawbacks of the main apparatus.

The stirred cell apparatus is a relatively simple set up and the measurement is relatively easy, as the evolution of the pressure inside the cell can provide the rate of absorption. However, this apparatus entails a major drawback related to the accuracy of the contact area between the liquid and the gas. Indeed, because of the stirring of the liquid phase, it seems difficult to assume that the contact surface

is flat. In addition, the stirring of the ammonia liquid would have entailed the vaporization of the ammonia and deposition on the walls of the cell. This gaseous ammonia would disturb the measurement of the pressure, and would result in a less accurate measurement. It also seems difficult to account for the change of the driving force, as the partial pressure of carbon dioxide varies during an experiment. In case the pressure is maintained at a constant value, as described earlier, it could be inaccurate to assume that the CO<sub>2</sub> loading of the solution remains constant, regarding the volumes of liquid and gas inside the cell.

The laminar jet absorber was recommended as the most accurate apparatus to measure the rate of absorption of a gas, in the case of fast reactions. However, in the system studied, the preliminary information that is available shows that the reaction of absorption is not particularly fast. In addition, this apparatus is not flexible, as the distance between the liquid nozzle and the receiver is limited. Therefore, the contact time would be limited, and the measurement of the rate of absorption challenging.

The disk column was discarded because of the disadvantages reported in 4.2.1.5. The apparatus might show some limitation to determine and model accurately the rate of absorption of carbon dioxide by a solvent.

The stopped flow apparatus was discarded because of the difficulty to perform accurate measurements for concentrated amine solutions.

The wetted wall column and wetted sphere apparatuses are currently used for a broad range of systems. They are flexible apparatuses, as the flow of gas and liquid can be varied, as well as the pressure in the system. They are precise systems that are very commonly used for absorption of carbon dioxide by aqueous alkanolamines.

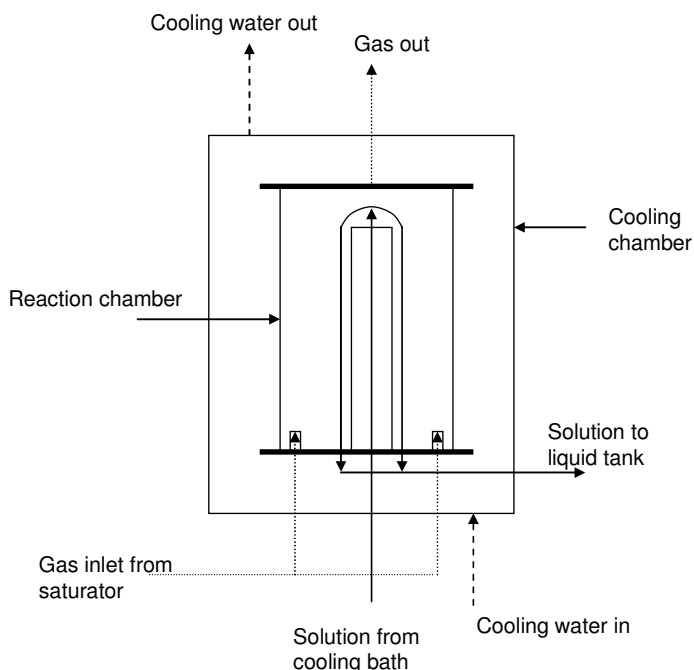
As the manufacturing of the wetted wall column apparatus seemed simpler, this experimental apparatus was selected. However, the use of this system entails two major challenges. First, it is a quite complex apparatus that requires various equipments. The design of the reaction chamber has to be specially precise and accurate. Second, the use of the apparatus is not trivial. Some time is required before measurements can be repeated and trusted. In addition, like some of the other types of apparatus mentioned, the characterization of the apparatus that permits the modeling of the gas and liquid side mass transfer coefficient is necessary.

#### **4.2.2 Description of the wetted wall column apparatus**

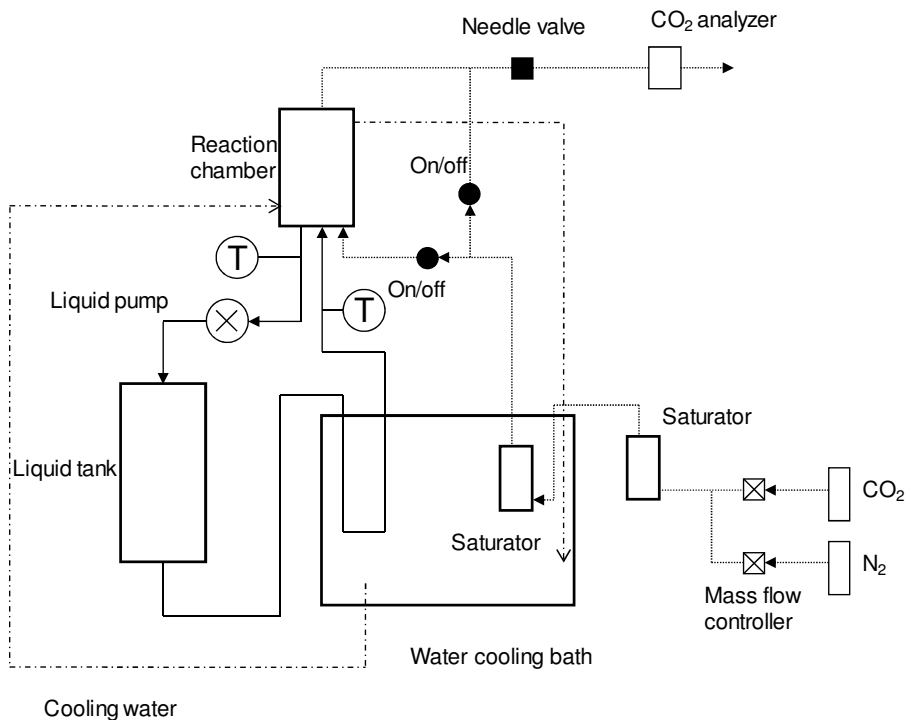
Measurements of the rate of absorption of carbon dioxide by different solvents were performed with a wetted wall column designed and constructed for this project. The design of the apparatus has been inspired by the one used for measuring the absorption rate of CO<sub>2</sub> in amine solutions at the University of Texas in Austin (Pacheco, 2000, Dugas, 2010). Discussions with researchers in Austin allowed for

improving the set up. It has been manufactured at the workshop of the Technical University of Denmark. More details regarding the apparatus can be found in Appendix A.

Figure 4-8 shows the experimental apparatus used in this work. It allows for counter-current contact between a liquid solvent and a well defined gas mixture. It shows a schematic overview of the reaction chamber and the circulation of the liquid solvent, the gas, and the cooling water. The reaction chamber consists of a glass tube in the center of which a stainless steel cylinder is fixed. The reaction chamber is enclosed in a second larger glass tube. The space between the two glass tubes is a heat exchange jacket in which water is circulated in order to maintain a constant and defined temperature. The solvent solution rises inside the stainless steel tube and then flows down, forming a thin film on the outer surface of it. The stainless steel tube has a height of 8.7 cm and an outer diameter of 1.2 cm. It reaches the bottom of the chamber where it flows back to a liquid tank. The glass tubes allows for observing the stability of the liquid film in the reaction chamber. The gas mixture of carbon dioxide and nitrogen is defined with mass flow controllers. The gas is introduced at the bottom of the reaction chamber and it flows upwards through the reaction chamber thereby allowing absorption of carbon dioxide in the liquid film. Figure 4-9 shows a schematic view of the overall experimental apparatus with all the different parts and the measuring devices included.



**Figure 4-8: Schematic view of the reaction chamber**



**Figure 4-9: Schematic view of the experimental apparatus**

Carbon dioxide and nitrogen are supplied from gas bottles with a molar purity of 99.995 and 99.996% respectively. The mixture of gases is made using Bronkhorst mass flow controllers. They allow for accurate mixing of a well-defined ratio of carbon dioxide and nitrogen but also control of the pressure. The flow rates of carbon dioxide and nitrogen are recorded. The total flow rate of gas is usually between 0.002 and 0.004 Nm<sup>3</sup>/min. The partial pressure of carbon dioxide is typically between 0 and 20 kPa. The gas flows through 1/8 inch pipes and flows through two water saturators, one at ambient temperature and another at the temperature of the experiment, as the second saturator is placed in the cooling bath. In this way it is ensured that the gas is saturated and has the correct temperature before reaching the contactor. On/Off valves allow for the by-pass of the reaction chamber. This permits the calibration of the CO<sub>2</sub> gas analyzer.

There are three evenly distributed gas inlets in the bottom of the reaction chamber to ensure a good distribution of the gas. They are elevated by 5mm in the reaction chamber in order to avoid the presence of MEA/ammonia solution in the gas pipes. Further there is one gas outlet located on the top center of the chamber.

Two non-dispersive infrared (NDIR) CO<sub>2</sub> probes (VAISALA CARBOCAP GMT 221) are used for two different concentration ranges (0-2% and 0-20%). The probes are able to measure the concentrations of carbon dioxide in gasses containing moisture. Therefore, the gas does not go through a condenser before its carbon dioxide content is measured.

The contact area between the gas and the liquid solvent can be calculated from the dimensions of the stainless steel cylinder and the homogeneous liquid solvent film on the surface. Hence, by measuring the inlet and outlet flows of carbon dioxide, it is possible to calculate the CO<sub>2</sub> absorption flux.

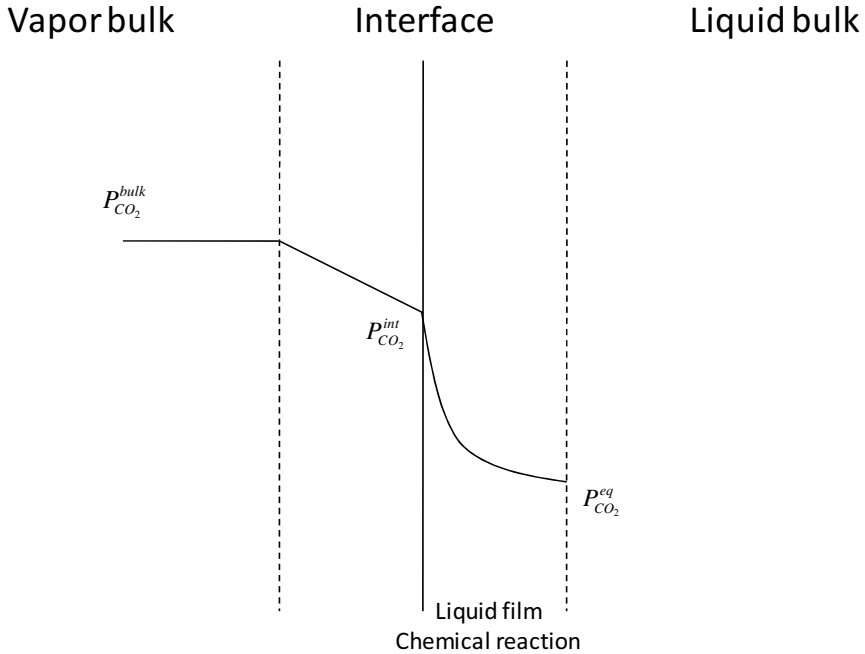
A water cooling bath (Julabo) is used to control the temperature in the experiment, from 5 to 41 °C. The water from the cooling bath is circulated in the glass jacket enclosing the reaction chamber.

The solvent solution is pumped through 1/4 inch pipes in a closed loop using a Cole-Paler EW-07001-40 micro pump. 4 mL/s is a typical flow rate that allows for a homogeneous and ripple-free film in the chamber. Three liquid outlets located at the bottom of the reaction chamber ensure the fast exit of the liquid and prevent from the formation of a stagnant liquid layer at the bottom of the chamber. A tank is included in the loop in order to ensure a large solvent volume of about 2.2 L and thereby a nearly constant loading during the experiments. The increase of the loading due to the absorption of carbon dioxide in the reaction chamber during an experiment using the solution with the fastest absorption rate was estimated to be 0.005 and therefore negligible. The liquid is pumped through the water cooling bath before it reaches the reaction chamber.

The temperature in the inlet and outlet liquid are measured using custom manufactured Pt100 1/10 DIN temperature probes from Beta. The experimental temperature is calculated as an average of these two temperatures. A typical temperature difference between the inlet and outlet is about 1 °C. The pressure at the entrance of the chamber was measured with a pressure transducer. The data from the temperature and CO<sub>2</sub> probes and from the pressure transducer were collected by a data acquisition box (Agilent 34970A).

### **4.2.3 Definition and measurement of the overall mass transfer coefficient**

According to Fick's first law, the flux of carbon dioxide is proportional to the carbon dioxide concentration gradient in the diffusion direction. The proportionality factor is the diffusion coefficient of carbon dioxide in the medium. Figure 4-10 shows a schematic representation of the mass transfer process of a diffusing gas into a liquid according to the two film model.



**Figure 4-10: Representation of the mass transfer process, inspired by Pacheco, 1998**

This representation is inspired by the two-film model. The flux can be expressed as the product between a mass transfer coefficient and the corresponding driving force, expressed as a difference of pressure. The mass transfer coefficients are functions of the diffusivity. Thus, the molar flux of a gaseous compound into a liquid that implies a chemical reaction can be expressed by two means.

First the diffusive flux of carbon dioxide from the vapor bulk to the gas film layer showed in Figure 4-10. This flux can be expressed by using the partial pressure of carbon dioxide as the driving force:

$$\varphi_{CO_2}^G = k_G (P_{CO_2}^{bulk} - P_{CO_2}^{int}) \quad (4.1)$$

Where  $P_{CO_2}^{bulk}$  is the bulk partial pressure of carbon dioxide in the gas phase and  $P_{CO_2}^{int}$  is the partial pressure of carbon dioxide at the gas-liquid interface, both expressed in Pa.  $\varphi_{CO_2}^G$  is the gaseous molar flux of carbon dioxide, expressed in mol/(m<sup>2</sup>·sec) and  $k_G$  is the gas-side mass transfer coefficient, expressed in mol/(m<sup>2</sup>·sec·Pa). It is a function of the gas properties. It accounts for the diffusion of carbon dioxide from the bulk vapor to the vapor-liquid interface as shown by the left part of Figure 4-10.

Second, this flux as shown in equation (4.1) can also be expressed as the diffusion flux at the liquid side instead of the gas side since there is a mass balance across the interface.

$$\phi_{CO_2}^L = k_G'(P_{CO_2}^{int} - P_{CO_2}^{eq}) \quad (4.2)$$

$\phi_{CO_2}^L$  is the molar liquid flux of carbon dioxide, expressed in mol/(m<sup>2</sup>·sec) as function of the mass transfer coefficient.  $P_{CO_2}^{int}$  is the partial pressure of carbon dioxide exerted by the liquid at the gas-liquid interface.  $P_{CO_2}^{eq}$  is the partial pressure of carbon dioxide of bulk liquid in Pa.  $k_G'$  is the liquid side mass transfer coefficient expressed in mol/(m<sup>2</sup>·sec·Pa). It is defined by:

$$k_G' = \frac{k_L^0 E_{CO_2}}{H_{CO_2}} \quad (4.3)$$

$k_L^0$  is the physical mass transfer coefficient in the liquid phase, expressed in m/sec. It reflects the transport of carbon dioxide from the gas-liquid interface to the bulk liquid assuming no liquid reaction.  $E_{CO_2}$  is the enhancement factor for carbon dioxide, accounting for the excess transport due to reaction. According to van Swaaij and Versteeg (1992), the enhancement factor  $E_{CO_2}$  of carbon dioxide can be defined as  $E_{CO_2} = \left(\phi_{CO_2}^L\right)_{\text{With Reaction}} / \left(\phi_{CO_2}^L\right)_{\text{Without Reaction}}$ .

$H_{CO_2}$  is the partition coefficient of carbon dioxide in the solvent, expressed in Pa·m<sup>3</sup>/mol. It is used in the conversion between liquid concentrations and partial pressures of carbon dioxide at the interface between the gas and the liquid. It is defined as the invert of the physical solubility of carbon dioxide in the solvent. It is function of both the temperature and the composition of the solvent. In a number of studies the above partition coefficient is typically called the Henry's constant even though the thermodynamic definition of the Henry's constant is not equal to the partition coefficient used. The partition coefficient converges toward the Henry's constant in pure water at infinite dilution. Therefore they are not alike for concentrated and high pressure solutions. In order to follow the description of previous studies, the actual partition coefficient used in this work is called Henry's constant in the remaining part of the derivations.

By applying the continuity of the flux at the interface, the transport through the gas film is equal to the transport through the liquid film:

$$\phi_{CO_2}^L = \phi_{CO_2}^G \quad (4.4)$$

Hence, by combining equations (4.1), (4.2) and (4.4), the flux can be expressed as the overall flux through both the liquid and gas films, by using the overall mass transfer coefficient  $K_G$  :

$$\varphi_{CO_2} = K_G(P_{CO_2}^{bulk} - P_{CO_2}^{eq}) \quad (4.5)$$

where  $\varphi_{CO_2}$  is the molar overall absorption flux of carbon dioxide, expressed in mol/(m<sup>2</sup>·sec),  $K_G$  is expressed in mol/(m<sup>2</sup>·sec·Pa).  $\frac{1}{K_G}$  represents the global resistance to the absorption through the gas film, interface, and liquid film. It can be expressed as the sum of the resistance from the gas side and from the liquid side:

$$\frac{1}{K_G} = \frac{1}{k_G} + \frac{1}{k'_G} \quad (4.6)$$

As described above the flux can be calculated using the process variables measured in the wetted wall column. This can be done knowing the contact area between the gas and the liquid and the amount of carbon dioxide absorbed per unit of time. Using mass balance principles and by assuming ideal gas law, the following expression of the flux is obtained, expressed in mol/(m<sup>2</sup>·sec):

$$\varphi_{CO_2} = \frac{P_{CO_2,in} - P_{CO_2,out}}{P} \frac{Q_g V_m}{A} \quad (4.7)$$

where  $V_m$  is the molar volume of the gas at the experimental conditions in the reaction chamber (mol/m<sup>3</sup>),  $Q_g$  is the total flow rate of gas at the entrance to the reaction chamber (m<sup>3</sup>/sec).  $Q_g$  is the inlet flow of carbon dioxide and nitrogen plus the gaseous flow of water and MEA/ammonia. The inlet flow rates of carbon dioxide and nitrogen are recorded by the mass flow controllers. The gaseous flow of MEA/ammonia and water in the chamber is calculated using the equilibrium calculations from the Extended UNIQUAC thermodynamic model available for the MEA-CO<sub>2</sub>-H<sub>2</sub>O (Faramarzi *et al.*, 2009) and the NH<sub>3</sub>-CO<sub>2</sub>-H<sub>2</sub>O (Darde *et al.*, 2010b, cf. Chapter 2) systems at the experimental conditions.  $P_{CO_2,in}$  and  $P_{CO_2,out}$  are the inlet and outlet partial pressures of carbon dioxide (Pa) and  $P$  is the total pressure of the system. The pressure is considered to be constant through the wetted wall column. The contact area  $A$  has been calculated with the geometry of the stainless steel pipe and by calculating the thickness of the liquid film. This last variable was estimated using a model from Bird *et al.* (1960) based on the momentum balance for a falling film. This model was then reused for the calculation of the physical liquid side mass transfer coefficient. The thickness of the liquid film in the reaction chamber  $\delta$  can be calculated as:



$$\delta = \sqrt[3]{\frac{3\eta_L Q_L}{\rho_L g L}} \quad (4.8)$$

Where  $\eta_L$  is the solvent viscosity,  $Q_L$  is the liquid flow rate,  $\rho_L$  is the liquid density,  $g$  is the gravitational acceleration and  $L$  is the perimeter of the wetted wall column.

The contact area between the liquid and the gas consists of the sum of two terms. First, the surface of a cylinder with the same height as the stainless steel tube (8.7 cm) and with the same diameter as the stainless steel tube (1.2 cm) plus two times the thickness of the liquid film. Second, the surface of the hemisphere with the same diameter as the cylinder to account for the area at the top of the stainless steel tube as shown in Figure 4-8. The area of the liquid film is 10% higher compared to the area of the stainless steel tube without a liquid film. It is therefore a significant effect.

Using equation (4.5) it is possible to determine the value of the overall mass transfer coefficient  $K_G$ . This is done by plotting the value of the flux as a function of  $P_{CO_2}^{bulk}$  at a given temperature, concentration of solvent, and CO<sub>2</sub> loading for various carbon dioxide partial pressures and by applying a linear regression, it is possible to obtain the value of  $P_{CO_2}^{eq}$  (for  $\phi_{CO_2} = 0$ ) and the value of  $K_G$  (slope of the line). In this work,  $P_{CO_2}^{bulk}$ , the bulk pressure of CO<sub>2</sub> in the reaction chamber, is estimated using the log mean average, as it is done by Pacheco (1998).

$$P_{CO_2}^{bulk} = \frac{P_{CO_2,in} - P_{CO_2,out}}{\ln\left(\frac{P_{CO_2,in}}{P_{CO_2,out}}\right)} \quad (4.9)$$

$P_{CO_2,in}$  is the partial pressure of carbon dioxide in the inlet of the chamber. It is determined with the measurements of the pressure in the chamber and of the carbon dioxide content in the gas when the reaction chamber is by-passed.  $P_{CO_2,out}$  is the partial pressure of carbon dioxide in the outlet. Similarly, it is determined with the measurements of the pressure in the chamber and of the carbon dioxide content in the outlet gas when it is circulated in the chamber.

#### 4.2.4 Experimental procedure

The measurement of the overall mass transfer coefficient was completed using the following steps in the laboratory:

- The system was flushed with nitrogen for at least 20 minutes, corresponding to more than 500 reaction chamber volumes.
- The pre-loaded solution was introduced in the liquid tank. It was circulated in the reaction chamber until the desired temperature was reached and a homogeneous liquid film on the

surface of the stainless steel cylinder in the reaction chamber could be obtained. When ammonia solution was used at low temperatures, pure nitrogen was introduced while the solution was circulated. This was done to prevent the ammonia solution from entering the gas pipes at the bottom of the chamber. This could have caused the formation of precipitate and disturbed the circulation of gases. It was visually ensured that the liquid level in the reaction chamber did not rise during the experiments.

- The gas with a defined total pressure and partial pressure of carbon dioxide first by-passed the reaction chamber until a stable concentration of CO<sub>2</sub> was measured. Hereby, the accuracy of the CO<sub>2</sub> probe could also be checked. The gas was then sent to the reaction chamber while the solvent solution was circulated until the CO<sub>2</sub> content in the outlet gas measured by the CO<sub>2</sub> probe was stable.
- The reaction chamber was by-passed again, and the two previous steps were repeated for a different partial pressure of carbon dioxide.

The carbon dioxide absorption flux was typically measured at 5 to 8 CO<sub>2</sub> partial pressures in order to determine the overall mass transfer coefficient accurately.

In this study, the CO<sub>2</sub> absorption rate was measured for aqueous MEA and aqueous ammonia solutions.

In the case of MEA, the solutions were prepared from pure MEA (Sigma Aldrich, purity > 99.0%) diluted to two desired concentrations. 10 and 30 wt% aqueous MEA solutions are used. The solutions were pre-loaded by bubbling carbon dioxide in the solution and by gravimetrically measuring the amount of carbon dioxide absorbed. The scale used had an accuracy of 0.01g for a mass of carbon dioxide added in the range 40-180g. The loadings used were 0.1, 0.2, 0.3 and 0.4 mol carbon dioxide/mol MEA.

In the case of ammonia, three concentrations were used in the experiments (1, 5 and 10 wt%). To prepare these solutions, 5.0 mol/L ammonia solutions (Sigma Aldrich) was used for 1 and 5 wt% solvent. 28 wt% ammonia solutions (Sigma Aldrich) were used for the more concentrated solvent. The solutions were loaded by gravimetrically adding ammonium bicarbonate. The solution was loaded gradually in order to prevent the increase of the temperature and the possible vaporization of ammonia. The loadings used were 0.2, 0.3, 0.4, 0.5, 0.6 and 0.8 mol carbon dioxide/mol ammonia. The weight of the added ammonium bicarbonate for a solution used during the experiment was in the range 20-600 g. All the solutions were made with distilled water and no further purifications were performed.

As no condenser was used to remove the moisture, ammonia or MEA in the gas phase, it was necessary to correct the value of the CO<sub>2</sub> probe by assessing the amount of water, MEA or NH<sub>3</sub> vaporized. This was done the same way as for the calculation of the gas flow rate (cf. 4.2.3). The pressure in the laboratory was measured in order to correct the CO<sub>2</sub> content measured by the CO<sub>2</sub> probe.

When ammonia or MEA solutions were used at a temperature higher than 21 °C, it was necessary to clean the compartment where the CO<sub>2</sub> content was measured by the CO<sub>2</sub> probe in order to remove the

condensed ammonia so it did not disturb the measurement by reacting with the unabsorbed carbon dioxide. In practice, for these experiments, for each of the carbon dioxide partial pressure studied, the carbon dioxide probe was taken out of the compartment for 15 minutes, which is a typical length during which the carbon dioxide content gets stabilized. The compartment was thoroughly cleaned using distilled water before the carbon dioxide probe was put back in place so that the CO<sub>2</sub> content could be measured. In the calculations, the partial pressures of water and ammonia in the outlet gas were considered to be equal to the ones at 21 °C, the laboratory temperature.

Measurements were not made for experimental conditions where precipitation of ammonium carbonate compounds occurred. As tested, the formation of precipitate disturbed the circulation of the solution and could lead to pipes clogging. Hence, measurements with 5 wt% aqueous ammonia solutions at loadings above 0.6 and temperatures below 21 °C and measurements with 10 wt% aqueous ammonia solutions at loadings above 0.5 and temperatures below 21 °C were not performed.

### 4.3 Rate of absorption and expression of the overall kinetic constant

#### 4.3.1 Overall kinetic constant using aqueous ammonia solutions

During the absorption of carbon dioxide into aqueous ammonia (or into aqueous solutions of primary alkanolamines like MEA), three main reactions should be considered at the gas-liquid interface, on the liquid side.

- First, the carbonic acid formation:



According to Blauwhoff *et al.* (1984), this reaction is considered to have a negligible contribution to the overall rate of absorption as this reaction is very slow compared to the other ones.

- Bicarbonate formation:



The reaction rate can be described as:

$$r_{CO_2-OH^-} = k_{OH^-} C_{CO_2} C_{OH^-} \quad (4.12)$$

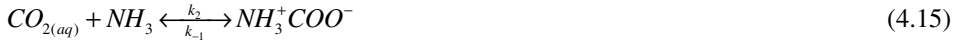
The expression of the reaction rate constant  $k_{OH^-}$ , given in m<sup>3</sup>/(mol·sec), has been proposed by Pinsent *et al.* (1956a)

$$\log k_{OH^-} = 10.635 - \frac{2895}{T} \quad (4.13)$$

- Finally, the carbamate formation:



According to Derks *et al.* (2009), similarly to the absorption of carbon dioxide by primary and secondary alkanolamines solutions, a zwitter-ion mechanism occurs in the case of ammonia. This mechanism has been proposed by Caplow in 1968 and reintroduced by Danckwerts in 1979. First, an ammonia molecule reacts with carbon dioxide to form a zwitter-ion that is later deprotonated in a second step. The nomenclature for the kinetic constant is the same as the one used by Vestee *et al.* (1996).



In reaction (4.16),  $B$  represents any base that is available in the solution. In the present case, it can therefore be a molecule of ammonia, water or a hydroxide ion present in the solution. In the case of  $CO_2$  absorption by aqueous Diisopropanolamine (DIPA) solutions, the contribution of the hydroxide ion is rather small, according to Versteeg *et al.* (1988a) and Little *et al.* (1992), because the deprotonation proceeds mainly by alkanolamine and water based on the experimental study by Blauwhoff *et al.* (1984). Hence, it is difficult to assess accurately the kinetic constant related to this reaction. Therefore, in this study, only the contributions of water and of ammonia have been considered for the deprotonation. At quasi steady state, as shown by Danckwerts (1979) and according to equations (4.15) and (4.16), the overall chemical rate of absorption of carbon dioxide by ammonia is given by:

$$r_{CO_2-NH_3} = k_2 C_{CO_2} C_{NH_3} - k_{-1} C_{NH_3^+COO^-} = C_{NH_3^+COO^-} \sum_b k_b C_B \quad (4.17)$$

Where  $\sum_b k_b C_B$  represents the contributions of the different bases in the system. Therefore:

$$r_{CO_2-NH_3} = \frac{C_{CO_2} C_{NH_3}}{\frac{1}{k_2} + \frac{k_{-1}}{k_2} \left( \frac{1}{\sum_b k_b C_B} \right)} \approx \frac{C_{CO_2} C_{NH_3}}{\frac{1}{k_2} + \frac{k_{-1}}{k_2} \left( \frac{1}{k_{H_2O} C_{H_2O} + k_{NH_3} C_{NH_3}} \right)} \quad (4.18)$$

where  $C_i$  represent the concentrations of compounds  $i$  in the liquid, given in  $\text{mol}/\text{m}^3$ , the constant  $k_2$  is given in  $\text{m}^3/(\text{mol}\cdot\text{sec})$ ,  $\frac{k_2 k_{H_2O} k_{-1}}{k_{-1}}$  and  $\frac{k_2 k_{NH_3}}{k_{-1}}$  are given in  $\text{m}^6/(\text{mol}^2\cdot\text{sec})$  and the rate  $r$  is expressed in  $\text{mol}/(\text{m}^3\cdot\text{sec})$ .

The overall kinetic rate constant  $k_{ov}$ , expressed in  $\text{sec}^{-1}$  is the sum of the contributions of the hydroxide ion and of the ammonia, as which results in the following expression based on equation (4.12) and (4.18).

$$k_{ov} = \frac{r_{CO_2-NH_3}}{C_{CO_2}} + \frac{r_{CO_2-OH^-}}{C_{CO_2}} = \frac{C_{NH_3}}{\frac{1}{k_2} + \frac{k_{-1}}{k_2} \left( \frac{1}{k_{H_2O} C_{H_2O} + k_{NH_3} C_{NH_3}} \right)} + k_{OH^-} C_{OH^-} \quad (4.19)$$

Several absorption models have been implemented in order to describe the physical process of absorption. Historically, the main ones are the two-film theory, proposed by Lewis and Whitman in 1924 and the penetration theory proposed by Higbie in 1935 and later on developed as the surface renewable theory by Danckwerts in 1951. Each of these approaches allows for modeling the mass transfer coefficients. These models use the Hatta number (Ha), defined by:

$$Ha = \frac{\sqrt{k_{ov} D_{CO_2,L}}}{k_L^0} \quad (4.20)$$

where  $D_{CO_2,L}$  is the diffusion coefficient of  $CO_2$  in the liquid phase.

The reaction during absorption of carbon dioxide in aqueous amine solutions is typically second order. In the case of second order reactions, the determination of the enhancement factor can be rather complex (van Krevelen, 1948). However, it is possible to apply conditions in which the concentrations of the reactants are constant in the solution, which implies that the reactant (in this case, MEA or ammonia) is not considerably depleted at the gas-liquid interface. This condition defines the pseudo first order reaction regime (Danckwerts, 1970). Under these conditions, for the film theory, the expression of the enhancement factor has been reported by van Swaaij *et al.* (1992) (equation (4.21)). In practice, when  $Ha$  is greater than 2, the enhancement factor can be approximated by the Hatta number.

$$E = \frac{Ha}{\tan Ha} \quad (4.21)$$

As reported by Kucka *et al.* (2003), the condition for a pseudo-first order reaction is given by:

$$2 < Ha \ll E_\infty \quad (4.22)$$

where  $E_\infty$  is the enhancement factor for a instantaneous reaction for which the absorbent is depleted at the liquid-gas interface. The fact that we are sufficiently away from the instantaneous reaction regime allows for assuming that the concentration of solvent is constant at the interface.  $E_\infty$  is defined by

$$E_\infty = 1 + \frac{D_{NH_3,L} C_{NH_3}^{bulk}}{2D_{CO_2,L} C_{CO_2}^{int}} \quad (4.23)$$

where  $D_{NH_3,L}$  and  $C_{NH_3}^{bulk}$  are the diffusion coefficient and the bulk concentration of ammonia in the liquid phase and  $C_{CO_2}^{int}$  is the concentration of carbon dioxide in the liquid phase at the gas-liquid interface. The correlation used for the diffusion coefficient of ammonia in the liquid phase is taken from Frank *et al.* (1996):

$$D_{NH_3,L} = (1.65 + 2.47x_{NH_3}) 10^{-6} \exp\left(-\frac{1996.6}{T}\right) \quad (4.24)$$

The apparent kinetic rate constant for the carbamate reaction is calculated from the overall kinetic rate constant  $k_{ov}$  by subtracting the contribution from the hydroxide ion as shown in equation (4.25).

$$k_{app} = k_{ov} - k_{OH^-} C_{OH^-} = \frac{C_{NH_3}}{\frac{1}{k_2} + \frac{k_{-1}}{k_2} \left( \frac{1}{k_{H_2O} C_{H_2O} + k_{NH_3} C_{NH_3}} \right)} \quad (4.25)$$

The apparent kinetic rate constant is commonly used in the literature (Derks *et al.*, 2009).

### 4.3.2 Overall kinetic constant using MEA solutions

Similar reactions as the one described in equation (4.10), (4.11), (4.15) and (4.16) occur in the case of MEA, reaction (4.10) having again negligible contribution compared to the other reactions. According to Versteeg *et al.* (1996), based on the different experimental studies available in the literature, when the carbamate formation is considered using the zwitter-ion mechanism, the second term of the denominator in equation (4.18) is negligible compared to the first one, and the rate of absorption can therefore be given by:

$$r_{CO_2,MEA} = k_2 C_{CO_2} C_{MEA} \quad (4.26)$$

Similarly to the case of ammonia, if the conditions of a pseudo first order regime are applied, meaning that MEA is not depleted at the gas-liquid interface (see equation (4.22)), the expression of the enhancement factor can be given by:

$$E = \frac{\sqrt{(k_2 C_{MEA} + k_{OH^-} C_{OH^-}) D_{CO_2}}}{k_L^0} \quad (4.27)$$

This simple expression for the enhancement factor for the absorption of carbon dioxide by aqueous MEA for first order regime has been commonly used and is satisfactory under these conditions.

#### 4.4 Characterization of the wetted wall column

As shown in equations (4.3) and (4.6), it is necessary to be able to model the gas side mass transfer coefficient  $k_G$  and the physical mass transfer coefficient in the liquid phase  $k_L^0$  to determine the liquid side mass transfer coefficient  $k_G'$  and the enhancement factor. These are determined from experiments as described in the following discussions.

##### 4.4.1 Determination of the gas side mass transfer coefficient, $k_G$

The gas side mass transfer coefficient can be determined by measuring the overall mass transfer coefficient for a system with a low and well known resistance. By measuring the overall resistance and by calculating the liquid side resistance, the gas side resistance can be determined by equation (4.6).

The characterization of the gas side mass transfer coefficient for a wetted wall contactor was done by Pacheco in 1998 and continued by Bishnoi and Rochelle in 2000. It was estimated by measuring the rate of absorption of CO<sub>2</sub> into an unloaded MEA solution. The kinetics of this reaction is well known, and the reaction is fast. Therefore the contribution of the liquid-side resistance is low and the gas side resistance can be determined accurately. A similar method was used in this study.

The overall mass transfer coefficient for the absorption of carbon dioxide by unloaded MEA solutions was determined by measuring the absorption flux at different partial pressures of carbon dioxide and by using equation (4.5).

When conditions for pseudo first order regime are applied, the liquid side mass transfer coefficient for the absorption of CO<sub>2</sub> by unloaded MEA solutions can be determined using equations (4.3) and (4.27) applying correlations for the kinetic rate constant, Henry's constant, and the diffusion coefficient.

The correlation from Hikita *et al.* (1977) was used in the calculation of the kinetic rate constant  $k_2$  as a function of the temperature, as shown by:

$$k_2 = 9.77 \cdot 10^7 \exp\left(-\frac{4955}{T}\right) \quad (4.28)$$

An empirical correlation was used for the Henry's law constant for carbon dioxide in MEA solutions, by Dang *et al.* (2003). It originates from the work of Licht and Weiland (1989). The correlation in  $\text{Pa} \cdot \text{m}^3 \cdot \text{mol}^{-1}$  is

$$H_{\text{CO}_2, \text{MEA}} = \alpha \cdot \exp\left(-\frac{2625}{T} + 12.2\right) \quad (4.29)$$

with

$$\alpha = \exp\left(\left(\frac{5076}{T} - 16.699\right)x_{\text{MEA}} + hI\right) \quad (4.30)$$

Temperatures are expressed in Kelvin,  $x_{\text{MEA}}$  is the mole fraction of MEA in the unloaded solution,  $h$  is the van Krevelen constant and  $I$  the ionic strength. In this study, similarly to Dang *et al.* (2003), the  $hI$  term has been neglected.

The calculation of the diffusivity of carbon dioxide in the aqueous MEA solution is determined using the  $\text{N}_2\text{O}$  analogy:

$$\frac{D_{\text{CO}_2, \text{MEA}}}{D_{\text{CO}_2, \text{water}}} = \frac{D_{\text{N}_2\text{O}, \text{MEA}}}{D_{\text{N}_2\text{O}, \text{water}}} \quad (4.31)$$

The correlations for the diffusivity of  $\text{CO}_2$  and of  $\text{N}_2\text{O}$  in water were obtained from Versteeg *et al.* (1988b), given in  $\text{m}^2/\text{sec}$  by

$$D_{\text{CO}_2, \text{water}} = 2.35 \cdot 10^{-6} \exp\left(-\frac{2119}{T}\right) \quad (4.32)$$

$$D_{\text{N}_2\text{O}, \text{water}} = 5.07 \cdot 10^{-6} \exp\left(-\frac{2371}{T}\right) \quad (4.33)$$

The correlation used for the diffusivity of  $\text{N}_2\text{O}$  in MEA solution was given by Ko *et al.* (2001). It takes into account both the temperature and the concentration of the amine in the solution.

$$D_{\text{N}_2\text{O}, \text{MEA}} = \left(5.07 \cdot 10^{-6} + 8.65 \cdot 10^{-10} C_{\text{MEA}} + 2.78 \cdot 10^{-13} C_{\text{MEA}}^2\right) \exp\left(\frac{-2371 - 9.34 \cdot 10^{-2} C_{\text{MEA}}}{T}\right) \quad (4.34)$$



The gas side mass transfer coefficient is dependent on the hydrodynamic conditions. It basically depends on the path and the velocity of the flow. The influence of these conditions is described in the mass transfer coefficient model of Hobler (1966). It is valid specifically for laminar-flow regime in wetted-wall columns. It comprises the Sherwood (Sh), Schmidt (Sc) and Reynolds (Re) numbers. Based on this similar assumption, Pacheco (1998) developed an empirical 2-parameter model of the following form:

$$Sh = \alpha Re^\beta Sc^\beta \left( \frac{d_s}{h} \right)^\beta \tag{4.35}$$

Using the definitions of

$$Sh = \frac{k_G d_s}{D_i^{Gas}}, \quad Re = d_s^2 N \frac{\rho}{\eta}, \quad Sc = \frac{\eta}{\rho D_i^{Gas}} \tag{4.36}$$

Where  $d_s$  is the difference between the radii of the inner glass tube and of the central tube (in the case of this apparatus and in this study, it is considered as a constant,  $d_s = 0.7\text{cm}$ ),  $\rho$  is the density of the gas,  $\eta$  is the dynamic viscosity,  $h$  is the height of the column (for this apparatus,  $h = 8.7\text{cm}$ ) and  $N$  is the mean gas velocity.  $\alpha$  and  $\beta$  are the parameters to be fitted. They were fitted using equations (4.6), (4.7), and (4.27). It should be noticed that the exponents for the Reynolds and the Schmidt in equation (4.35) are equal. This indicates that the influences of the viscosity and the density are only implicitly considered in the model.

The absorption flux has been measured for 10 and 30 wt% unloaded MEA solutions at 20 and 40 °C. Low concentrations of carbon dioxide in the gas phase were used in order to avoid the depletion of MEA at the interface. About 60 measurements were used to determine these parameters. The value of the parameters can be found in Table 4-1.

**Table 4-1: Value of the system parameters used to calculated the Sherwood number**

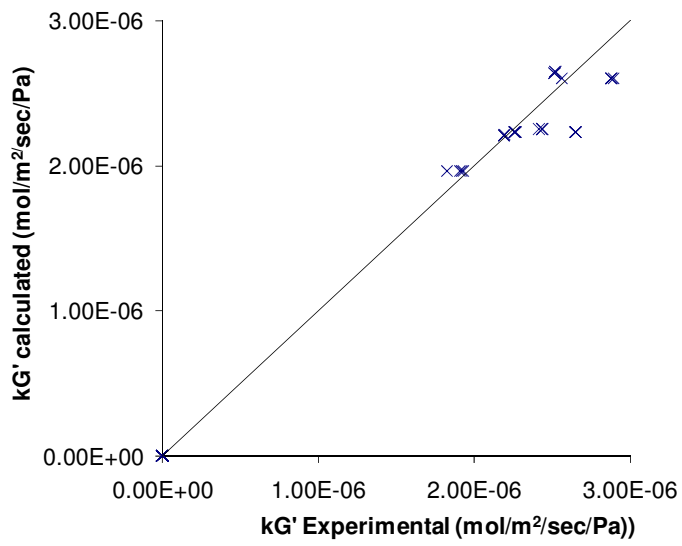
$\alpha$	1.53
$\beta$	1.02

These parameters show that at similar hydrodynamic conditions, the gas side mass transfer coefficient for the wetted wall column used in the present study is significantly higher (lower resistance) than the one found with the apparatus used by Pacheco *et al.* who obtained  $\alpha = 0.85$  and  $\beta = 1.05$ . The observed difference is probably due to the fact that the apparatus used in this work includes three gas inlets at the bottom of the reaction chamber, which improves the circulation of the gas in the chamber

and minimizes the gas resistance compared to the apparatus used by Pacheco *et al.* that only includes a single gas inlet.

The accuracy of the liquid side mass transfer coefficient  $k'_G$  depends on the accuracy of the gas side mass transfer coefficient. It can be calculated in two ways. Either using the expression of the enhancement factor for pseudo first order regime in unloaded MEA solutions (equations (4.3) and (4.27)). Or by measuring the overall mass transfer coefficient and subtracting the contribution from the gas side mass transfer coefficient using the model above. The two representations of  $k'_G$  should be in accordance with each other.

Figure 4-11 shows the comparison of the liquid side mass transfer coefficient  $k'_G$  calculated from equations (4.3) and (4.27) with  $k'_G$  obtained from the experimental measurements of the absorption flux of carbon dioxide in MEA solvent and using the Hobler's model (equation (4.35)). These measurements were used to fit the parameters used for the Sherwood number in Table 4-1. The average deviation obtained is 5.2%. The good agreement between the experimental and the calculated liquid side mass transfer coefficient shows that the gas side mass transfer coefficient is determined with sufficient accuracy.



**Figure 4-11: Comparison of the liquid side mass transfer coefficient calculated using the expression of the enhancement factor for the absorption of carbon dioxide by MEA solvent for the pseudo first order regime with the liquid side mass transfer coefficient calculated from the experimental measurements of the absorption flux of carbon dioxide in MEA solvents and from the calculation of the gas side mass transfer coefficient with the Sherwood number.**

Accounting for the formation of bicarbonate described in equation (4.11) had a very limited influence on the parameter determination. This was determined by discarding the second term in the parenthesis of equation (4.27). It barely affected the value of the liquid side mass transfer coefficient. This is due to the very low concentrations of the hydroxide ion.

It should be noted that the parameters that allows for calculating the Sherwood number (see Table 4-1) depend a lot on the correlation used for the Henry's law constant and the diffusivity of carbon dioxide in the solvent. The present correlations were chosen as they seemed to be best and sufficiently able to take the concentration of MEA into account. It should also be noted that these parameters are specific to the wetted wall column used in the experiments.

#### 4.4.2 Determination of the physical liquid mass transfer coefficient $k_L^0$

The physical mass transfer coefficient in the liquid phase  $k_L^0$  can be determined by using a fundamental model shown below and by making assumptions regarding the diffusion of gas. In the present study, the modeling  $k_L^0$  was done using the model proposed by Pigford (1941). It has been thoroughly described and applied for wetted wall column apparatus by Pacheco. In this model, the convective transport is considered to be in the direction of the flow, while the diffusive transport is in the perpendicular direction of the flow. The model depends on the variable  $\Theta$  that accounts for the carbon dioxide concentration change during the absorption. It is defined as.

$$\Theta = \frac{C_{CO_2,int} - C_{CO_2,outlet}}{C_{CO_2,int} - C_{CO_2,inlet}} \quad (4.37)$$

The model uses the dimensionless number  $\varepsilon$

$$\varepsilon = \frac{D_{CO_2,solvent} h}{u_{surf} \delta^2} \quad (4.38)$$

where  $h$  is the height of the column,  $u_{surf}$  is the velocity at the surface of the liquid and  $\delta$  is the thickness of the liquid film in the reaction chamber (see Figure 4-8). These two last parameters are estimated using a model from Bird *et al.* (1960) based on the momentum balance for a falling film, given by equations (4.8) and (4.39).

$$u_{surf} = \frac{\rho_L g \delta^2}{2\eta_L} \quad (4.39)$$

The expression of  $\Theta$  varies with the order of magnitude of  $\varepsilon$ . For the cases discussed here,  $\varepsilon$  was systematically lower than 0.01. Therefore, the following expression is valid under the used conditions.

$$\Theta = 1 - 3\sqrt{\frac{\varepsilon}{\pi}} \quad (4.40)$$

The liquid side mass transfer coefficient can then be obtained using an expression from Hobler (1966).

$$k_L^0 = \frac{Q_L}{A}(1 - \Theta) \quad (4.41)$$

In the present study, the physical mass transfer coefficient in the liquid phase is used to calculate the value of the Hatta number using equation (4.20). It is consequently used in order to check the conditions for pseudo first order regime by equation (4.22). This allows for using the simple enhancement factor expression, equation (4.21). In the pseudo first order regime the calculations of the absorption flux is not affected by the physical mass transfer coefficient in the liquid phase.

#### 4.5 *Liquid side mass transfer coefficient*

The liquid side mass transfer coefficient  $k_G'$ , introduced in equation (4.3), accounts for the physical and chemical mass transfer in the liquid film. Hence, the diffusion and the physical solubility of the carbon dioxide in the solvent as well as the effect from the chemical reactions are included in this factor. Hence, it is the factor that should be used when the mass transfer performance from a solvent is evaluated and compared with other solvents. As shown in equation (4.6), the liquid side mass transfer coefficient is determined from the measurement of the overall mass transfer coefficient  $K_G$  and from the modeling of the gas side mass transfer coefficient  $k_G$  (equation (4.35)).

The overall mass transfer coefficient was measured for aqueous ammonia solutions at ammonia concentrations between 1 and 10 wt%, loadings between 0 and 0.8, and temperatures between 6 and 41 °C. In these experiments, the resistance from the gas side has been minimized as discussed previously in order to increase the accuracy of the results.

An example of the determination of the overall mass transfer coefficient for a 5 wt% aqueous ammonia solution at 11 °C with a loading of 0.3 is given in Figure 4-12 where the carbon dioxide flux is plotted against the partial pressure of carbon dioxide. The slope of the curve is the value of  $K_G$ . According to equation (4.5), the equation of the linear trend line allows potentially for determining the equilibrium pressure of carbon dioxide in the solution. However, to determine a precise value of this property, measurements at low partial pressure of carbon dioxide are necessary. They were not performed because the calculation of the equilibrium pressure is not within the scope of this work and because the mass flow controllers and the carbon dioxide probes would not allow for a precise measurement of the y-intercepts. Figure 4-12 shows a negative value of the flux at  $P_{CO_2}^{bulk} = 0$  Pa which is in accordance to the behavior of equation (4.5) resulting in  $\varphi_{CO_2} = -K_G P_{CO_2}^{eq}$ .

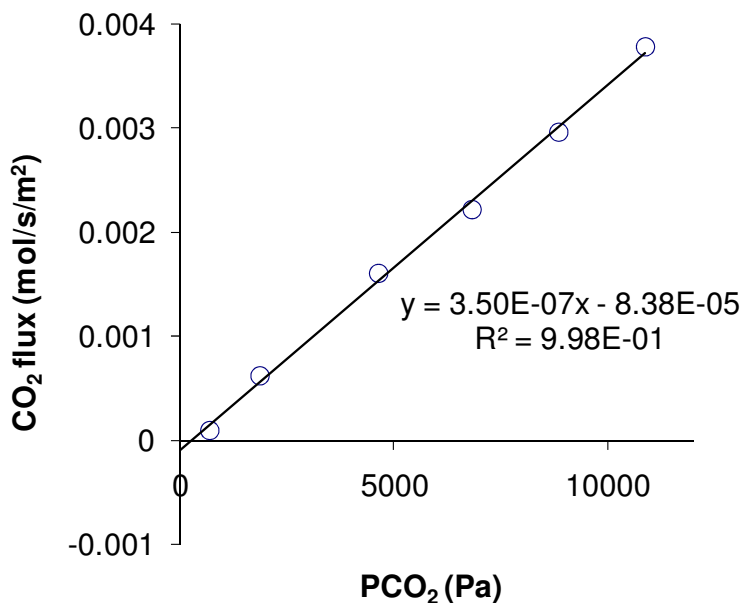


Figure 4-12: CO<sub>2</sub> absorption flux as a function of the partial pressure of CO<sub>2</sub> for a 5 wt% aqueous ammonia solution with a loading of 0.4 at 21 °C

#### 4.5.1 Considerations regarding the accuracy of the measurements

When experiments are carried out, especially using a newly built apparatus, it is essential to estimate the experimental uncertainty from the measurements. The influence of different experimental parameters must be evaluated.

The calculation of the absorption flux strongly depends on the contact area between the gas and the liquid. It was visually possible to observe that the falling film was homogenous and stable. The stability of the flow rate of liquid could also be checked. The flow rate of the liquid was varied in order to avoid any visible rippling effect.

The temperature was measured by temperature probes that had been calibrated from -1 to 50 °C prior to the experiments. For a given temperature of the cooling bath, it could be checked that the temperature reported by the probes was not varying over several weeks and the temperature of the solvent was therefore very stable and reliable. During an experiment, as soon as the chosen experimental temperature of the circulated solvent was reached, it was stabilized during the whole experiment without variation. As stated in 4.2.2, the temperature difference between the inlet and outlet liquids was lower than 1°C. This can be considered as the uncertainty of the temperature measurement.

The pressure transducer has been calibrated prior to the experiments between 0 and 20 bars. At low temperature, the pressure measured was very stable during an experiment. When the temperature was higher, the pressure was slightly more unstable due to the evaporation of water, but the variations observed were lower than 0.003 bar.

The flow rate of gas and the accuracy of the mixture of carbon dioxide and nitrogen are key parameter of the measurements. The mass flow controllers used were responsive and the change of partial pressure of carbon dioxide was fast. The flow rates of nitrogen and carbon dioxide for a given carbon dioxide partial pressure were very stable. However, the use of this equipment implied two limitations. First, it was not possible to make measurements at high pressure, because the flow rates of gas could not reach a stable value. Hence, during the measurements, the pressure in the reaction chamber was limited to 3 bar. Second, measurements at low partial pressure of carbon dioxide were not possible. The mass flow controllers used did not allow for a stable very low flow rate of carbon dioxide. This is a limitation as these measurements are necessary to determine accurately the equilibrium partial pressure of carbon dioxide for loaded solutions.

The main source of uncertainty from the experiment was related to the measurement of the carbon dioxide content in the outlet gas. Several factors affected the accuracy of the measurements. Some limitations came from the probes used. They were calibrated prior to the experiments. The validity of the calibration could be checked during the experiments while the reaction chamber was by-passed. After some weeks of measurements, the probe measuring the 0-2% range was discarded as its measurement quality decreased. This probe was not replaced. Hence, measurement with low carbon dioxide content could not be made. The 0-20% only required some minor adjustments of the calibration function and its validity was trusted until the end of the measurements. During the measurements, uncertainty was implied by the relative instability of the carbon dioxide content signal from the CO<sub>2</sub> probe. The fluctuations of the signal could reach up to 0.1%, which leads to an uncertainty of the flux up to 10%. The fluctuations were higher at high carbon dioxide content. For high temperature experiments, water and ammonia were vaporized from the chamber and were condensed in the reaction chamber, which lead to additional uncertainties. Efforts were made in order to limit the effect of the condensed ammonia by cleaning the reaction chamber and inserting the probe only after the cleaning and stabilization of the CO<sub>2</sub> content. In addition, the carbon dioxide content was corrected with the partial pressure of water and ammonia as well as with the pressure and temperature in the laboratory. However, for the high pressure, high ammonia concentrated and unloaded solutions, the results should be seen as indicative as stated below. No condenser was used for this apparatus, as the high content of condensed ammonia could have affected significantly the results, and the correction of the measurements would have been unreliable.

Many of the measurements presented here were repeated in order to check if it was possible to reproduce the results. At least five partial pressures of carbon dioxide were applied for each of the

measurements. When a low correlation coefficient was obtained from the linear regression, the measurements were systematically repeated.

#### 4.5.2 Liquid side mass transfer coefficient with aqueous MEA

The results for the liquid side mass transfer coefficient  $k'_G$  are given in Table 4-2 for 30 wt% MEA solutions for a loading from 0 to 0.4 for a temperature of 20 and 40 °C. They are determined by measuring the overall mass transfer coefficient for the different solutions and by calculating the gas side mass transfer coefficient using equation (4.35).

**Table 4-2: Liquid side mass transfer coefficient for 30.0 wt% MEA solutions at 20 and 40 °C**

	$k'_G \cdot 10^6$ (mol/(m <sup>2</sup> ·sec·Pa))				
Loading	0	0.1	0.2	0.3	0.4
20 °C	1.99	1.62	1.43	0.98	0.79
40 °C	2.58	2.15	1.85	1.53	1.14

For these experiments, the resistance from the gas side accounted for 5 to 25% of the total resistance. For all the experiments reported here, the conditions for the pseudo first order regime were respected. Hence, by using the Extended UNIQUAC thermodynamic model for the MEA-CO<sub>2</sub>-H<sub>2</sub>O system to calculate the concentration of free MEA and hydroxide ion as a function of the loading and the temperature and by using equations (4.3) and (4.27) as well as the correlations for the Henry's constant and the diffusivity of carbon dioxide in MEA solutions (equations (4.29), (4.32), (4.33) and (4.34)) it is possible to model the liquid side mass transfer coefficient. Figure 4-13 shows the results presented in Table 4-2 together with the results from the model. Experimental measurements of the liquid side mass transfer coefficient for 30 wt% MEA at 40 °C at difference loadings from Dang *et al.* (2003), Aboudheir *et al.* (2003), Dugas (2009), and Hartono (2009) have been included.

Figure 4-13 shows that the experiments at high loading from the present study are in a good agreement with the ones from the literature. At a loading of 0.25, the data by Dugas is significantly higher than the one observed in the present study. No experiments at lower loadings were made by Dugas. At these conditions, the system would become dominated by the gas side resistance and therefore their measurements would lack accuracy (Dugas, 2010). The results from Hartono *et al.* and from Aboudheir *et al.* at low loading are in relatively good agreement with the results from the present study.

Figure 4-13 also shows the good agreement between the experimental data and the modeling of the liquid side mass transfer coefficient used in this study. This agreement is valid for both temperatures. Hence, these results validate the modeling of the gas side mass transfer coefficient for this apparatus.

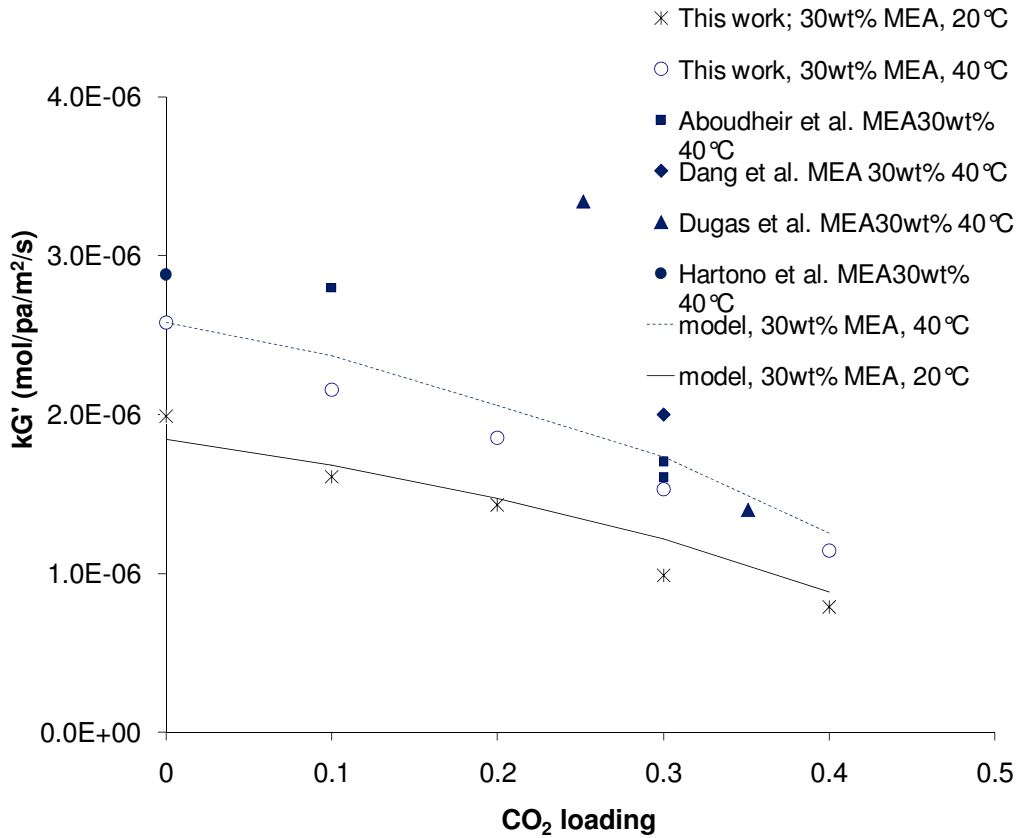


Figure 4-13: Liquid side mass transfer coefficient as a function of the loading for 30 wt% MEA solutions at 20 and 40 °C

### 4.5.3 Liquid side mass transfer coefficient with aqueous ammonia

Similarly, the results for the liquid side mass transfer coefficient for the aqueous ammonia solutions are given for 1, 5, and 10 wt% NH<sub>3</sub> solutions as a function of the loading and the temperature in Table 4-3, Table 4-4, and Table 4-5



**Table 4-3: Liquid side mass transfer coefficient for 1.0 wt% NH<sub>3</sub> solutions as a function of loading and temperature**

		$k'_G \cdot 10^6 \text{ (mol/(m}^2\text{·sec·Pa))}$				
Loading	0	0.2	0.4	0.6	0.8	
6 °C	<sup>a</sup>	0.22	0.13	0.14	0.09	
11 °C	0.27	0.21	0.18	0.28	0.08	
21 °C	0.31	0.23	0.20	0.14	0.11	
31 °C	0.41	0.39	0.35	<sup>a</sup>	0.13	

<sup>a</sup>: was not measured

**Table 4-4: Liquid side mass transfer coefficient for 5.0 wt% NH<sub>3</sub> solutions as a function of loading and temperature**

		$k'_G \cdot 10^6 \text{ (mol/(m}^2\text{·sec·Pa))}$						
Loading	0	0.2	0.3	0.4	0.5	0.6	0.8	
6 °C	0.61	<sup>a</sup>	0.39	<sup>a</sup>	0.35	0.10	<sup>a</sup>	
11 °C	0.74	0.47	0.40	0.23	0.22	0.16	<sup>a</sup>	
21 °C	0.90	0.53	0.39	0.34	0.31	0.17	<sup>a</sup>	
31 °C	1.51	0.90	0.70	0.61	0.53	<sup>a</sup>	0.16	

<sup>a</sup>: was not measured

**Table 4-5: Overall mass transfer coefficient for 10.0 wt% NH<sub>3</sub> solutions as a function of loading and temperature**

		$k'_G \cdot 10^6 \text{ (mol/(m}^2\text{·sec·Pa))}$			
Loading	0	0.2	0.4	0.5	
11 °C	1.35	0.97	0.58	0.37	
21 °C	1.50	1.00	0.51	0.36	
31 °C	2.4	1.58	1.21	<sup>a</sup>	

<sup>a</sup>: was not measured

The resistance of the gas side accounted for 5 to 15% of the total resistance for these experiments. The results for 10 wt% unloaded ammonia solutions at 31 °C should be considered with caution. It was not possible to repeat the results from the experiments with an uncertainty lower than 15%. This is probably due to the high amount of ammonia vaporized during the experiment despite the cleaning of the chamber where the content of CO<sub>2</sub> is measured, as described earlier. It could disturb the measurement of the CO<sub>2</sub> content and of the pressure. The values indicated in the table is the average value obtained from the different experiments. For the remaining solutions, based on the repetition of the experiments, the results are given with an uncertainty lower than 10%. The results included in the table are discussed below.

Figure 4-14, Figure 4-15 and Figure 4-16 show the liquid side mass transfer coefficient as a function of the CO<sub>2</sub> loading for aqueous ammonia and aqueous MEA solutions at various temperatures and concentrations.

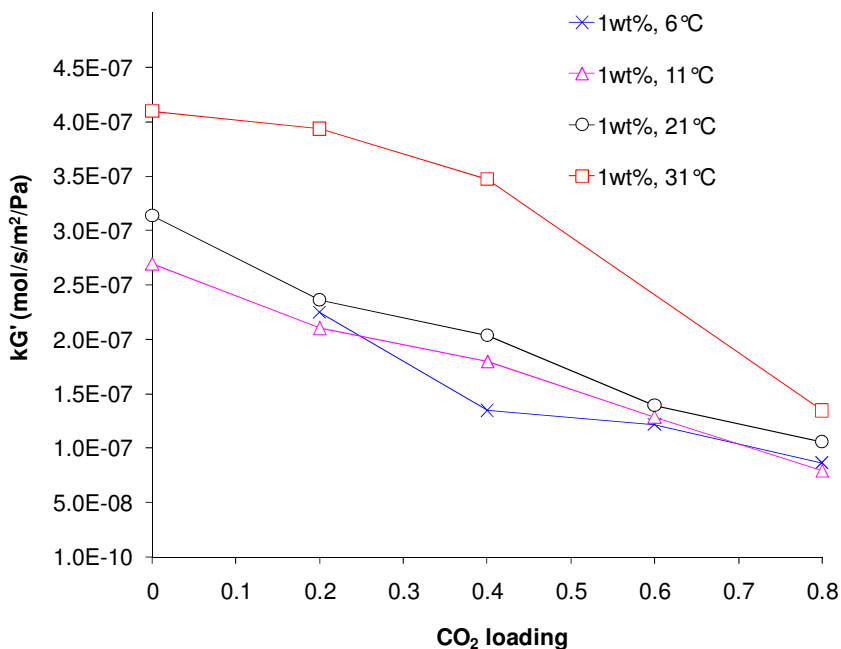


Figure 4-14: Liquid side mass transfer coefficient as a function of the CO<sub>2</sub> loading for 1 wt% ammonia solutions at various temperatures

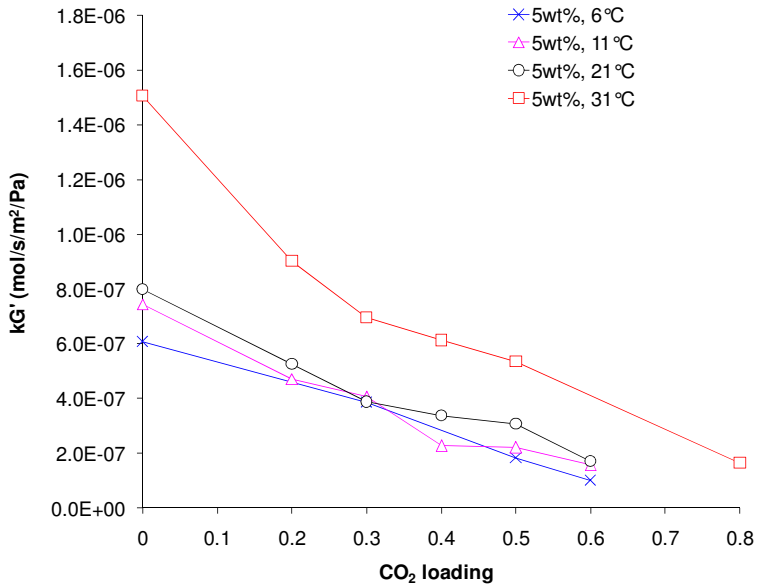


Figure 4-15: Liquid side mass transfer coefficient as a function of the CO<sub>2</sub> loading for 5 wt% ammonia solutions at various temperatures

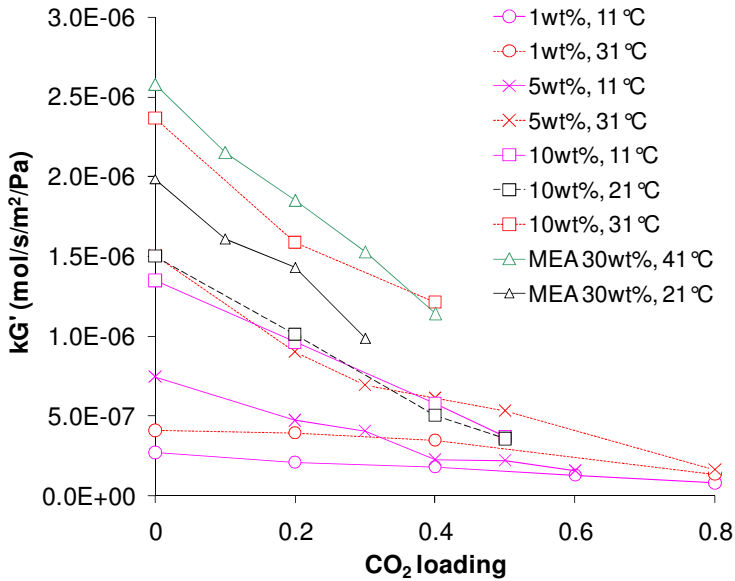


Figure 4-16: Liquid side mass transfer coefficient as a function of the CO<sub>2</sub> loading for 1, 5 and 10 wt% ammonia solutions at various temperatures and for 30 wt% MEA solutions at 21 and 31 °C

The results shown here follow generally a trend similar to the data of Puxty *et al.* (2010). However, for measurements at low concentration of ammonia (1 wt%), a significant increase of  $K_G$  as function of temperature is observed in this work. This is not the case in the work reported by Puxty *et al.* (2010). Their work represents the overall mass transfer coefficient  $K_G$ . However they did not quantify the resistance from the gas side during the experiments. In the work presented here, gas side resistance was also minimized but it still contributed up to 15% of the overall resistance. It is not possible to say whether Puxty *et al.* had a higher or lower gas side resistance than in the work here. The results are therefore in the end not completely comparable.

It can be observed from Figure 4-14, Figure 4-15, and Figure 4-16 that for all the concentrations and temperatures considered, the liquid side mass transfer coefficient decreases with the loading. When the loading reaches a value higher than 0.6, the mass transfer coefficient becomes very low which shows that the absorption is very slow at these concentrations and that reaching this loading would require a large contact area between the gas and the solvent in a capture process. However, even for the low concentrations of ammonia, the enhancement of the reaction is still occurring at a loading of 0.8, as pointed out by Puxty *et al.* (2010) (see Figure 4-14).

An increase of  $k'_G$  with the concentration of ammonia is observed within the ammonia concentration range considered here. By increasing the concentration from 1 to 10 wt%, the liquid side mass transfer coefficient for the unloaded solutions increases by about five times for the different temperatures.

The liquid side mass transfer coefficient globally increases with the temperature for all the ammonia concentrations considered. However, it can be noticed that the results at 6, 10, and 21 °C are close to each other. The difference is larger when the temperature increases from 21 to 31 °C.

This is an interesting result, as it shows that lowering the temperature of absorption from 21 to 11 °C in order to limit the vaporization of ammonia would not affect significantly the kinetics. On the other hand the lowering from 31 to 21 °C has a noticeable effect. Increasing the temperature from 6 to 31 °C entails an increase of  $k'_G$  by 1.5 to 2 times for unloaded solutions.

The comparison of the overall rate of absorption of carbon dioxide with aqueous ammonia and MEA solutions shows that the rate of absorption for 30 wt% MEA at 41 °C and 10 wt% ammonia solutions at 31 °C are equivalent (Figure 4-16). As reported by Puxty *et al.*, when the absorption at low temperature with aqueous ammonia is considered, the liquid side mass transfer coefficient is significantly lower than for MEA at 41 °C (which is a typical absorption temperature for processes based on MEA). At equal loading, the ratio of the liquid side mass transfer coefficients for 30 wt% MEA at 41 °C and 10 wt% ammonia solutions at 11 °C is comprised between 1.5 and 2. This means that the contact area between the gas and the liquid in the absorber should be multiplied by the same factor of 1.5 to 2 in order to reach the same absorption efficiency. For a packed tower with fixed diameter this would

indicate an increase a factor of 1.5 to 2 in height. Furthermore, when aqueous MEA solutions are used as a solvent, the loading range in the absorber is typically 0.2-0.5, while according to the CAP patent, the loading range is 0.3-0.7 (Gal, 2006). Looking at Figure 4-16, the ratio between the required contact areas for these two processes will be even larger than the ratio mentioned above (1.5 to 2) as it was calculated for equal loadings.

## 4.6 Overall chemical rate of absorption of CO<sub>2</sub> by aqueous ammonia

### 4.6.1 Modeling

The modeling of the overall chemical rate of absorption using the zwitter-ion mechanism has been made using absorption flux measurements of unloaded ammonia solutions.

The diffusivity and the Henry's law constant for carbon dioxide in aqueous ammonia solutions were taken from Derks *et al.* (2009). The diffusion coefficient of CO<sub>2</sub> is evaluated with the Stokes-Einstein equation:

$$D_{CO_2}^{NH_3} = D_{CO_2}^{H_2O} \left( \frac{\eta^{H_2O}}{\eta^{NH_3}} \right)^{0.8} \quad (4.42)$$

The correlation for the viscosities of water and aqueous ammonia solutions were taken from Frank *et al.* (1996).

$$\eta^{H_2O} = 1.18 \cdot 10^{-6} \exp\left(\frac{16400}{RT}\right) \quad (4.43)$$

$$\eta^{NH_3} = (0.67 + 0.78 \cdot x_{NH_3}) \cdot 10^{-6} \exp\left(\frac{17900}{RT}\right) \quad (4.44)$$

where  $x_{NH_3}$  is the mole fraction of ammonia in the unloaded solution.

The Henry's law constant for carbon dioxide in aqueous ammonia solution has been determined with the N<sub>2</sub>O analogy. The measurement of the physical solubility of N<sub>2</sub>O in aqueous ammonia solutions by Derks *et al.* (2009) showed that the presence of ammonia barely influenced the solubility in the temperature range 5-25 °C and concentration range 0-5 kmol/m<sup>3</sup>. This result has been confirmed by Qin *et al.* (2010) for a temperature in the range 11-50 °C and for a concentration up to 10 wt%. However, their experiments showed a dependency of the solubility of N<sub>2</sub>O with the temperature and the concentration of ammonia for loaded aqueous ammonia solutions. The solubility of carbon dioxide tends to decrease with the increase of the concentration of ammonia for loaded solutions. However, the lack of experiments did not allow for determining a consistent correlation. Therefore, in this study, the physical solubility of carbon dioxide in aqueous ammonia solutions has been considered to be equal to

the one in pure water. The correlation for the Henry's law constant for carbon dioxide in water is given in equation (4.32).

The kinetic parameters from equation (4.25) have been fitted using the temperature dependence defined in equation (4.45).

$$k_i = k_{i,283.15K} \exp\left(-\frac{Ea_i}{R}\left(\frac{1}{T} - \frac{1}{283.15}\right)\right) \quad (4.45)$$

The value of the parameters has been fitted by minimizing the least square deviation between the calculated and the measured absorption flux using equations (4.5), (4.6), (4.7) and (4.19). The Davidson-Fletcher-Powell algorithm was used to fit the parameters. The concentrations of water, free ammonia and hydroxide ions in the solvent at the defined ammonia concentration and temperature were calculated using the Extended UNIQUAC model available for the CO<sub>2</sub>-NH<sub>3</sub>-H<sub>2</sub>O system (Darde *et al.*, 2010b).

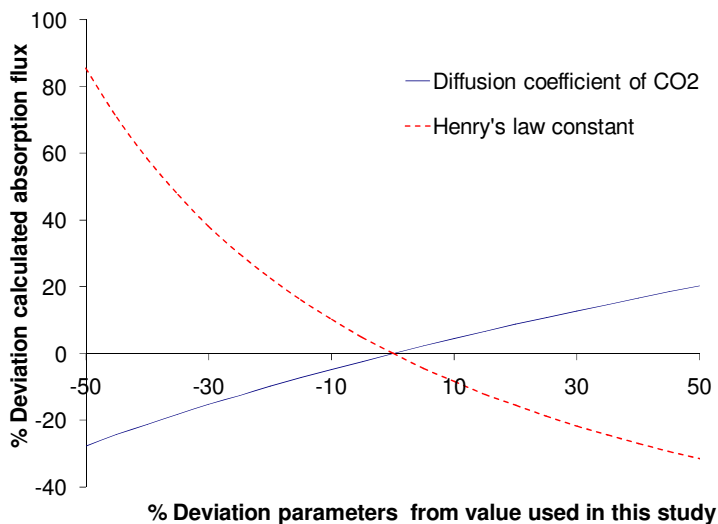
The expression of the enhancement factor from equation (4.21) is only available for measurements in the pseudo first order regime. Considering the unloaded solutions, the conditions defined in equation (4.22) were only satisfied for ammonia concentrations of 5 and 10 wt%. Hence, only the measurements for these concentrations were used to fit the kinetic parameters. As mentioned previously, the measurements of the flux using 10 wt% unloaded ammonia solution at 31 °C showed some uncertainties and were therefore not included in the parameter determination. The results for the parameter from equations (4.25) and (4.45) can be found in Table 4-6.

**Table 4-6: Kinetic parameters for the reaction of carbon dioxide in aqueous ammonia according to the zwitter-ion mechanism**

	$k_{i,283.15K}$	$\frac{Ea_i}{R}$
$k_2$	4.9 m <sup>3</sup> /(mol·s)	14000 K <sup>-1</sup>
$\frac{k_2 k_{NH_3}}{k_{-1}}$	2.1·10 <sup>-4</sup> m <sup>6</sup> /(mol <sup>2</sup> ·s <sup>2</sup> )	2200 K <sup>-1</sup>
$\frac{k_2 k_{H_2O}}{k_{-1}}$	7.1·10 <sup>-7</sup> m <sup>6</sup> /(mol <sup>2</sup> ·s <sup>2</sup> )	18000 K <sup>-1</sup>

As experienced for the case of MEA, the bicarbonate formation from equation (4.11) has a limited influence on the total absorption flux. The values of the parameters in Table 4-7 are affected by the experimental uncertainty as well as the correlations used for the diffusion coefficient and the Henry's

law constant of carbon dioxide in the aqueous ammonia solutions. The effect of the uncertainty of both the diffusion coefficient and the Henry's law constant of carbon dioxide in the aqueous ammonia solutions on the calculated absorption flux is shown in Figure 4-17, as it has been done by Paul *et al.* in 2009. The percentage deviation from the flux calculated with the physical parameters used in this study is plotted as a function of the deviation from the applied value of the diffusion coefficient and of the Henry's constant used in the calculation. The x axis shows the variation of the parameters given in percentage deviation from the actual values used in this study. Figure 4-17 shows that the Henry's law constant has a higher influence on the calculation of the flux than the diffusion coefficient. The experimental data from Qin *et al.* show that using the same value for the Henry's law constant in unloaded ammonia and pure water leads to a deviation of 5 to 10%. This might be caused by experimental uncertainties. As mentioned above, the Henry's law constant for carbon dioxide in loaded aqueous ammonia solutions is different from the one in pure water. The experiments from Qin *et al.* showed that the deviation between the actual Henry's law constant in loaded solution and the one in pure water could be up to 20%. Hence, this result could explain some uncertainties for the calculation of the absorption flux of carbon dioxide in loaded solutions. By underestimating the Henry's law constant, the model over estimates the liquid side mass transfer coefficient. The uncertainty regarding the diffusion coefficient is more difficult to evaluate. In general, Figure 4-17 shows that the uncertainty of both the diffusion coefficient and the Henry's law constant has a significant influence on the flux calculations. Therefore the parameters determined hereby should be considered with caution.



**Figure 4-17: Effect of the of the deviation (in%) of the diffusion and the Henry's law constant of carbon dioxide on the calculated absorption flux (in % deviation from the flux calculated with the Diffusion coefficient and the Henry's law constant used in this study)**

Figure 4-18 plots the measured and modeled carbon dioxide absorption flux for 5 and 10 wt% unloaded ammonia solutions at various temperatures as a function of the partial pressure of carbon dioxide in the chamber. It shows that the measured and the fitted absorption flux using the parameters from Table 4-6 are in good agreement.

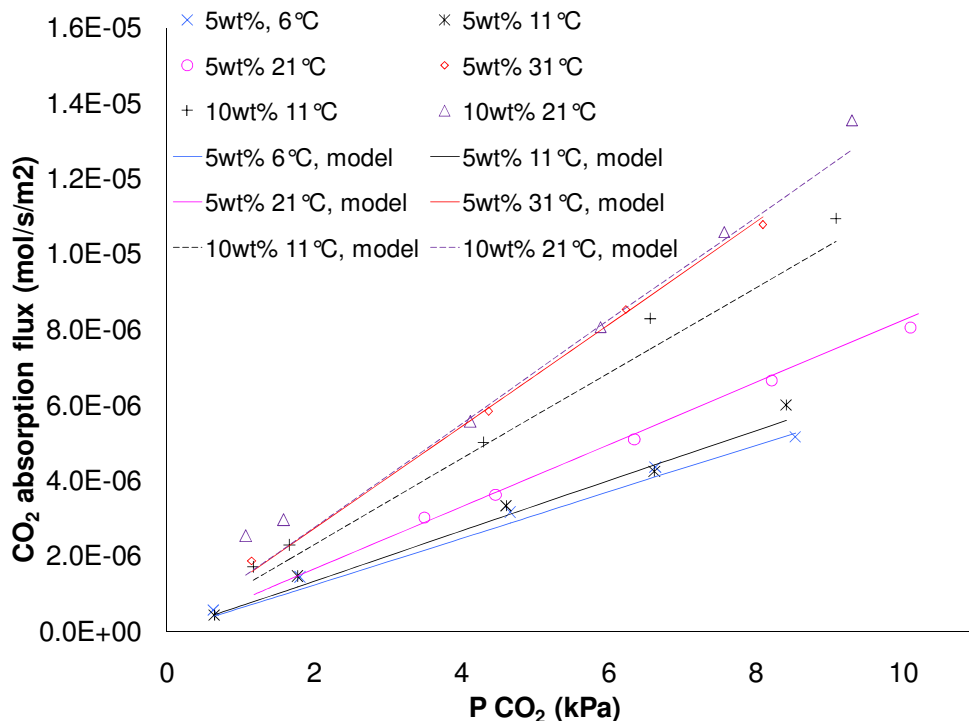


Figure 4-18: Measured and calculated absorption flux for 5 and 10 wt% unloaded ammonia solutions at various temperatures

#### 4.6.2 Comparison of the models

As mentioned previously, the rate of absorption has been modeled previously by several researchers. Pinsent (1956b) and Puxty *et al.* (2010) have modeled the overall kinetic rate constant in a similar way as it is done for MEA, by neglecting the contribution of the second reaction in the zwitter-ion mechanism. Derks *et al.* (2009) have modeled  $k_{ov}$  in the same way as it was done in this work, using a stirred cell set up. Qin *et al.* (2010) have recently measured the rate of absorption of carbon dioxide by unloaded aqueous ammonia solvents using a string of disc contactors. The rate of absorption was modeled using both the zwitter-ion and the termolecular mechanisms proposed by Crooks and Donnellan (1989) and modified by da Silva and Svendsen (2004). In this later mechanism, the



formation of ammonium carbamate ion is made in a complex single step reaction between a molecule of carbon dioxide, of ammonia and of a base present in the solution. It should be noted that the rate of absorption has been measured by Puxty *et al.* only for temperatures in the range 5-20 °C and for concentrations from 1 to 10 wt%, by Derks *et al.* for temperatures in the range 5-25 °C and for concentrations up to 12.5 wt% and by Qin *et al.* for temperatures in the range 25-49 °C and for concentrations up to 11 wt%. Hence, the temperature range of validity of their model does not cover the temperature range of the present work. The measurements from Pinsent were made at a concentration of ammonia up to 0.5 wt% and were therefore much lower than the one considered in this work.

Figure 4-19 and Figure 4-20 show the calculations of the overall kinetic rate constant as a function of the temperature for 5 and 10 wt% aqueous ammonia solutions as well as experimental results from this work, for 5 and 10 wt% unloaded solutions that were fitted to the present work's model and experimental results from Qin *et al.* (2010). The experimental results obtained with the 1 wt% solutions were not included as the pseudo first order regime conditions were not applied during the measurements. The lack of information regarding the gas side mass transfer coefficient in the work of Puxty *et al.* (2010) implies that no experimental data from this study could be included in these figures. The results from the experiments from Derks *et al.* are not available. The results from the model from Pinsent, Puxty *et al.*, Derks *et al.*, and Qin *et al.* were also included in Figure 4-19 and Figure 4-20. As mentioned before, these models do not cover the temperature and concentration ranges considered in the present study but they were extrapolated to these conditions.

As reported by Puxty *et al.* (2010) the results from Pinsent *et al.* (1956b) underestimate greatly  $k_{ov}$  compared to the other publications. It is probably due to the low concentration of ammonia used during the measurements. The results from the model from Puxty *et al.* are in a satisfactory agreement with the ones from the present study despite the difference in the chemical mechanisms considered though the results from Puxty are higher for 5 wt% NH<sub>3</sub> solutions. The values for  $k_{app}$  calculated with the model from Derks *et al.*, though in the same range, are systematically higher than the ones from the present work. The results from the model from Qin *et al.* are significantly lower than the ones from the present study and they do not show a strong influence of the temperature.

It should be noted that CSIRO have recently published the results from the operation of a pilot plant (Yu *et al.*, 2011). The overall mass transfer coefficient from the pilot plant was found to be significantly lower than the prediction of the model from Puxty *et al.* at similar conditions for 5 wt% solutions. This shows that it is not trivial to use the results from wetted wall columns experimental measurements for mass transfer calculations in packed columns. However, it should be noted that only the overall mass transfer coefficients are reported and compared in this study. Hence, the gas resistance is not considered. As hydrodynamic conditions vary significantly between wetted wall column measurements and absorption in a packed column, this might contribute to explain this difference.

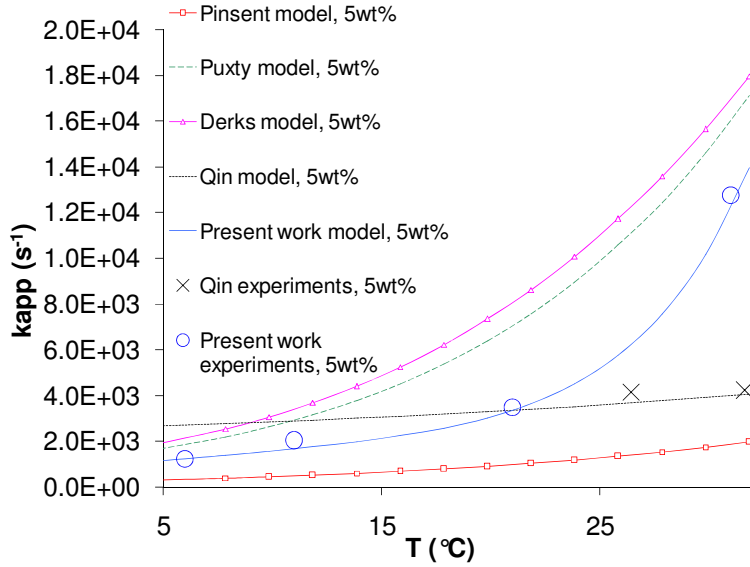


Figure 4-19: Comparison of the apparent kinetic rate constant models as a function of the temperature for unloaded 5 wt% aqueous ammonia solutions and experimental measurement from this study

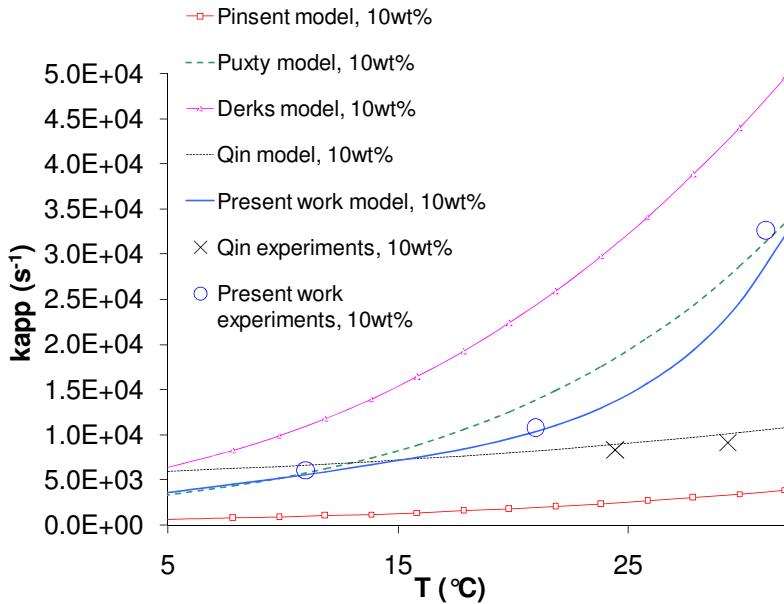
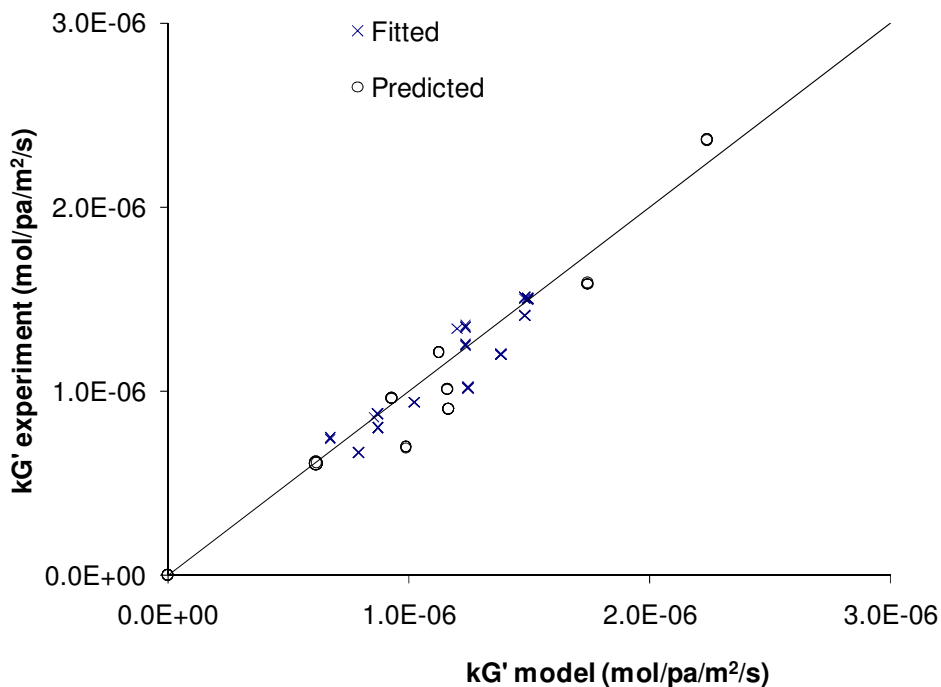


Figure 4-20: Comparison of the apparent kinetic rate constant models as a function of the temperature for unloaded 10 wt% aqueous ammonia solutions and experimental measurement from this study

The modeling of the overall kinetic constant allows for predicting the enhancement factor for loaded solutions, using again the thermodynamic model available for the  $\text{CO}_2\text{-NH}_3\text{-H}_2\text{O}$  system to calculate the concentrations of the species in the loaded solutions (Darde *et al.*, 2010b) (cf. Chapter 2). The comparison between the predicted enhancement factor and the measured one allows for evaluating the model. Again, the expression of the enhancement factor given in equation (4.21) is only valid under the pseudo first order regime. This is the case for the measurements of 5 wt% aqueous ammonia solutions at 31 °C for a loading lower than 0.5 and for the 10 wt% aqueous ammonia solutions at a loading of 0.2 at 11 and 21 °C and for a loading up to 0.4 at 31 °C.

Figure 4-21 shows the liquid side mass transfer coefficient  $k'_G$  calculated from the measurements of the overall mass transfer coefficient and from the modeling of the gas side mass transfer coefficient (equation (4.35)) as a function of the liquid side mass transfer coefficient calculated with the expression of the enhancement factor for the pseudo first order regime (equation (4.21)).



**Figure 4-21: Liquid side mass transfer coefficient calculated from the experimental measurements of the overall mass transfer coefficient of the absorption of carbon dioxide by aqueous ammonia solutions as a function of the liquid side mass transfer coefficient calculated from the expression of the enhancement factor for the pseudo first order regime using the value of the kinetic parameters for the reaction of carbon dioxide by ammonia solvent using the zwitter-ion mechanism determined in the present study.**

To calculate this coefficient, the value of the kinetic parameters for the reaction of carbon dioxide by aqueous ammonia according to the zwitter-ion mechanism determined in this study (Table 4-6) was used. The liquid side mass transfer coefficient for both the fitted data corresponding to the unloaded ammonia solutions and the predicted data corresponding to the loaded solutions are shown. The experimental measurements using loaded solutions were not used in the parameter estimation and are therefore predictions. The average deviation between the measured and the calculated liquid side mass transfer coefficient is 7.2% and 14.6% for the loaded solutions. It can be noticed that there is a tendency for the model to over predict the liquid side mass transfer coefficient for the loaded solutions. A reason may be that the model over predicts the solubility of carbon dioxide in loaded aqueous ammonia solutions by assuming a physical solubility of carbon dioxide equal to the one in water.

#### ***4.7 Conclusion***

The rate of absorption of carbon dioxide by aqueous ammonia solution has been studied using a wetted wall column apparatus. It allows for measuring the absorption flux of carbon dioxide by a solvent knowing the contact area between the gas and the solvent. The overall mass transfer coefficient for absorption of carbon dioxide in aqueous ammonia solutions was measured for ammonia concentration in the range 1 to 10 wt%, loading from 0 to 0.8 and temperature from 6 to 31 °C. Precipitation of ammonium carbonate compounds was avoided during the experiments. It was shown that the rate increases significantly with the temperature and the concentration of ammonia. It has though been shown that the increase of the rate between 6 and 21 °C is much lower than between 21 and 31 °C, which is a result of importance regarding the limitation of the vaporization of ammonia during the absorption of carbon dioxide in the context of the Chilled Ammonia Process.

The overall rate of absorption was compared with the rate measured for 30 wt% aqueous MEA solutions. It was shown that the rate of absorption using ammonia at the low absorption temperatures suggested for the Chilled Ammonia Process is significantly lower than the rate of absorption in a process based on MEA at typical temperatures around 41 °C. The use of aqueous ammonia solutions as a solvent at low temperatures would therefore require a larger contact area between the gas and the solvent.

Finally, using the measurements of the absorption flux for unloaded aqueous ammonia solution, the enhancement factor has been modeled by fitting six parameters to the overall kinetic rate constant. The small deviation between the predicted and the measured enhancement factor for loaded solutions showed that the model performs satisfactorily for the conditions where the pseudo first order regime could be applied. This model can be used in the future for a rate based simulation of the absorption of carbon dioxide by aqueous ammonia solutions.

#### ***4.8 Nomenclature***

A specific nomenclature is used for this chapter and is summarized below.

$A$	Contact area between the gas and the liquid in the reaction chamber ( $\text{m}^2$ )
$C_i$	Concentration compound $i$ ( $\text{mol}/\text{m}^3$ )
$D_{A,i}$	Diffusivity of compound $A$ in solvent $i$ ( $\text{m}^2/\text{sec}$ )
$D_A^{Gas}$	Diffusivity of compound $A$ in gas ( $\text{m}^2/\text{sec}$ )
$d_s$	Radii difference in the reaction chamber (m)
$E$	Enhancement factor
$E_\infty$	Enhancement factor in instantaneous reaction regime
$g$	Gravitational acceleration ( $\text{m}/\text{sec}^2$ )
$H_{A,i}$	Henry's law constant for specie $A$ in solvent $i$ ( $\text{Pa}\cdot\text{m}^3/\text{mol}$ )
$Ha$	Hatta number
$h$	Height of the wetted column (m)
$K_G$	Overall mass transfer coefficient ( $\text{mol}/(\text{m}^2\cdot\text{sec}\cdot\text{Pa})$ )
$k_i$	Kinetic rate constant for reaction $i$ ( $\text{m}^3/(\text{mol}\cdot\text{sec})$ )
$k_{app}$	Apparent kinetic rate constant ( $\text{sec}^{-1}$ )
$k_{ov}$	Overall kinetic rate constant ( $\text{sec}^{-1}$ )
$k_G$	Gas side mass transfer coefficient ( $\text{mol}/(\text{m}^2\cdot\text{sec}\cdot\text{Pa})$ )
$k_G'$	Liquid side mass transfer coefficient ( $\text{mol}/(\text{m}^2\cdot\text{sec}\cdot\text{Pa})$ )
$k_L^0$	Physical mass transfer coefficient in the liquid phase ( $\text{m}/\text{sec}$ )
$L$	Perimeter of the wetted wall column (m)
$N$	Mean gas velocity ( $\text{m}/\text{sec}$ )
$P$	Pressure (Pa)
$P_A$	Partial pressure of component $A$ (Pa)
$Q_g$	Gas flow rate ( $\text{m}^3/\text{sec}$ )
$Q_L$	Liquid flow rate ( $\text{m}^3/\text{sec}$ )
$R$	Molar gas constant ( $8.314 \text{ J}/(\text{mol}\cdot\text{K})$ )
$r$	Reaction rate ( $\text{mol}/(\text{m}^3\cdot\text{sec})$ )
$Re$	Reynolds number
$Sc$	Schmidt number
$Sh$	Sherwood number
$T$	Temperature (K)
$u_{surf}$	Velocity at the surface of the liquid ( $\text{m}/\text{sec}$ )
$V_m$	Gas molar volume
$x_i$	Mole fraction of specie $i$ in the liquid phase

#### Greek symbols

$\alpha$  and  $\beta$       Sherwood number parameters

$\phi_{CO_2}^G$	Gaseous molar flux of carbon dioxide (mol/(m <sup>2</sup> ·sec))
$\phi_{CO_2}^L$	Liquid molar flux of carbon dioxide (mol/(m <sup>2</sup> ·sec))
$\varepsilon$	Dimensionless parameters in Pigford's model
$\eta_L$	Liquid viscosity (Pa·sec)
$\rho$	Density (g/m <sup>3</sup> )
$\delta$	Liquid film thickness (m)
$\Theta$	Concentration change (Pigford model)

#### Superscripts

bulk	Bulk
eq	Equilibrium
in	Inlet
int	Liquid-gas interface
out	Outlet

## 4.9 References

- Aboudheir, A.P.; Tontiwachwuthikul, P.; Chakma, A.; Idem, R. Kinetics of the reactive absorption of carbon dioxide in high CO<sub>2</sub>-loaded, concentrated aqueous monoethanolamine solutions. *Chem. Eng. Sc.* **2003**, *58*, 5195.
- Barth, D.; Tondre, C.; Delpuech, J.J. Stopped-flow investigations of the reaction-kinetics of carbon-dioxide with some primary and secondary alkanolamines in aqueous solutions, *International Journal of Chemical Kinetics*, **1986**, *18*, 445.
- Blauwhoff, P. M. M.; Versteeg G. F.; Van Swaaij W. P. M. A study on the reaction between CO<sub>2</sub> and alkanolamines in aqueous solutions. *Chem. Eng. Sc.*, **1984**, *39*, 207.
- Bird, R. B.; Stewart, W. E.; Lightfoot, E.N. Transport Phenomena, *Wiley*, New York, **1960**.
- Bishnoi, S.; Rochelle, G. T. Absorption of carbon dioxide into aqueous piperazine: reaction kinetics, mass transfer and solubility. *Chem. Eng. Sc.*, **2000**, *55*, 5531.
- Cadours, R., Roquet, D. and Perdu, G. Competitive absorption-desorption of acid gas into water-DEA solutions, *Industrial & Engineering Chemistry Research*, **2007**, *4*, 233.
- Caplow, M. Kinetics of Carbamate Formation and Breakdown. *J. Am. Chem. Soc.*, **1968**, *90*, 6795.
- Crooks, J. E.; Donellan, J. P. Kinetics and Mechanism of the Reaction between Carbon Dioxide and Amines in Aqueous Solution. *J. Chem. Soc. Perkin Trans.*, **1989**, *II*, *4*, 331.
- Cullinane J. T.; Rochelle, G. T. Kinetics of carbon dioxide absorption into aqueous potassium carbonate and piperazine. *Ind. Eng. Chem. Res.*, **2006**, *45*, 2531.
- Danckwerts, P. V. Significance of Liquid-Film Coefficients in Gas Absorption. *Ind. Eng. Chem.*, **1951**, *43*, 1460.
- Danckwerts, P.V. Gas Liquid Reactions. *McGraw-Hill Inc*, New York, **1970**.
- Danckwerts, P. V. The Reaction of CO<sub>2</sub> with Ethanolamines. *Chem. Eng. Sc.*, **1979**, *34*, 443.

Dang, H.; Rochelle, G. T. CO<sub>2</sub> absorption rate and solubility in monoethanolamine / piperazine / water. *Separation Sci & Tech.*, **2003**, *38*, 337.

Darde, V.; Thomsen, K.; van Well, W. J. M.; Stenby, E. H. S. Chilled Ammonia Process for CO<sub>2</sub> capture. *Int. J. Greenhouse Gas Control*, **2010a**, *4*, 131.

Darde, V.; Thomsen, K.; van Well, W. J. M. and Stenby, E. H. S. Modeling of carbon dioxide absorption by aqueous ammonia solutions using the Extended UNIQUAC model. *Ind. Eng. Chem. Res.*, **2010b**, *49*, 12663.

Darde, V.; van Well, W. J. M.; Fosboel, P.; Stenby, E. H. S.; Thomsen, K. Experimental measurement and modeling of the rate of absorption of carbon dioxide by aqueous ammonia. **2011**, doi:10.1016/j.ijggc.2011.07.008

Da Silva, E. F.; Svendsen, H. F. Ab Initio Study of the Reaction of Carbamate Formation from CO<sub>2</sub> and Alkanolamines. *Industrial & Engineering Chemistry Research*, **2004**, *43*, 3413.

Derks, P. W. J.; Versteeg, G. F. Kinetics of absorption of carbon dioxide in aqueous ammonia solutions. *Greenhouse Gas Control Technologies 9, Energy Procedia*, **2009**, *1*, 1139.

Doraiswamy, L. K.; Sharma, M. M. Heterogeneous Reactions: analysis, Examples and Reactor Design, vol 2, *John Wiley*, New york, **1984**.

Dugas, R. Carbon dioxide Absorption, Desorption and diffusion in aqueous Piperazine and Monoethanolamine. Doctoral dissertation. The University of Texas, Texas, **2009**.

Faramarzi, L.; Kontogeorgis, G. M.; Thomsen, K.; Stenby E. H. Extended UNIQUAC model for thermodynamic modeling of CO<sub>2</sub> absorption in aqueous alkanolamine solutions. *Fluid Phase Equilib.*, **2009**, *282*, 121.

Frank, M. J. W.; Kuipers, J. A. M.; vanSwaaij, W. P. M. Diffusion coefficients and viscosities of CO<sub>2</sub>+H<sub>2</sub>O, CO<sub>2</sub>+CH<sub>3</sub>OH, NH<sub>3</sub>+H<sub>2</sub>O, and NH<sub>3</sub>+CH<sub>3</sub>OH liquid mixtures. *J. Chem. Eng. Data*, **1996**, *41*, 297.

Gal, E. Ultra cleaning combustion gas including the removal of CO<sub>2</sub>. World Intellectual Property, Patent WO 2006022885, **2006**.

Hartono, A. Characterization of diethylenetriamine (DETA) as absorbent for CO<sub>2</sub>. Doctoral dissertation Chemical Engineering. Trondheim, Norway, Norwegian University of Science and Technology., **2009**.

Higbie, R. The rate of absorption of a pure gas into a still liquid during a short time of exposure. *Transactions of the American Institute of Chemical Engineers*, **1935**, *31*, 365.

Hikita, H.; Asai, S.; Ishikawa, H.; Honda, M. The Kinetics of Reactions of Carbon Dioxide with Monoethanolamine, Diethanolamine and Triethanolamine by a rapid mixing method. *Chem. Eng. J. and Biochem. Eng. J.*, **1977**, *13*, 7.

Hobler, T. Mass Transfer and Absorbers, *Pergamon press*, Oxford, **1966**.

Ko, J-J.; Tsai, T-C.; Lin, C-Y.; Wang, H-M.; Li, M-H. Diffusivity of Nitrous Oxide in Aqueous Alkanolamine Solutions. *J. Chem. Eng. Data*, **2001**, *46*, 160.

Kucka, L.; Richter, J.; Kenig, E. Y.; Gorak, A. Determination of gas-liquid reaction kinetics with a stirred cell reactor, *Separation and Purification Technology*, **2003**, *31*, 163.

van Krevelen, D. W.; Hofstijzer, P. J. Kinetics of Gas-Liquid Reaction 1. General Theory. *Rec. Trav. Chim.*, **1948**, *67*, 563.

Kucka, L.; Richter, J.; Kenig, E. Y.; Gorak, A. Determination of gas-liquid reaction kinetics with a stirred cell reactor. *Sep. and Pur. Techno.*, **2003**, *31*, 163.

Lewis, J. B. The mechanism of mass transfer of solutes across liquid-liquid interfaces Part I: the determination of individual transfer coefficients for binary systems, *Chemical Engineering science*, **1954**, *3*, 248.

Lewis, W. K.; Whitman, W. G. Principles of Gas Absorption. *Ind. Eng. Chem.*, **1924**, *16*, 1215.

Li, J. L.; Henni, A.; Tontiwachwuthikul, P. Reaction kinetics of CO<sub>2</sub> in aqueous ethylenediamine, ethyl ethanolamine, and diethyl monoethanolamine solutions in the temperature range of 298-313 K, using the stopped-flow technique, *Industrial & Engineering Chemistry Research*, **2007**, *46*, 4426.

Licht, S.E. and Weiland, R.H. Density and Physical Solubility of Carbon Dioxide in Partial-Loaded Solution of MEA, DEA and MDEA and their blends. Presented at the Spring National Meeting, American Institute of Chemical Engineers, Houston, Texas, **1989**.

Littel, R. J.; Versteeg, G. F.; van Swaij W. P. M. Kinetics of CO<sub>2</sub> with primary and secondary amines in aqueous solutions—I. Zwitterion deprotonation kinetics for DEA and DIPA in aqueous blends of alkanolamines. *Chem. Eng. Sc.*, **1992**, *47*, 2027.

Pacheco, M.A. Mass transfer, kinetics and rate-based modeling of reactive absorption. Doctoral Dissertation, The University of Texas, Texas, **1998**.

Paul, S.; Ghoshal A. K.; Mandal, B. Kinetics of absorption of carbon dioxide into aqueous solution of 2-(1-piperazinyl)-ethylamine. *Chem. Eng. Sc.*, **2009**, *64*, 313.

Pigford, R. L.. Counter-Diffusion in a Wetted Wall Column. Doctoral Dissertation, The University of Illinois, Illinois, **1941**.

Pinsent, B. R. W.; Pearson, L.; Roughton, F. J. W. The kinetics combination of carbon dioxide with hydroxide ions. *Transaction of the Faraday society*, **1956a**, *52*, 1512.

Pinsent, B. R. W.; Pearson, L.; Roughton, F.J.W. The kinetics combination of carbon dioxide with ammonia, *Transaction of the Faraday society*, **1956b**, *52*, 1594.

Puxty, G.; Rowland. R; Attala, M. Comparison of the Rate of CO<sub>2</sub> Absorption into Aqueous Ammonia and Monoethanolamine. *Chem. Eng. Sc.*, **2010**, *65*, 915.

Qin, F.; Wanga, S.; Hartono, A.; Svendsen, H. F. Kinetics of CO<sub>2</sub> absorption in aqueous ammonia solution. *Int. J. Greenhouse Gas Control*, **2010**, *4*, 729.

Seo, D. J.; Hong, W. H. Effect of piperazine on the kinetics of carbon dioxide with aqueous solutions of 2-amino-2-methyl-1-propanol, *Industrial & Engineering Chemistry Research*, **2000**, *39*, 2062.

Telikapelli, V.; Kozak, F.; Leandri, J. F.; Sherrick, B.; Black, J.; Muraskin, D.; Cage, M.; Hammond, M.; Spitznogle, G. CCS with the Alstom Chilled Ammonia Process Development Program – Field Pilot Results. Presented at Greenhouse Gas Technology 10 (GHGT10), Amsterdam, **2010**.

Thomsen, K.; Rasmussen, P. Modeling of vapor–liquid–solid equilibrium in gas–aqueous electrolyte system. *Chem. Eng. Sc.*, **1999**, *54*, 1787.

Vaidya, P. D.; Mahajani, V. V.; Kinetics of the reaction of CO<sub>2</sub> with aqueous formulated solution containing monoethanolamine, N-methyl-2-pyrrolidone, and diethylene glycol, *Industrial & Engineering Chemistry Research*, **2005**, *44*, 1868 .

Vaidya P. D.; Kenig, E. Y. Gas-Liquid Reaction kinetics: a Review of Determination methods, *Chem. Eng. Comm*, **2007**, *194*, 1543.



van Swaaij, W. P. M.; Versteeg, G. F. Mass transfer accompanied with complex reversible chemical reactions in gas-liquid systems: an overview. *Chem. Eng. Sc.*, **1992**, *47*, 3181.

Versteeg, G. F.; Van Swaaij, W. P. M. On the kinetics between CO<sub>2</sub> and alkanolamines both in aqueous and non-aqueous solutions—I. Primary and secondary amines. *Chem. Eng. Sc.*, **1988a**, *43*, 573.

Versteeg, G. F.; Van Swaaij, W. P. M. Solubility and Diffusivity of acid gases (CO<sub>2</sub>, N<sub>2</sub>O) in aqueous alkanolamines solutions. *J. Chem. Eng. Data*, **1988b**, *33*, 29.

Versteeg, G. F.; Van Dijck, L. A. J.; Van Swaaij, W. P. M. On the kinetics between CO<sub>2</sub> and alkanolamines both in aqueous and non aqueous solutions: An overview. *Chem. Eng. Comm.*, **1996**, *144*, 113.

Xu, G. W.; Zhang, C. F.; Qin, S. J.; Wang, Y. W. Kinetics study on absorption of carbon- dioxide into solutions of activated Methyldiethanolamine, *Industrial & Engineering Chemistry Research*, **1992**, *31*, 921.

Yu, H.; Morgan, S.; Allport, A.; Cottrell, A.; Do, T.; McGregor, J.; Wardhaugh, L.; Feron, P. Results from trialling aqueous NH<sub>3</sub> based post-combustion capture in a pilot plant at Munmorah power station: Absorption. *Chemical Engineering Research and Design*, **2011**, *89*, 1204.

## 5 Validation of the Aspen User model and comparison with the e-NRTL model

### 5.1 Introduction

In order to evaluate the capture process, it is necessary to perform flow sheet calculations. Aspen Plus is a commercial simulator that has been widely used to simulate carbon dioxide capture processes. It allows for performing process optimization studies and has been used for different systems (e.g. Abu-Zhara *et al.* (2006), Oexmann *et al.* (2009), Plaza *et al.* (2009)). Its interface allows for building process configurations using built-in unit operations and routines. It is therefore a very valuable tool that offers a very large panel of possibilities. It is possible to perform equilibrium or rate based simulations, assuming that reliable thermodynamic and kinetic models are implemented.

When dealing with electrolyte solutions, the thermodynamic model that is implemented by default on Aspen Plus is the e-NRTL model proposed by Chen *et al.* (1982). This model has been successfully used for alkanolamine based systems. However, in the case of the CO<sub>2</sub>-NH<sub>3</sub>-H<sub>2</sub>O system, some issues have been identified regarding the performance of the default e-NRTL model available on Aspen Plus. Hence, it was decided to develop a user model that allows for implementing the Extended UNIQUAC model on Aspen Plus in order to be able to benefit from the performance of the thermodynamic model using the advanced features from the simulator. This work has been done by Bjørn Maribo-Mogensen from the Center for Energy Resources Engineering (CERE) at the Technical University of Denmark.

In this chapter, the Aspen Plus user model developed by Bjørn Maribo-Mogensen is described. It is then validated in order to show that the user model can reproduce the calculations from Extended UNIQUAC. By using the user model, the performances of the Extended UNIQUAC and e-NRTL models have been evaluated and the results for the simulation of a simple process configuration using both models have been compared. This work has been presented in two articles. Maribo-Mogensen *et al.* (2011) described the user model interface and its validation. Darde *et al.* (2011), in collaboration with Davide Bonalumi from Politecnico di Milano, described the comparison of Extended UNIQUAC with e-NRTL. These articles have been recently submitted for publication to Computers and Chemical Engineering and International Journal of Greenhouse Gas Control.

### 5.2 Description of the Aspen user model

#### 5.2.1 Introduction to the implementation of Extended UNIQUAC on Aspen Plus

The function of the Extended UNIQUAC user model (xUM) is to enable using the commercial simulator Aspen Plus with the Extended UNIQUAC model. The user model has been developed for Aspen Plus V 7.1 and 7.2 by Bjørn Maribo-Mogensen. Aspen Plus is extensible through the user model

interface described in their documentation (Aspen Plus, 2011). Once certain routines have been implemented in FORTRAN, Aspen Plus can load the user model in the form of a DLL. It can then be used in a similar way as the models available by default on Aspen Plus, such as the e-NRTL model. This section briefly describes the main features of the user model. More details can be found in Maribo-Mogensen *et al.* (2011).

Different routines have been included in the user model. It is first necessary to create a new thermodynamic model within Aspen. Practically, the base framework used for the thermodynamic model is common with the e-NRTL model. The property method is then changed in order to ensure that the necessary calculations by Extended UNIQUAC are taken into account. Hence, the calculations called by the DLL override the ones normally used by Aspen Plus when e-NRTL is used. This is done for the Gibbs energy and enthalpy of pure component in vapor, liquid and solid phases, and for the calculation of the activity coefficients. However, the main framework used by Aspen Plus to perform equilibrium calculations is not modified.

The model must be able to calculate activity coefficients and temperature derivatives by using the UNIQUAC parameters. To do so, the addition of non standard parameters on Aspen, such as the volume, surface area and interaction UNIQUAC parameters is necessary. Practically, these parameters are accessible in the properties/parameters section of Aspen Plus. The user model DLL retrieves all the parameters necessary for the calculations from Aspen Plus.

Subroutines are also necessary to calculate the thermal properties of a mixture. The calculations of the enthalpy and the Gibbs energy are based on the standard state properties, the activity coefficients and their temperature derivatives.

Hence, by adding the relevant parameters in the simulator, the Extended UNIQUAC model can be used in Aspen Plus in the same way as if e-NRTL was used. In order to avoid the time consuming task of typing all the UNIQUAC parameters, Bjørn Maribo-Mogensen has developed software that allows for exporting a text file containing all the parameters in an input Aspen Plus file. This input file includes the chemical reactions and all the parameters that are needed for the calculations. It also allows for converting the necessary standard state properties.

### **5.2.2 Main challenges related to the development of the user model**

Several challenges were faced during the development of the user model. Some of them are detailed below, more details can be found in Maribo-Mogensen *et al.* (2011).

First, the Extended UNIQUAC model is based on standard state Gibbs energies of formation that are for most of them taken from the NIST database (cf. Chapter 2). They are based on the molality scale. Hence, the equilibrium constants have to be converted to the rational scale. Similarly, Henry's law constants need to be converted. In addition, the correlations implemented on Aspen Plus for the partial liquid molar volume used in the pressure correction for VLE (Poynting factor, cf. equation (2.14)) are

different from the ones used in Extended UNIQUAC. This leads to minor difference with the results obtained with Extended UNIQUAC.

Then, with Extended UNIQUAC, the equilibrium constants are calculated using the Gibbs Helmholtz equation. The expression of the equilibrium constant is given by:

$$\ln K_j = -\sum_i v_{i,j} \frac{G_i^o}{RT} = a_j + b_j T + c_j \ln T + \frac{d_j}{T} + f_j \left( \frac{1}{T_\theta} - \frac{1}{T} \right) \ln(T - T_\theta) \quad (5.1)$$

Where  $a_i$ ,  $b_i$ ,  $c_i$ ,  $d_i$  and  $f_i$  are function of the parameters related the standard state Gibbs energy and enthalpy of formation and of the parameters of the heat capacity of component  $i$  (see equation (2.22)), and where  $T_\theta = 200$  K. Aspen Plus uses a four parameter correlation for the equilibrium constant:

$$\ln K_j = a_j^* + b_j^* T + c_j^* \ln T + \frac{d_j^*}{T} \quad (5.2)$$

Hence, the UNIQUAC parameters must be refitted so that the equilibrium constant is reproduced as accurately as possible with the Aspen Plus correlation. However, it has been observed that not a single set of parameters could reproduce accurately the equilibrium constant over a wide temperature range. In order to increase the accuracy of the user model, it is therefore proposed to be able to choose three different correlations, depending on the temperature range used. Hence, for each unit operation, the user chooses whether the correlation valid from -23 to 77 °C, -23 to 127 °C or -23 to 227 °C should be used, the first correlation being the most accurate at low temperature. Hence, up to 77 °C, the first correlation should be used, followed by the second one up to 127 °C. The third correlation should only be used for higher temperature.

### 5.2.3 Applicability and limitation of the user model

The user model can be used for any system for which Extended UNIQUAC parameters are available. CERE has developed an extensive parameter data base valid for 24 vapor component, 37 neutral liquid components, 41 anions, 35 cations and 886 solids. Most of these parameters are valid for a temperature from 0 to 110 °C (Thomsen *et al.*, 1996, Thomsen *et al.*, 1999).

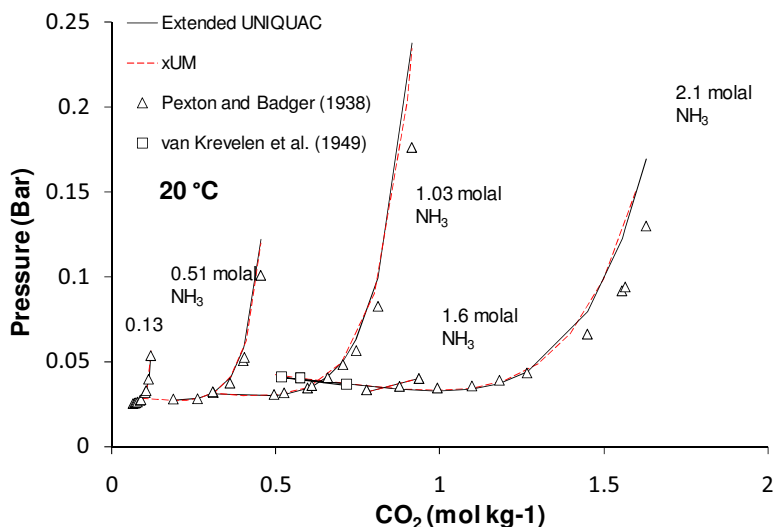
In this work, the user model has been applied to the simulation of the CO<sub>2</sub> capture using aqueous ammonia. All the species related to the CO<sub>2</sub>-NH<sub>3</sub>-H<sub>2</sub>O system, including the different solids, are considered in the calculations. As shown in Chapter 2, the UNIQUAC parameters for this system are valid up to a temperature of 150 °C. In addition, it is necessary to be able to simulate the composition of the flue gas from a power plant. UNIQUAC parameters for nitrogen as well as Henry's law constant correlations for a temperature up to 150 °C are available. Therefore, it is possible to use this compound in the simulations. The interaction parameters between sulfate species and compounds related to the CO<sub>2</sub>-NH<sub>3</sub>-H<sub>2</sub>O system are available in the original version of the Extended UNIQUAC (Thomsen *et*

*al.*, 1999). However, they have not been tested with the new version of the UNIQUAC parameters valid up to 150 °C. In addition, Henry's law constant for sulfur oxides would need to be implemented in the model. Hence, it cannot be used in the simulation with the current version of the thermodynamic model. In addition, in the absence of interaction parameters for oxygen or nitrous oxides, these compounds cannot be used in the simulations. This is a limitation to the user model, especially in the context of the simulation of the variant of the process developed by Powerspan, which combines the capture of carbon dioxide and sulfur oxides (McLarnon, 2009).

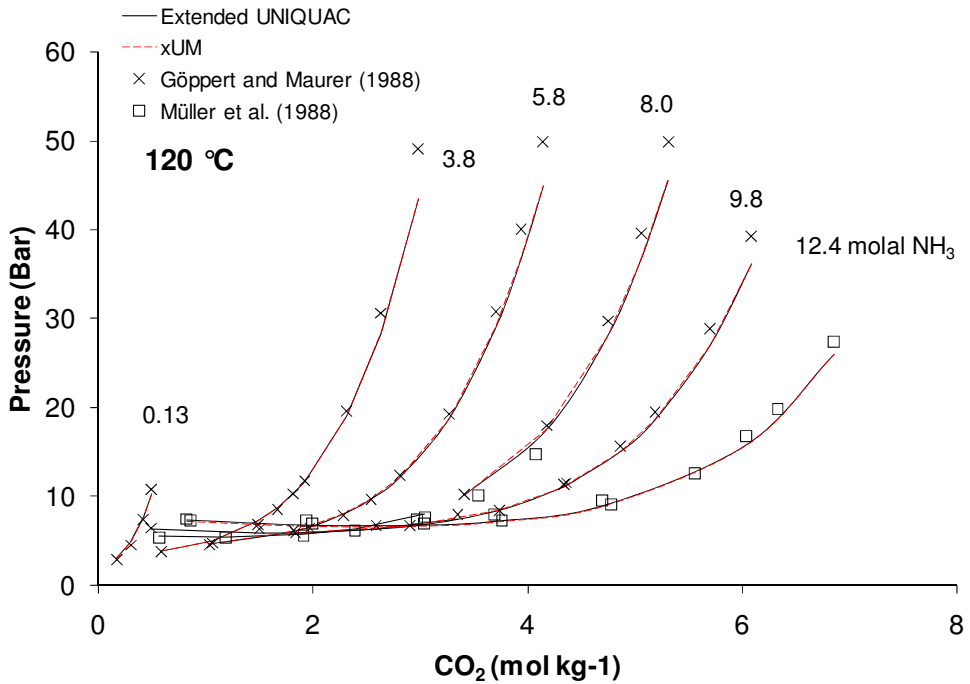
### 5.3 Validation of the interface

Many thermodynamic properties are important for the modeling of CO<sub>2</sub> capture processes. In this work the xUM is validated through the important electrolyte properties of VLE, SLE, and liquid speciation.

Figure 5-1 and Figure 5-2 show the comparison of the calculated bubble point pressure in the ternary CO<sub>2</sub>-NH<sub>3</sub>-H<sub>2</sub>O at 20 and 120 °C. Results of the xUM and of the Extended UNIQUAC model are shown. Experimental data have also been included to indicate the agreement between the model calculations and the experiments work. The figures show that at both low and high temperature, the results obtained with the Extended UNIQUAC model and the xUM agree completely. This conclusion is valid for temperature up to 180 °C, the highest temperature tested. In addition, it can be seen that the agreement between the model and the experiments is satisfactory, given the uncertainty for pressure measurements at high loading. The xUM may therefore successfully handle VLE (cf. Chapter 2).



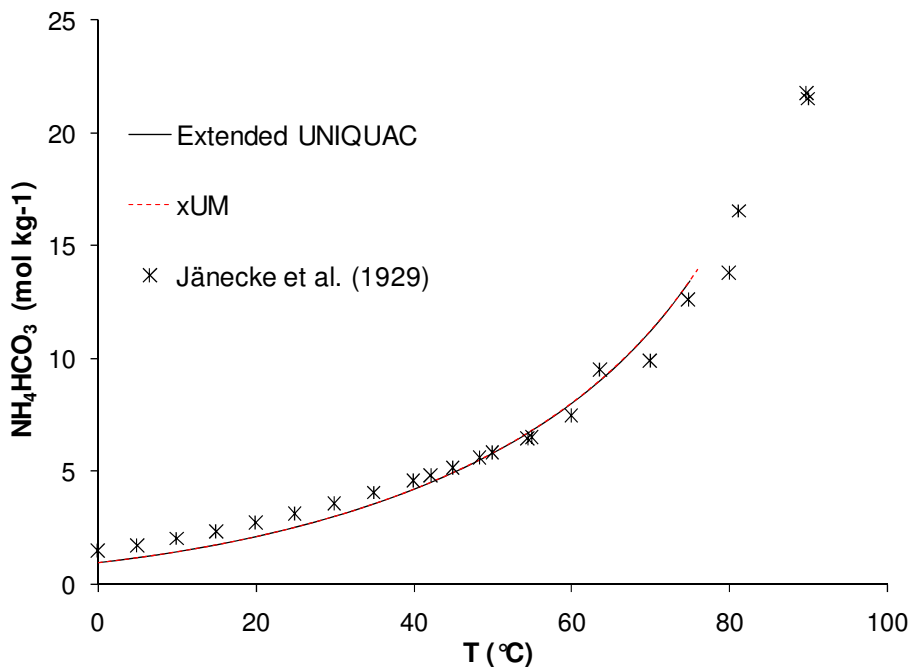
**Figure 5-1: Comparison of the results for the calculation of the bubble point pressure at 20 °C in a CO<sub>2</sub>-NH<sub>3</sub>-H<sub>2</sub>O mixture with the Extended UNIQUAC and the xUM. Experimental data by van Krevelen *et al.* (1949) and Pexton and Badger (1938) have also been included.**



**Figure 5-2: Comparison of the results for the calculation of the bubble point pressure at 120 °C in a CO<sub>2</sub>-NH<sub>3</sub>-H<sub>2</sub>O mixture with the Extended UNIQUAC and the xUM. Experimental data have also been included by Göppert and Maurer (1988) and Müller *et al.*(1988) have also been included.**

Figure 5-3 shows the calculation of the SLE behavior for ammonium bicarbonate as a function of the temperature using the extended UNIQUAC and xUM. Experimental data from Jänecke *et al.* (1929a, 1929b) have been included as well.

The figure shows the identical calculations of the xUM and the Extended UNIQUAC model for the whole range of temperature. Hence, the xUM implementation can successfully handle SLE behavior.



**Figure 5-3: Comparison of the results for the calculation of the solubility of ammonium bicarbonate as a function of the temperature with the xUM and the Extended UNIQUAC model. Experimental data from Jänecke *et al.* (1929a and 1929b) have also been included.**

Figure 5-4 and Figure 5-5 show the comparison of the speciation calculations for the mixtures of water, ammonia and carbon dioxide at 60 and 120 °C using the xUM, the Extended UNIQUAC, and the e-NRTL model. Experimental data are from Lichtfers (2000). It can be observed that the results using xUM are very close to the calculations of the Extended UNIQUAC model. This is valid at both high and low temperatures in the whole loading range. Conclusively, the xUM implementation and Extended UNIQUAC model perform identically and handles successfully the speciation calculations for a mixture of carbon dioxide, water and ammonia.

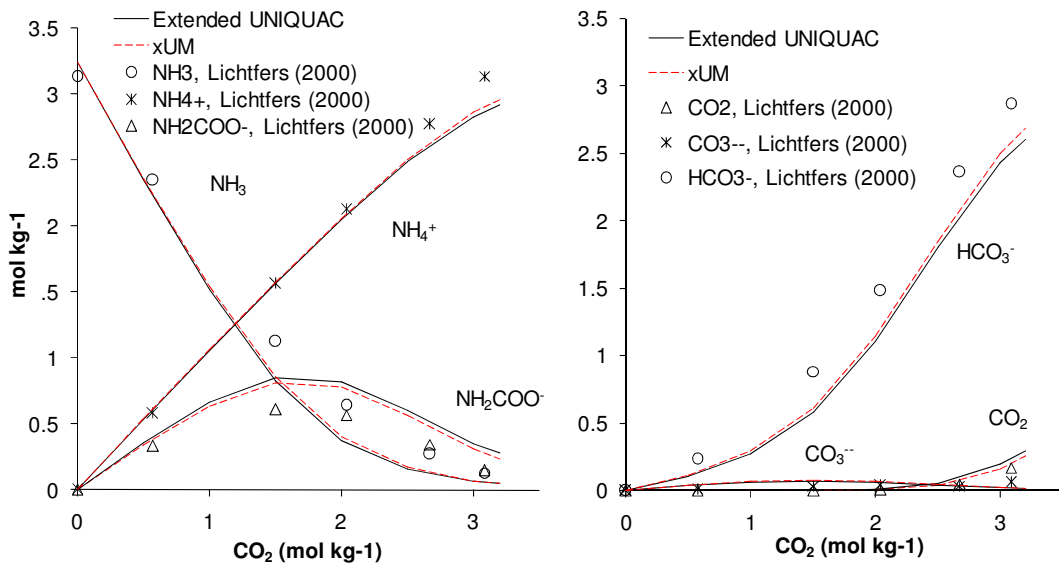


Figure 5-4: Speciation calculations expressed in molality, mol/kg water, for a mixture at 60 °C and for  $m(\text{NH}_3) = 3.25$  mol/kg water with the xUM and the Extended UNIQUAC. Experimental data are by Lichtfers (2000).

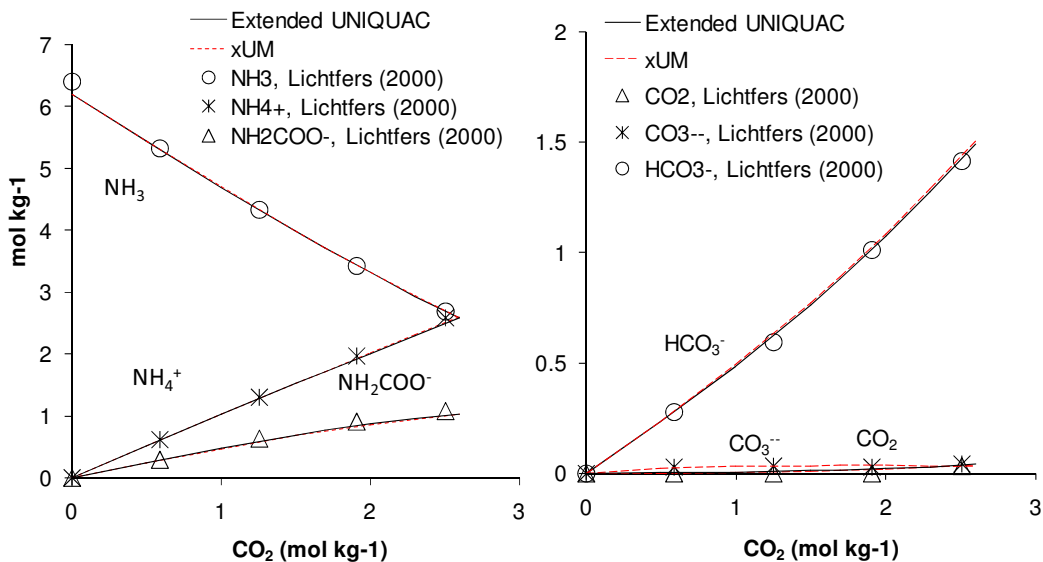


Figure 5-5: Speciation calculations expressed in molality, mol/kg water, for a mixture at 120 °C and for  $m(\text{NH}_3) = 6.20$  mol/kg water with the xUM and the Extended UNIQUAC. Experimental data are by Lichtfers (2000).



The above figures show that the results obtained with the Extended UNIQUAC model are similar to the Aspen Plus xUM. Key thermodynamic properties in electrolyte system have been compared and validated. The Aspen user model can therefore be accurately used for process simulation.

## **5.4 Comparison with the e-NRTL model**

### **5.4.1 Introduction**

The e-NRTL model is the model implemented by default on Aspen Plus. Hence, comparing the Extended UNIQUAC model with the e-NRTL for the system of interest is relevant. Files for process simulation of carbon dioxide capture processes for different solvents are available on the support website of Aspentech. These files are compatible with Aspen Plus V7.2. The file dedicated to CO<sub>2</sub> capture using NH<sub>3</sub> is identified with the ID 129521 released September 2010. This file includes the latest model parameters for the e-NRTL thermodynamic model for the system of interest. The previous version released for Aspen Plus V6.5 had been tested by Philip Fosbøl (2008). This study showed some solubility issues at high temperatures as well as inaccuracy of VLE calculations at high temperature. The new version of the e-NRTL model includes an update of the correlation for the equilibrium constant of the formation of ammonium bicarbonate, a modification of the correlation for the Henry's law constant for ammonia in water and the binary interaction parameters and heat capacity at infinite dilution have been refitted. It is this later version that is compared to the Extended UNIQUAC model in this study.

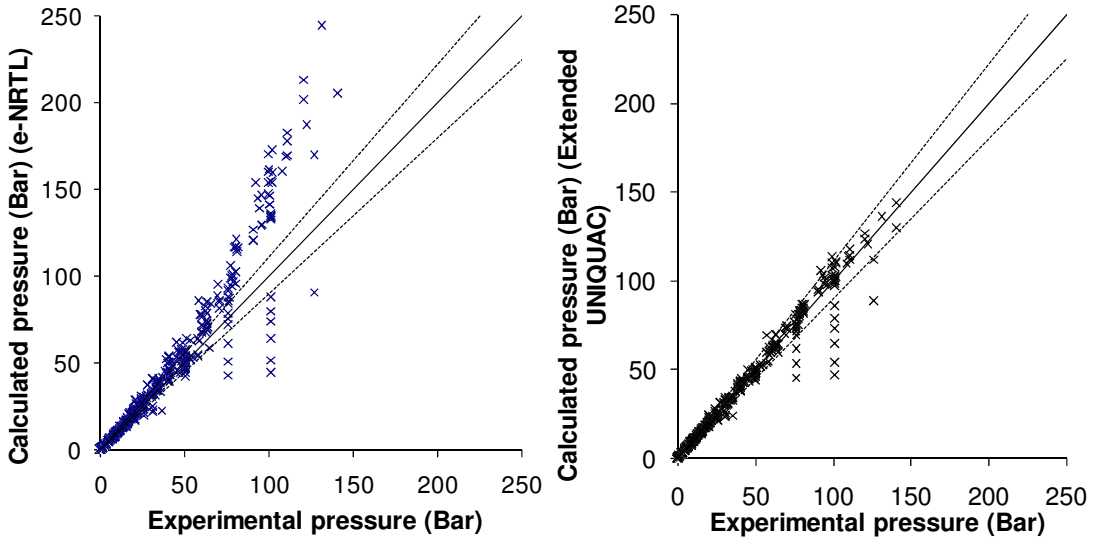
### **5.4.2 Evaluation of the thermodynamic models with experimental data**

Both models have been compared to existing experimental data available in the literature. As shown in Chapter 2, the data used in this section have been used to fit the Extended UNIQUAC model parameters. The list of experimental data used for the fitting the e-NRTL model is not available.

#### **5.4.2.1 Vapor-Liquid Equilibrium**

First, VLE data have been used. In the context of the simulation of the capture process, it is crucial that the VLE is well represented for the temperature and concentration ranges used.

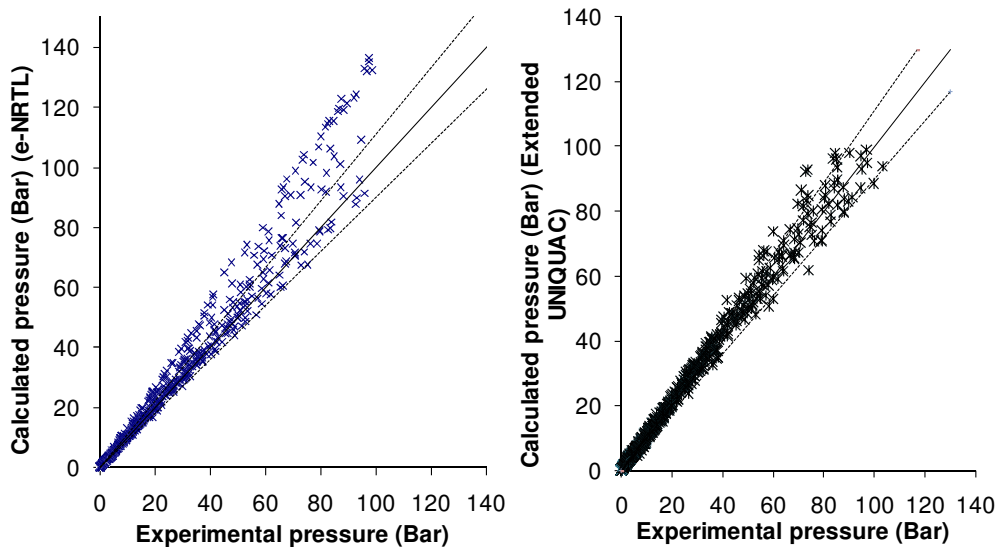
The binary systems CO<sub>2</sub>-H<sub>2</sub>O and NH<sub>3</sub>-H<sub>2</sub>O have been analyzed. Figure 5-6 shows the calculation of the bubble point pressure for the CO<sub>2</sub>-H<sub>2</sub>O system for both thermodynamic models compared with the experimental data taken from various publications for both thermodynamic models (cf. Chapter 2). The experimental temperature varies between 0 and 200 °C. 10% deviation dashed lines are added to the figure. It can be observed that the results using the xUM are significantly better than the ones observed with e-NRTL where the pressure is over estimated by the model for many of the data, especially for the high pressure data. Some of the experimental data are inconsistent for both models and seem to be unreliable, as pointed by Thomsen and Rasmussen (1999).



**Figure 5-6: VLE of the CO<sub>2</sub>-H<sub>2</sub>O system using Aspen Plus with e-NRTL (left) and Extended UNIQUAC (right). 10% deviation dashed lines have been included.**

Figure 5-7 shows the same calculations for the binary system NH<sub>3</sub>-H<sub>2</sub>O, using e-NRTL and the xUM. Various experimental data have been used (cf. Chapter 2). Again, the calculations using Extended UNIQUAC are in a better agreement with the experimental data. A significant number of data from various experiments at high pressure show a deviation higher than 20% compared to the model calculations.

The results for the binary systems show that the parameters from the e-NRTL model does not allow for representing the VLE in a satisfactory way for high pressure data.



**Figure 5-7: VLE of the  $\text{NH}_3\text{-H}_2\text{O}$  system using Aspen Plus with e-NRTL (left) and Extended UNIQUAC (right). 10% deviation dashed lines have been included.**

The study of the VLE calculations in the ternary system  $\text{CO}_2\text{-NH}_3\text{-H}_2\text{O}$  system is very relevant for the evaluation of the thermodynamic models. Figure 5-8 and Figure 5-9 respectively show the calculations with the xUM and the e-NRTL model for the bubble point partial pressures of carbon dioxide and ammonia at 20 °C as a function of the molality of carbon dioxide for different molalities of ammonia.

Figure 5-8 shows that the e-NRTL model is able to reproduce the partial pressure of carbon dioxide at 20 °C for all the concentrations and loadings considered with a high accuracy. Calculations with the xUM are satisfactory but not as accurate as with the e-NRTL model at high loading. At these conditions, the Extended UNIQUAC model overestimates slightly the partial pressure of carbon dioxide. Figure 5-9 shows the corresponding results for the partial pressure of ammonia. The Extended UNIQUAC model reproduces the partial pressure of ammonia precisely, while e-NRTL underestimates the ammonia vapor pressure at low loading conditions. For the highest ammonia concentration and the lowest loading range, the deviation between the experimental and the calculated partial pressure of ammonia reaches 30%. This would lead to an under-prediction of the ammonia slip from the absorber column in the context of a simulation of the  $\text{CO}_2$  capture process using aqueous ammonia.

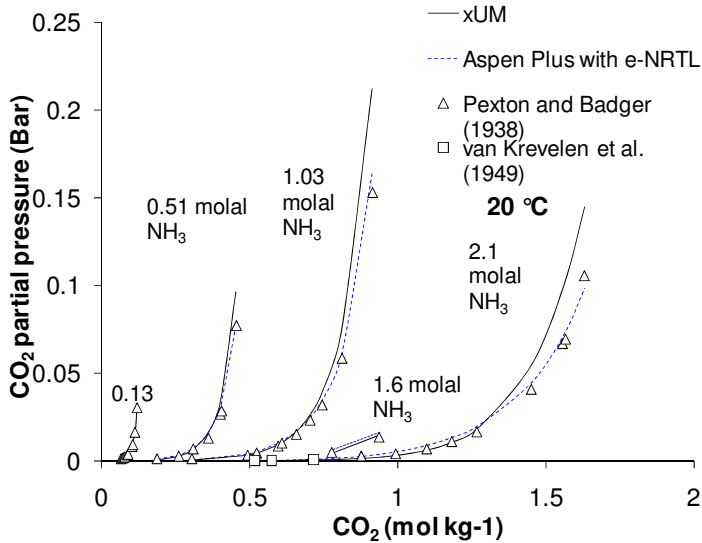


Figure 5-8: Comparison of the results for the calculation of the bubble partial pressure of carbon dioxide at 20 °C in a CO<sub>2</sub>-NH<sub>3</sub>-H<sub>2</sub>O mixture with the xUM and Aspen Plus with e-NRTL. Experimental data by van Krevelen *et al.* (1949) and Pexton and Badger (1938) have also been included.

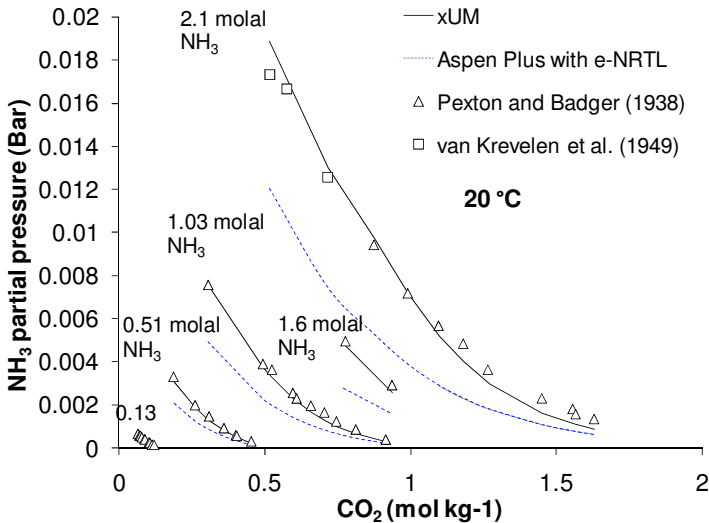


Figure 5-9: Comparison of the results for the calculation of the bubble partial pressure of ammonia at 20 °C in a CO<sub>2</sub>-NH<sub>3</sub>-H<sub>2</sub>O mixture with xUM and Aspen Plus with e-NRTL. Experimental data by van Krevelen *et al.* (1949) and Pexton and Badger (1938) have also been included.

Figure 5-10 and Figure 5-11 shows the calculations for partial pressure of carbon dioxide and ammonia for ternary mixtures at 40 °C for both models. Experimental data up to a molality of 11.8 are plotted. Both models are able to reproduce accurately the partial pressure of carbon dioxide for low ammonia concentration. It can be observed that at high ammonia concentration (11.8 molal), calculation by the e-NRTL model deviate significantly from the trend of the partial pressure. Figure 5-11 shows that the e-NRTL model under estimates slightly the partial pressure of ammonia, the results being better than at 20 °C.

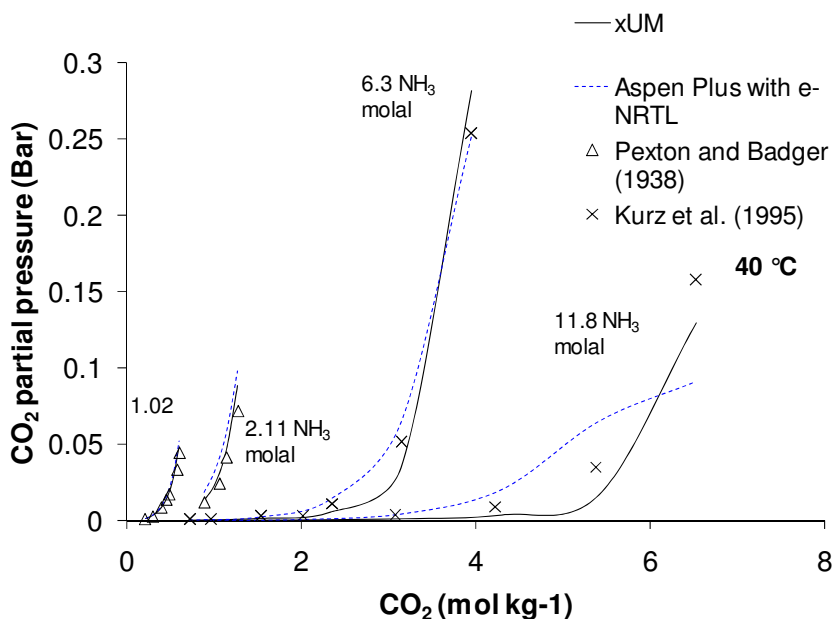
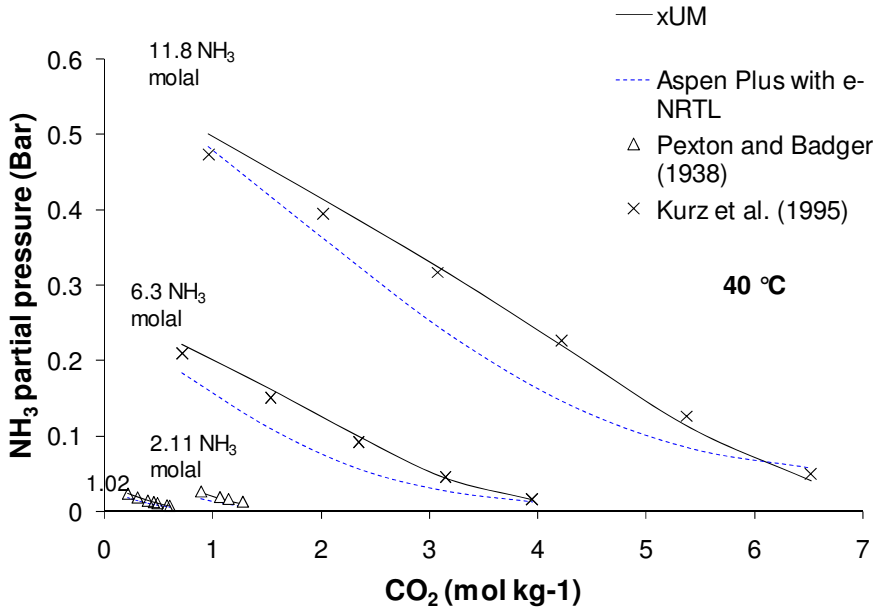
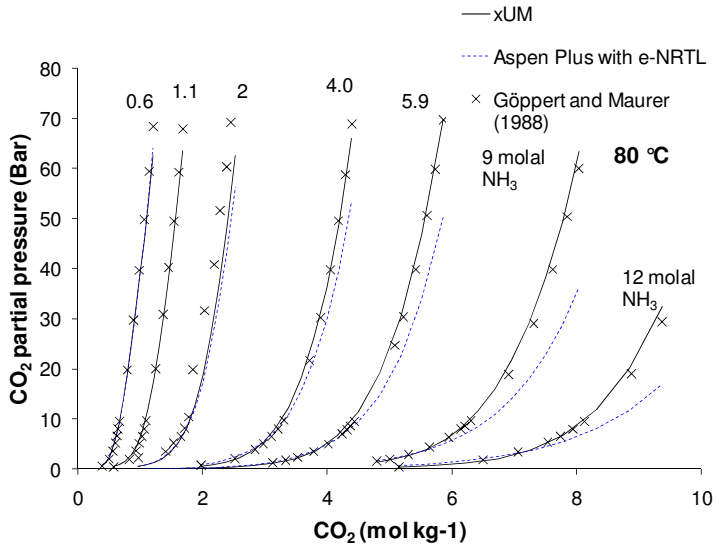


Figure 5-10: Comparison of the results for the calculation of the bubble partial pressure of carbon dioxide at 40 °C in a CO<sub>2</sub>-NH<sub>3</sub>-H<sub>2</sub>O mixture with xUM and Aspen Plus with e-NRTL. Experimental data by Pexton and Badger (1938) and Kürz *et al.* (1995) have also been included.

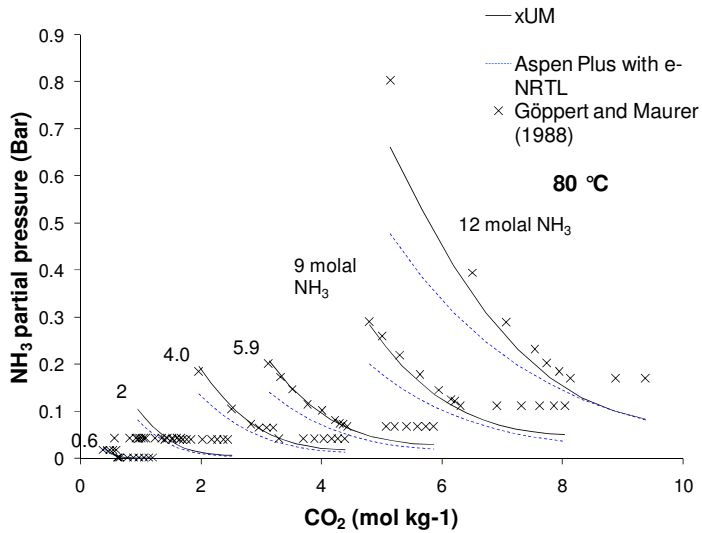


**Figure 5-11: Comparison of the results for the calculation of the bubble partial pressure of ammonia at 40 °C in a CO<sub>2</sub>-NH<sub>3</sub>-H<sub>2</sub>O mixture with xUM and Aspen Plus with e-NRTL. Experimental data by Pexton and Badger (1938) and Kürz *et al.* (1995) have also been included**

Figure 5-12 and Figure 5-13 show calculations of the partial pressures of carbon dioxide and ammonia at a temperature of 80 °C. Experimental data at high temperature and loading are included in the plots. It can be observed that at high ammonia concentration and high loading, the e-NRTL model calculates the partial pressure of carbon dioxide less accurately than the Extended UNIQUAC model. The latter performs well except for the very high loading range. Measuring the partial pressure of ammonia at high temperature and high loading is very challenging because of the low mole fraction of ammonia in the gas phase. Hence, the experimental data at high loading might be less accurate. The partial pressure of ammonia seems to remain constant when the molality of carbon dioxide increases, which might indicate that the detection limit of the sensor has been reached. As for the previous temperatures studied, the partial pressure of ammonia at low loading is not reproduced accurately by e-NRTL, while Extended UNIQUAC performs well.



**Figure 5-12: Comparison of the results for the calculation of the bubble partial pressure of carbon dioxide at 80 °C in a CO<sub>2</sub>-NH<sub>3</sub>-H<sub>2</sub>O mixture with xUM and Aspen Plus with e-NRTL. Experimental data by Göppert and Maurer (1988) have also been included.**



**Figure 5-13: Comparison of the results for the calculation of the bubble partial pressure of ammonia at 80 °C in a CO<sub>2</sub>-NH<sub>3</sub>-H<sub>2</sub>O mixture with xUM and Aspen Plus with e-NRTL. Experimental data by Göppert and Maurer (1988) have also been included.**

The evaluation of the models at higher temperature is especially relevant as it corresponds to the conditions at which the desorber operates. Figure 5-14 and Figure 5-15 shows the calculations for the partial pressure of carbon dioxide and ammonia at 100 °C as a function of the molality of carbon dioxide for different molality of ammonia. Experimental data for a molality of ammonia up to 14.3 and high loading are used for evaluation.

Both thermodynamic models estimate accurately the partial pressure of carbon dioxide for the data with limited loading. It can be seen that at high concentration and high loading, the e-NRTL model greatly under estimate the partial pressure of carbon dioxide while the calculations from the Extended UNIQUAC model are in a good agreement with the experimental data. Figure 5-15 shows that the experimental data are scattered, especially at high ammonia concentration. It can be observed that the e-NRTL model under estimates slightly the partial pressure of ammonia for low ammonia concentration. At higher concentrations, both models seem to under estimate this pressure.

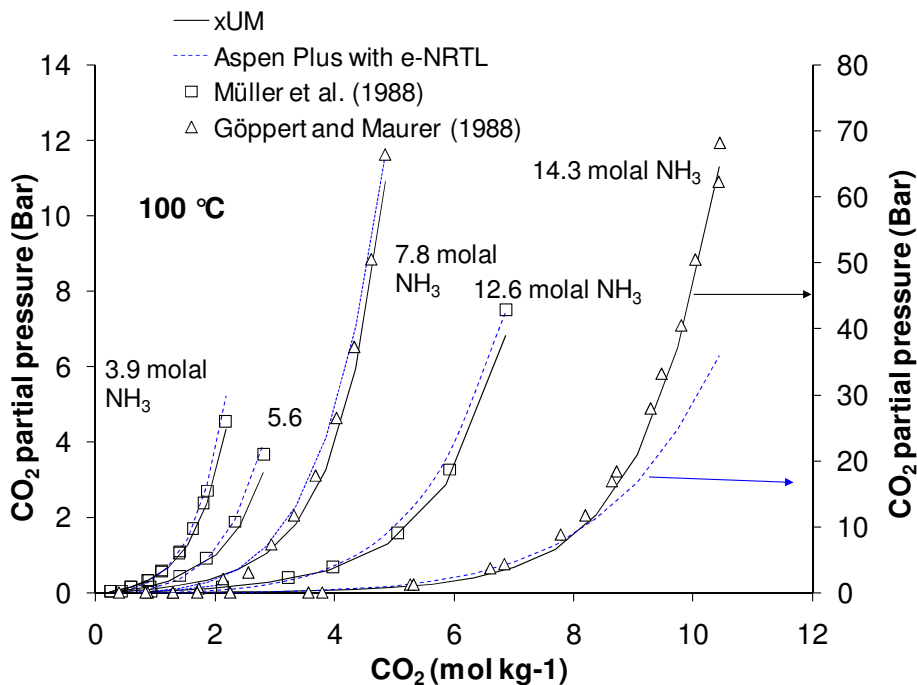
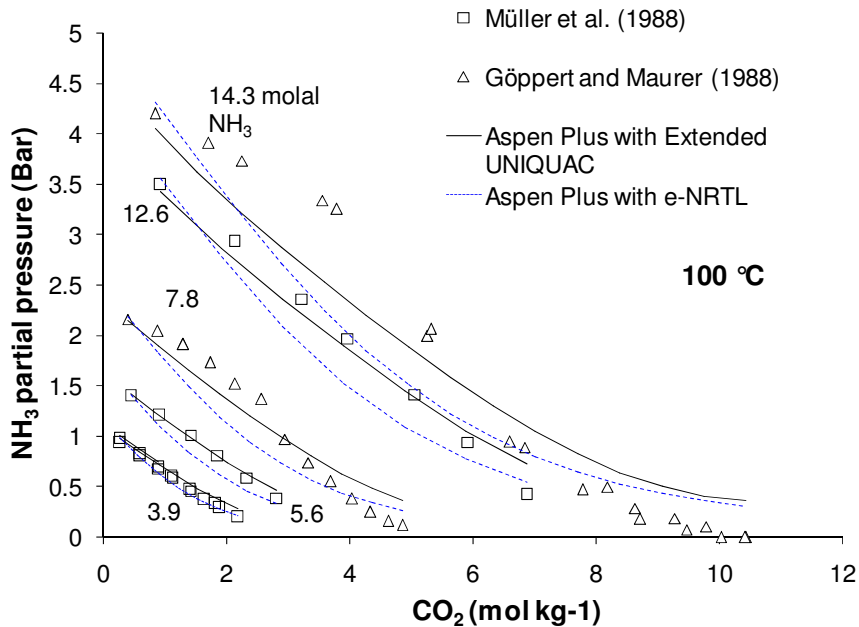


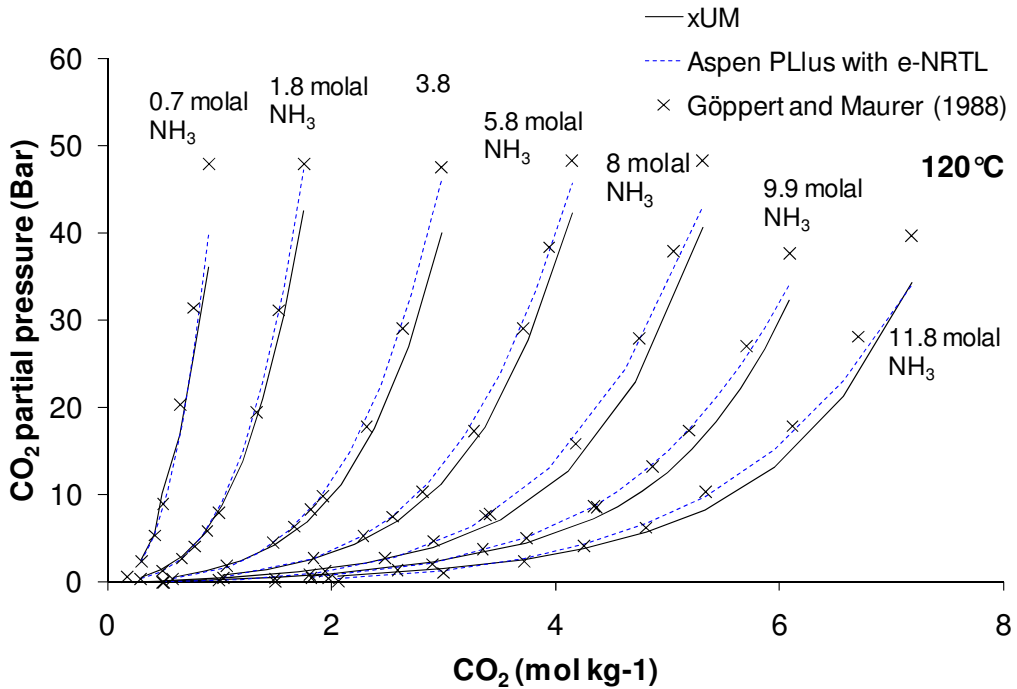
Figure 5-14: Comparison of the results for the calculation of the bubble partial pressure of carbon dioxide at 100 °C in a CO<sub>2</sub>-NH<sub>3</sub>-H<sub>2</sub>O mixture with xUM and Aspen Plus with e-NRTL. Experimental data by Müller *et al.* and Göppert and Maurer have also been included.





**Figure 5-15: Comparison of the results for the calculation of the bubble partial pressure of ammonia at 100 °C in a CO<sub>2</sub>-NH<sub>3</sub>-H<sub>2</sub>O mixture with xUM and Aspen Plus with e-NRTL. Experimental data by Müller *et al.* and Göppert and Maurer have also been included.**

Figure 5-16 shows the calculations for the partial pressure of carbon dioxide at 120 °C for different concentrations of ammonia and loadings. The experimental measurements of the partial pressure of ammonia show a low accuracy at high loading and high temperature. Hence, the data and calculations of the partial pressure of ammonia are not given here. It can be observed that the e-NRTL model performs better than Extended UNIQUAC for mixtures at high loading, where the Extended UNIQUAC model under estimates the partial pressure of carbon dioxide. For all the concentrations and loadings considered, the e-NRTL model calculates the carbon dioxide partial pressure accurately.



**Figure 5-16: Comparison of the results for the calculation of the bubble partial pressure of carbon dioxide at 120 °C in a CO<sub>2</sub>-NH<sub>3</sub>-H<sub>2</sub>O mixture with xUM and Aspen Plus with e-NRTL. Experimental data by Müller *et al.* and Göppert and Maurer have also been included.**

In conclusion, the e-NRTL model under estimates the partial pressure of ammonia in most cases. In the case of low loading, the deviation with the experimental data can be large. The calculations of the partial pressure of carbon dioxide are in general accurate for limited loadings and ammonia concentrations. For high concentrations and for high loadings, it can be seen that the e-NRTL model under estimates significantly this partial pressure at 40, 60, 80, 100 and 120 °C. The accuracy of the model for a molality of ammonia higher than 10 mol/kg (14.5 wt% NH<sub>3</sub>) and at high loading can therefore be doubted according to these results.

As presented in Chapter 2, the Extended UNIQUAC model performs very well for the calculation of the partial pressure of ammonia. This property is calculated accurately for the different concentrations and loadings considered up to 100 °C. For higher temperatures, the uncertainty of the experimental data does not allow for making conclusions. The Extended UNIQUAC model also calculates the partial pressure of carbon dioxide satisfactorily. At low temperature and high loading, the calculations slightly over estimate the CO<sub>2</sub> partial pressure. At high temperature and high loading, the Extended UNIQUAC model under estimates moderately the partial pressure.

### 5.4.2.2 Solid-Liquid Equilibrium

The simulation of the Chilled Ammonia Process requires a thermodynamic model that describes accurately SLE. It is required that the model can predict the nature and the amount of solid phase formed at the absorption temperature. It is also important to predict correctly at what temperature the solid phase disappears. Hence, the thermodynamic model must handle SLE for a large range of temperatures.

The Extended UNIQUAC and e-NRTL models do not handle the same solid compounds. The e-NRTL model only includes the formation of ammonium bicarbonate, while the Extended UNIQUAC model also handles the formation of 3 other solids (ammonium carbamate, ammonium carbonate and sesquicarbonate).

Figure 5-17 shows the calculation of the solubility of ammonium bicarbonate (ABC) as a function of the temperature for both thermodynamic models. These calculations are made at bubble point pressure and the pressure therefore increases when the temperature rises. Experimental data from Jänecke (1929a and 1929b) have been added. It can be seen that at low temperature, the calculation of the solubility of ABC is in good agreement with the experimental data for both models, the e-NRTL model being slightly more accurate. When the temperature exceeds 40 °C, the e-NRTL model over estimates the solubility of ABC while the results from the Extended UNIQUAC model remain in agreement with the experimental data. This figure shows that the solid formation at high concentration is not accurate with the e-NRTL model.

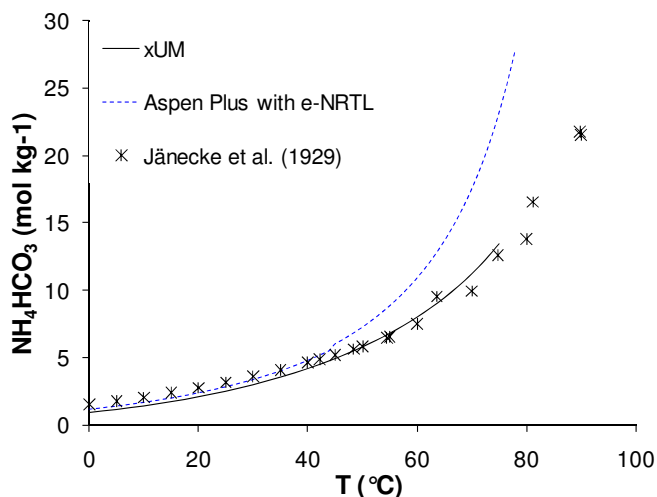


Figure 5-17: Comparison of the results for the calculation of the solubility of ammonium bicarbonate as a function of the temperature with xUM and Aspen Plus with the e-NRTL model. Experimental data by Jänecke (1929a and 1929b) have been added.

Figure 5-18 shows the calculations for both thermodynamic models of the loading at which ammonium bicarbonate and sesqui-carbonate precipitate as a function of the temperature for different molalities of ammonia. Again, these calculations are made at bubble point pressure and the pressure therefore varies for the different parts of the figure. Experimental data at different loadings from Jänecke have been included. In Figure 5-17, only data for a loading of 1 were used. The accuracy of the models can be evaluated by comparing with the experimental data the loading at which precipitation occurs, for a given temperature and molality.

It can be observed that the results at low ammonia concentration (3 mol/kg) are quite similar for both models and are in relative good agreement with the experimental data, e-NRTL being slightly more precise. For higher concentration of ammonia, it can be seen that the e-NRTL model estimates the formation of solid at a loading much lower than indicated by the experimental data. At 20 °C, e-NRTL predicts the appearance of ammonium bicarbonate at a loading from 0.34 to 0.25 when the ammonia concentration increases from 10 to 14 molal. The experimental data indicates that solid formation occurs for a loading larger than 0.5. Hence, for a molality up to 14 and for a temperature of 10 °C, no ABC is formed for a loading below 0.5.

The Extended UNIQUAC model allows for calculating accurately the solid formation, with the exception of one point at a temperature of 20 °C for a molality of ammonia of 13 where the Extended UNIQUAC calculates the formation of ammonium sesqui-carbonate instead of ABC. The other solids only appear for higher concentrations of ammonia.

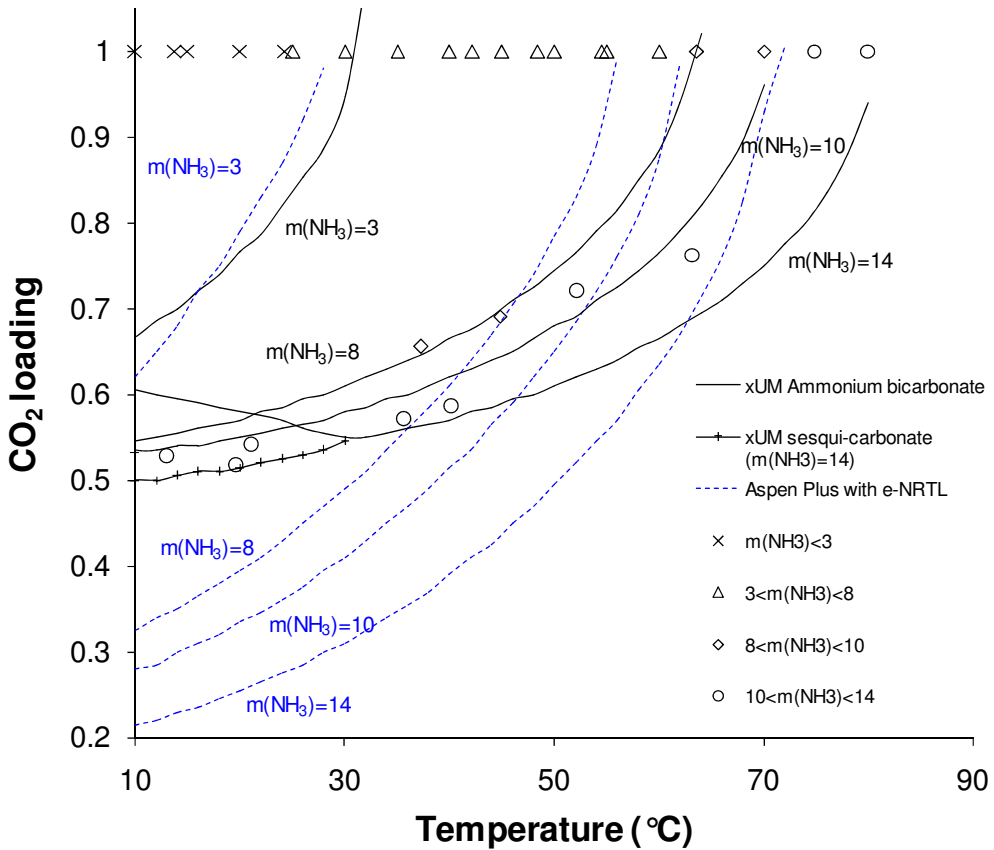


Figure 5-18: Comparison of the calculation of the loading at which ammonium bicarbonate and sesqui-carbonate precipitate as a function of the temperature for different molalities of ammonia with Extended UNIQUAC and the e-NRTL model. Experimental data for appearance of ammonium bicarbonate from Jänecke (1929a and 1929b) have been added.

### 5.4.2.3 Enthalpy calculations

Few enthalpy data for the ternary system  $\text{CO}_2\text{-NH}_3\text{-H}_2\text{O}$  are available in the literature. The data from Rumpf *et al.* (1998) reporting the measurements of enthalpy change from the partial evaporation of mixtures of carbon dioxide, ammonia and water have been used. The paper gives the weight and the pressure of the vapor phase produced and the energy consumption implied by the increase of the temperature of a given mixture of  $\text{CO}_2$ ,  $\text{NH}_3$  and  $\text{H}_2\text{O}$  (cf. Chapter 2). In this study, it is the mass of vapor produced that is used for the convergence in Aspen Plus, as the accuracy of the mass of vapor was found to be higher than the pressure measurement. The concentration of ammonia reaches up to 12

molal and the temperature is in the range 40-137 °C. The temperature increase is typically in the range 5-15 °C. The results with both models (see Figure 5-19) are very satisfactory given the uncertainty of the experimental data. The average deviation is below 4% for both models. This result is much better than the one reported for the Extended UNIQUAC model in Table 2-14. This is due to the low accuracy of the pressure measurements used in the flash calculations in Chapter 2.

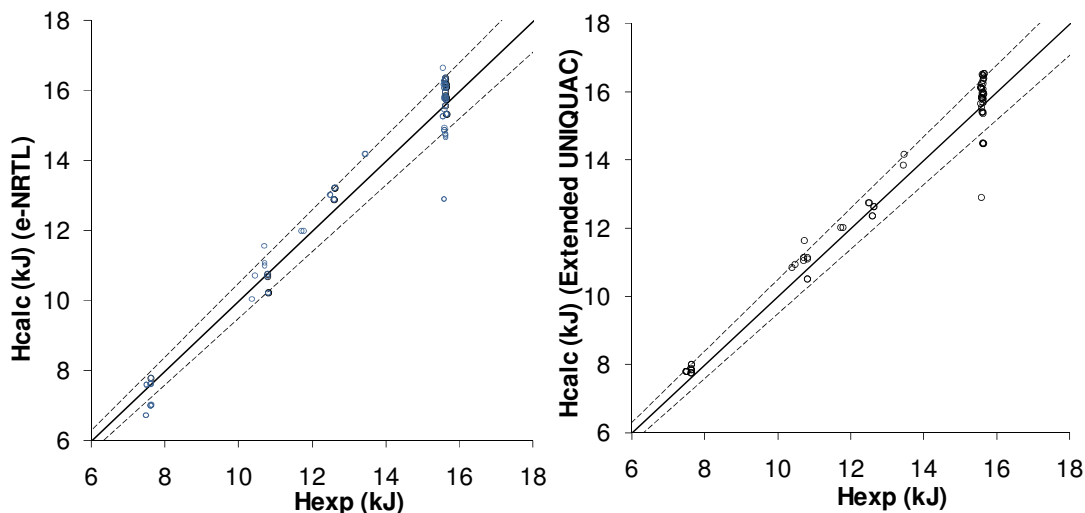


Figure 5-19: Heat of partial evaporation calculated with Aspen Plus with the e-NRTL model (left) and xUM (Right) as a function of the experimental data from Rumpf *et al.* (1998). 5% deviation dashed lines have been included

#### 5.4.2.4 Speciation

Figure 5-20 and Figure 5-21 show the speciation calculations as a function of the molality of carbon dioxide for both models, respectively at 60 °C with a molality of ammonia of 3.25 mol/kg and 120 °C with a molality of 6.2 mol/kg. Experimental data from Lichtfers have been plotted together with the calculated data. It can be observed that at 60 °C, both models perform relatively well. The Extended UNIQUAC model under estimates slightly the concentration of ammonia and bicarbonate and to some extent tends to over estimates the carbamate concentration. The e-NRTL model tends to overestimate the concentration of ammonia and bicarbonate and to under estimate the concentration of carbamate ion. At 120 °C, the results are very satisfactory for Extended UNIQUAC. However, the deviations reported for e-NRTL at 60 °C become very significant at 120 °C, especially at high loading. The low estimate of ammonium carbamate concentration could have consequences on the estimation of the heat requirement for the desorption.

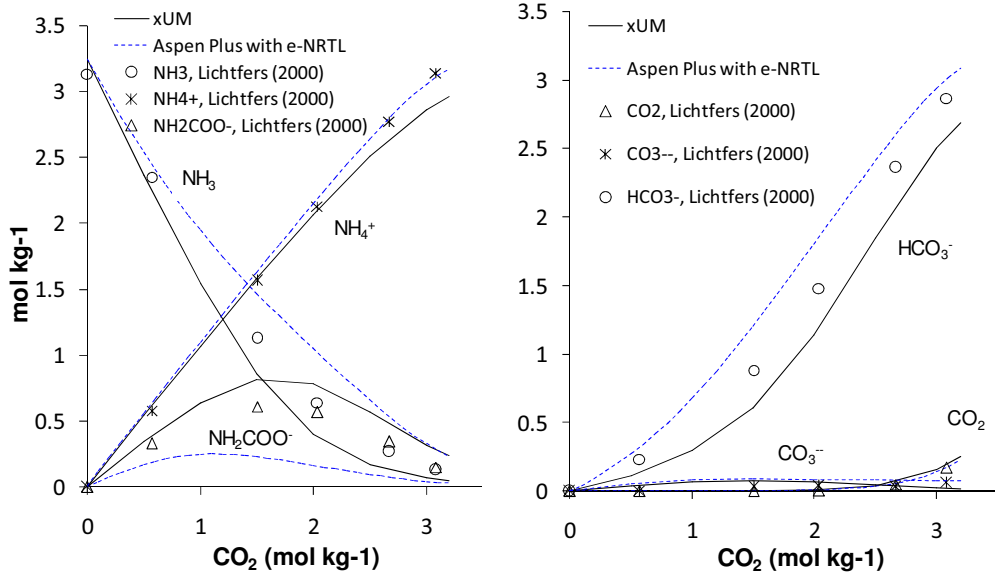


Figure 5-20: Speciation calculations with xUM and Aspen Plus with the e-NRTL model at 60 °C with a molality of ammonia of 3.25 mol/kg. Experimental data from Lichtfers (2000) have been added.

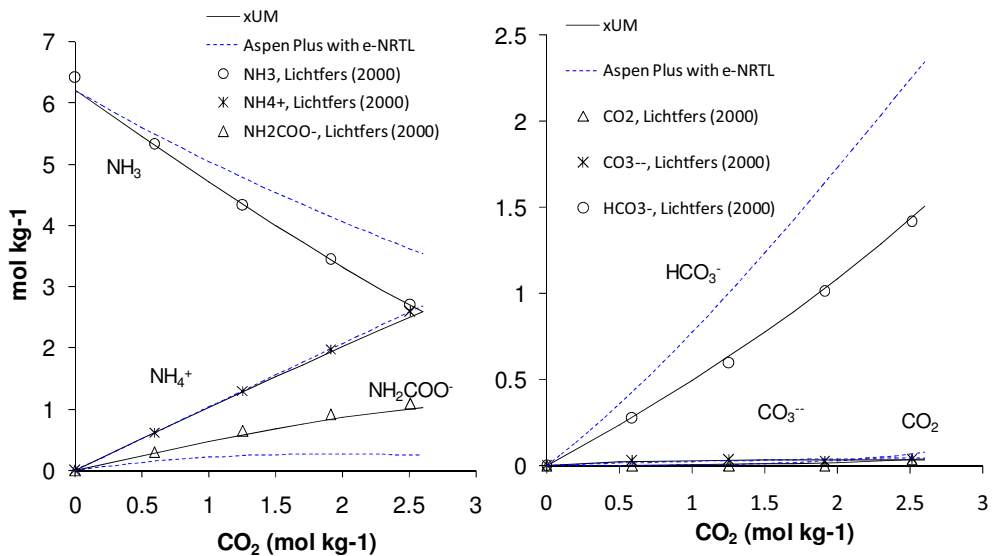


Figure 5-21: Speciation calculations with xUM and Aspen Plus with the e-NRTL model at 120 °C with a molality of ammonia of 6.2 mol/kg. Experimental data from Lichtfers (2000) have been added.

#### **5.4.2.5 Conclusion**

This analysis has revealed some of the limits of the thermodynamic models used. As shown in Chapter 2, the performance of the Extended UNIQUAC model for the CO<sub>2</sub>-NH<sub>3</sub>-H<sub>2</sub>O system is very satisfactory. The model was shown to over estimate slightly the partial pressure of carbon dioxide at low temperature and high loading and to under estimate it at high temperature, high loading and high ammonia concentration. The SLE calculations with this model were found to be very satisfactory up to a high concentration of ammonia. In addition, enthalpy and speciation calculations were in agreement with the experimental data up to a high temperature.

The e-NRTL model showed relatively good performance for the calculation of the partial pressure of carbon dioxide for limited concentrations of ammonia and limited loading. However, it was seen that the accuracy is lower at high concentrations and loadings. In addition, the partial pressure of ammonia is generally poorly estimated, especially for low loading solutions. The analysis of the SLE calculations shows that e-NRTL does not predict accurately solid formation. The results indicate that e-NRTL calculates the formation of ammonium bicarbonate for a loading much lower than the one observed with experimental data at low temperature. Finally, speciation calculations show that e-NRTL under estimates significantly the concentration of carbamate and over estimates the formation of bicarbonate for both tested temperatures.

These results show the importance of using a large data base from various types of experiments to derive the parameters of a thermodynamic model. In the case of the complex CO<sub>2</sub>-NH<sub>3</sub>-H<sub>2</sub>O system, it is especially relevant to ensure that the different properties of the system are well described by the model. The parameters from the version of the e-NRTL model tested would need to be refitted in order to increase the accuracy of the model.

### **5.4.3 Simulation of the CO<sub>2</sub> capture process using aqueous ammonia with e-NRTL and xUM**

#### **5.4.3.1 Description of the design specifications**

The CO<sub>2</sub> capture process has been simulated with both thermodynamic models by performing equilibrium calculations using common flow sheet and design specifications. The purpose of this study is to observe, quantify and interpret the difference in the calculations of the thermodynamic models. Therefore, a simple configuration of the process was chosen in order to simplify the comparison of the results.

The flue gas flow properties and composition are summed up in Table 5-1. As explained in 5.2.3, the xUM does not include oxygen, sulfur nor nitrous oxides. The composition of the flue gas was therefore simplified compared to a real flue gas from a coal fired power plant. It is expected that this simplification has only a minor influence on the simulation result.



**Table 5-1: Flue gas properties and composition**

<b>Flue gas flow rate (kg/s)</b>	781.8
<b>Temperature (°C)</b>	50
<b>Pressure (bar)</b>	1.016
<b>Mole fraction</b>	
<b>CO<sub>2</sub></b>	0.14
<b>H<sub>2</sub>O</b>	0.10
<b>N<sub>2</sub></b>	0.77

The absorber column is modeled as 3 flash units connected in series. The flue gas is cooled down with available cooling water, assumed to be at a temperature of 12 °C. A 5 °C temperature approach is used. Hence, the flue gas is cooled down to a temperature of 17 °C and reaches the bottom flash unit. The CO<sub>2</sub>-lean stream is chilled and flows to the top stage. The chilling is made in two steps. The solvent is first cooled down to a temperature of 17 °C using available cooling water. The cooled solvent is then chilled to a temperature of 10 °C using chilling water. This requires the consumption of electricity. In this study, the coefficient of performance (COP) is assumed to be 6. The solvent flow rate is varied so that 90% of the carbon dioxide is captured. The CO<sub>2</sub>-rich stream is then pressurized and reaches a heat exchanger where its temperature rises, before flowing to the CO<sub>2</sub> desorber column. It is modeled as 3 flash units connected in series. A design specification allows for varying the heat provided in the bottom flash unit in order to recover the carbon dioxide absorbed. A single flash unit models the condenser. The compression of the carbon dioxide stream is not included in the simulation. The CO<sub>2</sub>-lean stream reaches the lean-rich heat exchanger. The main design specification applied is a 5 °C difference at the cold side of the heat exchanger. In this simulation, no washing of the gas stream leaving the absorber is considered.

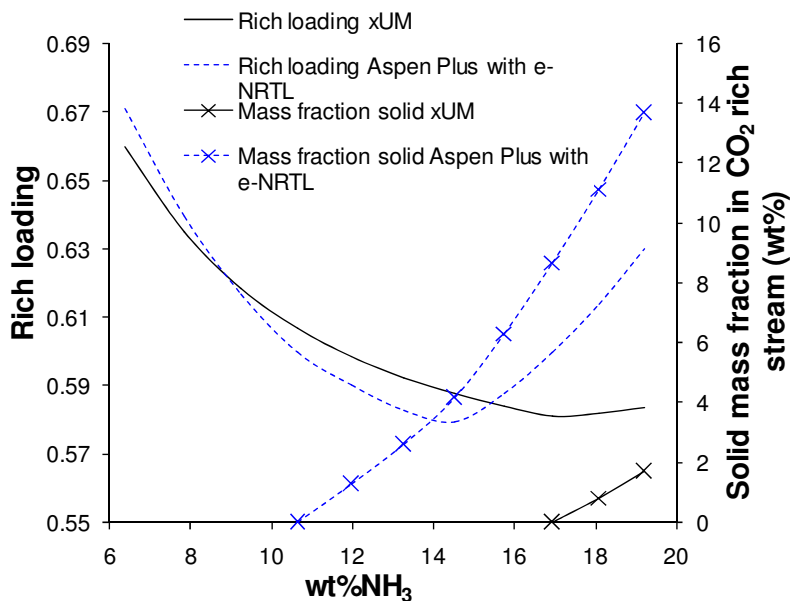
A base case scenario has been set up. The main boundary conditions and simulation inputs are summed up in Table 5-2. A sensitivity analysis on the main process parameters has been made using both models.

**Table 5-2: Boundary conditions for the base case scenario**

<b>Capture rate (%)</b>	90
<b>Initial ammonia concentration (wt%)</b>	9.25 (6.0 mol/kg H <sub>2</sub> O)
<b>Lean loading</b>	0.3
<b>Desorber pressure (bar)</b>	15
<b>Temperature of cooling water available (°C)</b>	12
<b>Temperature of chilled solvent (°C)</b>	10
<b>COP</b>	6
<b>Temperature difference in cold side heat exchanger (°C)</b>	5

### 5.4.3.2 Simulation results

The mass fraction of ammonia in the solvent has been varied from 6 to 19 wt% (3.7-13.8 mol/kg). Figure 5-22 shows the variation of the loading and the mass fraction of solid in the CO<sub>2</sub>-rich stream as a function of the carbon free mass fraction of ammonia in the solvent using the Extended UNIQUAC and the e-NRTL models. For all the concentrations considered, the solid phase consists exclusively of ammonium bicarbonate. Figure 5-22 shows that the e-NRTL and Extended UNIQUAC models calculate the formation of ammonium bicarbonate for a mass fraction of ammonia of respectively 11 and 17 wt%. This implies that the loading in the CO<sub>2</sub>-rich stream starts increasing for a lower ammonia concentration in the solvent for the e-NRTL model. The difference of results regarding the solid formation can be explained by the calculations presented in Figure 5-18. This difference would have a strong impact on the design of the equipment, especially the absorber and the heat exchanger. According to the e-NRTL model, these unit operations must be able to handle a much larger amount of solid than the amount predicted with the Extended UNIQUAC model.



**Figure 5-22: Rich loading and solid mass fraction in the CO<sub>2</sub>-rich stream as a function of the initial mass fraction of ammonia in the solvent.**

Figure 5-23 shows the calculation of the flow rate of CO<sub>2</sub>-lean stream and of the ammonia content in the gas stream exiting the absorber as a function of the carbon free mass fraction of ammonia in the solvent.

For the whole range of ammonia concentration considered, the e-NRTL model predicts a flow rate of solvent that is lower than the corresponding flow rate predicted with the Extended UNIQUAC model. The ammonia slip from the absorber is significantly lower according to e-NRTL compared to Extended UNIQUAC. This is explained by the difference of the VLE calculations at low temperature. This would have a strong impact on the required flow rate of washing stream used to lower the ammonia content in the exit gas and ultimately on the heat consumption in the ammonia stripper to recover the ammonia and regenerate the washing solvent.

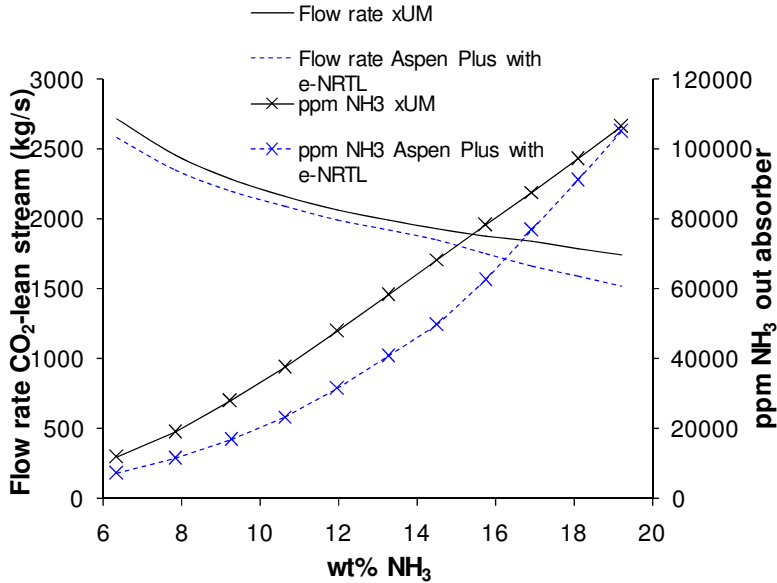
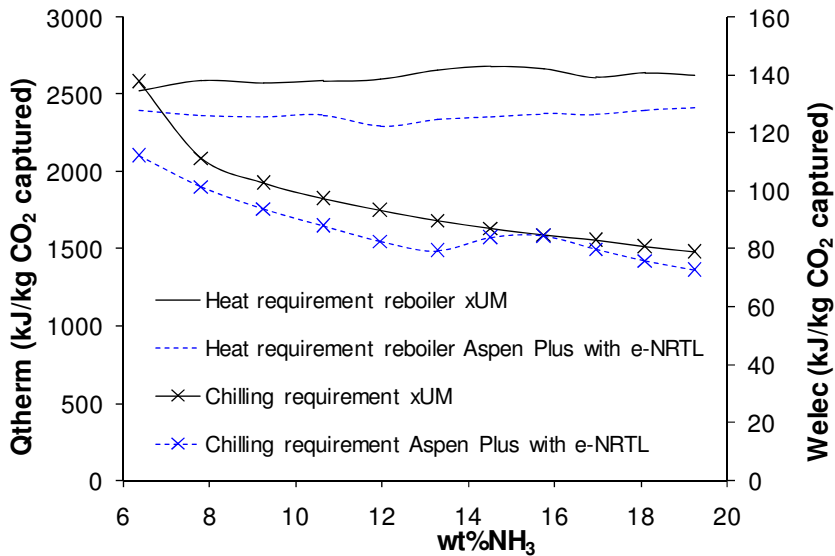


Figure 5-23: Flow rate of CO<sub>2</sub>-lean stream and ammonia content from the absorber calculated with e-NRTL and Extended UNIQUAC as a function of the carbon free mass fraction of ammonia in the solvent.

The shape of the rich loading predictions from Figure 5-22 can be qualitatively explained by the calculations shown in Figure 5-23. For a low concentration of ammonia in the solvent, the flow rate of solvent is lower with e-NRTL than with Extended UNIQUAC for a similar amount of carbon dioxide absorbed. Hence, the calculated rich loading is higher with NRTL than with UNIQUAC. When the ammonia concentration increases, the ammonia loss increases faster with Extended UNIQUAC than with e-NRTL. Hence, the rich loading decreases faster with e-NRTL than with Extended UNIQUAC. By increasing further the concentration of ammonia, the formation of solid entails a faster decrease of the solvent flow rate according to e-NRTL. At the same time, for high ammonia concentration, the prediction of ammonia losses from both models gets closer to each other. Hence, the rich loading calculated with e-NRTL increases and reaches a value higher than the one calculated with Extended UNIQUAC for a mass fraction of ammonia above 16 wt%.

Figure 5-24 shows the heat requirement in the desorber and the electricity requirement for the chilling calculated with both models as a function of the mass fraction of ammonia in the solvent.



**Figure 5-24: Heat requirement in the desorber and electricity requirement for the chilling calculated with e-NRTL and Extended UNIQUAC as a function of the carbon free mass fraction of ammonia in the solvent.**

The heat requirement is affected by different factors. High ammonia concentrations lead to lower solvent flow rates allowing for reducing the sensible heat required for the desorption. It also allows for reducing the reboiler temperature which entails a further reduction of the sensible heat. However, increasing the ammonia concentration implies the decrease of the temperature of the CO<sub>2</sub>-rich stream entering the desorber. This is due to the reduction of the reboiler temperature and to the fact that the carbon dioxide desorbed represents an increasing fraction of the enthalpy of the CO<sub>2</sub>-rich stream. Hence, less heat can be exchanged and transferred to the stream to heat it up. In the case where solids are present, a fraction of this heat will be used for the dissolution of the solid which also entails a reduction of the temperature of the CO<sub>2</sub>-rich stream entering the desorber and an increase of the heat consumption.

It can be observed that the heat requirement calculated with e-NRTL is significantly lower than the one observed with Extended UNIQUAC. The difference between the calculated heat requirements reaches 16%. Low quality heat from the power plant, the condenser or the compression section can be used to dissolve the solids present in the CO<sub>2</sub>-rich stream before it reaches the heat exchanger. This allows for decreasing significantly the heat requirement calculated with the e-NRTL model at high ammonia concentration. This would increase the difference between the calculations from the models and this difference would reach values up to 25%.

The electricity consumption for the chilling is also lower with e-NRTL than with Extended UNIQUAC. The main reason for this difference is the lower flow rate of solvent calculated with e-NRTL. The increase of the chilling requirement for a mass fraction of ammonia from 13 to 14 wt% is implied by the solid formation in the CO<sub>2</sub>-lean stream predicted by the model.

These results show that for similar conditions and design specifications, the results regarding the heat and electricity consumption vary a lot with the thermodynamic model used. For the conditions applied, e-NRTL tends to lower the heat and electricity consumptions compared to Extended UNIQUAC.

The heat requirement in the desorber depends on many factors such as the desorber pressure, the temperature of the stream entering the desorber, the flow rate of solvent and the loading of the CO<sub>2</sub>-rich stream. Hence, in order to compare the calculations of the models, it is necessary to apply similar boundary conditions. Figure 5-25 shows the heat requirement expressed in kJ/kg CO<sub>2</sub> captured and the capture rate calculated for both models as a function of the heat provided at the bottom stage of the desorber. These results were obtained by simulating the desorber section independently of the absorber. For this study and for both models, the initial ammonia concentration and the loading of the solvent entering the CO<sub>2</sub> desorber were set to 14.5 wt% and 0.52. The reboiler temperature was set to 119.9 °C and the desorber is operated at 15 bar. It corresponds to the composition and temperature obtained by simulating the process with the base case scenario conditions for a mass fraction of ammonia of 14.5 wt% using the e-NRTL model.

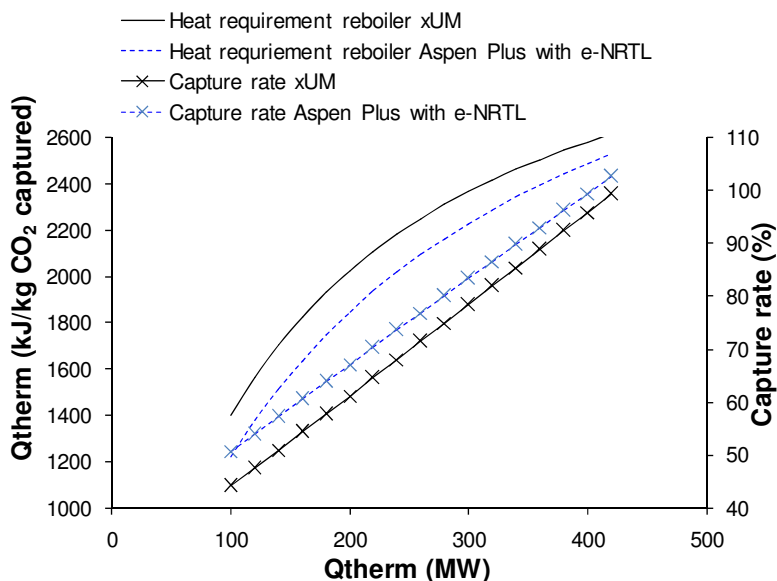


Figure 5-25: Heat requirement per mass carbon dioxide captured and capture rate calculated with e-NRTL and Extended UNIQUAC as a function of the heat consumption in the reboiler.

Figure 5-25 shows that for a given heat provided in the reboiler, e-NRTL predicts a higher capture rate than Extended UNIQUAC. For a heat consumption of 200 MW, the difference in the calculated capture rate is about 6 %-pts. Hence, at similar conditions, the heat required per mass carbon dioxide is lower for e-NRTL than for UNIQUAC. It is likely that this difference comes from the speciation calculations at high temperature. The low concentration of carbamate ion using the e-NRTL model compared to the Extended UNIQUAC model (see Figure 5-21) may affect the heat requirement calculations. This low concentration implies that ammonia reacts towards carbon dioxide in a way close to a tertiary amine, such as MDEA, which does not allow for forming a stable carbamate. This entails a low heat of desorption for these solvents compared to alkanolamines that are able to form stable carbamate, such as MEA.

#### **5.4.3.3 Conclusion of the simulation study**

The calculations from process simulation studies using e-NRTL and Extended UNIQUAC using similar boundary conditions showed significantly different results. The amount of solid ammonium bicarbonate in the CO<sub>2</sub>-rich stream entering the heat exchanger was calculated to be higher with e-NRTL. In addition, the prediction of the ammonia slip using Extended UNIQUAC was over estimated compared to e-NRTL. The calculated flow rate of the solvent to reach 90% capture efficiency was higher with Extended UNIQUAC than with e-NRTL. This leads to a significant discrepancy in the calculation of the heat and electricity requirements. e-NRTL predicted lower heat and electricity consumptions. By applying similar boundary conditions for the stream entering the desorber for both models, it was observed that the results were significantly different. Hence, the two thermodynamic models available for the NH<sub>3</sub>-CO<sub>2</sub>-H<sub>2</sub>O lead to significantly different calculations and conclusions regarding the performance of the process.

### **5.5 Conclusion**

A user model developed by Bjørn Maribo-Mogensen allowing for implementing the Extended UNIQUAC model on Aspen Plus has been evaluated. It has been shown that the Extended UNIQUAC user model could reproduce all the thermodynamic calculations from Extended UNIQUAC. Hence, it was validated as an accurate and valuable tool for process simulation.

The Extended UNIQUAC model implemented in Aspen was then compared to the latest version of the e-NRTL model for the CO<sub>2</sub>-NH<sub>3</sub>-H<sub>2</sub>O system. The comparison with the experimental data showed that Extended UNIQUAC generally performs better and can reproduce satisfactorily the large amount of experimental data used for the parameter fitting. e-NRTL underestimates the partial pressure of ammonia in many cases. In addition, partial pressure of carbon dioxide at high temperature and high ammonia concentration are not accurately represented. Furthermore, it was shown that the solid formation calculations with e-NRTL are not accurately represented. The model calculates precipitation of ammonium bicarbonate at a loading significantly lower than the one observed in the experimental data. Finally, speciation calculations using e-NRTL are less accurate than with Extended UNIQUAC.

At high temperature, the concentration of ammonium carbamate is underestimated by e-NRTL. This shows that the parameters from the e-NRTL model needs to be refitted and that the version tested in not satisfactory for process simulation.

Based on this comparison, a simple configuration of the CO<sub>2</sub> capture process was simulated with both thermodynamic models using similar boundary conditions. It was shown that the results obtained with the models are significantly different from each other. The solvent flow rate and the ammonia slip calculated with e-NRTL are especially lower than the ones observed with UNIQUAC. Solid formation in the CO<sub>2</sub>-rich stream is observed at a much lower ammonia concentration using e-NRTL than with UNIQUAC. This leads to a calculated heat requirement in the desorber up to 16% lower by using e-NRTL. By dissolving solid compounds in the CO<sub>2</sub>-rich stream by using low quality steam, this difference would reach 25%. By using similar compositions and temperature in the CO<sub>2</sub>-rich stream for both models, it has been shown that for a similar heat consumption, e-NRTL allows for desorbing more carbon dioxide. This is likely related to the low concentration of ammonium carbamate predicted by e-NRTL compared to Extended UNIQUAC.

By using the xUM, it is possible to perform a detailed process simulation study in order to evaluate the performance of the process. This study is detailed in the following chapter.

## 5.6 References

Abu-Zhara, M. R. M.; Schneider, L. H. J.; Niederer, J. P. M.; Feron, P. H. M. CO<sub>2</sub> capture from power plants: Part I. A parametric study of the technical performance based on monoethanolamine. *International Journal of Greenhouse Gas Control*, **2007**, *1*, 37.

Aspen Plus User Models, from Aspen Engineering 7.2 Documentation, [http://support.aspentech.com/Public%5CDocuments%5CEngineering%5CAspen%20Plus%5CV7.2/AspenPlusUserModelsV7\\_2-Ref.pdf](http://support.aspentech.com/Public%5CDocuments%5CEngineering%5CAspen%20Plus%5CV7.2/AspenPlusUserModelsV7_2-Ref.pdf), April 2011.

Chen, C. C.; Britt, H. I.; Boston, J. F.; Evans, L. B. Local Composition Model for excess Gibbs Energy of Electrolyte Systems. 1. Single Solvent, Single Completely Dissociated Electrolyte Systems. *AICHE J.*, **1982**, *28*, 588.

Fosbøl, P. L. The chilled ammonia process Evaluation of the energy requirements. Technical University of Denmark, internal report, **2008**.

Göppert, U.; Maurer, G. Vapor-liquid equilibria in aqueous solutions of Ammonia and Carbon Dioxide at Temperatures Between 333 and 393K. *Fluid Phase Equilibria*, **1988**, *41*, 153.

Jänecke, E. Über das System H<sub>2</sub>O, CO<sub>2</sub>, NH<sub>3</sub>. *Zeitschrift für Electrochemie*, **1929a**, *35*, 716.

Jänecke, E. Über die Löslichkeit von ammonbicarbonat in wasser bis zum schmelzpunkt. *Zeitschrift für Electrochemie*, **1929b**, *35*, 32.

van Krevelen, D. W.; Hoftijzer, P. J.; Huntjens, F. J. Compostion and vapour pressures of aqueous solutions of ammonia, carbon dioxide and hydrogen sulphide. *Recueil des travaux chimiques des Pays-Bas*, **1949**, *68*, 191.

Kurz, F.; Rumpf, B.; Maurer, G. Vapor-liquid-solid equilibria in the system NH<sub>3</sub>-CO<sub>2</sub>-H<sub>2</sub>O from around 310 to 470 K: New experimental data and modeling. *Fluid Phase Equilibria*, **1995**, *104*, 261.



- Lichtfers, U. Spektroskopische Untersuchungen zur ermittlung von Speziesverteilungen im System Ammoniak-Kohlendioxid-Wasser. Ph. D Dissertation, Kaiserslautern, Germany, **2000**.
- McLarnon, C., R.; Duncan, J. L. Testing of ammonia based CO<sub>2</sub> capture with multi-pollutant control technology. *Energy Procedia*, **2009**, *1*, 1027.
- Müller, G.; Bender, E.; Maurer, G. Vapor-liquid-equilibrium in the ternary system ammonia-carbon dioxide-water at high water contents in the range 373K to 473K. *Ber. Bunsenges. Phys. Chem.* **1988**, *92*, 148.
- Oexmann, J.; Kather, A. Post-combustion CO<sub>2</sub> capture in coal-fired power plants: Comparison of integrated chemical absorption processes with piperazine promoted potassium carbonate and MEA. Greenhouse Gas Technology 9, *Energy procedia*, **2009**, *1*, 799.
- Pexton, S.; Badger, E. H. M. The Examination of Aqueous solutions containing only NH<sub>3</sub> and CO<sub>2</sub>. *J. Soc. Chem Ind.*, **1938**, *57*, 107.
- Plaza, J. M.; Van Wagener, D.; Rochelle, G. T. Modeling CO<sub>2</sub> capture with aqueous monoethanolamine. *International Journal of Greenhouse Gas Control*, **2010**, *4*, 161.
- Rumpf, B.; Weyrich, F.; Maurer G. Enthalpy changes upon Partial Evaporation of Aqueous Solutions containing Ammonia and Carbon Dioxide. *Ind. Eng. Chem. Res.*, **1998**, *37*, 2983.
- Thomsen, K.; Rasmussen, P.; Gani, R. Correlation and prediction of thermal properties and behaviour for a class of aqueous electrolyte systems. *Chem. Eng. Sc.*, **1996**, *51*, 3675.
- Thomsen, K.; Rasmussen, P. Modeling of vapor-liquid-solid equilibrium in gas-aqueous electrolyte systems. *Chemical Engineering Science*, **1999**, *54*, 1787.

## **6 Simulation of CO<sub>2</sub> capture using aqueous ammonia using the Extended UNIQUAC model**

### **6.1 Introduction**

In order to make a process optimization study and to analyze thoroughly the potential of the process, flow sheet calculations are required. This allows for assessing the heat and electricity consumption by the different unit operations of a capture process. The results can be compared to the MEA-based process as a reference. A sensitivity analysis over the main process parameters can also be performed in order to study the optimization of the process. For this purpose, the user model d previously describe is used in order to implement the Extended UNIQUAC thermodynamic model in Aspen Plus. This chapter focuses on the simulation of the variant of the process with absorption at low temperature, the so-called Chilled Ammonia Process. It first includes the description of the two process configurations used and of the base case used in this study. Both process configurations allows for capturing 90 % of the carbon dioxide contained in the flue gas produced by a large scale power plant. In addition, they include water wash sections in order to reduce the emissions of ammonia to the atmosphere. The results from a sensitivity analysis of the main process parameters are then presented for both process configurations. Based on the results, the general performance of the process is analyzed and general conclusions are made.

### **6.2 Simulation of the CO<sub>2</sub> capture process using aqueous ammonia**

#### **6.2.1 Description of the process configurations**

This simulation study mainly focuses on the case of absorption at low temperature. The precipitation allows for increasing the CO<sub>2</sub> loading and the carrying capacity of the solvent. It can therefore lower the heat and power requirements for the desorption by lowering the flow rate of solvent. However, the unit operations used in the process must be able to handle the formation of solid matters during the absorption. One of the main concerns regarding the CAP is the vaporization of ammonia from the absorber as the ammonia has to be washed from the gas before it is released in the atmosphere. This washing and the recovery of the washing water implies additional heat consumption. The vaporization and the ammonia slip can be limited by applying a low temperature of absorption, a high CO<sub>2</sub> loading and by limiting the ammonia concentration (cf. Chapter 3). Optimized process configurations can contribute to limiting the ammonia slip. In this study, two main process configurations regarding the absorption have been considered in order to allow for the absorption of the carbon dioxide and for limiting the ammonia slip.

Configuration A is close to the configuration recently proposed by Alstom (cf. Figure 1-9, Kozak *et al.*, 2009). As shown in Figure 6-1, it uses a single RadFrac unit operation to model the absorber column. A RadFrac unit operation is commonly used in Aspen to model distillation and absorption processes. It

allows for modeling a packed column with a chosen number of equilibrium stages. In reality, when considering a CO<sub>2</sub> capture process from a large scale power plant, several absorber columns connected in series could be needed in order to limit the height of the absorber. The flue gas flows through two direct contact coolers (DCC) where its temperature is first cooled down to 20 °C with the available cooling water at 10 °C and then chilled down to 15 °C with chilling water at 5 °C. A 10 °C temperature approach is therefore applied in the DCC. The use of two DCC's allows for limiting the electricity consumption in the chiller by limiting the amount of cooling water to be chilled. The water content and volume of the flue gas decrease significantly through the DCC. A 5 °C temperature approach is applied for the liquid-liquid heat exchanger. Hence, the CO<sub>2</sub>-lean stream is cooled down to a temperature of 15 °C and chilled down to a temperature of 10 °C using chilled water at 5 °C before flowing to the top of the absorber. For the different chillers in the simulation, the heat exchanged is converted into electricity consumption using a COP of 5. The same value for the COP has been used by Mathias *et al.* (2010). By using a cyclone, the liquid and solid phases of the stream exiting the absorber are separated. A chosen fraction of the liquid phase is chilled down to 10 °C and recycled back to the top of the absorber while the rest of the stream constitutes the CO<sub>2</sub>-rich stream. This allows for reducing the temperature and increasing the loading at the top of the absorber column in order to reduce the vaporization of ammonia at the top of the absorber. In this configuration, chilled water is used for three different streams.

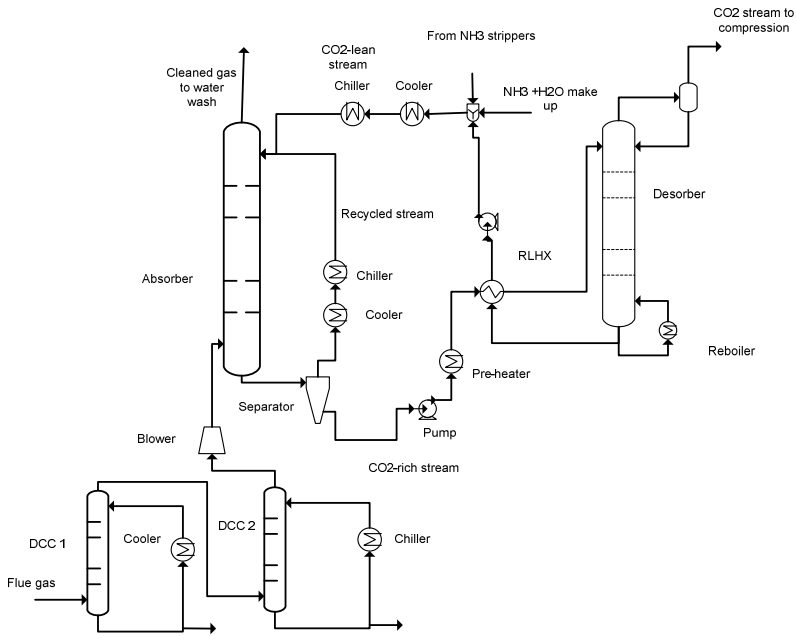


Figure 6-1: Schematic flow sheet of process Configuration A

Based on our experiences with modeling Configuration A, an alternative configuration is proposed in the present study. Configuration B, as shown in Figure 6-2, uses two RadFrac unit operations to model the absorber columns. They are connected in series. The CO<sub>2</sub>-lean stream and the flue gas are cooled down with the available cooling water to respectively 15 and 20 °C before they reach the first absorber where they are contacted counter-currently. Hence, the flue gas and the CO<sub>2</sub>-lean stream are not chilled before entering the absorber. The exit stream from the bottom of Absorber 1 is then chilled down to 10 °C. By using a cyclone, the solid and liquid phases are separated. The solid phase is introduced to the CO<sub>2</sub>-rich stream exiting the bottom of Absorber 2 while the liquid phase flows to the top of the second unit operation, Absorber 2. The gas exiting Absorber 1 is directly injected at the bottom of Absorber 2. Hence, this configuration allows for maintaining a low temperature and a high loading in the liquid at the top of Absorber 2 before the gas exits the absorption section and reaches the water wash. This set-up allows for reducing the ammonia slip from the gas stream exiting the absorber.

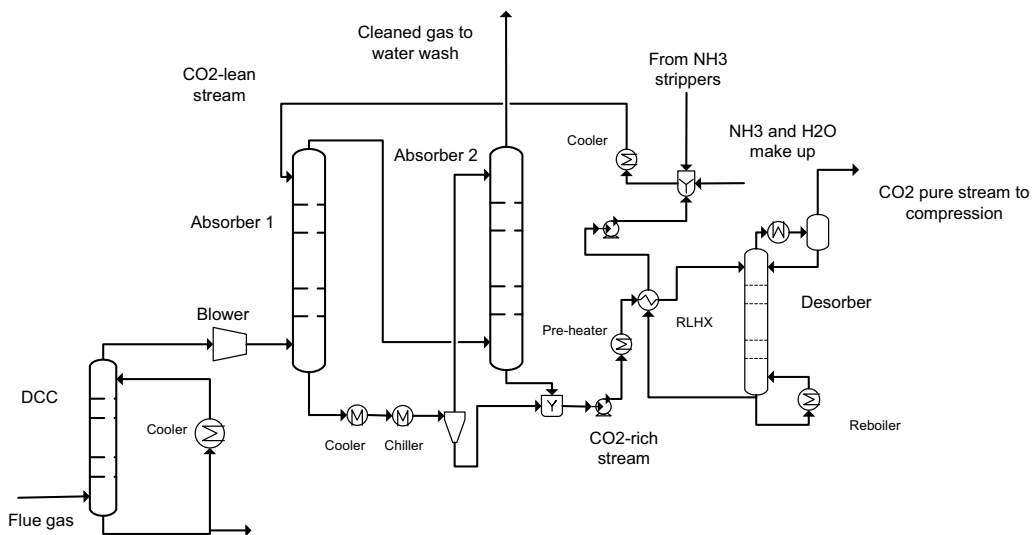


Figure 6-2: Schematic flow sheet of process Configuration B

## 6.2.2 Description of the flow sheet and design specifications

The main sections and unit operations of the flow sheet for both configurations are detailed in the following section.

The pressure drop to be overcome by the blower is the sum of the pressure drop in the piping, in the absorber and in the water wash unit operations. In equilibrium based calculations, this value is an input to the calculations. In the study of the simulation of the MEA-based process by Abu-Zahra *et al.* (2007), the pressure drop had been estimated as 0.048 bar. Due to slow absorption at low temperature, it is likely that the required height of the packing of the absorber and of the water wash unit operations

for the CAP is larger than for the MEA based process. In this study, the pressure drop for the flue gas is set to 0.08 bar.

The direct contact coolers are modeled as 5 equilibrium stage RadFrac columns. Water is circulated in order to cool down the flue gas before it reaches the absorber.

For Configuration A, the absorber is modeled as a 20-stage RadFrac column. For Configuration B, each of the absorbers is modeled as a 10-stage RadFrac column. Hence, the number of equilibrium stage for the absorption is similar for both configurations. The flow rate of CO<sub>2</sub>-lean stream is varied until a final capture rate of 90 % is reached.

As mentioned previously, the simulation is equilibrium based. Equilibrium models typically over predict the absorption abilities of a solvent. This leads to optimistic results compared to real capture plants. Hence, in order to obtain results that are closer to reality, Murphree efficiencies (ME) for carbon dioxide for the absorber columns have been specified. For a compound  $i$  at the equilibrium stage  $j$ , it is defined as:

$$ME_{i,j} = \frac{y_{i,j} - y_{i,j+1}}{y_{i,j}^* - y_{i,j+1}} \quad (6.1)$$

Where  $y_j$  is the mole fraction of compound  $i$  in the vapor leaving stage  $j$ ,  $y_{j+1}$  the mole fraction of compound  $i$  in the vapor entering stage  $j$  and  $y_j^*$  is the mole fraction of compound  $i$  in the vapor in equilibrium with the liquid entering stage  $j$ .

The ME is not an independent variable. However, in the absence of any pilot plant data available, it could not be calculated nor fitted. It has been shown previously that the rate of absorption of carbon dioxide by aqueous ammonia at low temperature is significantly lower than the one observed for the MEA-based process (cf. Chapter 4). As shown by Oexmann (2011), the ME for CO<sub>2</sub> in a 20-stage absorber column using 30 wt% MEA with 90% capture rate ranged between 0.15 and 0.45. It is chosen to use a ME lower than in the case of MEA. In the case of Configuration A, the ME for carbon dioxide for the absorber is set to 0.1. In the case of Configuration B, the ME for CO<sub>2</sub> for the first absorber is set to 0.2 for the different stages while it is set to 0.1 for the second, as the temperature in the second column is lower than in the first one due to the chilling of the solvent.

In this study, when solid precipitate is present in the CO<sub>2</sub>-rich stream, the stream is pre-heated before it reaches the rich-lean heat exchanger (RLHX) in order to dissolve the solids. The required temperature increase to dissolve the solids is calculated during the simulations. The low quality heat that can potentially be recovered from the overhead condenser at the top of the CO<sub>2</sub> desorber or from the stripped ammonia streams is used for this pre-heating. It allows for reducing the heat consumption in the CO<sub>2</sub> desorber. If no preheating was used, a significant amount of the heat gained from the CO<sub>2</sub>-lean

stream in the RLHX would be used to ensure the dissolution of the solid. Therefore, less heat would be used for the rise of the temperature of the CO<sub>2</sub>-rich stream. Hence, by using pre-heating, the temperature of the stream entering the desorber increases and the sensible heat in the desorber decreases (cf. Chapter 3 and Chapter 5). In all cases, the temperature difference at the cold side of the RLHX is set to 5 °C. It should be noted that in absence of solid in the CO<sub>2</sub>-rich stream, the pre-heating of the stream would not be beneficial as the temperature of the CO<sub>2</sub>-rich stream flowing to the desorber would not be affected by the pre-heating. It is therefore only used when the stream contains solid.

With Configuration B, for some sets of process parameters, the amount of low quality heat from the capture plant is not sufficient to dissolve the solid content. Hence, for these cases, the CO<sub>2</sub>-rich stream flowing to the RLHX still comprises solid particles. It is assumed that the performance of the RLHX is not affected by the presence of solids.

The CO<sub>2</sub>-rich stream is pressurized using a pump with an efficiency of 80%. The main heat exchanger is modeled as two heaters exchanging the same amount of heat. The temperature difference between the CO<sub>2</sub>-lean stream exiting the heat exchanger and the CO<sub>2</sub>-rich stream entering (cold side of RLHX) it is set to 5 °C.

The desorber is modeled as a 10-stage RadFrac column with a kettle type reboiler. The CO<sub>2</sub>-rich stream enters the top stage of the column. A flash unit at 40 °C models the overhead condenser for the gas exiting the desorber. This temperature allows for decreasing the volume of the gas and limiting the ammonia slip from the stripper. The carbon dioxide stream from the CO<sub>2</sub> desorber reaches a 5-stage compressor with an efficiency of 80% with inter-cooling at 40 °C to reach a final pressure of 110 bar.

Despite the low temperature at the top of the absorber, the gas exiting the absorber has a high ammonia content. It is therefore necessary to wash this stream before it is released to the atmosphere. This washing is made in two steps as shown in Figure 6-3. The gas first flows to Water Wash 1, a 10-stage RadFrac column where it is contacted with a washing stream that mainly consists of water. The washing stream is preliminary chilled down to a temperature of 10 °C before entering the column. This chilling temperature for the washing stream is kept constant in all the simulations. The flow rate of the stream is varied until a content of ammonia lower than 300 ppm is reached. The ammonia recovered is then stripped off in the NH<sub>3</sub> stripper 1 column. The stripped stream that contains ammonia, carbon dioxide and water is sent back to the CO<sub>2</sub>-lean stream and to the absorber. The regenerated washing stream flows back to the water wash column. A design specification allows for varying the heat duty in the reboiler so that the composition of the washing stream remains constant. A second water wash column is then used to lower the ammonia content in the exhaust gas to a value lower than 10 ppm. Similarly to the first water wash section, a stripper is used to regenerate the washing solvent and recover the ammonia. The water purity of the washing stream used is higher than for the first water wash. For the sake of simplicity in the simulation, two strippers are used. In the case of a real capture plant, a single ammonia stripper would probably be used. The regenerated washing streams would be

taken from different heights in the ammonia stripper in order to match with the purity requirement of the two water wash sections.

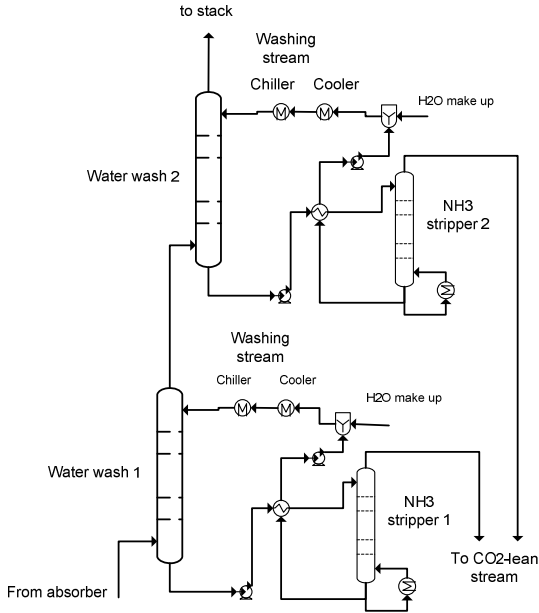


Figure 6-3: Schematic flow sheet of the water wash section

### 6.2.3 Boundary conditions for the base case scenario

A base case scenario has been chosen in order to perform a parameter sensitivity analysis.

The flue gas that is considered in the simulation exits the flue gas desulphurization unit (FGD unit). Its composition and flow rate are taken from a power plant with a gross power output of 1100 MW<sub>elec, net</sub> (Kather *et al.*, 2011). The parameters related to the flue gas can be seen in Table 6-1. As mentioned previously, the user model does not handle oxygen, argon or sulfur compounds (cf. Chapter 5). Therefore they have been replaced by nitrogen in the simulation.

Based on the information of the CAP patent, a base case scenario has been set up in order to analyze the performance of the capture process. The main process parameters of the base case scenario and the main general design specifications are summed up in Table 6-2. A capture rate of 90% is a value that is commonly used in the literature. A mass fraction of ammonia of 7.8% corresponds to a molality of ammonia of about 5 mol/kg water. The temperature of the available cooling water used is rather low and therefore corresponds to a cold location.

**Table 6-1: Flue gas parameters**

	<b>Real Flue gas</b>	<b>Simulation</b>
	<b>Mole Fraction</b>	<b>Mole Fraction</b>
<b>H2O</b>	0.11	0.11
<b>CO2</b>	0.14	0.14
<b>N2</b>	0.71	0.75
<b>O2</b>	0.03	-
<b>Ar</b>	0.01	-
<b>SOx</b>	10ppm	-
<b>Total Flow (kmol/sec)</b>	34.8	34.8
<b>Total Flow (kg/sec)</b>	1021	1021
<b>Total Flow (m3/sec)</b>	917	917
<b>Temperature (°C)</b>	48.49	48.49
<b>Pressure (bar)</b>	1.01325	1.01325

**Table 6-2: Process parameters for the base case scenarios and main design specifications**

<b>Capture rate (%)</b>	90
<b>Ammonia concentration (carbon free) (wt%)</b>	7.8
<b>Lean loading</b>	0.33
<b>Desorber pressure (bar)</b>	10
<b>Temperature approach liquid-liquid heat exchanger (°C)</b>	5
<b>Temperature approach DCC (°C)</b>	10
<b>Temperature difference cold side RLHX (°C)</b>	5
<b>Cooling water temperature (°C)</b>	10
<b>Chilled water temperature (°C)</b>	5
<b>Chilling temperature (°C)</b>	10
<b>COP</b>	5
<b>Recycling rate (Configuration A) (%)</b>	50



## 6.3 Results and discussion

### 6.3.1 Base case scenario

The analysis of the process must take both the heat and electricity requirements into account. Table 6-3 includes the results for the base case scenario for both process configurations. It can be seen that the heat requirement in the CO<sub>2</sub> desorber, the flow rate of CO<sub>2</sub>-lean stream are in the same range for both configurations. The value calculated for the heat consumption for desorption is significantly lower than the one observed with the MEA-based process, 3700 kJ/kg CO<sub>2</sub> captured during the CASTOR project (Knudsen *et al.*, 2008). This comparison is only indicative, as the power consumption for the desorption of carbon dioxide depends on the required quality of the steam. The heat requirement in the NH<sub>3</sub> strippers varies significantly for Configuration A and B. The variation is due to the large difference in the ammonia slip from the absorber. For both process configurations, the reboiler temperature of the NH<sub>3</sub> strippers is systematically lower than the one of the CO<sub>2</sub> desorber. Hence, a lower steam quality could be used to strip the ammonia if it is available. The larger solid formation in case of Configuration B is due to the lower temperature and the higher loading of the CO<sub>2</sub>-rich stream caused by the use of the second absorber with inter-cooling.

The desorption at high pressure allows for reducing the electricity requirement during the compression of carbon dioxide. For the base case scenario of Configuration B, the sum of the electricity requirements for the chilling and for the compression of the CO<sub>2</sub> pure stream represents about 75 % of the compression duty observed for a conventional capture process with a desorber pressure at 2 bar, calculated in this study as 340 kJ/kg CO<sub>2</sub> captured. The chilling duty is larger for Configuration A, as it includes the chilling of the flue gas and of the recycling stream on top of the chilling of the CO<sub>2</sub>-lean stream. The sum of the chilling and compression duty is in the same range as the compression duty observed for conventional capture processes. It must be noted that the chilling duty heavily depends on the temperature of the cooling water available.

For Configuration A, CO<sub>2</sub> absorption occurs for 95% in the absorber and 5% in the washing sections for the base case scenario. The results for Configuration B show that most of the CO<sub>2</sub> capture occurs in Absorber 1. For the base case scenario, 72 % of the CO<sub>2</sub> is captured in Absorber 1, 16.5 % in Absorber 2 and 1.5% in the water wash sections. Absorber 2 also allows for reducing significantly the ammonia slip. The ammonia content in the gas stream exiting absorber 1 is about ten times higher than the one in the stream exiting absorber 2. This higher percentage of the carbon dioxide capture in the washing section for Configuration A is a consequence of the higher ammonia slip which implies the use of a larger flow rate of cooling water to reach a final ammonia content in the exit gas of 10 ppm.

The higher solid fraction for Configuration B can be explained by a higher loading and a lower temperature of the CO<sub>2</sub>-rich stream. This implies that a higher amount of heat is required for pre-heating in order to dissolve the solids before the CO<sub>2</sub>-rich stream reaches the heat exchanger. In the case of the base case scenario with Configuration A, this heat allows for increasing the temperature of

the stream from 21 to 23 °C. For Configuration B, the temperature increases from 15 to 25 °C. For the base case scenario, this heat can be recovered from the overhead condenser and the stripped ammonia. For the base case scenario, the total heat that can be recovered and used is about 850 kJ/kg CO<sub>2</sub> captured.

The CO<sub>2</sub> gas stream exiting the condenser at a pressure of 10 bar has a significant ammonia content that is reduced during the compression due to the inter cooling. It should be noted that the liquid stream from the condenser that is introduced to the top of the CO<sub>2</sub> desorber is a slurry. Depending on the cases, the mass fraction of the solid in that stream can reach 60 wt%. The minimum temperature to apply in the condenser in order to avoid the formation of solid for the base case scenario and for both configurations is 72 °C. Increasing the temperature in the overhead condenser results in a reduction of the heat requirement in the CO<sub>2</sub> desorber. However, it also increases the ammonia content of the CO<sub>2</sub>-stream leaving the condenser that is then required to be washed in order to remove its ammonia content before the captured carbon dioxide is compressed. Another option is to introduce the slurry stream exiting the condenser in the CO<sub>2</sub>-lean stream and to chill it down before injecting it to the absorber. However, this option implies a small increase of the heat requirement. In this study, as shown in Figure 6-1 and Figure 6-2, the slurry stream is brought back to the desorber. This will in reality require an adequate design of the piping system that is not within the scope of this study. The temperature in the overhead condenser of 40 °C ensures limiting the ammonia content in the CO<sub>2</sub> pure stream but entails the solid formation in the stream from the condenser.

**Table 6-3: Results base case scenario for Configuration A and Configuration B**

	<b>Configuration A</b>	<b>Configuration B</b>
<b>Heat requirement CO<sub>2</sub> desorber (kJ/kg CO<sub>2</sub> captured)</b>	2533	2461
<b>Heat requirement NH<sub>3</sub> stripper 1 (kJ/kg CO<sub>2</sub> captured)</b>	279	115
<b>Heat requirement NH<sub>3</sub> stripper 2 (kJ/kg CO<sub>2</sub> captured)</b>	129	52
<b>Temperature CO<sub>2</sub>-rich entering CO<sub>2</sub> desorber</b>	114	113
<b>Temperature reboiler CO<sub>2</sub> desorber (°C)</b>	131	130
<b>Temperature reboiler NH<sub>3</sub> stripper 1 (°C)</b>	98	98
<b>Temperature reboiler NH<sub>3</sub> stripper 2 (°C)</b>	100	100
<b>NH<sub>3</sub> content gas out absorber 1 (ppm)</b>	-	18690

Temperature gas out absorber 1 (°C)	-	18.3
NH <sub>3</sub> content gas out absorber 2 (ppm)	10105	1860
Temperature gas out absorber 2 (°C)	11.8	10.2
NH <sub>3</sub> content gas out water wash 2 (ppm)	10.9	8.7
Electricity requirement chilling solvent (kJ/kg CO <sub>2</sub> captured)	143	88
Electricity requirement chilling flue gas (kJ/kg CO <sub>2</sub> captured)	14.6	-
Electricity requirement compression (kJ/kg CO <sub>2</sub> captured)	177	177
Mass fraction solid CO <sub>2</sub> -rich stream (%)	0.8	2.8
Pre-heating CO <sub>2</sub> -rich stream to dissolve solid content, can be taken from heat integration condenser and stripped ammonia (kJ/kg CO <sub>2</sub> captured)	176	650
Rich CO <sub>2</sub> loading	0.66	0.68
Flow rate CO <sub>2</sub> -lean stream (kg/sec)	3140	2980
Total flow rate washing water streams (kg/sec)	332	170
NH <sub>3</sub> content before compression in CO <sub>2</sub> pure stream (ppm)	76	76
NH <sub>3</sub> content after compression in CO <sub>2</sub> pure stream (ppm)	< 1	< 1

A sensitivity analysis of the main process parameters has been made for both process configurations.

### 6.3.2 Results sensitivity analysis Configuration A

The main process parameters for Configuration A are listed below. Their influence on the heat and electricity requirements has been studied.

- The ammonia concentration in the solvent
- The lean loading
- The chilling temperature
- The desorber pressure
- The recycling rate for the liquid phase of the stream exiting the absorber.

### 6.3.2.1 Effect of the ammonia concentration

Figure 6-4 shows the influence of the concentration of ammonia in the solvent on the heat requirements for the CO<sub>2</sub> desorber, NH<sub>3</sub> strippers and on the ammonia slip from the absorber. The mass fraction of ammonia in the solvent is varied from 4 to 11 wt% (2.4 to 7.3 molal NH<sub>3</sub>) leaving the other process parameters from the base case unchanged (see Table 6-2). As shown in Figure 6-4, the ammonia content in the gas stream exiting the absorber varies between 4500 and 19000 ppm. This rising ammonia slip leads to an increase of the heat requirement in the NH<sub>3</sub> strippers when the concentration increases, reaching 950 kJ/kg CO<sub>2</sub> captured for the highest concentrations studied.

When the ammonia concentration increases, the heat requirement in the CO<sub>2</sub> desorber decreases for a mass fraction of ammonia up to 9 %. For higher mass fractions, the heat requirement in the CO<sub>2</sub> desorber remains quite stable. Different effects explain this trend:

- Increasing the concentration of ammonia entails the drop of the flow rate of solvent, as more carbon dioxide can be captured per kilogram of solvent. This entails the decrease of the sensible heat required in the desorber. The drop of flow rate is faster for the low concentration range.
- When the ammonia concentration increases and reaches high value, the difference between the temperature of the CO<sub>2</sub>-rich stream entering the desorber and the CO<sub>2</sub>-lean stream exiting it increases. It is explained by two effects:
  - First, the temperature of the CO<sub>2</sub>-rich stream from the heat exchanger decreases. This is due to the rise of the CO<sub>2</sub> content per kilogram solvent in the CO<sub>2</sub>-rich stream which leads to an increasing difference in heat capacities of the CO<sub>2</sub>-lean and rich streams in the heat exchanger. The calorimetric value of the carbon dioxide that is desorbed represents a growing proportion of the heat that is transferred from the CO<sub>2</sub>-lean to the CO<sub>2</sub>-rich stream.
  - Second, when the ammonia concentration in the solvent increases, the ammonia slip increases (cf. Figure 6-4). Hence, the flow rate of washing stream necessary to reduce the ammonia content in the flue gas rises, and the amount of CO<sub>2</sub> captured in the water wash sections increases. This CO<sub>2</sub> stripped with the ammonia in the NH<sub>3</sub> strippers is mixed with the CO<sub>2</sub>-lean stream. This entails that the over-stripping of the CO<sub>2</sub>-rich stream is required which leads to the increase of the reboiler temperature.
  - This increase of the temperature difference in the desorber causes a rise of the required temperature increase in the reboiler and therefore of the sensible heat. This analysis is only valid for a constant temperature difference at the cold side of RLHX.

In addition, for high ammonia concentration range, the calculated rich loading decreases. This is due to the increase of the equilibrium partial pressure of carbon dioxide when the ammonia concentration

increases at constant temperature and loading for high loading range. The decrease of the rich loading entails a slower decrease of the solvent flow rate for the high concentration range.

Therefore, for this process configuration, using high ammonia concentration in the solvent does not allow for reducing the global heat requirement. In addition, a further increase of the concentration would lead to an increase of the solid content in the CO<sub>2</sub>-rich stream. As not enough low quality heat might be available in the capture plant, some solid content might reach the RLHX and therefore cause the decrease the temperature of the CO<sub>2</sub>-rich stream entering the CO<sub>2</sub> desorber. This would lead to an increase of the heat requirement in the desorber. The minimum heat requirement is observed for a mass fraction of ammonia of about 8.5 wt% and has a value of 2930 kJ/kg CO<sub>2</sub> captured.

Figure 6-5 shows the total heat requirement as a function of the concentration of ammonia in the solvent for different recycling rates. For each ammonia concentration, there is a recycling rate that corresponds to a minimum of the heat requirement. In addition, it can be seen that the higher is the ammonia concentration, the higher is the recycling rate where the minimum for the heat requirement can be observed. A high recycling rate allows for increasing the loading and decreasing the temperature at the top of the absorber. It therefore allows for limiting the ammonia slip which is especially relevant for high ammonia concentration solvents. The recycling rate therefore has to be optimized to the solvent concentration in order to decrease the heat consumption.

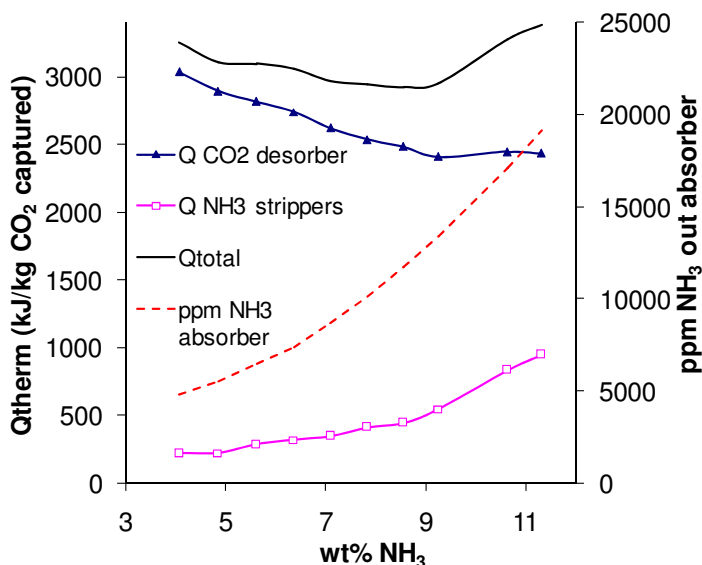


Figure 6-4: Heat requirement and ammonia content in the gas stream exiting the absorber as a function of the ammonia concentration in the solvent

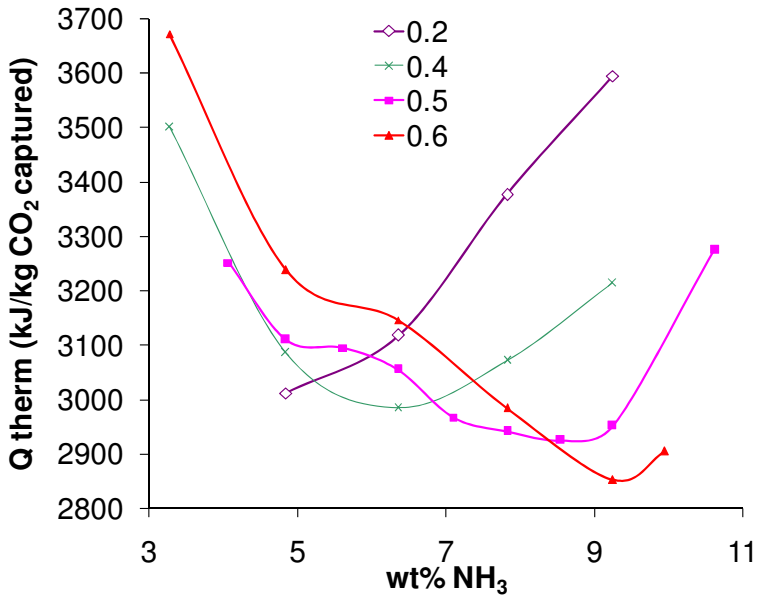


Figure 6-5: Total heat requirement as a function of the ammonia concentration in the solvent for different recycling rates

Figure 6-6 shows the electricity chilling duty and the flow rate of the CO<sub>2</sub>-lean stream as a function of the ammonia concentration. The decrease of the solvent flow rate when the concentration of ammonia in the solvent increases implies the drop of the chilling duty.

Figure 6-7 shows the electricity consumption from the chilling of both the solvent and the flue gas as a function of the concentration of ammonia in the solvent for different recycling rates. It can be observed that the chilling duty increases with the recycling rate and decreases when the concentration of ammonia in the solvent increases. As previously mentioned, the power savings from the compression compared to a conventional capture process are estimated at 160 kJ/kg CO<sub>2</sub> captured. From Figure 6-7, it can be seen that the chilling duty exceeds this reduced power duty for most of the cases analyzed.

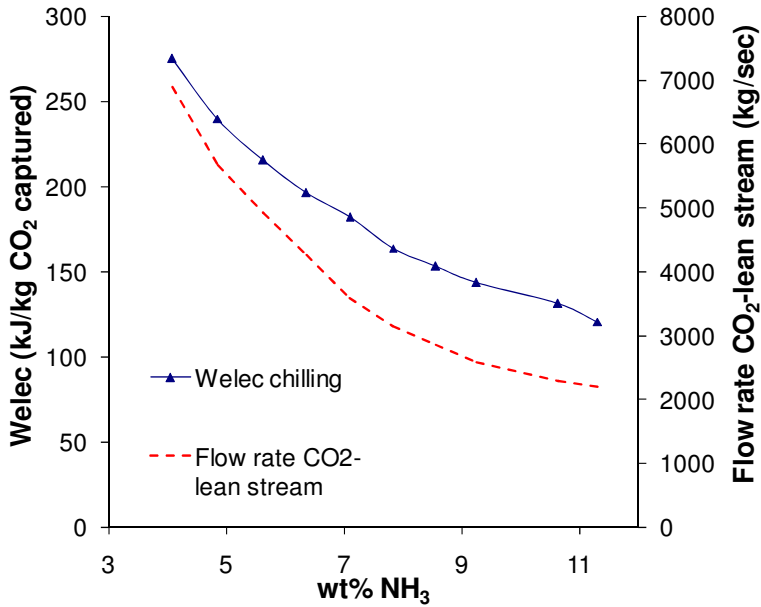


Figure 6-6: Chilling duty and flow rate of the CO<sub>2</sub>-lean stream as a function of the concentration of ammonia in the solvent

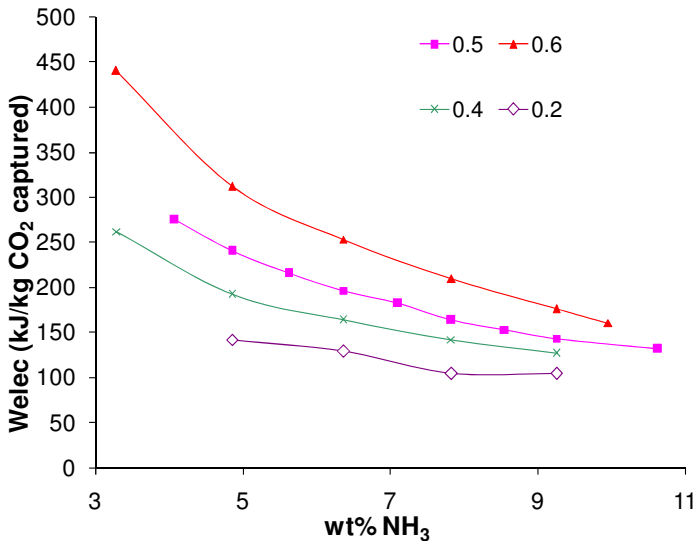


Figure 6-7: Electricity requirement from the chilling of the solvent and flue gas as a function of the concentration of ammonia in the solvent for different recycling rate

### 6.3.2.2 Effect of the lean loading

The influence of the lean loading on the different heat consumptions for a recycling rate of 0.5 and on the ammonia content in the gas stream exiting the absorber is shown in Figure 6-8. The loading is varied between 0.24 and 0.4. The main effect of the lean loading on the heat requirement can be seen on the heat consumption in the NH<sub>3</sub> strippers. When the lean loading increases, the ammonia slip drops. Consequently, the heat requirement in the NH<sub>3</sub> strippers decreases. The heat consumption decreases from 670 to 320 kJ/kg CO<sub>2</sub> captured for the loading range considered.

The heat consumption in the CO<sub>2</sub> desorber varies between 2500 and 2630 kJ/kg CO<sub>2</sub> captured. It reaches a weak minimum for a loading of 0.33. Increasing the loading has three effects:

- First, the increase of the required flow rate of solvent to reach 90% capture rate, which tends to increase the required sensible heat.
- Second, the decrease of the reboiler temperature, which leads to the decrease of the sensible heat.
- Third, similarly to the effect of the ammonia concentration, the decrease of the ammonia slip has a positive effect on the heat requirement (cf. 6.3.3.1).

It is the balance of these two effects that explain the trend of the heat consumption in the CO<sub>2</sub> desorber.

By increasing the lean loading from 0.24 and 0.4, the rich loading decreases from 0.67 to 0.62 and the solid content in the CO<sub>2</sub>-rich stream follows the same trend. This can be explained by the increase of the required flow rate of the solvent.

Overall, by increasing the lean loading, the global heat requirement reaches a minimum of 2950 kJ/kg CO<sub>2</sub> captured. A similar trend may be observed when the recycling rate is varied instead of the lean loading.

Figure 6-9 shows the global heat requirement as a function of the lean loading for different recycling rates. It can be seen that when the recycling rate increases, the minimum observed for the heat requirement occurs at a lower loading. As shown in Figure 6-10, the electricity requirement for the chilling of the flue gas and solvent increases with both the lean loading and the recycling rate.



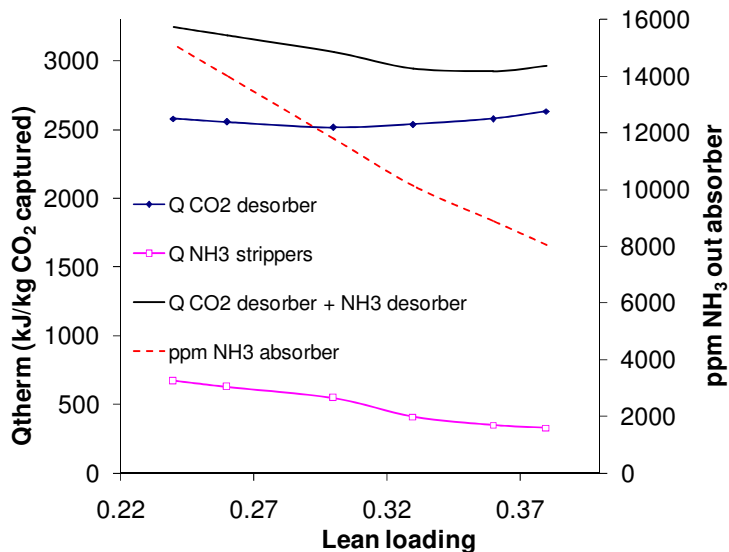


Figure 6-8: Heat requirement and ammonia content in the gas stream exiting the absorber as a function of the lean loading

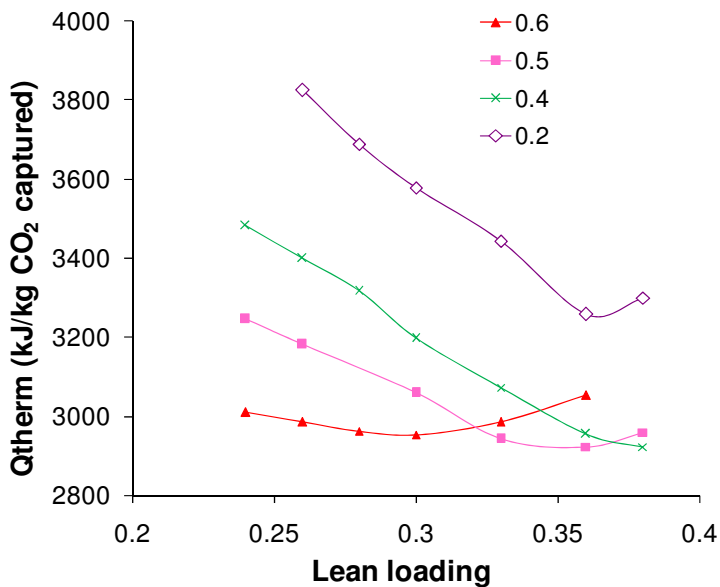


Figure 6-9: Total heat requirement as a function of the lean loading for different recycling rates

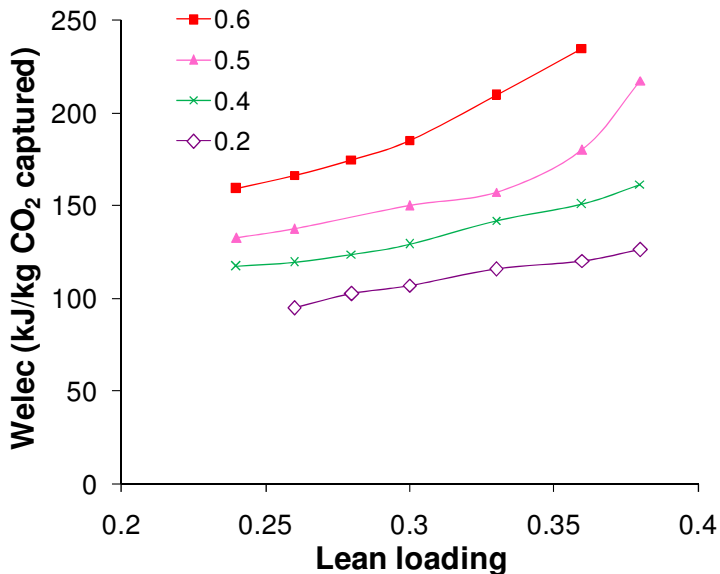


Figure 6-10: Electricity requirement from the chilling of the solvent and flue gas as a function of the loading for different recycling rates

### 6.3.2.3 Effect of the chilling temperature

Figure 6-11 shows the heat requirement in the CO<sub>2</sub> desorber and the NH<sub>3</sub> strippers, the total heat consumption and the chilling duty as a function of the chilling temperature. The temperature is varied between 7 and 19 °C. When the chilling temperature exceeds 15 °C, the cooling of the solvent can be made with the available cooling water and no chilling is required for the solvent. However, the chilling temperature of the washing stream is maintained at 10 °C. It can be seen that both the heat consumption in the CO<sub>2</sub> desorber and the NH<sub>3</sub> strippers rise when the chilling temperature increases. This is explained by the increase of the required solvent flow rate and the rise of the volatility of ammonia when the temperature increases. Figure 6-11 therefore shows the high beneficial effect of lowering the temperature in the absorber towards heat consumption. The heat requirement with a chilling temperature of 20 °C reaches a value close to 4000 kJ/kg CO<sub>2</sub> captured. Hence, using such a concentration of ammonia at this temperature is not competitive with a process using 30 wt% MEA. Figure 6-11 shows that lowering the chilling temperature implies an increase of the chilling duty that reaches a value of 250 kJ/kg CO<sub>2</sub> captured for a temperature of 7 °C. Lowering the temperature also favors the formation of solid. The solid content in the CO<sub>2</sub>-rich stream reaches 3.5 wt% for a chilling temperature of 7 °C.

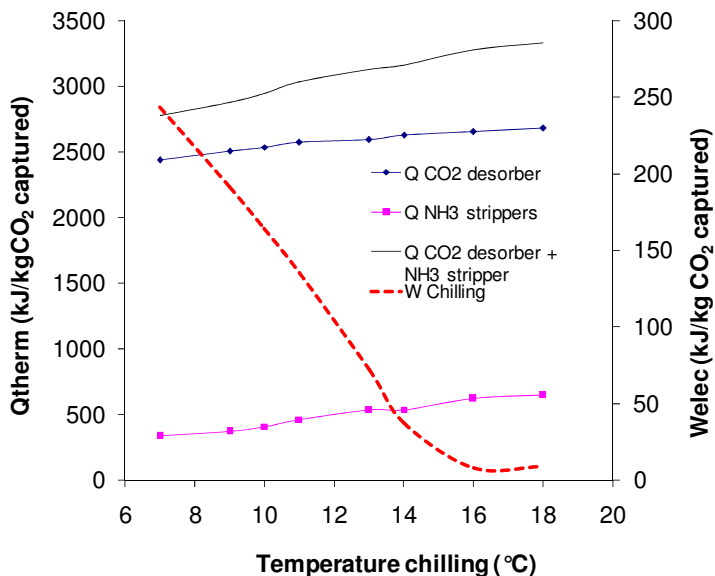


Figure 6-11: Heat requirement and chilling duty as a function of the chilling temperature

The effect of the desorber pressure is analyzed for Configuration B (see section 6.3.3.4).

### 6.3.3 Results sensitivity analysis Configuration B

The same process parameters as for the Configuration A have been studied with the exception of the recycling rate that is not relevant for this process configuration.

#### 6.3.3.1 Effect of the ammonia concentration

Figure 6-12 shows the heat requirement in the CO<sub>2</sub> desorber and NH<sub>3</sub> strippers as a function of the concentration of ammonia in the solvent. The mass fraction of ammonia in the solvent is varied from 6.5 to 10.8% which corresponds to a molality of about 4.1 to 7.1 mol/kg. Figure 6-13 shows the calculated electricity requirement for the chilling of the solvent and the flow rate of the CO<sub>2</sub>-lean stream as a function of the ammonia concentration.

It can be observed that by increasing the ammonia concentration, the heat consumption in the CO<sub>2</sub> desorber is barely affected for the range of ammonia concentration considered. This trend was already observed for Configuration A for high concentration range. The effects reported in 6.3.2.1 can explain this behavior. The drop of the flow rate of solvent can be seen in Figure 6-13.

The increase of the ammonia concentration in the solvent at constant lean loading entails the rise of the ammonia slip from the absorber, from 1300 to 3400 ppm. This implies an increase of the heat

requirement in the NH<sub>3</sub> strippers from 140 to 350 kJ/kg CO<sub>2</sub> captured. It can be noticed that the values are much lower than for the previous process configuration. This can be explained by the lower temperature through Absorber 2 and the higher loading at the top of Absorber 2 compared to Configuration A.

Due to the high loading at the top of Absorber 2, it is not possible to reach 90% capture rate with low ammonia concentration in the solvent. At these conditions, the equilibrium partial pressure of CO<sub>2</sub> at the top of Absorber 2 gets too close to the wanted CO<sub>2</sub> partial pressure in the gas leaving the absorber (0.015-0.02 bar) (cf. Figure 3-5). Hence, Configuration B is not suitable for very low ammonia concentration in the solvent for this high capture rate.

Solid content that consists of ammonium bicarbonate is formed in the second absorber. The mass fraction of solid in the CO<sub>2</sub>-rich stream varies between 1.7 and 3.5%. The global heat requirement varies between 2600 and 2800 kJ/kg CO<sub>2</sub> captured, reaching a weak minimum for 8 wt% NH<sub>3</sub>. It can be observed that the calculated heat requirement is very promising when compared to the 3700 kJ/kg CO<sub>2</sub> captured found for the MEA-based process (Knudsen *et al.*, 2008). Figure 6-12 shows that increasing the concentration does not allow for reducing significantly the global heat requirement. It also shows that using a low concentration of ammonia in the solvent with this process configuration allows for reaching a low heat consumption.

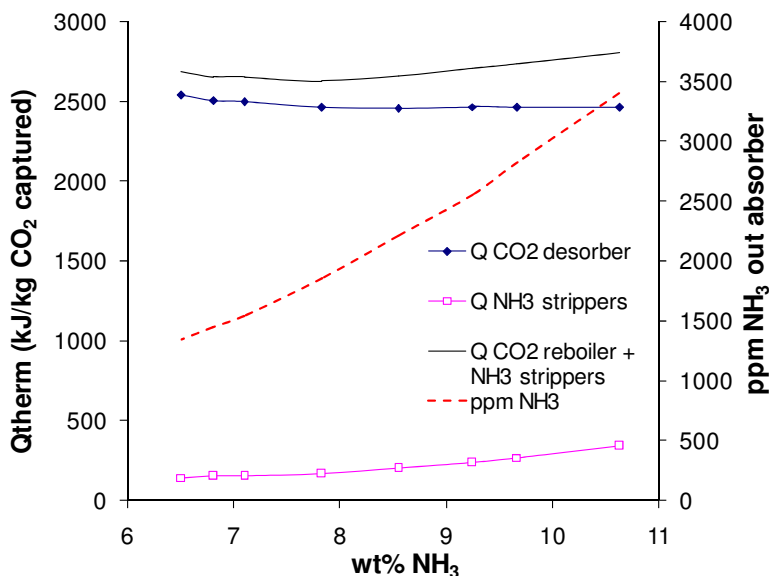


Figure 6-12: Heat requirement and ammonia content in the gas stream exiting Absorber 2 as a function of the ammonia concentration in the solvent

Figure 6-13 shows that the electricity requirement for the chilling and the flow rate of the solvent follow the same trend, the decrease of the electricity requirement being slightly slower due to the extra chilling duty for the precipitation. The value of the chilling duty for low ammonia concentration represents about half of the compression duty. It may also be observed that the chilling duty is much lower than the one observed with Configuration A. This is due to the fact that chilling of the flue gas and of the recycled stream is not required for Configuration B.

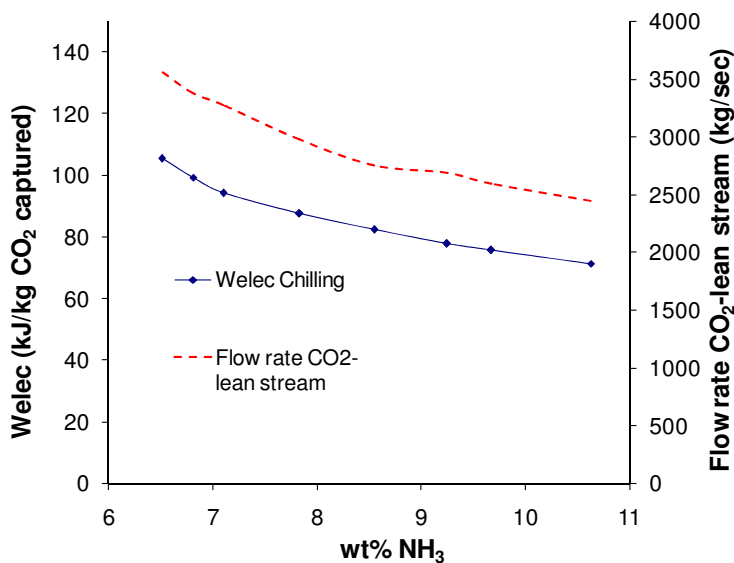


Figure 6-13: Electricity requirement for the chilling of the solvent and flow rate of the CO<sub>2</sub>-lean stream as a function of the concentration of ammonia in the solvent

### 6.3.3.2 Effect of the lean loading

The influence of the lean loading on the heat requirement and the rich loading can be seen in Figure 6-14. The heat requirement in the CO<sub>2</sub> desorber decreases when the loading increases and reaches values lower than the ones observed with Configuration A. This behavior can be explained by the increase of the rich loading for the lean loading range considered. This implies the fast decrease of the temperature of the reboiler and the reduction of the heat requirement, despite the increase of the solvent flow rate. The loading of the stream exiting Absorber 1 increases as well. Therefore, the ammonia slip and the heat requirement in the NH<sub>3</sub> strippers decrease slightly.

In the case of Configuration A, with an increasing lean loading, the rich loading would show a maximum and decrease for high lean loading range. The lower temperature applied in Absorber 2 for Configuration B permits reaching higher loading than with Configuration A according to the equilibrium calculations. Due to mass transfer limitations, reaching such high loading might not be

feasible. This reflects the limitations induced by the use of equilibrium calculations during the simulation.

When the lean loading has a high value (above 0.35), not enough heat can be recovered from the overhead condenser and from the stripped ammonia stream to dissolve the solid content of the CO<sub>2</sub>-rich stream. Hence, the CO<sub>2</sub>-rich stream reaching the RLHX contains some solid. This explains why the heat requirement in the CO<sub>2</sub> desorber remains stable. Higher lean loading would entail a rise of the heat consumption in the CO<sub>2</sub> desorber.

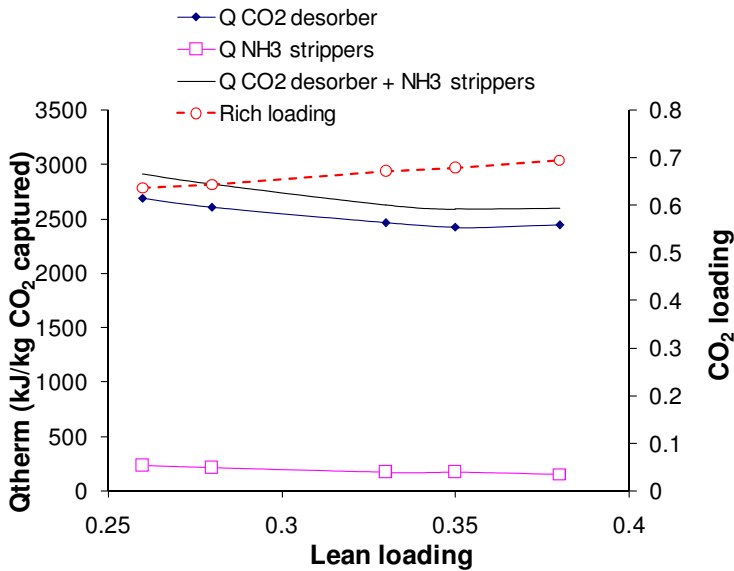


Figure 6-14: Heat requirement and rich loading as a function of the lean loading

### 6.3.3.3 Effect of the chilling temperature

Figure 6-15 shows the influence of the chilling temperature on the heat requirements. For this specific analysis, the mass fraction of ammonia in the solvent has been set to 9.3 %. The temperature has been varied between 6 and 14 °C. It can be seen that decreasing the chilling temperature allows for decreasing the heat requirement in the CO<sub>2</sub> desorber and the NH<sub>3</sub> strippers as the low temperature leads to a drop of the ammonia slip from the absorber. However, for chilling temperature below 8 °C, not enough heat required for pre-heating can be recovered and the heat requirement in the desorber rises. The solid content in the CO<sub>2</sub>-rich stream reaches 6 wt% for a chilling temperature of 6 °C. The electricity requirement from the chilling decreases from 125 to 11 kJ/kg CO<sub>2</sub> captured when the temperature increases from 6 to 14 °C. Hence, similarly to Configuration B, the reduction of the chilling temperature causes a large increase of the chilling duty.

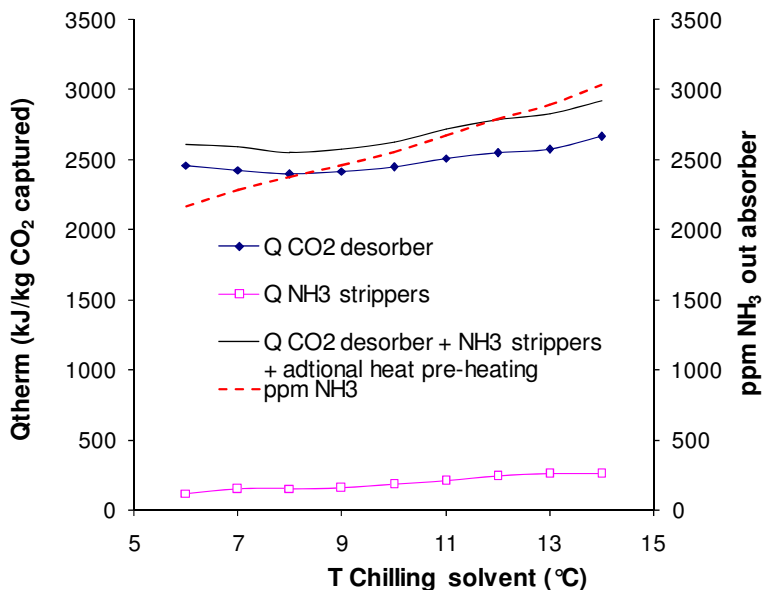


Figure 6-15: Heat requirement and ammonia content in the gas stream exiting absorber 2 as a function of the chilling temperature of the solvent for 9.3 wt% NH<sub>3</sub>

### 6.3.3.4 Effect of the desorber pressure

Figure 6-16 shows the heat requirement and the reboiler temperature as a function of the desorber pressure, varied from 1.5 to 30 bar. It shows that the heat requirement decreases rapidly when the desorber pressure increases from 1.5 to 12 bar. The decrease carries on more slowly from 12 to 30 bar. Increasing the desorber pressure implies the rise of the reboiler temperature. Hence, the required steam to ensure the desorption has a higher quality, which will affect the efficiency of the power plant delivering the steam negatively. The global decrease in the heat requirement is due to the increase of the ratio of equilibrium partial pressure of carbon dioxide and water when the temperature increases (Tobiesen and Svendsen, 2006). This behavior is typical to solvent with a high heat of absorption of carbon dioxide (Oexmann, 2011).

Figure 6-17 shows the electricity consumption from the compression and the chilling as a function of the desorber pressure. The compression duty decreases from 370 to 90 kJ/kg CO<sub>2</sub> captured when the pressure increases from 1.5 to 30 bars. The decrease of the electricity consumption is faster for a rise of the pressure from 1.5 to 10 and becomes more limited for higher pressures. It can be seen that the chilling duty for the base case is about 88 kJ/kg CO<sub>2</sub> captured. This value is lower than the power savings during the compression compared to a conventional process (160 kJ/kg CO<sub>2</sub>). For the base case and for this configuration, the chilling duty is therefore compensated by the savings from the compression of the CO<sub>2</sub> stream with a pressurized desorption.

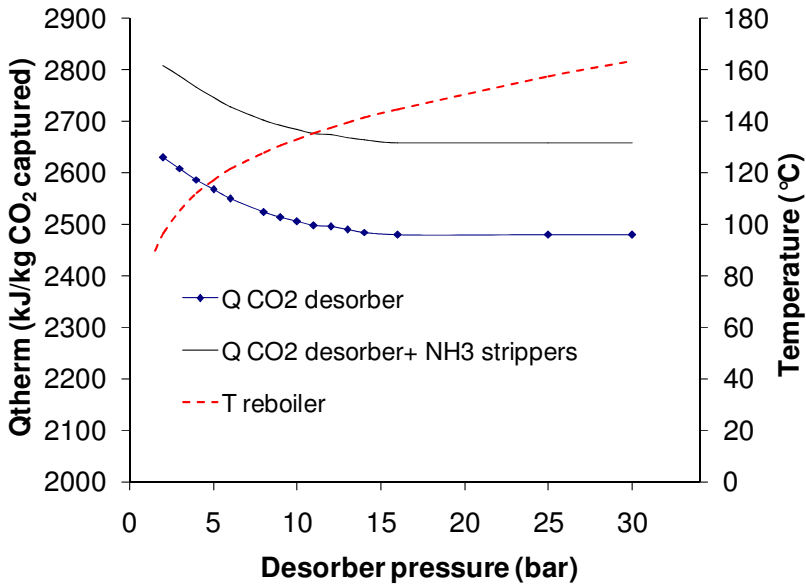


Figure 6-16: Heat requirement as a function of the desorber pressure

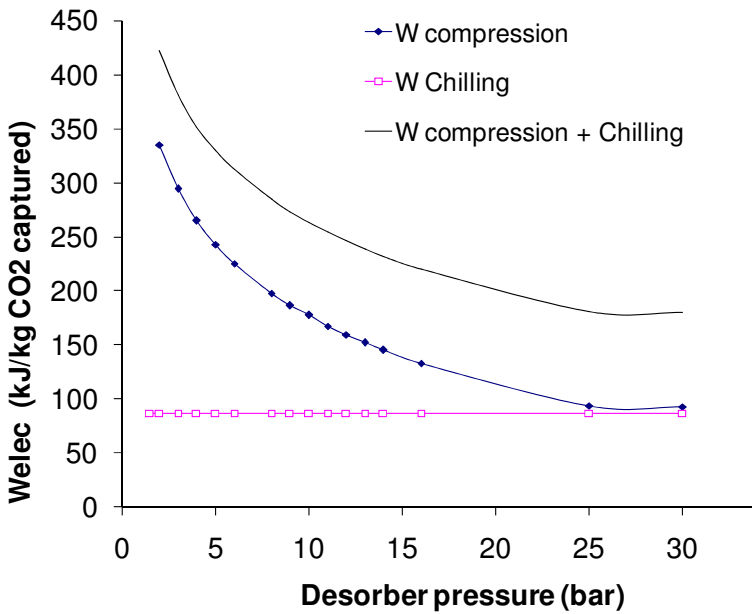


Figure 6-17: Electricity requirement for the compression and for the chilling as a function of the desorber pressure



### 6.3.4 Discussion regarding the simulation

The quality of the simulation results is affected by the use of equilibrium calculations that do not take into account mass transfer limitations. Because of the lack of pilot plant data, some of the design specifications were chosen based on studies of other capture processes. The results that have been shown are highly dependent on some of the major assumptions made during the simulation, such as the value of the ME in the absorber, the number of equilibrium stages for the absorbers and desorbers or the use of the temperature difference of 5 °C for the heat exchanger. As these assumptions are based on studies with similar processes, this work allows for making a good estimation of the potential of the process and for showing the influence of the main parameters.

The influence of the value of the ME in the absorber has been particularly studied. For the base case scenario with Configuration A, by increasing the ME from 0.1 to 0.15, the required flow rate of solvent decreases from 3140 to 2720 kg/s. Consequently, the rich loading increases from 0.66 to 0.71. The heat requirement in the CO<sub>2</sub> desorber is therefore affected, decreasing from 2530 to 2300 kJ/kg CO<sub>2</sub> captured. Hence, the heat and electricity consumptions are sensitive to the ME in the absorber. The ME should be fitted to pilot plant data as a function of the ammonia concentration, the temperature, the gas composition and the loading to account for the deviation from equilibrium. This would improve the accuracy of the simulation.

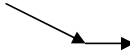
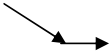
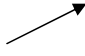
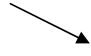

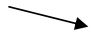
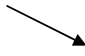
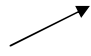

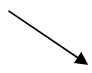
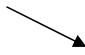
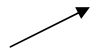
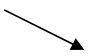
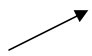


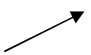

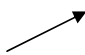
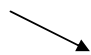
In addition, the dimensions of the absorber columns are strongly affected by the rate of absorption of carbon dioxide by aqueous ammonia. Some of the sets of parameters described resulted in a high loading regime for a low absorption temperature and a low driving force. This might not be compatible with an absorber with a feasible size. A method that permits the evaluation of the absorber height based on the simulation results is described in Chapter 7.

### 6.3.5 Analysis of the simulation results

The simulation results showed some significant differences between the two process configurations studied. The results with Configuration B were significantly better than with Configuration A regarding the heat and electricity requirements. For Configuration B, most of the absorption of carbon dioxide occurs in the first absorber where the loading of the solvent is lower and the driving force higher.

The results have shown that the optimization of the process is not trivial. The main process parameters have an effect on the heat requirement in both the CO<sub>2</sub> desorber and the NH<sub>3</sub> strippers and on the global electricity consumption. Table 6-4 summarizes the qualitative effect of the main process parameters on the heat requirement in the CO<sub>2</sub> desorber and NH<sub>3</sub> strippers, the temperature of the reboiler of the desorber and the chilling duty.

**Table 6-4: Summary of the qualitative effects of the increase of process parameters on various outputs of the process**

	<b>Qtherm CO<sub>2</sub> desorber</b>	<b>Temperature reboiler</b>	<b>Qtherm NH<sub>3</sub> strippers</b>	<b>Welec Chilling</b>
<b>Concentration NH<sub>3</sub></b>				
<b>Recycling rate</b>				
<b>Lean loading</b>				
<b>Desorber pressure</b>				
<b>Chilling temperature</b>				

The performance of the process is shown to be very promising, especially for Configuration B where a total heat requirement lower than 2700 kJ/kg CO<sub>2</sub> captured is calculated for the base case, maintaining a low electricity requirement for the chilling. Configuration A also shows a very competitive heat requirement (3000 kJ/kg CO<sub>2</sub> captured for the base case) but causes a rise in the electricity consumption for the chilling.

The ammonia concentration in the solvent is one of the key parameter for the process. Increasing the ammonia concentration in the low concentration range implies a decrease of the heat consumption in the CO<sub>2</sub> desorber. When the mass fraction of ammonia exceeds 8.5 wt%, the heat consumption in the CO<sub>2</sub> desorber remains stable. The rise of the concentration of ammonia also implies the increase of the volatility of ammonia and therefore of the heat requirement in the ammonia strippers. Hence, for both process configurations studied, that using a concentration of ammonia larger than 11 wt% does not imply a reduction of the global heat requirement. The study also shows that the use of a low concentration of ammonia in the solvent with limited or no precipitation can also be competitive with the MEA-based process.

The lean loading is also a significant parameter for the heat and electricity consumptions. Increasing the loading up to a certain limit permits the decrease of the heat requirement in both the CO<sub>2</sub> desorber and the NH<sub>3</sub> strippers. In addition, increasing the loading allows for reducing the reboiler temperature and therefore reducing the steam quality. It also enhances the formation of solid in the CO<sub>2</sub>-rich stream, which therefore requires more heat to dissolve its solid content during the pre-heating. This heat can in most cases be taken from heat integration with the overhead condenser and the stripped ammonia. However, at high lean loadings, with configuration B, not enough low quality heat can be recovered from the capture plant. In all cases, the heat required for dissolving the solids will affect the integration with the power plant, as this heat can no longer be used for this purpose. Mass transfer limitations not considered in these equilibrium calculations might also affect the actual performance of Configuration B, especially for high lean loadings.

In case of Configuration A, increasing the recycling rate allows for reducing the heat requirement in the NH<sub>3</sub> strippers by reducing the ammonia slip. In addition, it entails the decrease of the temperature of the reboiler. However, it causes the rise of the chilling and pumping duty. Overall, the qualitative effects of this parameter are similar to the lean loading.

The chilling temperature was shown to have a large impact on the heat requirement in the NH<sub>3</sub> strippers as well as on the electricity requirement. Again, a compromise must be found to optimize the configuration of the process and lower the global power consumption. In the case of Configuration A, assuming a low temperature for the available cooling water (10 °C), the chilling duty reaches values significantly higher than the power reduction for the compression due to the pressurized desorption. This conclusion also depends on the COP of the chillers.

The increasing desorber pressure allows for diminishing the heat requirement in the desorber and for reducing the power duty during the compression of the carbon dioxide stream. However, the rise of the desorber pressure entails the increase of the temperature in the reboiler and consequently the quality of the stream and the global power duty for the desorption.

The study of the heat and electricity requirements shows the high potential of this capture process. However, in order to optimize the configuration of the process and to make a more accurate comparison with the MEA-based process, an integration study with a power plant is necessary.

## **6.4 Conclusion**

The performance of the Chilled Ammonia Process has been analyzed by performing flow sheet calculations by using the Extended UNIQUAC model implemented in Aspen Plus. The simulations were equilibrium based. Two process configurations for the absorption section were analyzed and compared. They both allow for absorbing carbon dioxide from flue gas at low temperature in order to limit the ammonia vaporization. This low temperature implies the formation of solid compounds. The

flow sheet also included the washing and stripping of the ammonia from the gas exiting the absorber so that the final ammonia content in the exhaust gas is 10 ppm.

A base case scenario was set up based on the information from the CAP patent and the previous studies. The simulation results showed the high potential of the process for a low heat requirement. The configuration with 2 absorber columns and chilling of the solvent before it flows to the top of the second absorber showed the best results with a total heat consumption lower than 2700 kJ/kg CO<sub>2</sub> captured. The chilling duty has been evaluated and compared to the power savings during the compression thanks to the high desorber pressure. If cooling water is available at 10 °C, the chilling duty is in the same range as the power savings due to pressurized compression for both configurations.

A sensitivity analysis on the main process parameters, such as the ammonia concentration, the lean loading, the chilling temperature, the recycling rate and the desorber pressure was done for both process configurations. It could be seen that the optimization of the process is not trivial. The parameters affect the different heat and electricity consumptions and therefore the global power duty. Main conclusions on the influence of the different process parameters could be made based on the simulation results. For both configurations, the use of a high concentration of ammonia in the solvent does not lead to a decrease of the global heat consumption. The large amount of solid in the CO<sub>2</sub>-rich stream may imply the rise of the heat consumption in the desorber. Overall, the results showed that the heat and electricity requirements using a low concentration of ammonia could be very competitive with MEA-based processes.

In order to assess the drop of the efficiency of a power plant, an integration study is pursued in the next chapter. It takes into account the required quality of the steam and analyzes thoroughly the electricity consumption by taking the pumping of the cooling water and solvent, the blower and the chilling into account. As the results are based on equilibrium calculations, it is necessary to estimate the packing height requirement for the absorber column of the process. This permits ensuring that the results obtained correspond to an absorber column with a feasible size.

## 6.5 References

- Abrams, D. S.; Prausnitz, J. M. Statistical thermodynamics of liquid mixtures: A new expression for the excess Gibbs energy of partly or completely miscible systems. *AIChE J.*, **1975**, *21*, 116.
- Abu-Zahra, M. R. M.; Schneiders, L. H. J.; Niederer, J. P. M.; Feron, P. H. M. CO<sub>2</sub> capture from power plants: Part I. A parametric study of the technical performance based on monoethanolamine. *International Journal of Greenhouse Gas Control*, **2007**, *1*, 37.
- Chen, C. C.; Britt, H. I.; Boston, J. F.; Evans, L. B. Local Composition Model for excess Gibbs Energy of Electrolyte Systems. 1. Single Solvent, Single Completely Dissociated Electrolyte Systems. *AIChE J.*, **1982**, *28*, 588.
- Darde, V.; Thomsen, K.; van Well, W. J. M.; Stenby, E. H. S. Chilled Ammonia Process for CO<sub>2</sub> capture. *International Journal of Greenhouse Gas Control*, **2010a**, *4*, 131.

Darde, V.; Thomsen, K.; van Well, W. J. M.; Stenby, E. H. S. Modeling of carbon dioxide absorption by aqueous ammonia solutions using the Extended UNIQUAC model. *Ind. Eng. Chem. Res.*, **2010b**, *49*, 12663.

Darde, V.; van Well, W. J. M.; Fosboel, P.; Stenby, E. H. S.; Thomsen, K. Experimental measurement and modeling of the rate of absorption of carbon dioxide by aqueous ammonia. **2011**, doi:10.1016/j.ijggc.2011.07.008

Gal, E. Ultra cleaning combustion gas including the removal of CO<sub>2</sub>. World Intellectual Property, Patent WO 2006022885, **2006**.

Kather, A.; Linnenberg, S.; Oexmann, J. POSEIDON PostCombustion CO<sub>2</sub>-Abtrennung: Evaluierung der Integration, Dynamik und Optimierung nachgeschalteter Rauchgaswäschen. Förderkennzeichen PTJ/BMWi/0327785, **May 2011**.

Knudsen, J. N.; Jensen, J. N.; Biede, O. Castor SP2: experiments on pilot plant. CASTOR-ENCAP-CACHET-DYNAMIS Common Technical Training Workshop, Lyon, France, **2008**.

Kurz, F.; Rumpf, B.; Maurer, G. Vapor-liquid-solid equilibria in the system NH<sub>3</sub>-CO<sub>2</sub>-H<sub>2</sub>O from around 310 to 470 K: New experimental data and modeling. *Fluid Phase Equilibria*, **1995**, *104*, 261.

Mathias, P. M.; Reddy, S.; O'Connell, J. P. Quantitative Evaluation of the Aqueous-Ammonia Process for CO<sub>2</sub> capture fundamental Data and Thermodynamic Analysis. *Int. J. Greenhouse Gas Control*, **2010**, *4*, 174.

Mogensen, B., Darde, V., Fosboel, P., Thomsen, K., Kontorgeorgis, G., 2011. Implementation of the Extended UNIQUAC Model for Electrolyte Systems in Aspen Plus through the User. Submitted to Computers and Chemical Engineering.

Oexmann, J.; Kather, A. Minimising the regeneration heat duty of post-combustion CO<sub>2</sub> capture by wet chemical absorption: The misguided focus on low heat of absorption solvents. *International J. of Greenhouse Gas Control*, **2010**, *4*, 36.

Oexmann, J. PostCombustion CO<sub>2</sub> Capture: Energetic Evaluation of Chemical Absorption Processes in CoalFired Steam Power Plants, PhD dissertation, Hamburg University of Technology, Germany, **2011**.

Tobiesen, F. A.; Svendsen, H. F. Study of a Modified Amine-Based Regeneration Unit. *Ind. Eng. Chem. Res.*, **2006**, *45*, 2489.

## **7 Integration study of the CO<sub>2</sub> capture process using aqueous ammonia**

### **7.1 Introduction**

In order to study the performance of the CO<sub>2</sub> capture process using aqueous ammonia and to compare it with other capture processes, it is necessary to evaluate the impact of the process on a power plant. This is done through an integration study. The capture process and carbon dioxide compressor have been implemented into a hard coal steam power plant simulator. The flow sheet calculations are coupled with the power plant simulation in order to calculate the efficiency penalty induced by the capture of carbon dioxide.

The influence of various process parameters has been studied. Both process configurations presented earlier have been considered. In addition, the variants of the process implying the absorption at low (0-10 °C) and high (above 20 °C) temperatures have been investigated. In order to study the influence of the location of the plant, two cooling water temperatures are considered. To examine the feasibility of the equilibrium calculations, the size of the absorber columns has been evaluated for the different cases by using the modeling of the rate of absorption of carbon dioxide by aqueous ammonia (cf. Chapter 4).

This integration study has been made in collaboration with Sebastian Linnenberg, from the Hamburg University of Technology (TUHH), institute of Energy Systems. He performed the simulation of the power plants and of the compressor in order to calculate the efficiency penalty based on the simulation results. He designed the chiller system used in these simulations. He has also participated in the interpretation of the results. A paper presenting some of the results has been recently submitted for publication in International Journal of Greenhouse Gas Control.

### **7.2 Modeling methodology**

The purpose of this work is to investigate the performance of a CO<sub>2</sub> capture process using aqueous ammonia for two different configurations, two different power plants and different process parameters. It is therefore required to analyze the interaction and the effect of the capture process and of the carbon dioxide compressor on the power plant. Hence, the different parts must be modeled accurately.

#### **7.2.1 Power plant**

This study consists of analyzing the effect of the implementation of a carbon dioxide capture process on an existing power plant. In order to analyze the influence of the location of the power plant, this study has been made for two cooling temperatures. Hence, two power plants have been modeled and simulated:

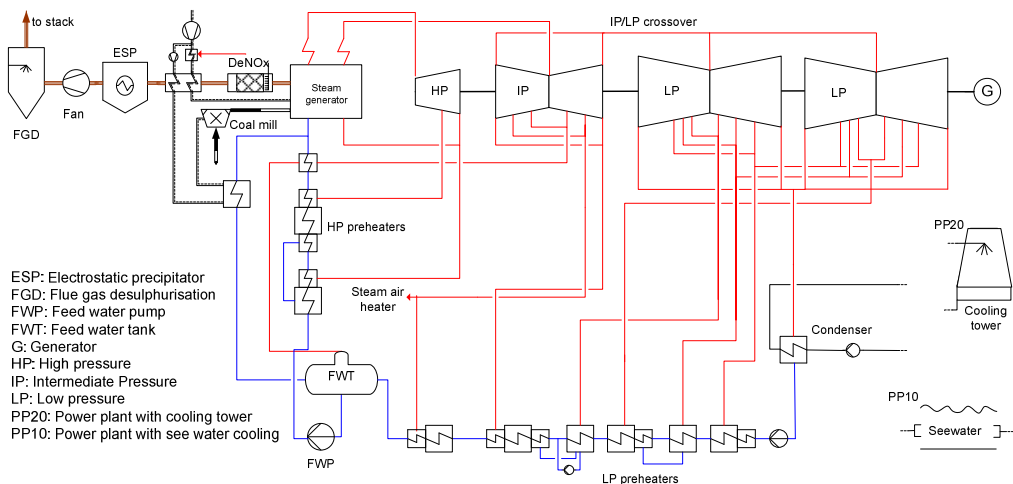
- PP20 represents a power plant located in the land side, where no sea water can be used for cooling. These power plants typically operate natural draft cooling towers in order to generate water at a temperature in the range 16-20 °C, depending on the ambient temperature and

humidity and on the process used. In this study, the cooling water available is assumed to be produced at 20 °C. Similarly to Pfaff *et al.* (2010), it is assumed that the cooling water temperature gain is 10 °C.

- PP10 represents a power plant at a costal location cooled down with sea water. In this study, its temperature is assumed to be 10 °C. It is also assumed that the cooling water temperature gain is 10 °C.

The simulation of the power plant has been performed by Sebastian Linnenberg using the commercial software *EBSILON Professional 9.00*. It is an adequate tool to represent power plant processes.

The power plants modeled in this study are both supercritical state-of-the-art hard coal fired power plants with a gross power output of 1100 MW<sub>elec</sub>. Figure 7-1 shows a schematic flow sheet of the power plants (Kather *et al.*, 2011). The main modeling parameters can be found in Table 7-1. The difference in the net efficiency of the power plants can be mainly explained by the lower condenser pressure of PP10 resulting from the lower cooling water temperature (Pfaff *et al.*, 2010). The compositions of the flue gas from PP10 and PP20 are identical. However, the flow rate of flue gas from PP20 is about 2% higher than the one from PP10. All the heat and electricity consumptions reported are expressed in kJ per kilogram carbon dioxide captured. Hence, the results of the integration from both power plants are comparable.



**Figure 7-1: Schematic flow sheet of the power plant (Kather *et al.*, 2011)**

**Table 7-1: Main process parameters for the power plants PP10 and PP20**

	<b>PP10</b>	<b>PP20</b>
<b>Gross (output) capacity (MW<sub>elec</sub>)</b>	1100	1100
<b>Net efficiency (%)</b>	46.6	45.4
<b>Live steam conditions (°C, bar)</b>	600, 285	600, 285
<b>Reheated steam conditions (°C, bar)</b>	620, 60	620, 60
<b>Condenser pressure (mbar)</b>	28	50
<b>Cooling water temperature (°C)</b>	10	20
<b>Flue gas CO<sub>2</sub> concentration (vol.-%, dry)</b>	13.9	13.9
<b>Flue gas O<sub>2</sub> concentration (vol.-%, dry)</b>	3.3	3.3

## **7.2.2 CO<sub>2</sub> capture process**

### **7.2.2.1 Simulation of the capture process**

The capture process is simulated in the same way as it has been presented in Chapter 6. Similar design specifications are used in the integration study. The study is made for both configuration A and B.

### **7.2.2.2 Considerations regarding the convergence of the simulation**

In this integration study, some of the parameters have been varied in a broader range than in Chapter 6. The use of RadFrac columns in Aspen Plus causes some difficulties regarding the convergence of the calculations during the simulation. These difficulties are especially linked to the solid formation in the absorber. When a high amount of precipitate is occurring, the convergence of the absorber column becomes more difficult to reach. In addition, equilibrium calculations can lead to convergence issues due to the incompatibility of the set of process parameters with a 90% capture rate.

These issues brought some limitations to the simulations. It was not possible to reach convergence for some cases, especially for high ammonia concentration and high loading in the CO<sub>2</sub>-lean stream. In addition, because of the use in series of two RadFrac unit operations, the use of configuration B entailed significant difficulties to reach convergence of the simulation, especially at high ammonia concentrations. Hence, only a limited amount of results is available for this process configuration.

### **7.2.2.3 Dimensions of the absorber column**

Given the low rate of absorption of carbon dioxide by aqueous ammonia solvent, it is necessary to prove that the capture process can be built with a feasible size for the absorber column. In this work, the absorber dimensions are estimated based on the method described by Abu Zahra *et al.* (2007) and Oexmann *et al.* (2008). The required height of packing of each equilibrium stage is calculated using the



modelling of the rate of absorption of carbon dioxide by aqueous ammonia from (cf. Chapter 4) and the results from the column profile from the simulation results.

The diameter of the column is calculated using the work from Kister (1992) based on the maximum flow rates of gas and liquid through the column.

First, the flow parameter  $F_{LV}$  follows equation (7.1).

$$F_{LV} = \frac{\max(m_L)}{\max(m_G)} \sqrt{\frac{\rho_G}{\rho_L}} \quad (7.1)$$

where  $\max(m_L)$  and  $\max(m_G)$  are respectively the maximum mass flow rates liquid and gas phases in the column, expressed in kg/s and where  $\rho_L$  and  $\rho_G$  are the densities of liquid and gas phases calculated at the same stages as the corresponding maximum flow rates. The densities are expressed in kg/m<sup>3</sup>. Hence, the column is designed considering a theoretical stage at which the maximum flow rates of gas and liquid are observed.

The flooding-point capacity factor  $C$ , expressed in m/s, allows for calculating the superficial velocity. It follows equation (7.2).

$$C = 0.3084 \frac{CP}{\sqrt{0.3084 F_p}} \left( \frac{\rho_L}{10^6 \eta_L} \right)^{0.05} \quad (7.2)$$

where  $CP$  is the capacity parameter. It is determined by using the Generalized Pressure Drop Correlations (GPDC) specific to the packing used (Kister, 1992). It is function of the flow parameter  $F_{LV}$ . The structured packing MELLAPAK 252Y by Sulzer is used in this study.  $F_p$ , expressed in m<sup>-1</sup>, is the packing factor, also specific to the packing used.  $\eta_L$  is the dynamic viscosity of the liquid phase, expressed in N•s/m<sup>2</sup>.

A 0.75 factor is used to design the column for 75% of the velocity at the flooding point. In addition, a security factor of 0.85 is typically used. Hence, the superficial velocity  $u_{sf}$  expressed in m/s follows equation (7.3).

$$u_{sf} = \frac{0.75 \cdot 0.85 \cdot C}{\sqrt{\frac{\rho_G}{\rho_L - \rho_G}}} \quad (7.3)$$

The cross sectional area  $A_{CS}$ , expressed in m<sup>2</sup>, can then be calculated with equation (7.4):

$$A_{CS} = \frac{\max(V_G)}{u_{sf}} \quad (7.4)$$

where  $\max(V_G)$  is the maximum volumetric flow rate expressed  $m^3/s$ .

The simulation results allow for determining the different properties needed at each stage of the column. Hence, the required cross sectional area can be calculated. Based on the number of columns considered, it is then possible to calculate the required diameter of the column(s).

The required height of the packing of each of the stage of the column can then be estimated by calculating the required contact area to absorb the amount of carbon dioxide transferred from the gas to the liquid. Using the film theory, the mole flow of carbon dioxide  $\Delta n_{CO_2,i}$  transferred at stage  $i$  from the gas to the liquid phase can be expressed as a function of the mass transfer flux and the contact area between the gas and the liquid:

$$\Delta n_{CO_2,i} = \varphi_{CO_2,i} A_i \quad (7.5)$$

Where  $\varphi_{CO_2,i}$  is the mass transfer flux expressed in  $mol/(m^2 \cdot sec)$  and  $A_i$  is the contact area between the gas and the liquid for stage  $i$ .

By using the two-film model to represent the mass transfer process and by applying the continuity of the flux from the gas to the liquid, the mass transfer flux can be expressed as shown in equation (4.5):

$$\varphi_{CO_2,i} = K_G \Delta P_{CO_2,i} = \frac{\Delta P_{CO_2,i}}{\frac{1}{k_G} + \frac{H_{CO_2}}{k_L^0 E_{CO_2}}} \quad (7.6)$$

In this study, similarly to Oexmann *et al.* (2008), the gas side mass transfer coefficient  $k_G$  is determined by using the correlation by Bravo *et al.* (1985) for the Sherwood number for the gas phase  $Sh_G$ :

$$Sh_G = 0.0338 Re_G^{0.8} Sc_G^{0.333} \quad (7.7)$$

And with:

$$k_G = \frac{D_{CO_2,G} Sh_G}{d_{eq}} \quad (7.8)$$

$Re_G$  and  $Sc_G$  are the Reynolds and Schmidt numbers for the gas phase,  $D_{CO_2,G}$  is the diffusion coefficient of carbon dioxide in the gas phase, expressed in  $m^2/s$  and  $d_{eq}$  is the equivalent diameter, specific to the packing. For the MELLAPACK 252Y,  $d_{eq} = 0.018m$ .

The physical liquid side mass transfer coefficient  $k_L^0$  is determined by using the Bravo Fair correlation (Bravo *et al.*, 1996).

$$k_L^0 = 2\sqrt{\frac{D_{CO_2,L}u_{eff,L}}{\pi \cdot S}} \quad (7.9)$$

Where  $u_{eff,L}$  is the effective velocity of the liquid, expressed in m/s and  $S$  is the packing specific length, equal to 0.017 m in the case of MELLAPACK 252Y. The correlation presented in Chapter 4 for the partition coefficient of carbon dioxide in aqueous ammonia and the diffusion coefficient are used here.

As the pseudo first order regime was not necessarily reached, the expression of the enhancement factor for second order irreversible reaction from van Krevelen and Hoftijzer (1948) was used:

$$E = \frac{Ha \sqrt{\frac{E_\infty - E}{E_\infty - 1}}}{\tanh\left(Ha \sqrt{\frac{E_\infty - E}{E_\infty - 1}}\right)} \quad (7.10)$$

The modeling of the overall kinetic rate constant  $k_{ov}$  described in Chapter 4 was used in this study. It should be noticed that this model is based on experimental data using aqueous ammonia solutions with a concentration up to 10 wt% for a temperature up to 21 °C and with a concentration of ammonia up to 5 wt% for a temperature up to 31 °C. During the simulation, the temperature in the absorber may exceed this temperature.

The theoretical contact area between the gas and the liquid can therefore be calculated. In this study, a safety factor of 25% is used in the final calculation. By using the value of the diameter of the column, it is then possible to estimate the required height of the packing for each of the equilibrium stages.

The total height of the column is obtained by adding 25% of the column diameter to the calculated packing height. This accounts for the necessary space at the bottom of the column in order to secure an even gas flow distribution, at the top of the column. In addition, 0.75 meter is added for each 10 meters of packing for the liquid distributors, liquid collectors and supporting grid.

### 7.2.3 Mechanical chiller system

Mechanical chillers are required to provide cooling water at low temperature necessary to chill the solvent and flue gas during the capture. The COP mainly depends on the type of chiller used, the available cooling water, the temperature difference between the inlet and outlet and the chilling temperature. In this integration study, the chillers considered have been designed using information from Cofely Refrigeration GmbH. The technology used is a mechanical chiller using ammonia as a refrigerant using screw type chiller compressors. A temperature difference in the liquid-liquid heat exchanger of 5 °C is considered. Hence, in order to chill the solvent to a temperature of 10 °C, a 5 °C chilling water produced by the chiller is required. Table 7-2 shows the results for the calculation of the COP as a function of the cooling water temperature.

Table 7-2: Design parameter for the mechanical chiller

	PP10	PP20
Cooling water temperature at inlet (°C)	10	20
Cooling water temperature at outlet (°C)	20	30
Supply temperature (°C)	5	5
COP (-)	9.2	6.6

In this integration study, the influence of the chilling temperature is studied. The manufacturer provided estimation of the COP for a chilling water of 10 °C. It was therefore necessary to determine the coefficient of performance for the different chilling temperatures studied. They were estimated by Sebastian Linnenberg by using the software COOLPACK (cf. Figure 7-2).

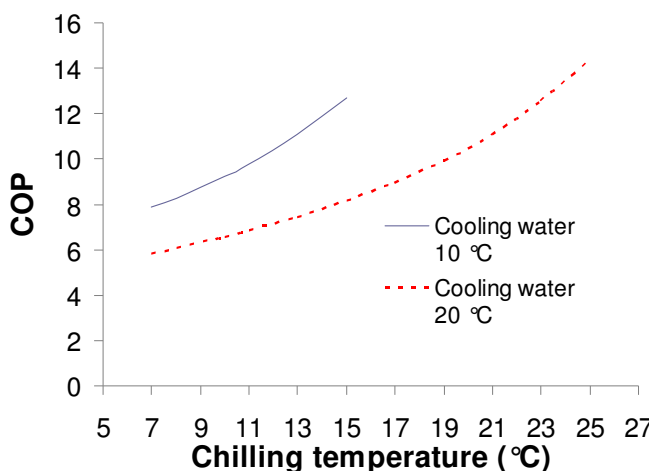


Figure 7-2: COP as a function of the chilling temperature for the two cooling water temperatures

## 7.2.4 Compressors

The compression duty represents a significant part of the efficiency penalty induced by the carbon dioxide capture. During the integration study, unlike in Chapter 6, the compressors are simulated with EBSILON *Professional 9.00* in order to increase the accuracy and to facilitate the integration study between the compressor and the power plant. The simulation of the compressors and their interaction with the power plant has been handled by Sebastian Linnenberg.

As the effect of the desorber pressure on the efficiency penalty is studied, different configurations for the compressors are used, depending on the desorber pressure (inlet pressure). The outlet CO<sub>2</sub> pressure is fixed at 110 bar. In this study, an integrally-gearred (radial) compressor with 6, 4 or 2 stages, correspondingly 3, 2 or 1 intercoolers and an after-cooler is considered. The pressure ratio of a single stage lies in the range of 2 to 1.4. These assumptions leads to three different compressor configurations (see Table 7-3). The power duty for the compression as a function of the inlet pressure is shown in Figure 7-3.

**Table 7-3: Description of the configurations for the compressors**

<b>Configuration</b>	<b>a</b>	<b>b</b>	<b>c</b>
<b>No. of stages</b>	6	2	2
<b>No. of intercoolers</b>	3	2	1
<b>No. of after-coolers</b>	1	1	1
<b>Inlet pressure range (bar)</b>	2 - 14	15 - 28	29 - 30
<b>Discharge pressure (bar)</b>	110	110	110

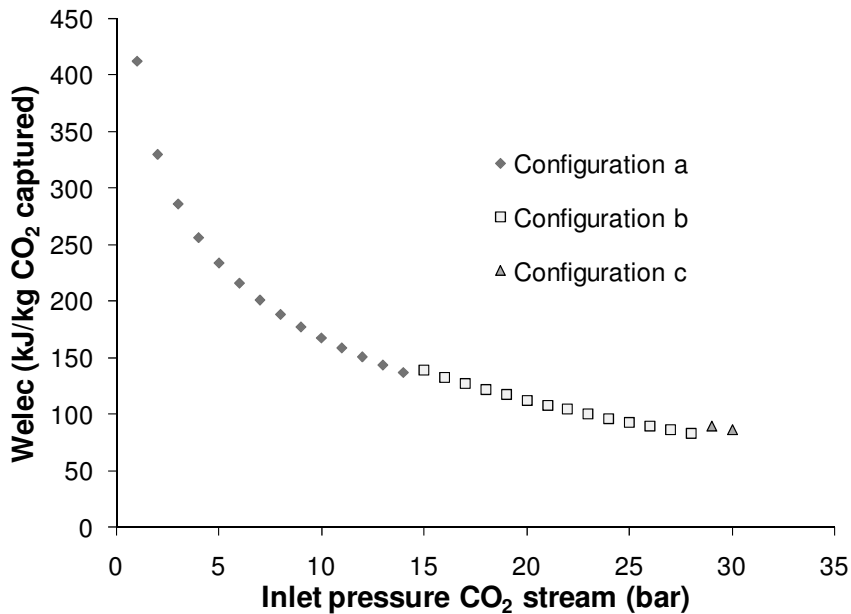


Figure 7-3: Power duty for the compression for the three compressor configurations studied.

### 7.2.5 Integration with CO<sub>2</sub> capture unit

The principles of the integration study are summarized in Figure 7-4. The simulation of the power plant provides the flow rate, composition, temperature and pressure of the flue gas. In this study, only full load and steady state operation of the power plant is considered. The simulation of the capture process allows for determining the necessary outputs. The power duty from the chilling is calculated from the COP described in section 7.2.3 based on the results of the simulation of the capture process. The cooling duty allows for calculating the power duty required for the pumping of the cooling and chilling water. Hence, the electricity consumption from the pumping, chilling, pumping of cooling water and compression can be determined. Based on the reboiler temperatures and the heat requirements, the pressure and quantity of steam required and the amount of heat available from the reboiler condensates are calculated. The power reduction induced by the steam extraction is determined. In addition, by extracting steam to the reboiler and condensing it, the pumping of cooling water to the turbine condenser is reduced. This reduction of auxiliary power is taken into account in the calculation of the efficiency. Hence, based on the simulation outputs, the net power output and net efficiency can be determined, and the distribution of the different contributors to the efficiency penalty can be calculated. It should be noted that no waste heat integration from the capture plant is considered in this study. The heats from the over-head condenser or the stripped ammonia are not integrated in the steam cycle. In the case of the CAP, they are used to dissolve the solids in the CO<sub>2</sub>-rich stream (cf. Chapter 6).

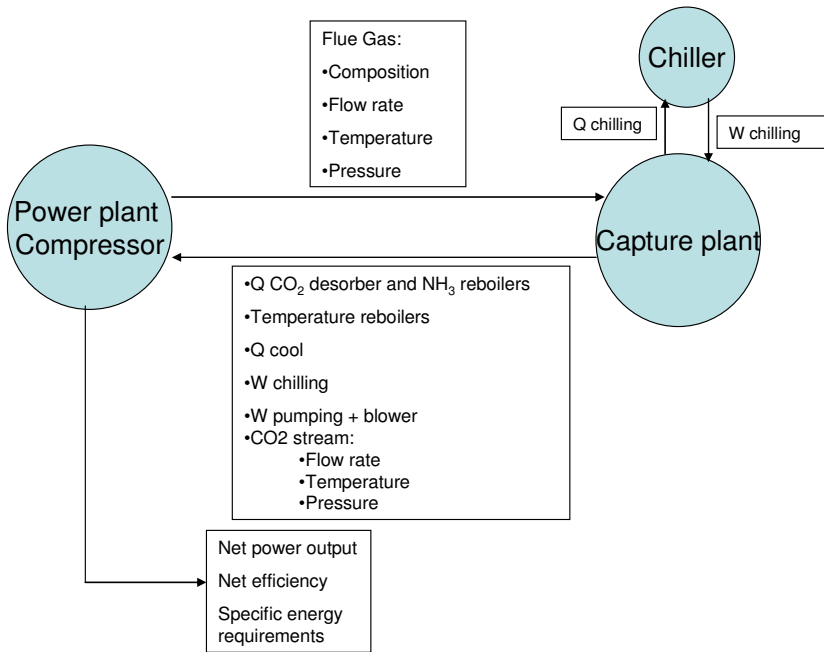


Figure 7-4: Schematic principle of the integration of the capture process

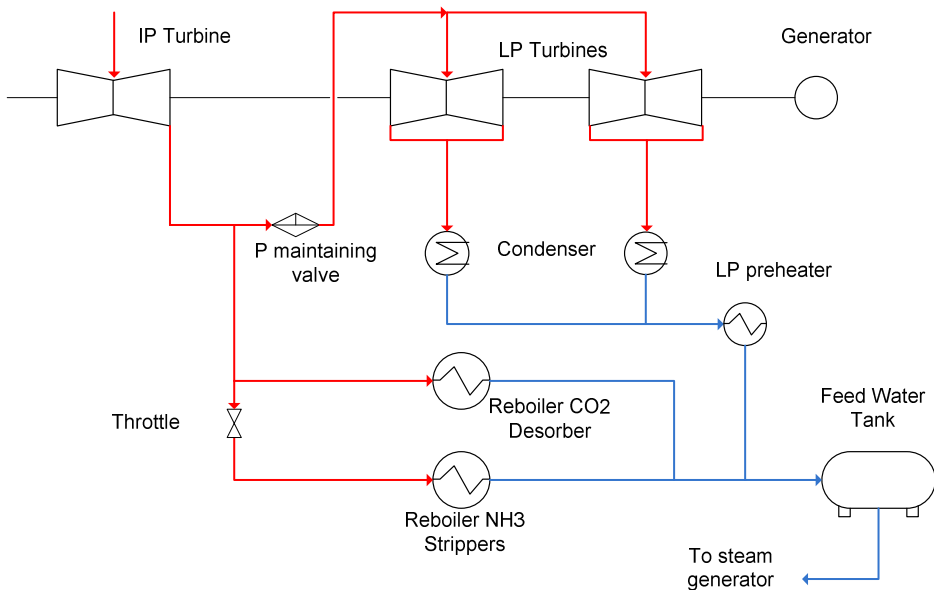


Figure 7-5: Flow sheet the of the integration of the capture process with the steam cycle

The heat required for the regeneration of the solvent and of the washing stream is provided by extracting steam from the water-steam cycle shown in Figure 7-5. A similar flow sheet for the MEA process has been described by Oexmann (2011). Typically, the steam is extracted at low pressure from the crossover pipe between the intermediate pressure (IP) and low pressure (LP) turbine cylinders (Lucquiaud, 2011). At full load, without CO<sub>2</sub> capture, the pressure at the IP/LP crossover for PP10 and PP20 is 3.9 bar. A 10 °C temperature approach is applied in the reboiler. In addition, a pressure loss of 0.4 bar in the pipe from the IP/LP to the capture unit is considered. Using the results from the simulation of the capture process, these assumptions allow for calculating the required pressure of the steam. In order to keep the steam at the pressure required by the CO<sub>2</sub> capture process for the case the pressure is larger than 3.9 bar, a pressure maintaining valve is placed downstream the branch to the reboiler, in the pipe leading to the LP turbine. In the capture process, steam is required for the CO<sub>2</sub> desorber and for the NH<sub>3</sub> strippers. The required steam quality for the reboiler of the NH<sub>3</sub> strippers is systematically lower than the one for the reboiler of the CO<sub>2</sub> desorber. In this integration study, the excessive pressure is reduced using a throttle. Hence, the lower requirement of the steam quality for the reboiler of the NH<sub>3</sub> strippers is not advantageous for the power plant considered. If steam extraction at a lower pressure level were available, the excess pressure could be used in the low pressure turbine and the efficiency penalty would be reduced.

In this retrofit study, independently of their temperature, the condensates from the reboilers are forwarded to the feed water tank and back to the steam-water cycle.

### **7.3 Results**

The integration study has been made for both process configurations. The effect of the different parameters on the heat and electricity consumptions resulted in similar trends for both configurations (cf. Chapter 6). As the use of configuration B resulted in additional convergence problems, the main analysis of the integration study is made for configuration A.

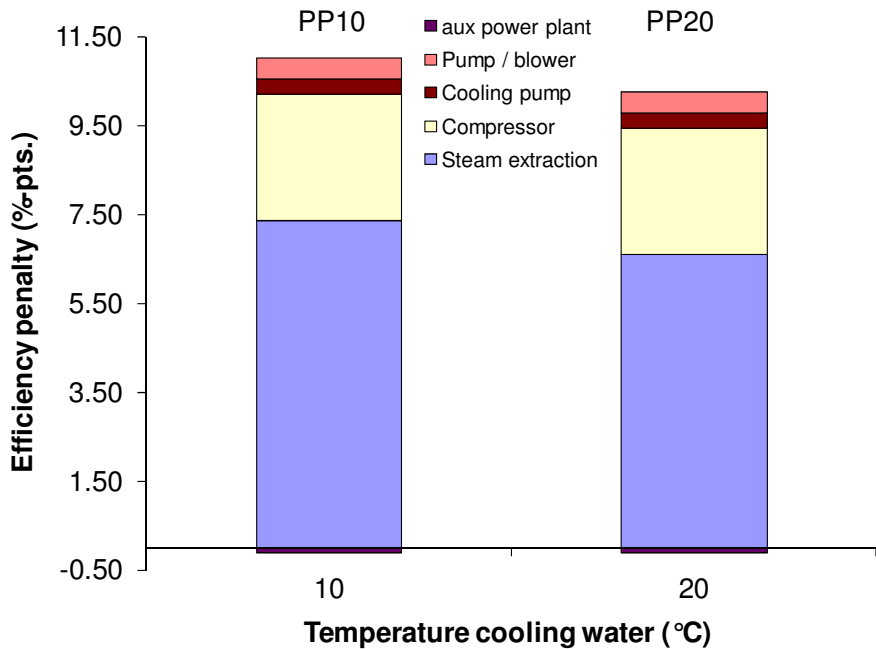
#### **7.3.1 Reference process with MEA**

In order to evaluate the performance of the capture process using aqueous ammonia, it is necessary to compare the results from the integration study of the MEA-based process with both PP10 and PP20. The results from the integration of the MEA-based process are derived from the POSEIDON project (Kather *et al.*, 2011). The simulation of the capture process has been made using a rate-based model for the CO<sub>2</sub>-MEA-H<sub>2</sub>O system. The boundary conditions for the optimum case considered in this study are included in Table 7-4. Figure 7-6 shows the distribution of the efficiency penalty from a CO<sub>2</sub> capture process using 30 wt% MEA for both power plants for the different contributors and for the optimum cases. The net efficiency penalties obtained are 10.9 %-pts. for PP10 (leading to an efficiency of 35.7%) and 10.2 %-pts. for PP20 (leading to an efficiency of 35.2%).



**Table 7-4: Boundary conditions**

<b>CO<sub>2</sub> capture rate (%)</b>	90
<b>Reboiler duty (kJ/kg CO<sub>2</sub> captured)</b>	3470
<b>Reboiler temperature (°C)</b>	120.3
<b>Desorber pressure (bar)</b>	2
<b>Power duty of pumps and blower (kJ/kg CO<sub>2</sub> captured)</b>	110
<b>Cooling Duty (kJ/kg CO<sub>2</sub> captured)</b>	3860



**Figure 7-6: Distribution of the efficiency penalty from a CO<sub>2</sub> capture process using 30 wt% MEA for PP10 and PP20 (Kather *et al.*, 2011)**

The cooling water temperature has only a limited effect on the heat and electricity consumption of the capture process. However, the pressure of the condenser of the low pressure turbines of PP10 is significantly lower than the one of PP20. This implies that a larger fraction of power is produced by the low pressure turbine compared to PP20. Hence, steam extraction from the IP/LP cross over leads to a larger efficiency penalty for PP10.

### 7.3.2 Results configuration A

In this integration study, the process parameters that are studied are:

- The concentration of ammonia in the solvent
- The cooling water temperature ( $T_{cool}$ )
- The desorber pressure ( $P_{des}$ )
- The lean loading (LL)
- The recycling rate (RR)
- The chilling temperature ( $T_{chill}$ )

The parameters studied are similar to the ones in Chapter 6. In addition, the influence of the cooling water temperature is analyzed.

#### 7.3.2.1 Effect of the ammonia concentration

The influence of the various parameters on the performance of the process is studied for three mass fractions of ammonia in the solvent: 5.6, 7.8 and 10.0 wt%. These correspond to a molality of ammonia of 3.5, 5.0 and 6.5 mol/kg water. Figure 7-7 shows this distribution for the three ammonia concentrations considered in the study for a pressure of 10 bar, for a recycling rate of 0.3 and a lean loading of 0.33. This shows that for the three cases, the dominant contributor is the steam requirement in the CO<sub>2</sub> desorber. The efficiency penalty induced by the steam extraction to the CO<sub>2</sub> desorber varies between 63 and 55% of the total penalty by increasing the concentration of ammonia from 5.6 to 10.0 wt%. By adding the contribution for the NH<sub>3</sub> strippers, the global penalty from steam extraction reaches 70-75% of the total penalty. Increasing the concentration of ammonia from 5.6 to 10.0 wt% implies a significant rise of the steam extraction from the ammonia strippers, leading to an increase of the efficiency penalty from 0.8 to 2.3 %-pts. On the other hand, the efficiency penalty from the pumping and the blowing duties decreases from 1.3 to 1 %-pts. These observations show that despite the major contribution of the steam extraction for the CO<sub>2</sub> desorber, the chilling and pumping duties and the steam consumption due to the ammonia slip are important factors to consider during the optimization of the process.

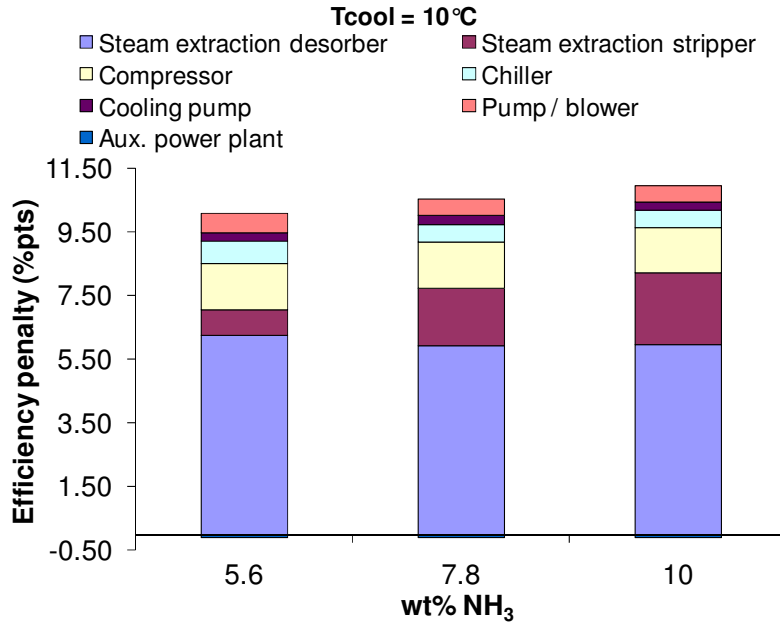


Figure 7-7: Net efficiency penalty from the different contributors for 5.6 wt% NH<sub>3</sub>, 7.8 wt% NH<sub>3</sub> and 10.0 NH<sub>3</sub> wt%, for RR = 0.3, LL = 0.33, Pdes = 10 bar, Tchill = 10 °C, Tcool = 10 °C

### 7.3.2.2 Effect of the cooling water temperature

The cooling water temperature does not affect the capture process itself. However, the chilling duty and the duty for the pumping of cooling water are affected by this parameter. In addition, as mentioned in 7.3.1, due to the lower condenser pressure of the LP turbine, the efficiency penalty from steam extraction at similar conditions is higher for PP10 than for PP20 (see Table 7-5).

Table 7-5: Efficiency penalty for the various contributors for Tcool = 10 °C and Tcool = 20 °C for 7.8 wt% NH<sub>3</sub>, RR = 0.3, LL = 0.33, Tchill = 10 °C and Pdes = 10 bar.

Efficiency penalty (%-pts.)	Tcool = 10 °C (PP10)	Tcool = 20 °C (PP20)
Steam extraction desorber	5.9	5.4
Steam extraction stripper	1.8	1.6
Compressor	1.4	1.4
Chiller	0.6	2.4
Pump / blower	0.5	0.5
Cooling pump	0.3	0.3
Aux power plant	-0.1	-0.1
Net efficiency penalty	10.5	11.7

### 7.3.2.3 Effect of the desorber pressure

The qualitative effect of the desorber pressure can be found in Chapter 6. Figure 7-8 shows the influence of the desorber pressure on the net efficiency penalty of the overall process for the different contributors for the case 7.8 wt% NH<sub>3</sub>, RR = 0.3, LL = 0.33 and T<sub>cool</sub> = 10 °C. The increasing net efficiency penalty for desorber pressures smaller than 4 bars can be explained by limitations of the IP-turbine. The low desorber pressure leads to a lower quality for the steam extraction. This leads to an increase of the volumetric flow rate of steam in the last stage of the IP turbine. The pressure of the steam required by the capture unit drops below the nominal pressure at the IP/LP cross-over (3.9 bar). To avoid damages in the last turbine stages of the IP turbine the specific exhaust volume flow in the IP turbine(actual volume flow/nominal volume flow), which increases with a decreasing steam quality, is limited to 1.4. When this limit is reached, the pressure is not reduced further and the throttle is used to reach the required pressure level, leading to an increased efficiency penalty from steam extraction.

It can be observed that the net efficiency penalty shows a minimum at a desorber pressure of 4 bar. Depending on the set of process parameters, the optimum pressure is comprised between 4 and 10 bar. Operating the desorber at a pressure higher than 10 bar is therefore not beneficial. This is observed for all the sets of parameters tested in this study. It should however be noted that this conclusion is specific to the power plant used.

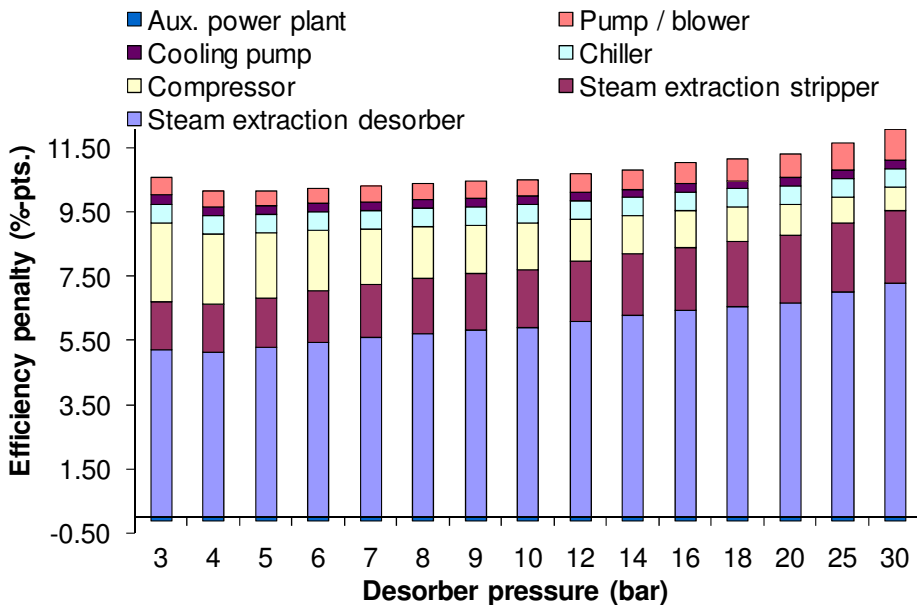


Figure 7-8: Influence of the desorber pressure on the efficiency penalty for the various contributors, for 7.8 wt% NH<sub>3</sub>, RR = 0.3, LL = 0.33, T<sub>chill</sub> = 10 °C and T<sub>cool</sub> = 10 °C.

### 7.3.2.4 Effect of the lean loading and of the recycling rate

The lean loading and the recycling rate have similar qualitative effects on the heat requirement in the NH<sub>3</sub> strippers and the electricity requirement (cf. Chapter 6, Table 6-4). Hence, the sensitivity analysis is given for these two parameters together.

The effects of the lean loading and of the recycling rate on the efficiency penalty largely depend on the ammonia concentration in the solvent. In the case of a low ammonia concentration in the solvent (5.6 wt% NH<sub>3</sub>, cf. Figure 7-9), an increase of the lean loading or of the recycling rate strongly affects the chilling and pumping duties and the heat requirement in the NH<sub>3</sub> strippers. The effect of the lean loading and recycling rate on these three contributors to the efficiency penalty should therefore be considered. In the case of a high ammonia concentration (10.0 wt% NH<sub>3</sub>, cf. Figure 7-10), the flow rate of solvent is lower. Hence, the chilling and pumping duties are less affected by the loading and recycling rates. However the ammonia slip and therefore the heat requirement in the NH<sub>3</sub> strippers vary significantly with these parameters. The contribution of the efficiency penalty from the steam extraction for the ammonia strippers is very high for low recycling rate and lean loading. Due to convergence issues, it was not possible to get results for a broader range of recycling rates using this concentration of ammonia.

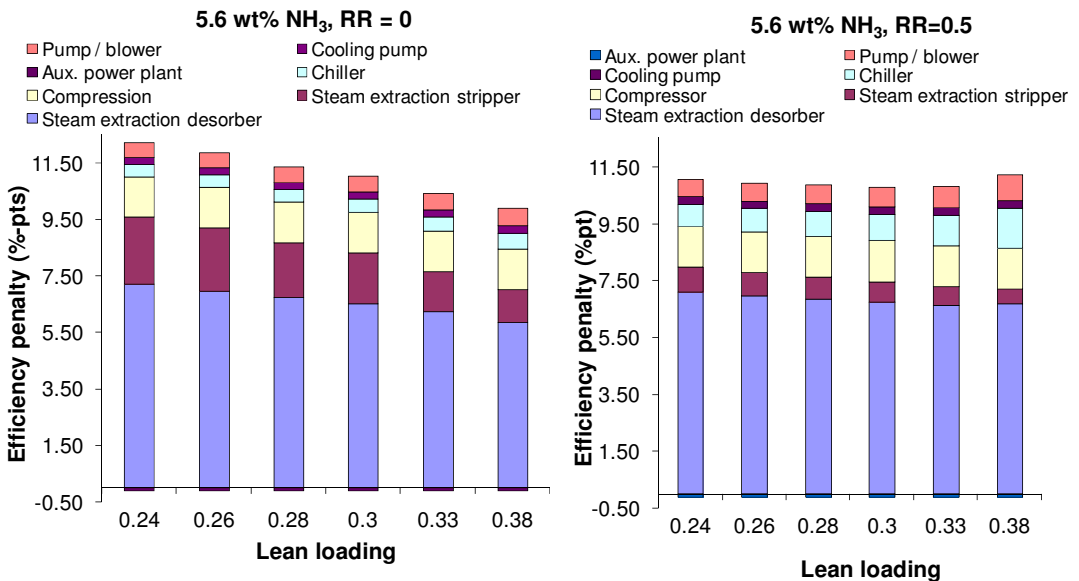


Figure 7-9: Efficiency penalty from the steam extraction for the CO<sub>2</sub> desorber and the NH<sub>3</sub> strippers, the chilling duty and the pumping and blower duties as a function of the lean loading for RR = 0 (left) and RR = 0.5 (right) for 5.6 wt% NH<sub>3</sub>, T<sub>chill</sub> = 10 °C, T<sub>cool</sub> = 10 °C and P<sub>des</sub> = 10 bar.

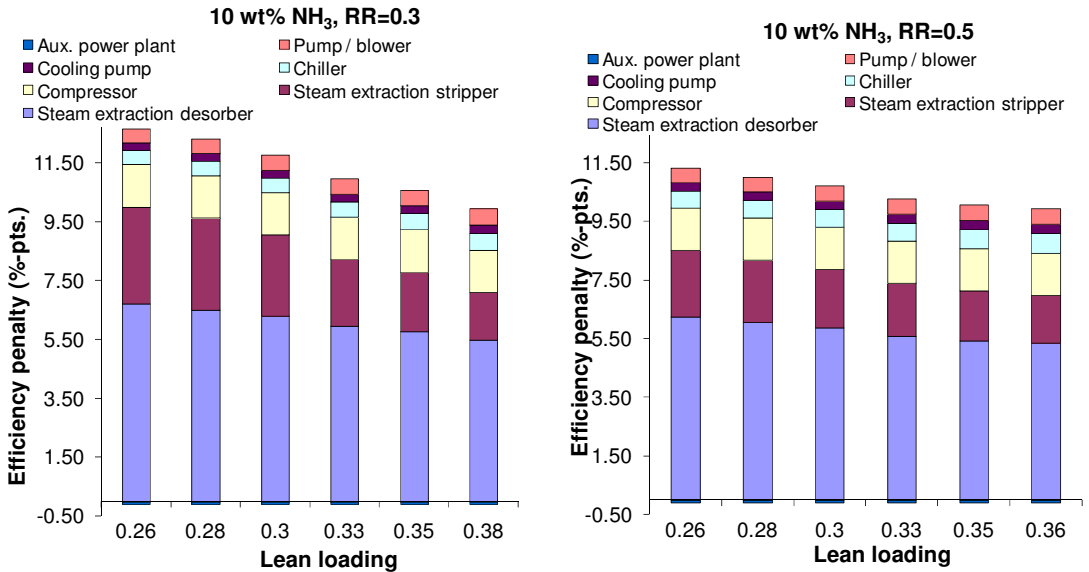


Figure 7-10: Efficiency penalty from the steam extraction for the CO<sub>2</sub> desorber and the NH<sub>3</sub> strippers, the chilling duty and the pumping and blower duties as a function of the lean loading for a recycling rate of 0.3 (left) and 0.5 (right) for 10.0 wt% NH<sub>3</sub>, T<sub>chill</sub> = 10 °C, T<sub>cool</sub> = 10 °C and P<sub>des</sub> = 10 bar.

### 7.3.2.5 Study of the cross dependency of the process parameters

In order to account for the cross dependency of the effects of the process parameters on the efficiency penalty, the desorber pressure, the lean loading and the recycling rate have been varied. The chilling temperature has been maintained at 10 °C. This study has been made for the three ammonia concentrations. Hence, general conclusions regarding the performance of the process for a low chilling temperature can be made.

#### Case of 5.6 wt% NH<sub>3</sub>

Figure 7-11 shows the influence of the lean loading on the net efficiency penalty for a recycling rate of 0, 0.3, 0.5 and 0.7 and for a pressure of 4 and 10 bar for 5.6 wt% NH<sub>3</sub>, T<sub>chill</sub> = 10 °C, T<sub>cool</sub> = 10 °C. Figure 7-12 shows similar calculations for T<sub>cool</sub> = 20 °C. It can be observed that for both cooling water temperatures considered, the best results are obtained without recycling of the exit stream of the absorber. As explained above, an increase of the recycling rate entails an increase of the chilling and pumping duties, while the heat requirement in the NH<sub>3</sub> strippers only moderately decreases due to the low ammonia concentration.

For T<sub>cool</sub> = 10 °C, the minimum net efficiency penalty is obtained without recycling for a desorber pressure of 10 bar. It reaches a value of about 9.6 %-pts. for a lean loading in the range 0.4-0.42 (cf.

Figure 7-11). The results are better for a desorber pressure of 10 bar for high lean loadings because of the restriction of the volume flow rate in the IP turbine when the required steam pressure decreases. Hence, a process using aqueous ammonia for absorption at low temperature without solid formation in the absorber leads to a net efficiency penalty about 1.3 %-pts. lower than the one observed with aqueous MEA (cf.7.3.1), assuming, that a low temperature cooling water is available.

For  $T_{cool} = 20\text{ }^{\circ}\text{C}$ , it occurs for a desorber pressure of 4 bar for a lean loading in the range 0.33-0.38. The minimum net efficiency penalty is 10.7 %-pts. (cf. Figure 7-12), which is larger than what is observed with MEA (10.2 %-pts).

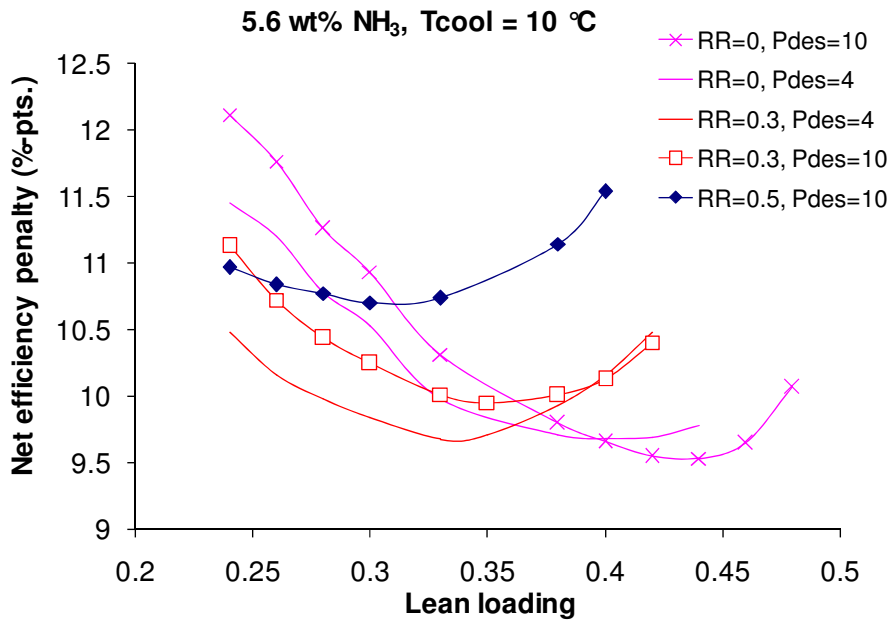
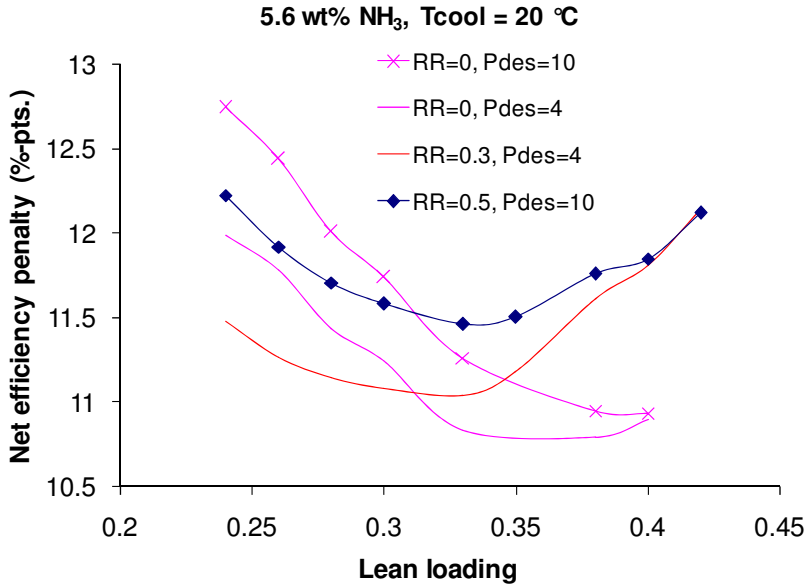


Figure 7-11: Influence of the lean loading, the recycling rate and the desorber pressure on the efficiency penalty for 5.6 wt% NH<sub>3</sub>, T<sub>chill</sub> = 10 °C, T<sub>cool</sub> = 10 °C



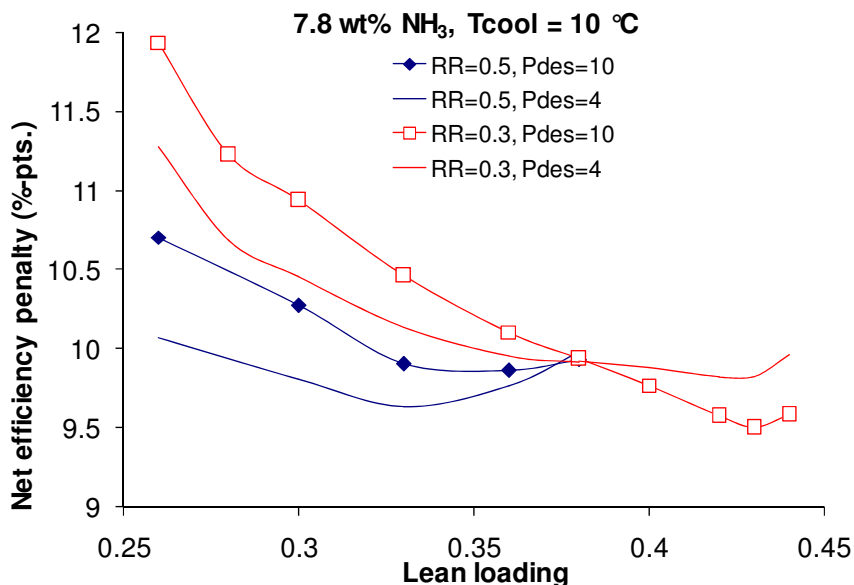
**Figure 7-12: Influence of the lean loading, the recycling rate and the desorber pressure on the efficiency penalty for 5.6 wt% NH<sub>3</sub>, T<sub>chill</sub> = 10 °C, T<sub>cool</sub> = 20 °C**

### Case of 7.8 wt% NH<sub>3</sub>

Figure 7-13 shows calculations similar as Figure 7-11 for an ammonia concentration of 7.8 wt% NH<sub>3</sub>. For the case where cooling water is available at 10 °C, the minimum new efficiency penalty is obtained for a desorber pressure of 10 bars and a recycling rate of 0.3 for a loading of 0.43. At these conditions, the process entails solid formation during the absorption. The calculated efficiency is about 9.5 %-pts., about 1.4 %-pts. lower than what is observed with MEA. It can be observed that this minimum is obtained for a narrow lean loading range.

If cooling water is available at 20 °C, the minimum is obtained for a recycling rate of 0.3 and a desorber pressure of 4 bar, for a loading of 0.42. Another local minimum is obtained for a recycling rate of 0.5 for a lower loading. The minimum calculated net efficiency penalty is 11.1 %-pts. It is therefore higher than what is observed with MEA.

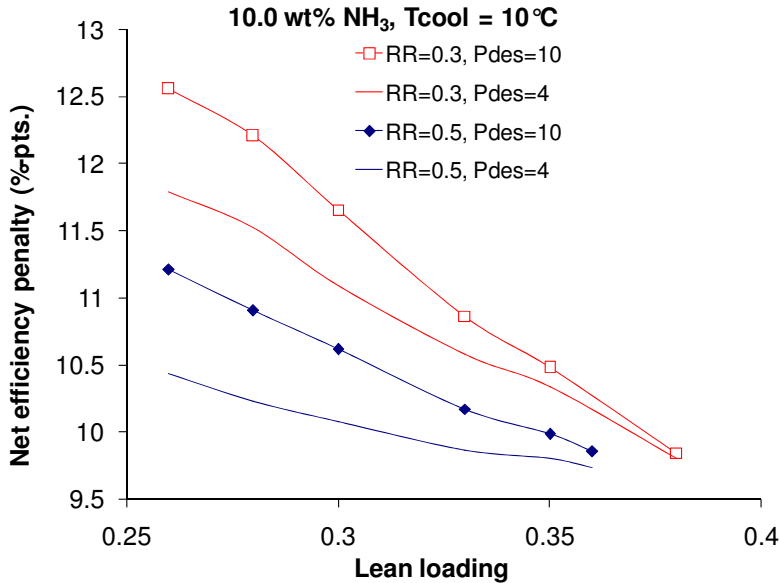




**Figure 7-13: Influence of the lean loading, the recycling rate and the desorber pressure on the efficiency penalty for 7.8 wt% NH<sub>3</sub>, T<sub>chill</sub> = 10 °C, T<sub>cool</sub> = 10 °C**

### Case of 10.0 wt% NH<sub>3</sub>

Figure 7-14 shows similar plots for 10.0 wt% NH<sub>3</sub> and T<sub>cool</sub> = 10 °C. The convergence issues experienced by simulating the capture process for high loading ranges when high ammonia concentration was used did not allow for reaching a minimum in the net efficiency penalty. The lowest value of the net efficiency penalty calculated with 10.0 wt% NH<sub>3</sub> is about 9.7 %-pts for a recycling rate of 0.5, a desorber pressure of 4 bar and a lean loading of 0.35. It is about 1.2 %-pts lower than what is observed with MEA. Hence, because of the high penalty from the steam extraction to the ammonia strippers, the global efficiency penalty calculated with the high ammonia concentration is not lower than the one found with a low ammonia concentration. The results for T<sub>cool</sub> = 20 °C resulted in a minimum efficiency penalty of about 11 %-pts., which is significantly higher than what is observed with MEA.



**Figure 7-14: Influence of the lean loading, the recycling rate and the desorber pressure on the efficiency penalty for 10.0 wt% NH<sub>3</sub>, T<sub>chill</sub> = 10 °C, T<sub>cool</sub> = 10 °C**

Hence, the three concentrations studied for a chilling temperature of 10 °C lead to an efficiency penalty lower than the one observed with MEA assuming that cooling water at 10 °C is available. The minimum efficiency penalties are quite close for the three ammonia concentrations. When cooling water at 20 °C is available, the penalty induced by the process is systematically higher than the one observed with MEA. Hence, the CAP with Configuration A is only competitive if cooling water at low temperature is available.

### 7.3.2.6 Effect of the chilling temperature

Figure 7-15 shows the effect of the chilling temperature on the efficiency penalty for the different contributors for 5.6 wt% NH<sub>3</sub>, RR=0.3, LL = 0.33, Pdes = 10 bar for both T<sub>cool</sub> = 10 °C and T<sub>cool</sub> = 20 °C.

For T<sub>cool</sub> = 10 °C, increasing the chilling temperature from 7 to 17 °C entails the rise of the efficiency penalty from the steam extraction for the NH<sub>3</sub> strippers from 0.7 to 1.8%-pts. while the contribution from the chilling duty decreases from 1.3 to 0.0 %-pt. For T<sub>cool</sub> = 20 °C, when T<sub>chill</sub> increases from 7 to 25 °C, the contribution to the efficiency penalty from steam extraction to the NH<sub>3</sub> strippers rises from 0.6 to 2.5 %-pts. and the contribution from the chilling duty decreases from 3.6 to 0.2 %-pt. For T<sub>chill</sub> = 25 °C, the remaining chilling duty corresponds to the chilling of the washing stream that occurs at 10 °C for all the simulations (cf. 6.2.2).

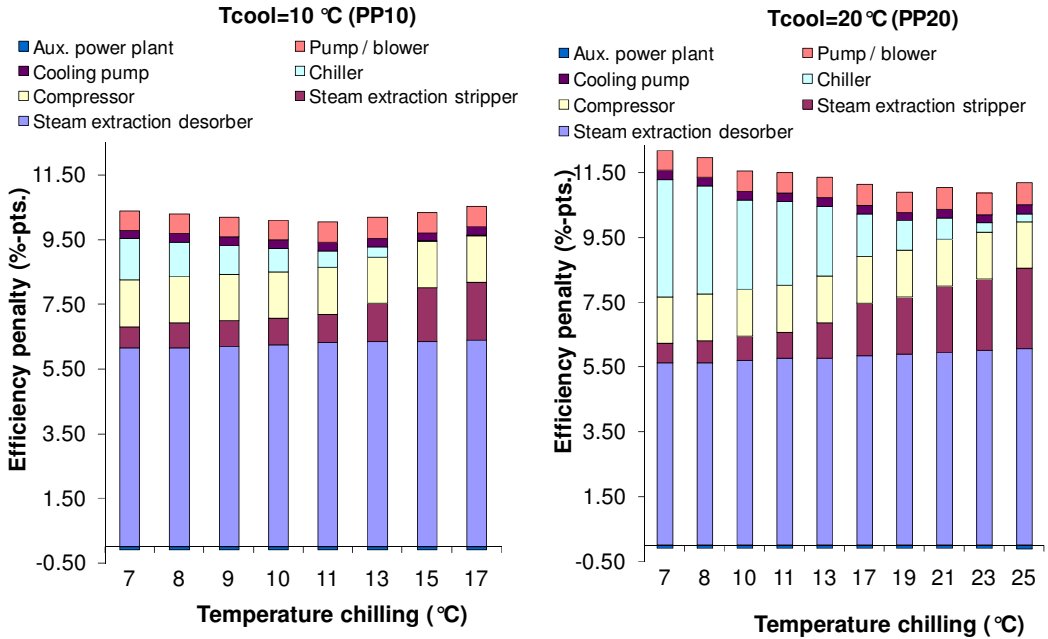
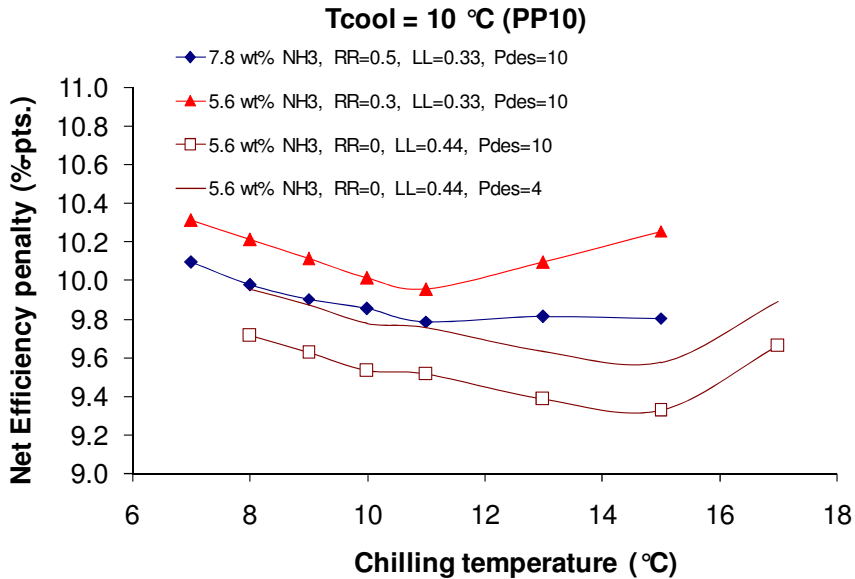


Figure 7-15: Influence of the chilling temperature on the efficiency penalty for the various contributors for 5.6 wt% NH<sub>3</sub>, RR = 0.3, LL = 0.33, Pdes = 10bar, Tcool 10 °C (left) and Tcool = 20 °C (right)

The influence of the chilling temperature on the efficiency penalty has been studied for various combinations of ammonia concentrations, recycling rates, lean loadings and desorber pressures for a cooling temperature at 10 °C (cf. Figure 7-16). It shows that the optimal temperature for the various cases studied is between 10 and 15 °C. Hence, despite the power consumption from the chilling, it is beneficial to absorb carbon dioxide at low temperature when low temperature cooling water is available for most sets of parameters. The minimum efficiency penalty is observed for 5.6 wt% NH<sub>3</sub>, without recycling for a lean loading of 0.44, a pressure in the desorber of 4 bar and for a chilling temperature of 15 °C, meaning that only cooling water is used and no chilling is required for the solvent and the flue gas. The value for this efficiency penalty is 9.4 %-pts.



**Figure 7-16: Influence of the chilling temperature on the net efficiency penalty for Tcool = 10 °C**

Similar calculations have been made for Tcool = 20 °C (cf. Figure 7-17). The optimum chilling temperature is usually higher than 20 °C. A minimum net efficiency penalty of 10.2 %-pts. can be obtained for Tchill = 21 °C. However, the efficiency penalty does not compete with the one obtained with MEA (10.2 %-pts.). Hence, by using Configuration A, it is not possible to reach an efficiency penalty lower than the one observed with MEA if cooling water at 20 °C is used. It can be observed that for high chilling temperature, it is recommended to use low concentration of ammonia. The use of high concentration of ammonia in the solvent entails a very high efficiency penalty from steam extraction to NH<sub>3</sub> strippers.

The results shown are strongly affected by the COP used. Hence, for a more thorough study of the effect of the chilling temperature on the performance of the process, a more detailed modeling of the refrigeration system would be required.

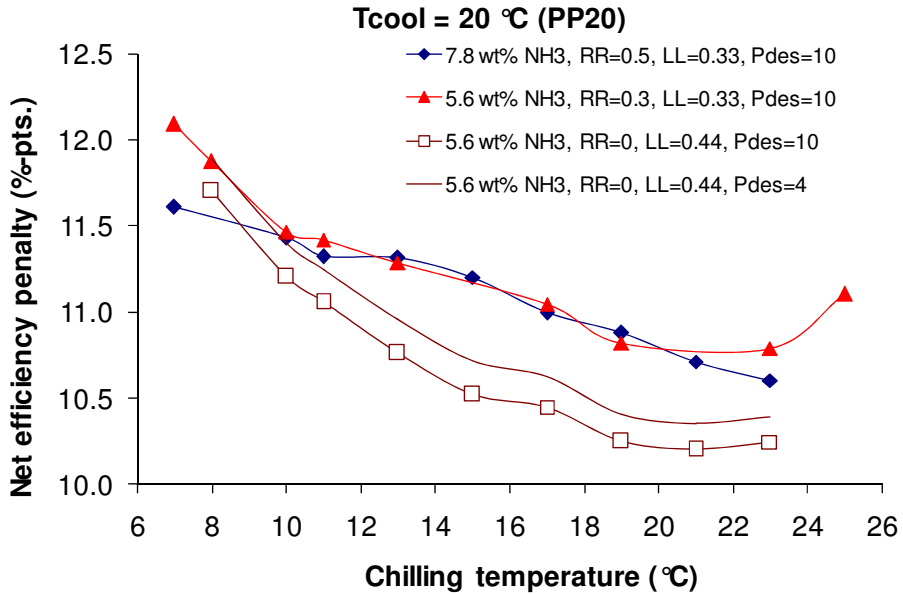


Figure 7-17: Influence of the chilling temperature on the net efficiency penalty for T<sub>cool</sub> = 10 °C

### 7.3.2.7 Calculation of the dimension of the absorber columns

Using the method described in 7.2.2.3, the dimensions of the absorber have been estimated. The calculation of the diameter of the column is mainly affected by the volumetric flow rate of the gas and by the densities of liquid and gas in the column. Hence, the diameter is not much affected by the loading and the recycling rate. For the different cases considered, the calculated value of the diameter of the column is about 24 m. In this study, in order to compare fairly the packing height requirement for the different cases, this value is considered as constant. Due to the limitations from the transportation, construction and operation of such a large column, 2 columns with a diameter of 17 m or 3 columns with a diameter of 14 m might be recommended.

The packing height requirement of each stage depends on the rate of absorption of carbon dioxide by aqueous ammonia. It is therefore strongly influenced by the temperature and the free ammonia concentration in the solvent.

The absorber column is modeled as a packed column. It is assumed in this study that the mass transfer obtained with the packing is not affected by the formation of solid. In reality, in case of absorption implying precipitation, a spray column might be necessary, which would lower the mass transfer compared to packed columns. Figure 7-18 shows the estimate of the height of the absorber column as a function of the lean loading for different ammonia concentrations and recycling rates for a chilling

temperature of 10 °C. For some cases at low loading and low recycling rate, the temperature in the column exceeded the temperature range applied for the experiments used for the modeling of the kinetic rate of absorption (see Chapter 4). Hence, these results should be considered with caution. The column height tends to increase with the lean loading and with the recycling rate. This is due to the decrease of the temperature and the increase of the loading in the column. In addition, the packing height requirement decreases when the ammonia concentration in the solvent increases due to the increase of the temperature and of the concentration of free ammonia in the solvent.

For the cases where a minimum was found for the efficiency penalty, the absorber height is in the range 50-60 m. By using the same method for a process using aqueous MEA, Abu-Zhara *et al.* (2007a) estimated a column height of 29 m (Oexmann *et al.*, 2008). Hence, a column approximately twice as high is required for the process using aqueous ammonia. A single absorber column 60 m high might not be feasible, but by using 2 or 3 absorbers, it is possible to reach the required packing height. This study therefore shows that a higher capital cost is required for the absorber compared to the MEA-based process. However, the required packing height to reach 90% capture rate is compatible with a real capture process.

These results are based on the rate of absorption of carbon dioxide by ammonia solvent, and the uncertainty related to the modeling of the absorption rate described in Chapter 4 should therefore be considered. Especially, the overestimation of the physical solubility of carbon dioxide in loaded solutions according to the experimental data from Qin *et al.* (2011) may lead to an under prediction of the packing height requirement. The experiments of Qin show that the solubility of carbon dioxide in ammonia solutions decreases with the loading, which would lead to a decrease of the liquid side mass transfer coefficient  $k'_G$ .

As shown in 6.3.4, the ME affects strongly the required flow rate of solvent. Decreasing the ME with a constant capture rate implies a rise of the flow rate of solvent. In the absorber, this tends to reduce the temperature and decrease the loading. The calculation of the enhancement factor is therefore affected by the ME. For all the cases studied here, decreasing the ME implies the increase of the enhancement factor.

In addition, the concentration profile in the absorber is heavily affected by the ME. Lowering the ME while maintaining a constant capture rate and number of equilibrium stages during the simulation implies the increase of the driving force for the absorption of carbon dioxide. Consequently, the absorption flux increases and the packing height requirement decreases. The value of the packing height requirement therefore depends on the value of the ME applied during the simulations. More explanations regarding the effect of the ME on the packing height of the absorber can be found in Appendix B.

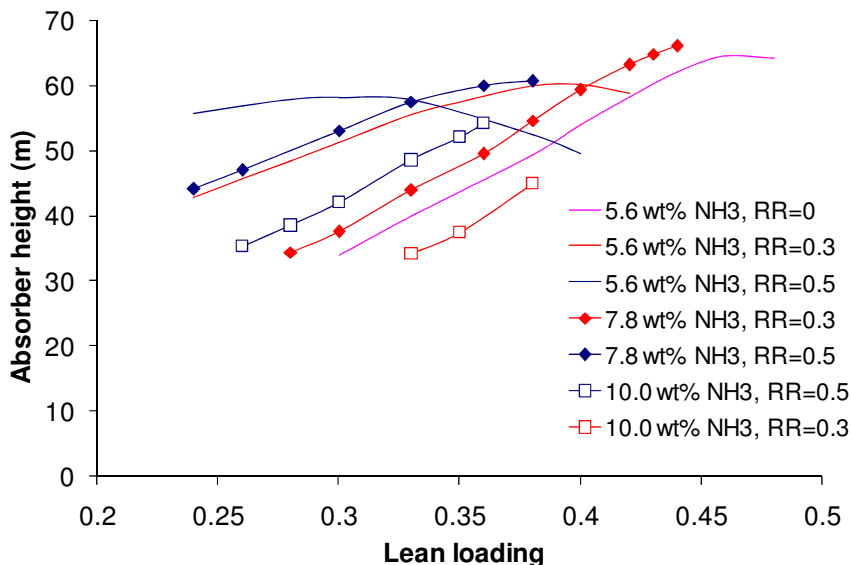


Figure 7-18: Calculation of the absorber height for  $T_{\text{chill}} = 10\text{ }^{\circ}\text{C}$

### 7.3.2.8 Water wash column dimensions

By using a method similar to the one described in 7.2.2.3 applied to the absorption of ammonia, it is possible to estimate the packing height requirement for the water wash sections. In this study, the value of the enhancement factor for the absorption of ammonia by the solvent has been set to 1. It was therefore assumed that there was no effect from a chemical reaction to enhance the washing of ammonia. The equilibrium partial pressures of ammonia in the washing stream have been calculated with the Extended UNIQUAC model. The physical solubility of ammonia used in the calculation was set to be equal to the one in pure water. For the case where the highest ammonia slip from the absorber was observed, assuming a diameter of 24 m for the column, the packing height requirement reached a value of 17 m for the first water wash column.

## 7.3.3 Results Configuration B

### 7.3.3.1 Effect of the lean loading

The effect of the pressure in the desorber for Configuration B is similar to the one reported in 7.3.2.3.

Figure 7-19 shows the influence of the lean loading on the different contributors to the net efficiency penalty. For a lean loading up to 0.35, the net efficiency penalty due to the steam extraction to the  $\text{CO}_2$  desorber decreases with the lean loading and reaches values lower than what is observed with Configuration A at the same ammonia concentration for a recycling rate of 0.3. It can be explained by

the lower heat requirement in the desorber and the lower temperature of the reboiler due the higher rich loading compared to Configuration A.

Compared to Configuration A, the penalty from the steam extraction for the NH<sub>3</sub> strippers also shows lower value (when LL increases from 0.26 to 0.38, from 0.6 to 0.45 %-pt. compared to 1.5 to 0.75 %-pts. for Configuration A for RR = 0.5 and 7.8 wt% NH<sub>3</sub>. As only one stream is chilled down, the chilling requirement is also lower than what is observed with Configuration A when recycling is used.

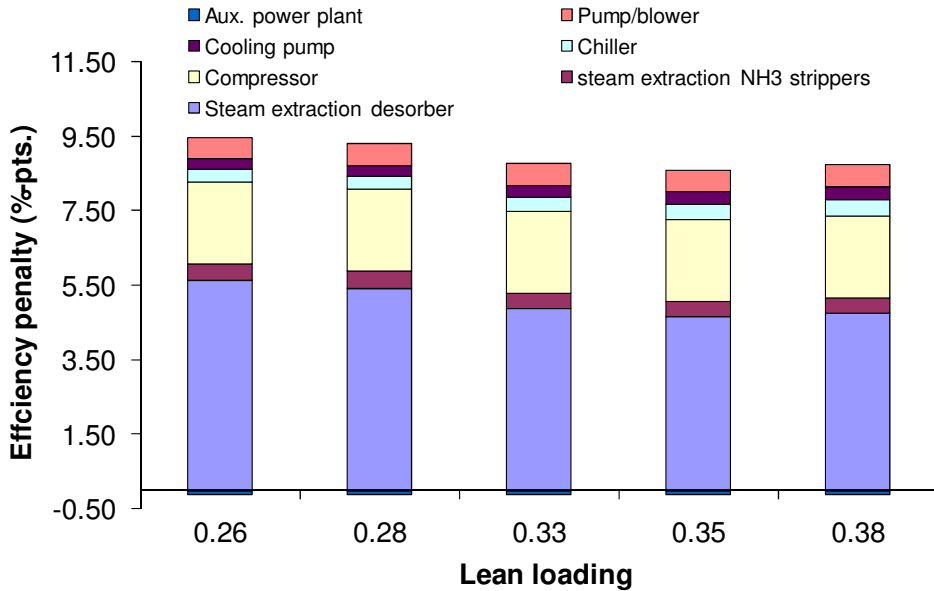
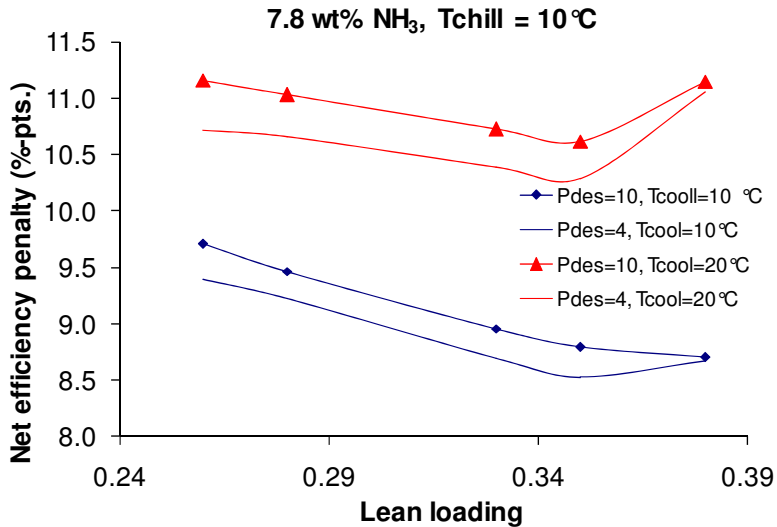


Figure 7-19: Net efficiency penalty for the different contributors for 7.8 wt% NH<sub>3</sub>, T<sub>chill</sub> = 10 °C and T<sub>cool</sub> = 10 °C

Figure 7-20 shows the effect of the lean loading on the efficiency penalty for 7.8 wt%NH<sub>3</sub>, T<sub>chill</sub> = 10 °C, for P<sub>des</sub> = 10 bar and P<sub>des</sub> = 4 bar and for T<sub>cool</sub> = 10 °C and T<sub>cool</sub> = 20 °C. It can be observed that for the range of lean loading considered, for T<sub>cool</sub> = 10 °C, a minimum for the net efficiency penalty is found for P<sub>des</sub> = 4 bar, T<sub>cool</sub> = 10 °C and LL = 0.35. The value obtained is 8.5 %-pts., which is about 2.4 %-pts. lower than what is found with 30wt% MEA. It is also significantly lower than the calculations with Configuration A. Hence, this study has shown that Configuration B shows a very high potential for reducing the efficiency penalty induced by a carbon capture process.

For T<sub>cool</sub> = 20 °C, the net efficiency penalty reaches a minimum for a lean loading of 0.35 and a pressure in the desorber of 4 bar. The efficiency drop does not compete with the one found with 30 wt% MEA.





**Figure 7-20: Effect of the lean loading, the desorber pressure and the cooling water temperature on the efficiency penalty for 7.8 wt% NH<sub>3</sub> and Tchill = 10 °C**

### 7.3.3.2 Calculation of the dimension of the absorber columns

Using a similar method as the one presented in 7.2.2.3, it is possible to estimate the diameters and height of the absorber columns. According to the calculations, the diameters of the columns have a value close to the one calculated for Configuration A. In order to compare the calculation of the height of the column for both configurations, the diameter of both absorbers has been set to the same value as the one calculated with Configuration A (24 m). By increasing the lean loading from 0.26 to 0.38, the height of the Absorber 1 increases from 25 to 35 m. It should be noted that for some of the cases, the temperature in the column exceeded by 7 °C the temperature range (6-31 °C) of the experiments used for the modeling of the kinetic rate of absorption of CO<sub>2</sub> by aqueous ammonia. In this study, the same correlations for the kinetic constant as the one given in Chapter 4 were used when the temperature exceeded 31 °C. These calculations should therefore be considered with caution. The low height compared to the one observed with Configuration A is explained by the high temperature through the column compared to Configuration A.

For Absorber 2, for 7.8 NH<sub>3</sub> wt%, all the cases studied, the calculations lead to a required height of packing larger than 200 meters. This high value can be explained by the very low driving force occurring in Absorber 2 due to the low partial pressure of carbon dioxide in the gas phase and the high loading of the solvent. In addition, at low temperature and high loading, the rate of absorption of carbon dioxide by the solvent is very low. This packing height is not compatible with a real process due

to the issue and cost implied by the construction of such column and the resulting pressure drop that would increase the duty from the blower.

Given the large reduction of the net efficiency penalty for a capture rate of 90%, Configuration B using 7.8 NH<sub>3</sub> wt% may have the potential for showing good performance at a lower capture rate. However, it needs to be ensured the lower packing height would still allow for reducing the ammonia content in the flue gas. By using the same method as the one used to estimate the height of the water wash sections, it is possible to estimate the packing height requirement for the cleaning of the ammonia from the gas phase in Absorber 2. Similar assumptions were made regarding the physical solubility and the enhancement factor. The results from the simulation with a 90% CO<sub>2</sub> capture rate have been used. The packing height requirement for the cleaning of ammonia in Absorber 2 was found to be comprised between 10 and 17 m. Hence, providing the packing height of Absorber 2 is higher than 17 m, it is possible to decrease the ammonia slip from Absorber 2 to a level close to the one observed in the simulation.

### **7.3.3.3 Analysis of the results with Configuration B**

The high value for the packing height requirement of Absorber 2 could reflect that the value of the ME applied in Absorber 1 and Absorber 2 are not adapted. As stated earlier, pilot plant data would be necessary to determine the correct ME. A lower value for the ME would allow for increasing the driving force and decreasing the packing height requirement (cf. Appendix B). However, it should be noticed that a lower ME in Absorber 2 might imply issues related to the high equilibrium partial pressure of the solvent on top of Absorber 2 (cf. 6.3.3.1 and Chapter 3). This entails that it might not be possible to reach 90% capture efficiency. In addition, as shown in 6.3.4, lowering the ME would affect the flow rate of the solvent and therefore the net efficiency penalty. Simulations with a lower ME and a lower capture rate would be necessary to investigate further the potential of this process configuration. Due to convergence issues, this study could not be conducted. The rest of this analysis is made for a ME of 0.2 in Absorber 1 and 0.1 in Absorber 2.

In Chapter 6, it has been shown that about 72% of the carbon dioxide is captured in Absorber 1. The amount of carbon dioxide captured in Absorber 2 is limited. Hence, reducing the height of Absorber 2 compared to the calculated value would still allow for reaching a decent capture rate. Assuming that, for an identical solvent flow rate, the height of Absorber 2 allows for capturing one fifth of what the simulation results show, the final capture rate would reach a value in the range 77-80%. As the ammonia slip from the absorber would keep a level close to the one observed in the simulation and as the flow rate of the solvent would be unchanged, by neglecting the change of the rich loading, it can be assumed the absolute values of the heat and electricity requirements would remain close to the simulation results. Hence, it is possible to estimate the specific heat and electricity requirements, expressed in kJ/kg CO<sub>2</sub> captured and to calculate the corresponding efficiency penalty for a capture rate of 90%. For the optimum case, the net efficiency penalty converted to the 90% capture rate would

reach about 9.6 %-pts. Hence, based on these assumptions, the optimum net efficiency penalty with both process configurations would be in the same range.

By increasing the concentration of ammonia in the solvent, it is possible to increase the driving force in the column and therefore reduce the packing height requirement to more reasonable values with 90% capture rate. However, this would imply the formation of solid in the CO<sub>2</sub>-rich stream and the rise of the heat requirement in the desorber. Due to convergence issues, the integration study with high concentration of ammonia in the solvent has not been conducted.

Overall, this study shows that Configuration B has the potential for lowering the efficiency penalty. However, different limitations inherent to this process configuration have been identified. The use of a robust rate-based model would be required to evaluate more accurately the performance of the process with Configuration B and to draw conclusions regarding its potential for a reduced efficiency penalty combined a reasonable capital cost.

## **7.4 Conclusion**

The performance of the CO<sub>2</sub> capture using aqueous ammonia has been evaluated through an integration study. This study has been done for two cooling water temperatures. Hence, two power plants with the same gross power output have been simulated and used in this study.

It has been shown that for both power plants and both process configurations, the pressure in the desorber resulting in the lowest efficiency penalty was comprised between 4 and 10 bar depending on the process parameters. Therefore, operating the desorber at a higher pressure is not recommended because of the high steam quality required for the power plants considered.

Regarding Configuration A, for the case where cooling water temperature at 10 °C is available, it has been shown that the absorption at low temperature was beneficial. An efficiency penalty significantly lower than the one found using MEA could be reached for the three ammonia concentrations considered. Hence, the process variant with absorption at low temperature without precipitation during the absorption has shown better performance than the MEA process. The reduction of the net efficiency penalty of the power plant compared to the MEA process reached 1.4 %-pts. The size of the absorber column has been evaluated for the optimal cases. It was observed that a packing height about twice as high as what is needed for the MEA-based process is required.

The net efficiency penalty obtained with Configuration B reached a value of 8.5 %-pts, about 2.4 %-pts lower than what is obtained with MEA. However, the estimation of the height of Absorber 2 has shown that reaching a capture rate of 90% would not be feasible. It is estimated that the use of a lower absorber column and the decrease of the capture rate would lead to performance close to the ones observed with Configuration A.

For the case where cooling water at 20 °C is available, the efficiency penalty calculated for both process configurations was systematically higher than the one observed using aqueous MEA solutions, both for absorption at low and high temperature.

## 7.5 References

- Abu-Zahra, M. R. M., Schneiders, L. H. J., Niederer, J. P. M., Feron, P. H. M. CO<sub>2</sub> capture from power plants: Part I. A parametric study of the technical performance based on monoethanolamine. *International Journal of Greenhouse Gas Control*, **2007a**, *1*, 37
- Bravo, J. L.; Rocha, J. A.; Fair, J. R. Mass transfer in Gauze Packings. *Hydrocarbon. Proc.*, **1985**, *64*, 91.
- Kather, A.; Linnenberg, S.; Oexmann, J. POSEIDON PostCombustion CO<sub>2</sub>-Abtrennung: Evaluierung der Integration, Dynamik und Optimierung nachgeschalteter Rauchgaswäschen. Förderkennzeichen PTJ/BMWi/0327785, **May 2011**.
- Kister, H. Z. Distillation design. McGraw-Hill, New York, **1992**.
- van Krevelen, D.; Hoftijzer, P. Kinetics of gas-liquid reactions I General theory. *Recueil des Travaux Chimiques des Pays-Bas et de la Belgique*, **1948**, *67*, 563.
- Linnenberg, S.; Kather, A. Evaluation of an Integrated Post-Combustion CO<sub>2</sub> Capture Process for Varying Loads in a Coal-Fired Power Plant using Monoethanolamine, 4<sup>th</sup> International Conference on Clean Coal Technologies, Dresden, Germany, **2009**.
- Lucquiaud, M.; Gibbins, J. On the integration of CO<sub>2</sub> capture with coal-fire power plants: A methodology to assess and optimise solvent-based post combustion capture systems. *Chem. Eng. Res. Des.*, **2011**, doi:10.1016/j.cherd.2011.03.003
- Oexmann, J.; Hensel, C.; Kather, A. Post-combustion CO<sub>2</sub>-capture from coal-fired power plants: Preliminary evaluation of an integrated chemical absorption process with piperazine-promoted potassium carbonate. *International Journal of Greenhouse Gas control*, **2008**, *2*, 539.
- Oexmann, J. PostCombustion CO<sub>2</sub> Capture: Energetic Evaluation of Chemical Absorption Processes in Coal Fired Steam Power Plants, PhD dissertation, ISBN-13: 9783869556338, Hamburg University of Technology, Germany, **2011**.
- Qin, F.; Wanga, S.; Hartono, A.; Svendsen, H. F. Kinetics of CO<sub>2</sub> absorption in aqueous ammonia solution. *Int. J. Greenhouse Gas Control*, **2010**, *4*, 729.
- Pfaff, I.; Oexmann, J.; Kather, A. Optimised integration of post-combustion CO<sub>2</sub> capture process in Greenfield power plant. *Energy*, **2010**, *35*, 4030-4041.
- Rocha, J. A.; Bravo, J. L.; Fair, J. R. Distillation columns containing structured packings: A comprehensive model for their performance. 2. mass-transfer model. *Industrial & Engineering Chemistry Research*, **1996**, *35*, 1660.



## 8 Conclusions and recommendations

### 8.1 Conclusive remarks

CO<sub>2</sub> capture is a promising method to reduce carbon dioxide emissions from the power sector significantly. The implementation of CO<sub>2</sub> capture processes can therefore contribute tackling the problem of climate change. In this thesis, the performance of the CO<sub>2</sub> capture process using aqueous ammonia has been evaluated. This study is based on the development of a thermodynamic model, an experimental study of the kinetic rate of absorption of CO<sub>2</sub> by aqueous ammonia solvent, the simulation of the capture process and an integration study of the capture process with a power plant.

In this work, the Extended UNIQUAC thermodynamic model for the CO<sub>2</sub>-NH<sub>3</sub>-H<sub>2</sub>O system originally proposed by Thomsen and Rasmussen (1999) has been upgraded. By using additional ternary vapor-liquid equilibrium experimental data in various concentration ranges, its valid temperature range has been extended up to 150 °C. Furthermore, experimental data measuring enthalpy change from partial evaporation, speciation, heat capacity, enthalpy of solution and the enthalpy of dilution have been used. 43 model parameters and standard state properties have been refitted using about 3700 data points. The new version of the Extended UNIQUAC model describes accurately the vapor-liquid-solid equilibrium, the speciation and the thermal properties of a mixture of carbon dioxide, ammonia and water for a temperature in the range 0-150 °C.

Using this tool, a preliminary thermodynamic analysis of the Chilled Ammonia Process has been performed. Based on the patent from the process, the compositions of the main streams of the process have been calculated for different ammonia concentrations in the solvent. The study showed the ability for the three ammonia concentrations to capture CO<sub>2</sub> from coal-fired power plants at low temperature. The presence of ammonium bicarbonate precipitate has been shown in the absorber for high concentration of ammonia in the solvent. The study has also confirmed the high ammonia slip from the absorber despite the low temperature of absorption. Increasing the loading, reducing the temperatures and the ammonia concentration in the solvent are the three means to reduce the ammonia slip. The potential for operating the CO<sub>2</sub> desorber at high pressure has also been identified. A reference configuration has been set up in order to estimate the heat requirement for the desorption of CO<sub>2</sub> based on equilibrium calculations and assumptions regarding the process. This study showed the high potential for the reduction of the heat requirement compared to monoethanolamine-based process.

The rate of absorption of carbon dioxide by a solvent is a crucial factor to consider when dealing with CO<sub>2</sub> capture. It is closely linked to the required size of the absorber and hence to the capital cost of the capture process. A wetted wall column apparatus has been designed and built. It was used to measure the overall mass transfer coefficient of carbon dioxide by aqueous ammonia solvents for a temperature from 6 to 31°C, a mass fraction of ammonia up to 10 wt% and a loading up to 0.8. These measurements were compared to the mass transfer coefficient using 30 wt% MEA solutions. It was observed that at

low temperature, the mass transfer coefficient obtained with loaded ammonia solutions was significantly lower than the one observed with loaded MEA at 40°C. This shows that the variant of the process with absorption at low temperature would imply a larger contact area between the gas and the solvent. Based on the experimental measurements using unloaded solutions, the chemical rate of absorption of carbon dioxide by aqueous ammonia has been modeled. The calculations of the model have been compared with the experimental measurements using loaded solutions. It has been shown that the model is able to predict accurately this rate of absorption.

In order to evaluate the process, flow sheet calculations are required. This study uses the Extended UNIQUAC user model (Maribo-Mogensen et al., 2011) that allows for the implementation of the Extended UNIQUAC model in the commercial simulator Aspen Plus. It has been shown that the user model could reproduce accurately the thermodynamic calculations from Extended UNIQUAC up to a high temperature. Hence, it has been proven that the user model is an accurate tool for process simulation on Aspen Plus. The Extended UNIQUAC model has been compared to the e-NRTL model available by default on Aspen Plus for the CO<sub>2</sub>-NH<sub>3</sub>-H<sub>2</sub>O system. By comparing both models with available experimental data, it was shown that the Extended UNIQUAC model performed better than the e-NRTL model. The partial pressure of ammonia was found to be under estimated by the e-NRTL model for a large temperature range. In addition, the calculations regarding the formation of solids were not accurate. Finally, the speciation calculations showed that the e-NRTL model under estimated the concentration of ammonium carbamate at high temperature. The CO<sub>2</sub> capture process was then simulated using both thermodynamic models using similar boundary conditions with a simple configuration of the process. This study has shown that the predictions of the models differ. The heat requirement in the CO<sub>2</sub> desorber calculated with the e-NRTL model was significantly lower than the one obtained with the Extended UNIQUAC model at similar boundary conditions.

Using Aspen Plus coupled with the Extended UNIQUAC model, the CO<sub>2</sub> capture process has been simulated by performing equilibrium calculations. In order to account for the deviation from the equilibrium, low Murphree efficiencies for CO<sub>2</sub> in the absorber have been specified. Two different process configurations that allow for limiting the ammonia slip from the absorber have been studied. A base case scenario was set up. The influence of the main process parameters on the heat and electricity consumption was analyzed by performing sensitivity analysis. It was shown that increasing the concentration of ammonia in the solvent does not imply a decrease of the heat consumption because of the rise of the ammonia slip from the absorber. The chilling duty was compared to the compression savings by operating the desorber at elevated pressure for different cases. For both configurations, heat requirement significantly lower than what is observed with MEA could be obtained. The process implying absorption at low temperature showed to have the potential to be competitive with MEA-based process.

In order to estimate the effect of the implementation of the capture process on a power plant, an integration study has been performed. This work, in collaboration with the Hamburg University of

Technology (TUHH), allowed for estimating the net efficiency penalty induced by the capture process and by the compression of carbon dioxide. A sensitivity analysis for the main process parameters was performed again. The influence of the location of the plant was also considered by doing this analysis for two cooling water temperatures. The study has shown that the process with absorption at low temperature resulted in a significantly reduced net efficiency penalty compared to the MEA-based process, providing that low temperature cooling water was available. In addition, based on the modeling of the rate of absorption of CO<sub>2</sub> by aqueous ammonia, an estimate of the dimension of the absorber column was provided. For one of the configurations, it resulted in an absorber column approximately twice as high as what is required for MEA. For the other configuration that showed a lower net efficiency penalty, the calculations for one of the absorber columns resulted in a very high packing height requirement. Hence, reaching 90% capture rate with this configuration might not be feasible, but the configuration still showed potential for good performance at a lower capture rate.

## ***8.2 Challenges and recommendations***

There are several directions in which this study could be carried on and improved.

Regarding the thermodynamic model, additional ternary vapor-liquid equilibrium data at temperature lower than 20 °C would allow for ensuring that the calculations of the model are accurate at low temperature. In addition, it would be interesting to develop the model so that additional species, such as sulfur oxides or nitrous oxides can be used in the simulation. This would permit the detailed study of the variant of the process developed by Powerspan that absorbs CO<sub>2</sub> and SO<sub>x</sub> simultaneously. The Extended UNIQUAC parameters for the corresponding species are available, but the interaction parameters between the different species would need to be re-fitted to the new ammonia parameters.

The kinetic study could be carried on as well. Kinetic measurements at higher temperature are required to model the rate of absorption up to 40 °C. Because of the volatility of ammonia, these measurements would be challenging. The experimental study of the solubility of CO<sub>2</sub> in loaded aqueous ammonia solutions would improve the accuracy of the model. In addition, it would be interesting to study the effect of the use of promoters to aqueous ammonia solution. This could allow for improving the performance of the solvent.

Regarding the simulation, several aspects could be developed or improved.

- Different chilling systems could be tested, especially direct chilling system might allow for limiting the chilling duty.
- Investigating the performance of the process using higher concentration of ammonia and different process configurations might allow for improving the performance of the process, especially for cooling water at high temperature.



- The use of equilibrium calculations implies uncertainty regarding the ability for the simulation to predict the absorption behavior in a real packed column. The Murphree efficiencies used in the simulation to reflect the deviation from equilibrium have been assumed. This assumption affects the results strongly. Pilot plant data would allow for fitting the Murphree efficiency in the absorber as a function of the ammonia concentration, the temperature, the partial pressure of carbon dioxide and the loading. The development of a rate-based model would allow for improving the accuracy of the study. It would require simulating the wetted wall column experiments with Aspen Plus and fitting the parameters for the kinetic rate constant for each of the chemical reactions, including the reverse reactions. The rate based model should also include the vaporization and absorption of ammonia. It should be checked that the assumption used in the study considering the enhancement factor can be set to be equal to one is valid.
- Using a rate-based model, Configuration B could be optimized. More process configurations could be tested. The many studies dealing with the simulation of MEA-based capture process could be used to improve the process configurations. The split of the CO<sub>2</sub>-rich stream to the desorber and the use of inter-cooling in the absorber are among solutions that have proven to reduce the power consumption of the capture.
- In case a robust rate-based model is available, the development of a model that accounts for the dynamics would be interesting. The load of the power plant is varying and the capture plant therefore has to adapt to this variation. As the capture process using aqueous ammonia is more complex than the MEA-based process, it would be especially interesting to investigate how the process would react to a high variation of the load, such as the temporary shut down of the power plant. In addition, while operating a capture process, having the possibility to vary the CO<sub>2</sub> capture rate would probably be a strong asset to deal with peak consuming hours.
- Finally, based on the results of the present study, it would be possible to make a preliminary assessment of the capital cost of the process and to compare it with the MEA-based process. The size of the absorber column has been estimated. The cost of the chillers, the blower and the stripper could also be assessed based on information from supplier or from the literature. The influence of the process parameters on the dimension of the main heat exchangers could be studied. The effect of the presence of solid for the high concentration cases should also be considered.

## 9 Appendix

### 9.1 Appendix A

#### 9.1.1 Additional information regarding the Wetted Wall column apparatus

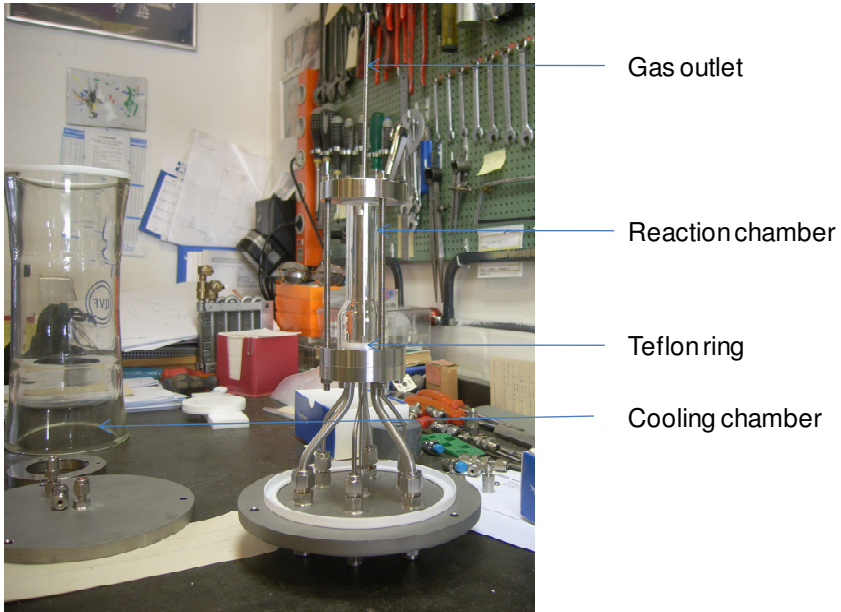
The wetted wall column has been built at the workshop of DTU. The design of the apparatus was inspired by the wetted wall column used by Pacheco (1998) and Dugas (2010). Figure 9-1 shows a picture of the stainless steel tube with its base. In white, the teflon ring allows for ensuring the reaction chamber is hermetic. It includes holes for the three gas inlets and the three liquid outlets. It can be observed that the shape of the teflon ring and the location of the liquid outlet (close to the center) allow for an efficient flow of the liquid out of the reaction chamber. In addition, it allows for preventing the formation of a stagnant layer at the bottom of the stainless steel tube. The gas inlets and liquid outlets are evenly distributed at the bottom of the chamber.

On the base holding the stainless steel tube, one of the gas inlets can be seen. It is elevated in order to prevent from the gas to bubble in the solvent before it is introduced in the chamber.

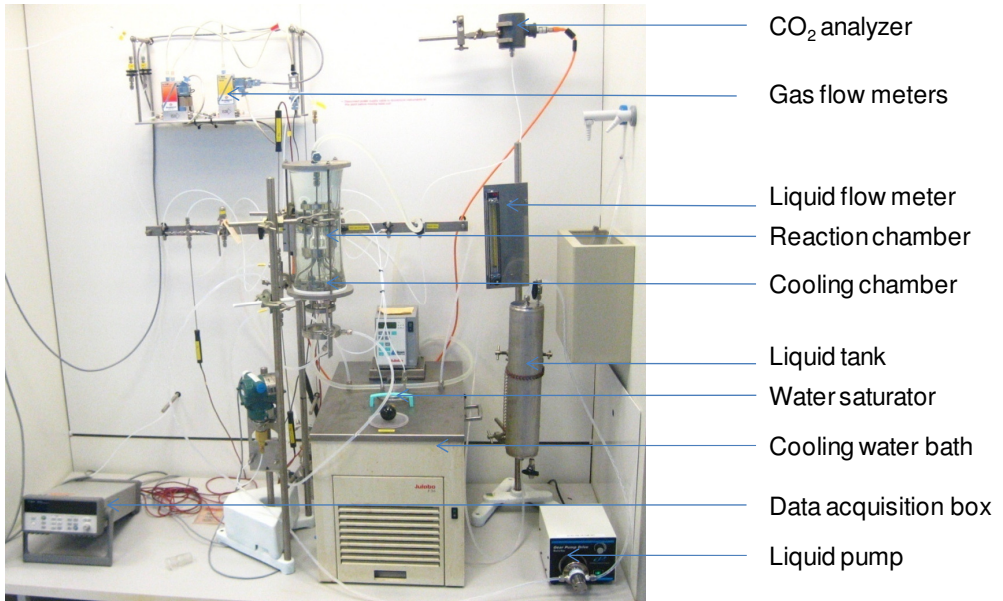
Figure 9-2 shows a picture of the reaction chamber. The teflon ring has been attached to the base. Figure 9-3 shows an overview of the experimental apparatus with the different units.



Figure 9-1: Picture of the stainless steel tube, the holding base and the Teflon ring



**Figure 9-2: Picture of the reaction chamber**



**Figure 9-3: Overview of the experimental apparatus**

### 9.1.2 References

- Dugas, R. Carbon dioxide Absorption, Desorption and diffusion in aqueous Piperazine and Monoethanolamine. Doctoral dissertation. The University of Texas, Texas, **2009**.
- Pacheco, M.A. Mass transfer, kinetics and rate-based modeling of reactive absorption. Doctoral Dissertation, The University of Texas, Texas, **1998**.

### 9.2 Appendix B

This section analyses the effect of the variation of the ME in the simulations. For the sake of simplification, this analysis is made for Configuration A for a chilling temperature of 10 °C. In the simulations, the capture rate has a constant value of 90% and the composition and flow rate of the flue gas is constant. Hence, by changing the value of the ME, if the variation of the ammonia slip from the absorber is neglected, the amount of carbon dioxide absorbed in the absorber column can be considered as constant.

For a given set of parameters, lowering the ME in the absorber while maintaining a constant capture rate implies that a larger flow rate of solvent is required. The effects of this phenomenon on the rate of absorption have been described in 7.3.2.7.

The variation of the ME also affects the concentration profile in the column. Figure 9-4 shows the McCabe-Thiele diagram for the absorber for 7.8 wt% NH<sub>3</sub>, RR= 0.5, LL = 0.33, T<sub>chill</sub> = 10 °C for ME = 0.1 and ME = 0.15.

The partial pressures of carbon dioxide at the bottom and at the top of the column are similar for both MEs, as the amount of CO<sub>2</sub> captured in the absorber is very close for both cases. Hence, the mole fractions of carbon dioxide in the gas phase at the top and at the bottom of the column are similar for the operating lines with both MEs.

As the flow rate of solvent is higher, the CO<sub>2</sub> loading and consequently the mole fraction of free carbon dioxide in the liquid phase reaches lower values for ME = 0.10 than for ME = 0.15.

The lower temperature implies that for a given mole fraction of carbon dioxide in the liquid phase, the equilibrium partial pressure of carbon dioxide is slightly lower for ME = 0.10 than for ME = 0.15.

Figure 9-4 shows that by lowering the ME keeping a constant capture rate, the difference between the operational and equilibrium partial pressure of carbon dioxide increases in the column. Hence, the driving force for the mass transfer increases.

During a simulation, if the amount of carbon dioxide absorbed is constant and if the number of equilibrium stage is unchanged, decreasing the ME for carbon dioxide in the absorber therefore leads to the decrease of the packing height requirement in the absorber.

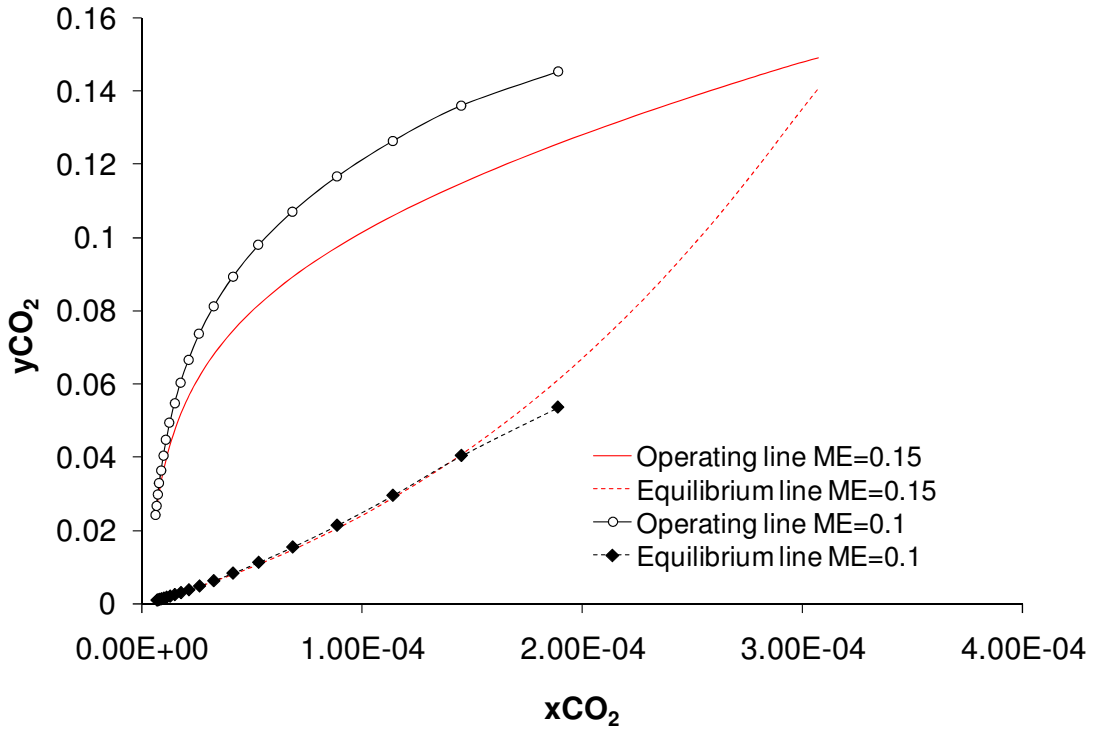


Figure 9-4: Operating and equilibrium CO<sub>2</sub> concentration profile in the absorber for 7.8 wt% NH<sub>3</sub>, RR=0.5, LL=0.33, T<sub>chill</sub> = 10 °C for ME = 0.1 and ME = 0.15



## **9.3 Appendix C**

### **9.3.1 List of publications**

Darde, V.; Thomsen, K.; van Well W. J. M.; Stenby E. H. Chilled ammonia process for CO<sub>2</sub> capture, *Int. J. Greenhouse Gas Control*, **2010**, *4*, 131.

Darde, V., Thomsen, K., van Well, W.J.M. and Stenby, E.H.S. Modeling of carbon dioxide absorption by aqueous ammonia solutions using the Extended UNIQUAC model. *Ind. Eng. Chem. Res.*, **2010**, *49*, 12663-12674.

Darde, V.; van Well, W. J. M.; Fosboel, P.; Stenby, E. H. S.; Thomsen, K. Experimental measurement and modeling of the rate of absorption of carbon dioxide by aqueous ammonia. **2011**, doi:10.1016/j.ijggc.2011.07.008.

In addition, 3 papers have been recently submitted for publication in scientific journals.

### **9.3.2 List of presentations at international conferences**

ICPWS XV, Berlin, Germany, September 2008 – oral presentation.

GHGT9, Washington, USA, November 2008 – oral presentation.

Copenhagen Climate Congress, Copenhagen, Denmark, March 2009 – poster presentation.

IEAGHG 12<sup>th</sup> capture network meeting, Regina, Canada, September 2009 – oral presentation.

SIMS50, Fredericia, Denmark, October 2009– oral presentation.

GHGT10, Amsterdam, the Netherlands, September 2010 – oral presentation.

PCCC1, Abu Dhabi, May 2011 – oral presentation.

Center for Energy Resources Engineering  
Department of Chemical and  
Biochemical Engineering  
Technical University of Denmark  
Søltofts Plads, Building 229  
DK-2800 Kgs. Lyngby  
Denmark

Phone: +45 4525 2800  
Fax: +45 4525 4588  
Web: [www.cere.dtu.dk](http://www.cere.dtu.dk)

ISBN : 978-87-92481-56-6